Carbon and nitrogen acquisition of the diazotroph *Trichodesmium* in a high CO_2 world

Dissertation
zur Erlangung des akademischen Grades eines
Doktors der Naturwissenschaften
- Dr. rer. Nat. -
am Fachbereich 2 (Biologie/Chemie)
der Universität Bremen

vorgelegt von

Sven Alexander Kranz

Bremen,
März, 2010

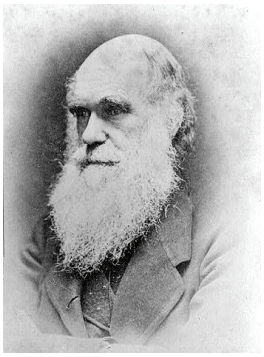

March 18th. 1839 - We sailed from Bahia. A few days afterwards, when not far distant from the Abrolhos Islets, my attention was called to a reddish-brown appearance in the sea. The whole surface of the water, as it appeared under a weak lens, seemed as if covered by chopped bits of hay, with their ends jagged. These are minute cylindrical confervae, in bundles or rafts of from twenty to sixty in each. Mr. Berkeley informs me that they are the same species (Trichodesmium erythraeum) with that found over large spaces in the Red Sea, and whence its name of Red Sea is derived. Their numbers must be infinite: the ship passed through several bands of them, one of which was about ten yards wide, and, judging from the mud-like colour of the water, at least two and a half miles long.

The Voyage of the Beagle – Charles Darwin

Danksagung

I am committed to many people who crossed my way during the time as a PhD student, giving me a life next to this thesis or at least a smile once a day. There are too many to name them all, but the next pages are for those who directly contributed to the success of this piece of work:

In erster Linie möchte ich mich bei Björn Rost für Deine unendliche Geduld, Deiner Entfesselungskunst für meine oft gordischen Gedankenknoten sowie Deinem Talent, mich immer wieder aufzubauen bedanken. Natürlich sollte Deine wissenschaftliche Expertise hier nicht zu kurz kommen: es gibt keinen, der C-Isotopenfraktionierung so geschmackvoll erklären kann und mit dem es so viel Spaß macht, wissenschaftliche Probleme zu erörtern und nach Erklärungen zu suchen. Hier muss ich mich natürlich auch bei Anneli, Deiner wunderbaren Frau sowie Deinen 3 bezaubernden Kindern bedanken und entschuldigen. Entschuldigt, dass ich Euren Mann/Vater manchmal bis spät abends für mich beansprucht habe. Danke, dass Ihr das „ertragen und erlaubt“ habt.

Weiterhin bedanke ich mich bei Prof. Dieter Wolf-Gladrow, dass Du es mir ermöglicht hast, in Deiner Arbeitsgruppe am AWI Fuß zu fassen sowie für Deine Bereitschaft, meine gesammelten Werke zu lesen, zu korrigieren und zu bewerten.

Ebenso bedanke ich mich bei Prof. Kai Bischof für die Bereitwilligkeit, diese Arbeit zu bewerten, sowie die Bereitschaft als Prüfer zur Verfügung zu stehen.

Bei Christoph Völker bedanke ich mich für die schnellen Korrekturen, sowie die spontane Bereitschaft als Prüfer einzuspringen.

Ein besonderer Dank verdient Klaus-Uwe Richter. Ohne Dich würde der Laden hier nicht ganz so rund laufen und viele meiner Experimente wären nicht möglich gewesen! Danke für alles.

רבה תודה Orly Levitan for the great and productive time in the lab. I’m still sorry that you haven’t had the chance to see Bremerhaven in the light during your 1 month internship at the AWI. I will never forget our state-transition dance, the whiteboard full of black, green and red arrows and cryptic letters after each day. Although you missed the sun in Bremerhaven, we had lots of fun in the sun on Cape Verde. Night work has pros and cons ☺. Hier bedanke ich mich auch bei

Stefanie Sudhaus vom IFM Geomar. Danke für die Einladung an diesem Experiment teilzunehmen. Es war harte aber schöne Arbeit und hat mir einen guten Einblick in die Wissenschaft außerhalb des Labors gegeben.

I thank Peter Ralph for the invitation to investigate *Trichodesmium* in the wonderful city of Sydney. I learned a lot during this stay, especially not to leave the track and that *Trichodesmium* is not just a bag of chlorophyll. Looking forward to coming back to your lab.

Thanks Katherina and Javier for hosting me during my stay in Down Under. You gave me back my smile and you showed me, how to separate work and life (sorry I failed in this discipline). I also really enjoyed your stay here in Bremerhaven, even it developed into a small "SO Disaster" with a ripped filament (I'm still sorry for that). I will never forget the time with you!

Auch bedanke ich mich bei den Mitgliedern des Doktorandenteams 2007-2009: Maria, Sönke, Conny, Lasse, Friederike, Susann, Donata und Thomas. Zusammen haben wir einiges erreicht! Es hat wirklich Spaß gemacht mit Euch.

Weiterhin bedanke ich mich bei allen Mitarbeitern und Alumni der Biogeoscience. Besonders hervorheben möchte ich allerdings Sebastian S. und Sevrine. Mit Euch hatte ich vom Anfang meines PhDs an sehr viel Spaß. Lys, thanks for all your corrections and that you accompanied my often late hour work in the last month (even though it was not voluntary ;-)). Meinen Büromitstreitern Morten und Sebastian R. danke ich für die angeregten wissenschaftlichen Diskussionen sowie Korrekturen. Maya danke ich dafür, dass sie es über 2 Jahre mit mir in einer Wohnung ausgehalten hat, sowie für Ihre Freundschaft, die ich des Öfteren mal sehr strapaziert habe. Scarlett, Ulrike, Gerald, Karin und Anja danke ich für Euer Dasein in dieser Arbeitsgruppe und Eure Hilfsbereitschaft sowie den wissenschaftlichen Austausch. Dörte, danke für Deine Hilfe in allen Belangen der Bürokratie. Danke auch an alle anderen und für die leckeren Kuchen!

Abschließend will ich mich noch bei meinen Liebsten bedanken: Ma, Pa, danke für Eure Unterstützung und Euer Verständnis. Christiane, vielen lieben Dank für das Leben, das Du mir neben der Doktorarbeit gegeben hast.

Table of contents

Summary
&
Zusammenfassung

1 SUMMARY

The main motivation for this thesis was to describe the responses of the N_2 fixing cyanobacterium *Trichodesmium* to elevated pCO_2 and to provide a detailed understanding of underlying processes. The focus was hereby to characterize inorganic carbon acquisition and its interaction with photosynthesis and N_2 fixation. Based on these findings, the potential influence of *Trichodesmium* on the ecosystem and elemental cycles in the future oceans was assessed.

First, a comparison of the ^{14}C disequilibrium technique and membrane inlet mass spectrometric (MIMS) approaches on modes of carbon acquisition was conducted. This method comparison provided experimental confirmation of key assumptions and demonstrated strengths and weaknesses of the different approaches. The ^{14}C disequilibrium technique was found to be a robust and accurate method to determine the preference of inorganic C species (CO_2 and/or HCO_3^-) taken up by phytoplankton cells. The MIMS approach obtained nearly identical results on the contribution of HCO_3^- and CO_2 relative to net carbon fixation. In addition, the C fluxes measured by MIMS provided details on the kinetics of HCO_3^- and CO_2 uptake. Regarding extracelluar carbonic anhydrase (eCA), the two methods differed in their estimates on activities. Errors in the ^{14}C-based estimates on eCA activities were also much higher than those obtained by the MIMS approach. In view of the applicability, the ^{14}C disequilibrium technique has a significant advantage for field studies, whereas MIMS approaches are required for a more detailed characterization of the carbon concentrating mechanism (CCM). Both methods were applied in subsequent studies on *Trichodesmium*.

Second, *Trichodesmium* was incubated to different CO_2 concentrations (150, 370, and 1000 µatm pCO_2) to test for its CO_2 sensitivity. In these acclimations, the production of particulate organic carbon (POC) and particulate organic nitrogen (PON) was strongly stimulated under 1000 µatm pCO_2. To explain this effect, modes of carbon acquisition were characterized by means of MIMS and ^{14}C disequilibrium technique. *Trichodesmium* was found to operate an efficient CCM based primarily on the uptake of HCO_3^-. Apparent affinities for DIC decreased with increasing CO_2 concentrations. Changes in affinities were even more pronounced over the diurnal cycle, being inversely correlated with N_2 fixation. Activities for eCA were low and did not change with pCO_2, indicating a minor role of this enzyme in carbon acquisition. The presence of an efficient CCM clearly negates a direct effect of ambient CO_2 on the carboxylation efficiency of ribulose-1,5-bisphosphate carboxylase/oxygenase (RubisCO) in *Trichodesmium*. Instead, the findings point to changes in resource allocation as an explanation for the observed CO_2-sensitivity.

Summary

To determine the effect of energy availability on the CO_2-sensitivity, *Trichodesmium* was subsequently grown under a matrix of low and high levels of pCO_2 (150 and 900 µatm) and irradiance (50 and 200 µmol photons m^{-2} s^{-1}). Growth rates as well as cellular C and N content increased with increasing CO_2 and light levels in the cultures. The CO_2-dependent stimulation in POC and PON production was highest under low light. To understand these CO_2-effects and their modulation by light, energy sources (gross photosynthesis) and sinks (C-aquisition, N_2 fixation, Mehler reaction) were assessed by means of mass spectrometry and gas chromatography. Gross photosynthesis was found to increase with light, yet being insensitive to CO_2. High CO_2 levels, however, stimulate rates of N_2 fixation and prolonged its duration. Although HCO_3^- was the dominant carbon source for C fixation in all treatments, CO_2 uptake increased under elevated pCO_2. Mehler reaction was generally low under growth condition but instantaneously induced when cells were exposed to high light, indicating that this process rather functions as photo-protective than O_2-scavenging mechanism in *Trichodesmium*. In summary, the observed stimulation in growth and production rates under elevated pCO_2 cannot be explained by changes in energy production via PSII activity but it can be attributed to the CO_2-dependent regulation in CCM and N_2 fixation. Owing to this improved "energy use efficiency" under elevated pCO_2, *Trichodesmium* is likely to benefit from ocean acidification.

In addition to the experiments looking at the effect of changes in carbonate chemistry on *Trichodesmium*, the consequences of a bloom situation on carbonate chemistry was investigated under different availabilitiy of inorganic phosphorus (P). During exponential growth, the concentration of DIC decreased while pH increased until cell densities peaked in all treatments. Once P became depleted, DIC decreased even further and total alkalinity (TA) dropped. These pronounced changes in carbonate chemistry were accompanied by precipitation of $CaCO_3$, subsequently identified as aragonite. Under P-replete conditions, however, TA remained constant, DIC returned to initial concentrations and no aragonite was formed in the post bloom phase. The ability of *Trichodesmium* to shift carbonate chemistry from equilibrium was further investigated by applying a diffusion-reaction model to the data. These findings demonstrate the capability of *Trichodesmium* to induce precipitation of aragonite from seawater as a function of P availability. Possible consequences on the marine carbon cycles are discussed.

ZUSAMMENFASSUNG

Ziel dieser Arbeit war es, die Reaktion des N_2-fixierenden Cyanobakteriums *Trichodesmium* auf eine Erhöhung von atmosphärischem CO_2 zu beschreiben und ein detailliertes Prozessverständnis der gefundenen Effekte zu erlangen. Der Schwerpunkt der Forschung lag hierbei auf der Charakterisierung des Kohlenstofferwerbs und dessen Wechselwirkung mit Fotosynthese sowie N_2-Fixierung. Auf Grundlage der erzielten Ergebnisse wurden zukünftige Veränderungen im marinen Ökosystem sowie von Stoffkreisläufen abgeschätzt.

Zu Beginn der Doktorarbeit wurden zwei Ansätze zur Bestimmung des Kohlenstofferwerbs von Phytoplankton miteinander verglichen. Dieser Vergleich bestätigte Schlüsselannahmen der "^{14}C disequilibrium"-Technik sowie Methoden der Membran-Einlass Massenspektrometrie (MIMS) und zeigte deren Stärken und Schwächen. Die "^{14}C disequilibrium"-Technik ist ein robuster and präziser Ansatz zur Spezifizierung der Kohlenstoffaufnahme (CO_2 und/oder HCO_3^-) von Phytoplankton. Der MIMS-Ansatz zeigte nahezu identische Ergebnisse in Bezug auf den Anteil von HCO_3^- und CO_2 relativ zur Netto-Kohlenstofffixierung. Des Weiteren ergaben die Kohlenstoffflussmessungen mittels MIMS detaillierte Angaben über HCO_3^-- und CO_2-Aufnahmekinetiken. Bei der Bestimmung der Aktivität von extrazellulärer Karboanhydrase (eCA) unterschieden sich beide Ansätze in ihren Abschätzungen. Der methodische Fehler der "^{14}C disequilibrium"-Technik war hierbei erheblich größer als die Fehler des MIMS-Ansatzes. Hinsichtlich der Anwendbarkeit zeigte sich, dass die "^{14}C disequilibrium"-Technik bedeutende Vorteile für den Einsatz in Feldstudien hat, wohingegen der MIMS-Ansatz für eine genauere Charakterisierung der Kohlenstoff-Konzentrierungsmechanismen (CCM) erforderlich ist. Beide Methoden wurden in den nachfolgenden Studien mit *Trichodesmium* angewendet.

Um die Sensitivität von *Trichodesmium* auf Veränderungen in der CO_2 Konzentration zu untersuchen, wurde dieses Cyanobakterium an verschiedene CO_2 Partialdrücke (pCO_2) von 150, 370 und 1000 µatm akklimatisiert. Ein starker Anstieg der Produktion des partikulären organischen Kohlenstoffs (POC) sowie des partikulären organischen Stickstoffs (PON) konnte hierbei unter 1000 µatm pCO_2 gemessen werden. Um diese CO_2-bedingten Veränderungen besser verstehen zu können, wurde der Kohlenstofferwerb mit Hilfe der MIMS- und der "^{14}C disequilibrium"-Technik charakterisiert. Es zeigte sich, dass *Trichodesmium* einen effizienten CCM besitzt, der hautsächlich auf aktiver Aufnahme von HCO_3^- basiert. Die apparenten Affinitäten für gelösten anorganischen Kohlenstoff (DIC) reduzierten sich dabei mit erhöhten CO_2 Konzentrationen. Über den Tagesverlauf waren die Veränderungen in diesen Affinitäten noch ausgeprägter und mit der Aktivität der N_2-Fixierung antikorreliert. Für *Trichodesmium* wurde nur eine geringe Aktivität von eCA gemessen, welche unabhängig vom pCO_2 der

Akklimatisation war und somit eine nur geringe Rolle im CCM von *Trichodesmium* spielt. Die Existenz eines effizienten CCM in *Trichodesmium* beweist eindeutig, dass Veränderungen im pCO_2 keinen direkten Einfluss auf die Karboxilierungseffizienz der Ribulose-1,5-Bisphosphate Carboxylase/Oxygenase (RubisCO) hat. Die gemessene CO_2-Sensitivität scheint stattdessen durch Veränderungen im zellulären Energiehaushalt hervorgerufen zu werden.

Um Auswirkungen von Energieverfügbarkeit auf die CO_2-Sensitivität zu bestimmen, wurde *Trichodesmium* in einer Matrix aus niedrigen und hohen Konzentrationen von pCO_2 (150 und 900 µatm) und Licht (50 und 200 µmol photons m^{-2} s^{-1}) akklimatisiert. Die Wachstumsraten sowie zelluläre Kohlenstoff- und Stickstoffgehalte steigerten sich durch erhöhte pCO_2 sowie erhöhte Lichtintensitäten in den Kulturen. Die CO_2-abhängige Steigerung in der POC und PON Produktion war unter der niedrigen Lichtintensitäten am größten. Um diese Reaktionen und ihre Regulierung durch Licht zu verstehen, wurden die zelluläre Energieproduktion (Brutto-Fotosyntheseraten) sowie energieverbrauchende Prozesse (Kohlenstoff-Aufnahme, N_2-Fixierung, Mehler Reaktion) über MIMS und Gas-Chromatographie abgeschätzt. Die Brutto-Fotosyntheseraten steigerten sich mit erhöhter Lichtintensität, waren jedoch unbeeinflusst von pCO_2. Erhöhte CO_2-Konzentrationen zeigten jedoch einen Stimulierungseffekt auf Raten sowie Dauer der N_2-Fixierung über den Tagesverlauf. Obwohl HCO_3^- die hauptsächliche Kohlenstoffquelle für C-Fixierung in allen Akklimatisationen darstellte, steigerte sich die CO_2-Aufnahme unter erhöhtem pCO_2. Unter den Akklimatisationsbedingungen wurde nur eine niedrige Aktivität der Mehler Reaktion gemessen, welche sich allerdings stark steigerte, sobald die Zellen höherer Lichtintensität ausgesetzt waren. Diese Beobachtungen deuten darauf hin, dass die Mehler Reaktion eher zum Schutz der Fotosynthese bei hohen Lichtintensitäten als zur Senkung der zellulären O_2-Konzentrationen fungiert. Zusammenfassend zeigt sich, dass die beobachtete Erhöhung der Wachstums- sowie der Produktionsraten unter erhöhtem pCO_2 nicht durch eine Veränderung in der Fotosyntheseaktivität und demzufolge der primären Energieproduktion erklärt werden kann. Die starke CO_2-Sensitivität kann vielmehr auf die CO_2-abhängige Regulation des CCMs und der N_2-Fixierung zurückgeführt werden. Aufgrund der verbesserten „Energienutzungs-Effizienz“ unter erhöhtem pCO_2 wird *Trichodesmium* voraussichtlich von der Ozeanversauerung profitieren.

Ergänzend zu den Studien über die Auswirkungen von veränderter Karbonatchemie auf *Trichodesmium*, wurden die Effekte einer Blütensituation von diesem Cyanobakterium auf die Karbonatchemie unter verschiedener Phosphatverfügbarkeit (PO_4^{3-}) betrachtet. Die Ergebnisse zeigten, dass während des Zellwachstums die DIC-Konzentration abnahm wohingegen der pH im Medium anstieg. Dieser Trend war unter allen Bedingungen bis zum Erreichen der

maximalen Zellkonzentration vergleichbar. Nach vollständiger Aufnahme von PO_4^{3-} verringerte sich DIC auch nach Erreichen der maximalen Zellkonzentration weiter. Außerdem wurde ein Abfallen der Alkalität (TA) im Medium beobachtet. Diese ausgeprägten Veränderungen in der Karbonatchemie korrelierten mit einer Ausfällung von aragonitischem $CaCO_3$. In dem Ansatz, bei dem PO_4^{3-} nicht aufgebraucht wurde, blieb TA konstant und DIC kehrte zu den initialen Konzentrationen zurück. Auch konnte hier keine Aragonitfällung beobachtet werden. Um die Veränderung in der Karbonatchemie in Aggregaten von *Trichodesmium* abschätzen zu können, wurde ein "diffusion-reaction" Modell verwendet. Diese Studie zeigt das Potential von *Trichodesmium*, Aragonitfällung in Abhängigkeit von Phosphatverfügbarkeit in Seewasser zu induzieren. Mögliche Auswirkungen auf den marinen Kohlenstoffkreislauf wurden diskutiert.

General introduction

2 General introduction

2.1 Setting the scene

In the Hadean, around 4.6 billion years ago, life would have been impossible for most modern life forms due to a hostile environment. Average temperatures of about 100°C and a primal atmosphere devoid of oxygen, mainly composed of water vapor, dinitrogen (N_2), carbon dioxide (CO_2) and methane (CH_4) prevailed (Holland, 1984; Kasting et al., 1988; Kasting and Siefert, 2002). With Earth's cooling, water vapor condensed and in the Archaean (4 billion years ago), the ancestral ocean became home to the first prokaryotic life forms. These so-called Archaea exploit a large variety of sources for biomass production, ranging from organic compounds and the use of NH_4^+, metal ions or even hydrogen gas as energy source. About one billion years later, prokaryotic life forms evolved, able to use sunlight for energy production, the so-called photoautotrophic bacteria (Xiong et al., 2000; Blankenship, 2001).

Cyanobacteria were the first using sun energy to split the water molecules for the production of biochemical energy (Des Marais, 2000), which was used to convert CO_2 into biomass. These prokaryotes and their descendants changed the destiny of our planet, altering the atmosphere by consuming CO_2 and producing O_2 via the process of photosynthesis. Initially, the O_2 reacted mainly with iron-containing minerals and as soon as those were oxidized, O_2 started to accumulate in the atmosphere (Rye and Holland, 1998; Farquhar et al., 2000). It took another 1.5 billion years before the eukaryotic photosynthetic organisms entered the scene (Javaux et al., 2001). All these photosynthetic organisms strongly influenced environmental conditions and climate by driving many of the global elemental cycles.

Although environmental conditions have undergone major changes over geological time, the presently observed global change is occurring at an unprecedented rate, mainly caused by changes in land use and the burning of fossil fuel (Solomon et al., 2007). A large proportion of the anthropogenically released CO_2 is absorbed by the oceans, buffering the increase of this greenhouse gas in the atmosphere and thus global warming. However, the CO_2 uptake by the oceans causes complex changes in the carbonate chemistry that are reflected by a decreasing pH (Wolf-Gladrow et al., 1999; Solomon et al., 2007). This process, often referred to as ocean acidification, is likely to affect marine organisms in general and phytoplankton in particular (Raven et al., 2005; Rost et al., 2008).

Marine phytoplankton comprises approximately 5000 species (Sournia et al., 1991; Tett and Barton, 1995) and represents about one percent of the photoautotrophic vegetation on Earth. Despite their little overall biomass, these photoautotrophs are responsible for about half of the

global primary production (Field et al., 1998). This apparent paradoxon is caused by the capacity for rapid growth and a corresponding high turnover. Despite the high variety in phytoplankton, only a relatively small number of species dominate elemental cycling. Among these key species, marine N_2 fixing cyanobacteria, so-called diazotrophs, play an important role in the nitrogen cycle, thus marine productivity and Earth's climate (Zehr and Ward, 2002). It is a key question in climate research, marine ecology and biogeochemistry to understand the complex interplay between ecosystem functioning and climate variability.

2.2 The marine carbon cycle

Understanding the responses and feedbacks of phytoplankton to changes in atmospheric CO_2 requires the knowledge of processes influencing the CO_2 exchange between ocean and atmosphere. The uptake of atmospheric CO_2 by the ocean is mediated by the so-called physical and biological carbon pumps (Volk and Hoffert, 1985). The physical pump describes the vertical carbon flux resulting from differences in CO_2 solubility of warm and cold water. As warm surface water moves from low to high latitudes, successive cooling results in an increasing solubility for CO_2. Owing to deep-water formation at high latitudes, this cold water, rich in dissolved inorganic carbon (DIC), is then transported to the deep ocean (Fig. 1).

Biological fixation of DIC into biogenic matter, its subsequent sinking, remineralization and/or dissolution drives the biological pumps, which are thought to cause about 75% of the vertical DIC gradient (Sarmiento et al., 1995). These pumps can be separated into the organic carbon pump and the carbonate pump. The organic carbon pump is driven by photosynthetic CO_2 fixation into particulate organic carbon (POC), causing a drawdown of CO_2 from the atmosphere into the ocean (Fig. 1). Organisms that precipitate calcium carbonate ($CaCO_3$) and sink to depth provide a CO_2 source for the atmosphere. This counterintuitive effect is caused by consumption of DIC as well as total alkalinity (TA) during the process of calcification (Zeebe and Wolf-Gladrow, 2007). The extent of both biological pumps, expressed in the so-called rain ratio ($CaCO_3$: POC), largely determines the flux of CO_2 between surface ocean and atmosphere, and was estimated to range between 0.05 and 0.25 in the contemporary ocean (Sarmiento et al., 2002). Cyanobacteria are known to be important primary producers (Paerl and Bebout, 1992; Waterbury, 2005) and a source for reactive nitrogen (Karl et al., 1997), and thus play a key role in the marine carbon cycling (Capone et al., 1997; Partensky et al., 1999; Waterbury, 2005).

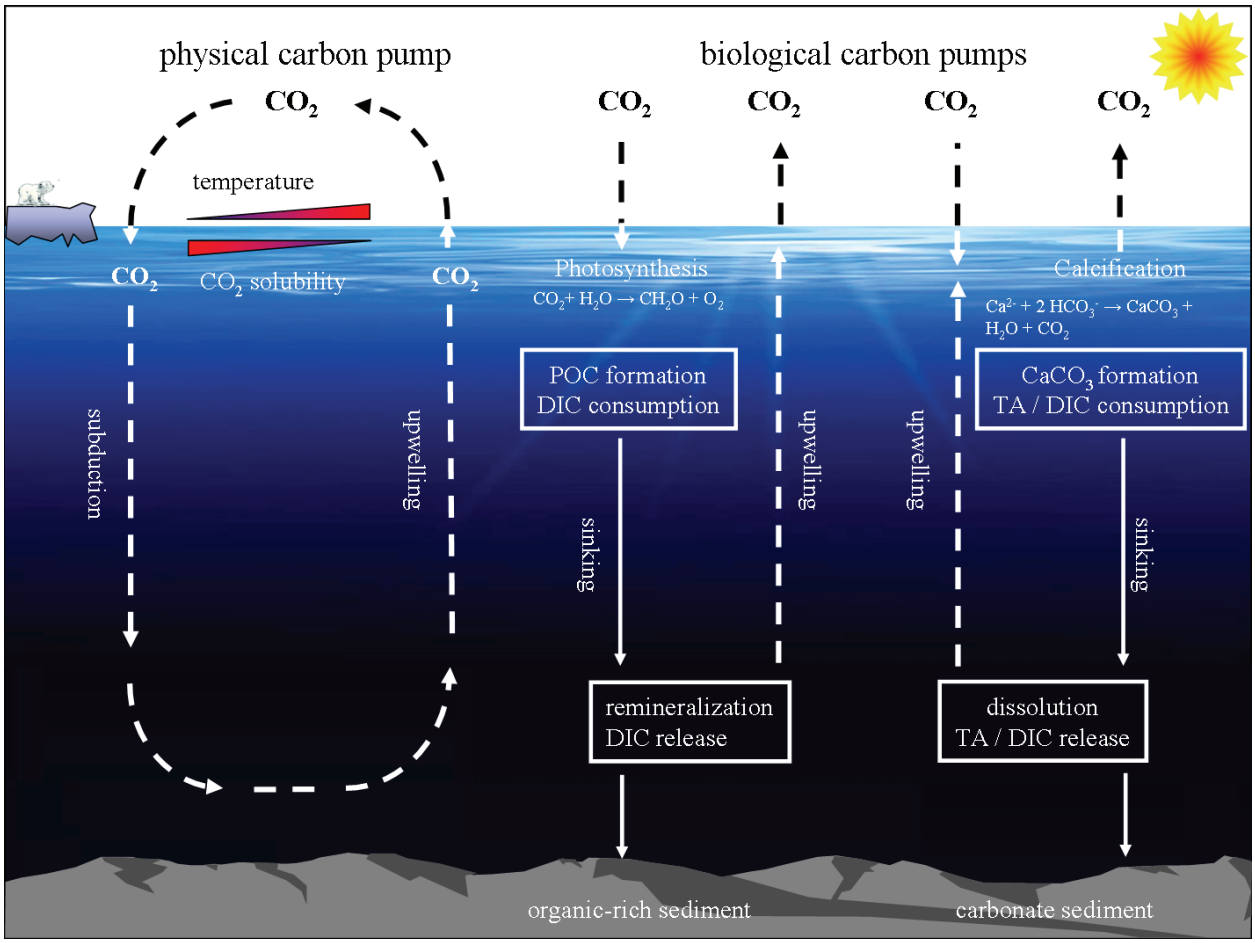

Figure 1: Schematic illustration of the physical and biological driven carbon pumps (see text). Solid lines indicate the flow of particulate carbon and dotted lines indicate mass redistribution by physical-chemical processes such as gas exchange or water mass movements. Abbreviations: DIC – dissolved inorganic carbon; POC – particulate organic carbon; TA – total alkalinity.

2.2.1 Seawater carbonate chemistry

To understand global carbon cycles and biological processes involved in C assimilation, the basics of the carbon system have to be known. Next to N_2 (71%), O_2 (21%) and Argon (1%), CO_2 (0.038%) is the most abundant gas in the contemporary Earth's atmosphere. When atmospheric CO_2 dissolves in seawater, it follows Henry's law (see Eq. 1):

$$[CO_2] = \alpha \times pCO_2. \quad (1)$$

where $[CO_2]$ is the concentration of dissolved (aqueous) CO_2, α represents the temperature- and salinity-dependent solubility coefficient and pCO_2 denotes the atmospheric partial pressure of CO_2. Despite the relatively low concentration of CO_2 in the atmosphere compared to N_2 or O_2, the relative amount of inorganic carbon in the ocean is an order of magnitude higher. This is caused by the fact that CO_2 is not simply dissolved in seawater like other gases, but it reacts with the water and forms carbonic acid (H_2CO_3), which subsequently dissociates to the anions bicarbonate (HCO_3^-) and carbonate (CO_3^{2-}):

$$CO_2 + H_2O \rightleftharpoons H_2CO_3 \rightleftharpoons HCO_3^- + H^+ \rightleftharpoons CO_3^{2-} + 2H^+ \quad (2)$$

The $[CO_2]$ usually comprises $[H_2CO_3]$, which exists only in very low concentrations. The sum of the three dissolved species $[CO_2]$, $[HCO_3^-]$ and $[CO_3^{2-}]$ is summarized as dissolved inorganic carbon (DIC):

$$DIC = [CO_2] + [HCO_3^-] + [CO_3^{2-}] \quad (3)$$

While the [DIC] in the surface ocean is relatively constant, the proportion of the DIC species vary as a function of pH (Fig. 2), temperature and salinity. An increase in temperature and/or salinity will increase the relative proportion of $[CO_3^{2-}]$ with respect to $[CO_2]$ and $[HCO_3^-]$.

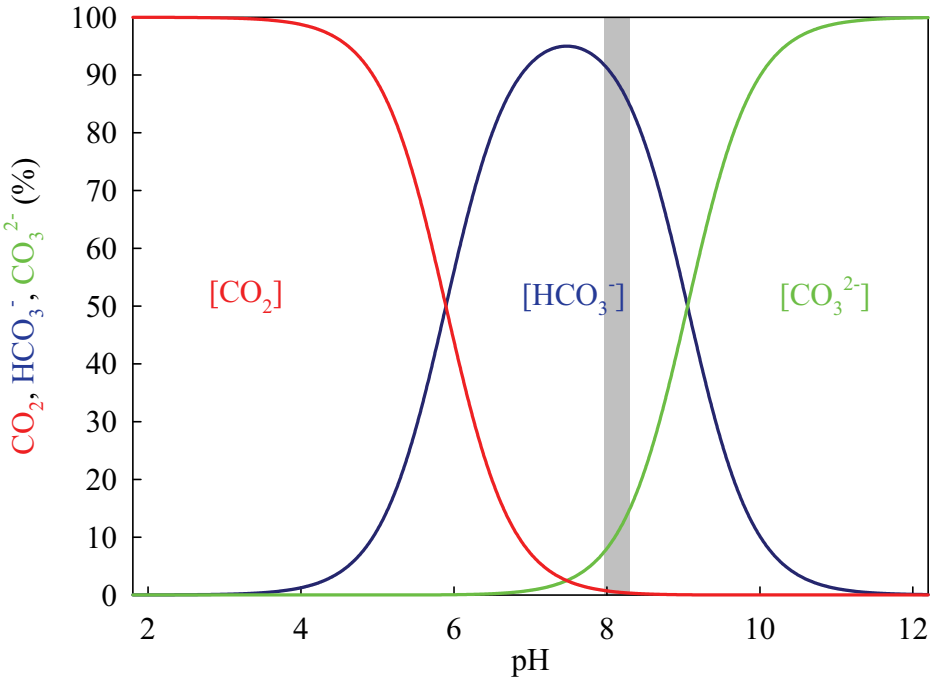

Figure 2: Relative proportions of CO_2, HCO_3^- and CO_3^{2-} in seawater as a function of pH (20°C, S=34). In the contemporary ocean, the pH is around 8.0 to 8.3 (indicated by the grey bar). Thus, HCO_3^- represent about 85-94%, followed by CO_3^{2-} with 5-15%, while CO_2 comprises only 0.3-1.2% of DIC. Please note that the relative proportions of the DIC species control the pH and not vice versa (modified after Zeebe and Wolf-Gladrow, 2007).

For an accurate description of the carbonate system, total alkalinity (TA) is required. This parameter can be regarded as an electrochemical charge balance or the buffer capacity. The surplus of strong cations (e. g. Na^+, Mg^{2+}, Ca^{2+} K^+, Sr^+) over strong anions (e. g. Cl^-, CO_4^{2-} NO_3^-, F^-) in seawater is balanced by the charge of weak ions and defines TA (Dickson, 1981):

$$TA = [HCO_3^-] + 2[CO_3^{2-}] + [B(OH)_4^-] + [OH^-] - [H^+] + [X] \quad (4)$$

While most of the charge difference between strong cations and strong anions is compensated by $[HCO_3^-]$ and $[CO_3^{2-}]$, other constituents such as $[Si(OH)_3^-]$, $[HPO_4^{2-}]$, $[PO_4^{3-}]$ or $[NH_3]$, here defined as X, only have minor influence on TA. For a more detailed description of alkalinity in seawater the reader is referred to Wolf-Gladrow et al. (2007).

Various biogeochemical processes affect DIC as well as TA (Fig. 3). Invasion or release of CO_2 into seawater changes DIC, while TA remains constant. The production of organic matter decreases DIC due to photosynthetic CO_2 fixation. The concomitant increase in TA is caused by NO_3^- uptake, which is compensated by H^+ or OH^- exchange of the cell to keep electroneutrality (C:N ratio according to Redfield was assumed). Remineralization changes DIC and TA in the opposite direction. The precipitation of $CaCO_3$ reduces DIC by 1 and TA by 2 units, thereby increasing CO_2 levels and decreasing pH. Dissolution of $CaCO_3$ has the reverse effect.

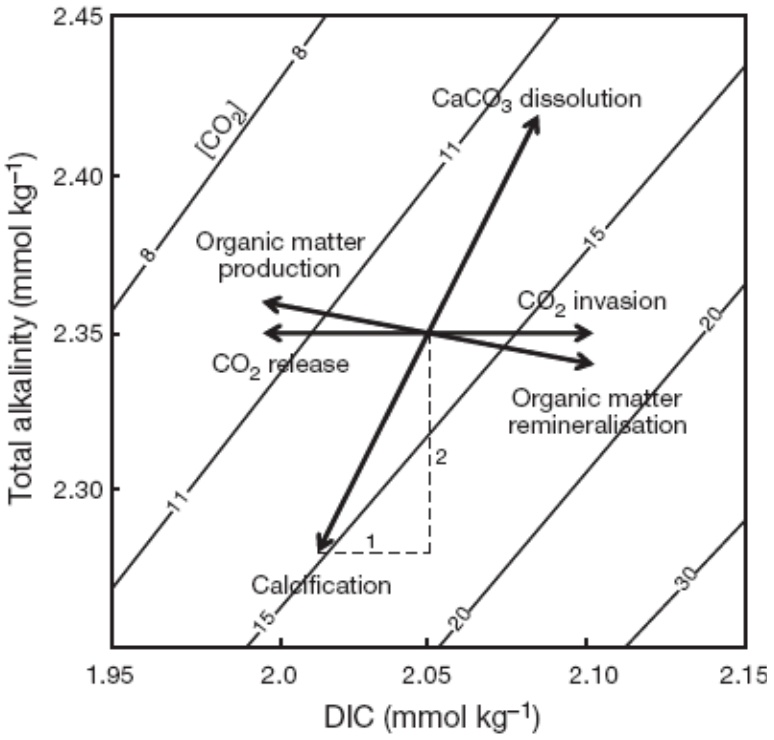

Figure 3: Effect of various processes (arrows) on dissolved inorganic carbon (DIC) and total alkalinity (TA). Lines indicate levels of constant dissolved CO_2 (in µmol kg^{-1}) as a function of DIC and TA. See text for details (modified after Zeebe and Wolf-Gladrow, 2007).

2.3 The marine nitrogen cycle

The flow of nitrogen compounds between the oceans and the atmosphere is central to life, as nitrogen is a fundamental component of biomass. In most of the oceans' surfaces, bio-available nitrogen sources like ammonia (NH_4^+), nitrate (NO_3^-) and nitrite (NO_2^-) are scarce (Capone, 2000) and therefore often restrict primary production. Only a few phytoplankton species like some marine bacteria and cyanobacteria are able to make use of the abundant N_2 for growth and biomass buildup. As a product of N_2 fixation processes, cells often release NH_4^+ (Mulholland et al., 2004), which subsequently can be oxidized by nitifying bacteria to NO_2^- and NO_3^- (Fig. 4) at the oceans' surface. As these dissolved inorganic nitrogen sources are used by phytoplankton species to build particulate organic nitrogen (PON), most of it will sooner or later sink and become remineralized. After ammonification, NH_4^+ can be oxidized to NO_2^- and subsequently to

NO_3^-. When upwelled, these nitrogen sources, become available for phytoplankton biomass production (Gruber and Sarmiento, 1997).

In so-called oxygen minimum zones of the ocean, the process of denitrification reduces NO_3^- to NO_2^-, nitric oxide (NO), nitrous oxide (N_2O) and subsequently to N_2. The anammox reaction, a recently discovered process, directly converts NH_4^+ and NO_2^- to N_2 (Devol, 2003; Kuypers et al., 2005). The gaseous products of both processes (NO, N_2O, N_2) can be lost from the oceanic system via exchange with the atmosphere (Gruber and Sarmiento, 1997; Devol, 2003).

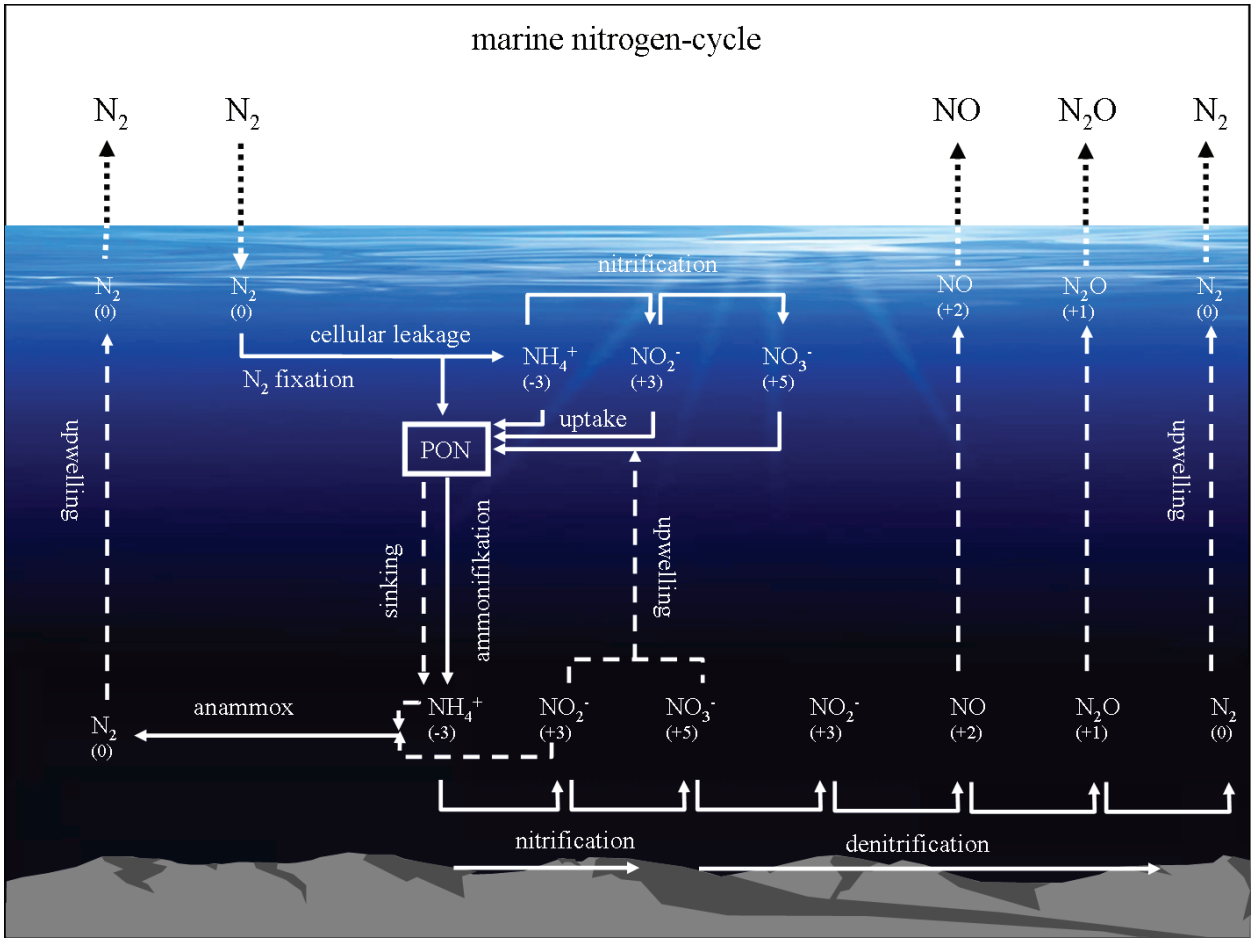

Figure 4: Schematic representation of the marine N cycle showing the major N fluxes. Atmospheric deposition and riverine input of NH_4^+, NO_3^- and dissolved organic nitrogen is not shown here. Solid lines indicate processes that involve biology. Dotted lines indicate mass redistribution by physical-chemical processes such as gas exchange or water mass movements. Numbers in parentheses refer to the valence of N in each molecule or ion. Abbreviation: PON – particulate organic nitrogen.

Nitrogen fixation and denitrification/anammox are generally assumed to dominate the flow of nitrogen into and out of the ocean, respectively (Capone, 2001; Gruber, 2005; Capone and Knapp, 2007). Human activity, however, affects the nitrogen cycle via the use of fertilizers or increasing atmospheric N deposition, causing eutrophication of costal areas and the open ocean (Codispoti et al., 2001; Doney et al., 2007). Model calculations on N_2 fixation and denitrification suggest a depletion of nitrogen in the contemporary oceans (Codispoti et al., 2001). Although

this apparent N loss is not yet supported by geochemical evidence (Karl et al., 2002), it may reflect an underestimation of important processes like N_2 fixation. The latter process has been proposed to be a key in several interactions and feedbacks between the ocean and atmospheric CO_2 (Falkowski, 1997).

2.4 Cyanobacteria and *Trichodesmium*

Within the phylogenetic tree of life, cyanobacteria are classified in the domain of bacteria. These organisms are found in Antarctic melt water ponds as well as in hot springs, hyper-saline lakes and arid areas such as the dry valleys in Antarctica as well as the Atacama Desert and thus are nearly ubiquitous in all ecosystems (Rai et al., 2000). Cyanobacteria are also associated with fungi in a symbiosis called lichens, or with eukaryotes and higher plants. As an ancestor of eukaryotic photoautotrophs, this phylum is of significant interest in the endosymbiotic theory which describes the origin of specialized organelles inside eukaryotes (Mereschkowsky, 1905; Margulis, 1971, 1996).

Marine cyanobacteria like the species *Synechococcus* and *Prochlorococcus* present two of the most abundant organisms on Earth, yet they were only discovered around 30 years ago (Johnson and Sieburth, 1979; Waterbury et al., 1979). Despite being less than 1 µm in size, they contribute essentially to marine carbon cycling as well as the food web (Paerl and Bebout, 1992; Waterbury, 2005). As one of the most important diazotrophs, *Trichodesmium* is a key player in the marine nitrogen cycle. The N_2 annually fixed by this species is calculated to range between 60 and 110 Tg (Capone et al., 1997; Gruber and Sarmiento, 1997; Mahaffey et al., 2005), which is proposed to support up to 50% of the primary production in the tropical and subtropical oceans (Paerl and Bebout, 1992; Capone et al., 1997). The ecology and physiology of this important diazotroph is described in the following.

2.4.1 Ecology of *Trichodesmium*

Trichodesmium was first described by Ehrenberg in 1830, classifying this genus within the order of oscillatoriales (Ehrenberg, 1830). Today, five different *Trichodesmium* species have been differentiated. Morphologically, *Trichodesmium spp.* cells range between 5 and 20 µm in diameter, forming filaments that consist of up to 340 single cells. These trichoms are found in the ocean as single filaments or as aggregates (Fig 5 A, B). Aggregates occur as puffs, spherically arranged filaments, and tufts, elongated rafts (Paerl and Bebout, 1988; Paerl, 1994).

As a photoautotroph, *Trichodesmium spp.* thrives in the oceans upper layer down to 100 m with maximal abundance at 20-40 m depth (La Roche and Breitbarth, 2005 and references therein). Its distribution is restricted to warmer waters in between the 20°C isotherm (Fig. 5 D).

Notably, highly-stratified oligotrophic waters favor its growth and occurrence (Capone et al., 1997). Under optimal conditions, blooms can cover up to 10^6 km^2 of the ocean surface (i.e. Fig. 5 C; Capone et al, 1998). With cell densities of up to 5.7 x 10^9 cells L^{-1} (Suvapepun, 1992), such blooms strongly influnece primary production and ecosystem structure. Besides, mass development of *Trichodesmium* can have detrimental effects on higher trophic levels as some strains produce toxins causing massive mortality of zooplankton and fish (Sato et al., 1966; Hawser et al., 1992) or human respiratory diseases ("Trichodesmium fever").

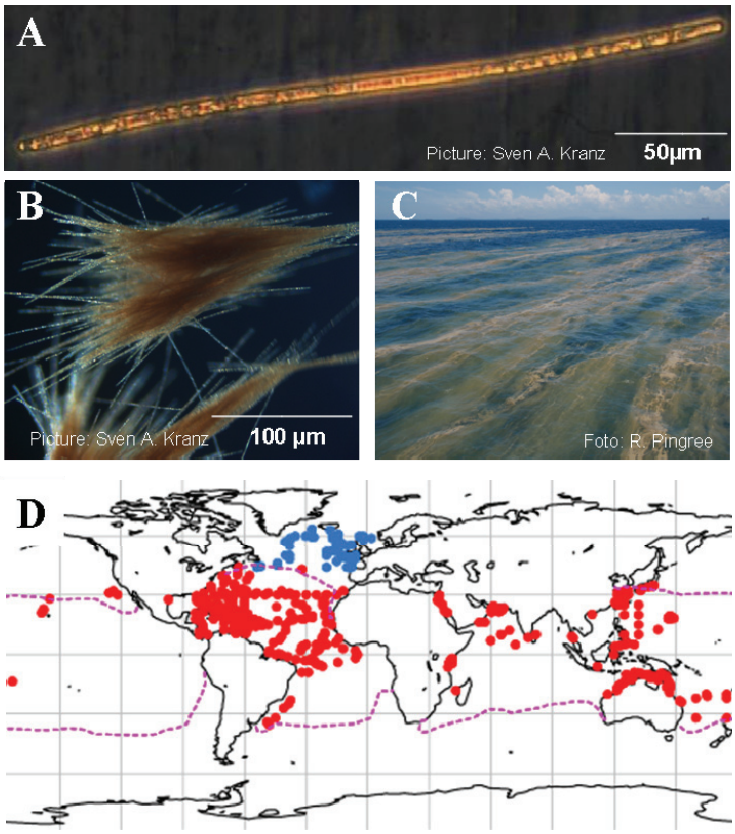

Figure 5: Morphology and distribution of *Trichodesmium*. A) Single filament of *Trichodesmium erythraeum* IMS101, consisting of ~40 cells. B) Filaments of *Trichodesmium erythraeum* IMS101 aggregated as a tuft. One aggregate can contain several hundreds of filaments. C) Typical appearance of *Trichodesmium* during late bloom situation, also called sea sawdust (Great Barrier Reef; Heron Island. D) Global distribution of *Trichodesmium* based on field studies (La Roche and Breitbarth, 2005). The pink line represents the 20°C isotherm, red dots indicate physiologically active cells, blue dots inactive inactive cells. The distribution is likely to be much larger than indicated by these observations.

Although relatively slow-growing, *Trichodesmium* is a highly competitive genus due to a number of adaptations to oligotrophic waters. Next to to the ability to fix N_2, inorganic nitrogen and other nutrients can be obtained from deeper layers as *Trichodesmium* can vertically migrate by regulating its buoyancy (Villareal and Carpenter, 1990). Moreover, organic nutrients like phosphonates can be taken up (Dyhrman et al., 2006). High irradiances can be tolerated by effective photochemical quenching mechanisms (Subramaniam et al., 1999). Regarding predation, the ability to form aggregates may effectively reduce grazing pressure (La Roche and Breitbarth, 2005).

Recent studies on *Trichodesmium* observed strong responses in growth, POC production and N_2 fixation under elevated pCO_2 (Barcelos é Ramos et al., 2007; Hutchins et al., 2007; Levitan et al., 2007). The underlying processes responsible for the CO_2-sensitivity in this genus are currently unknown. In the following, physiological key processes are outlined.

2.4.2 PHYSIOLOGY OF *TRICHODESMIUM*

In contrast to eukaryotic photosynthetic organisms, cyanobacteria lack organelles (like chloroplasts or mitochondria) and thus have to operate all metabolic pathways in one compartment. In fact, some biochemical pathways even share the same protein complexes. To avoid futile cycling and disadvantageous feedbacks, most pathways are therefore tightly regulated (Fig. 6).

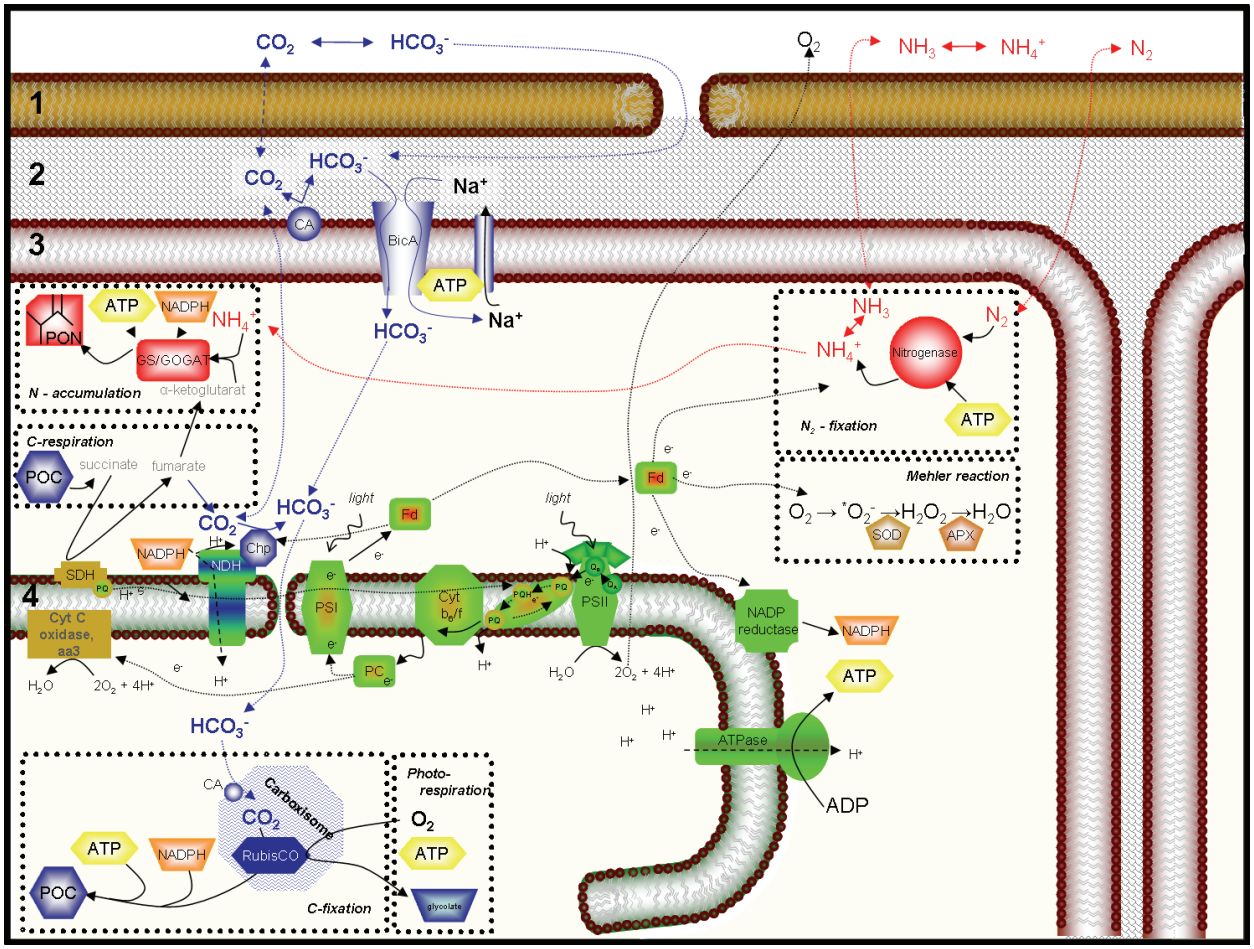

Figure 6: Schematic representation of major cellular complexes involved in energy flow (electron, ATP, NADPH+H^+, N_2 fixation, carbon acquisition, carbon fixation, carbon respiration, Mehler reaction) in *Trichodesmium*. Photosynthetic complexes are green, respiratory complexes are marked in brown, N_2 fixation and assimilation is marked in red and complexes involved in carbon acquisition and fixation are blue. The shared metabolic components are indicated by a mix of the respective colors. Dotted lines represent diffusive fluxes, solid lines represent fluxes where protein or enzymes are involved. (1) illustrates the outer membrane (2) illustrates periplasmatic space, consisting of a glycolipid layer (3) the plasma membrane and (4) the thylacoid membrane. Thylakoids are invaginations of the plasma membrane. Abbreviations: ADP – adenosine-5'-diphosphate; APX – ascorbate-peroxidase; ATP – adenosine-5'-triphosphate; ATPase – adenosine-5'-triphosphat synthase; BicA – BicA (HCO_3^--transporter); CA – carbonic anhydrase; Cyt b_6/f – cytochrome b_6/f protein complex; Cyt C oxidase aa3 – cytochrome C oxidase; e^- – electron; Fd – ferredoxin; GS/GOGAT – glutaminsynthase/glutamine-2-oxoglutarate-amidotransferase; H^+ – Proton; NADPH – nicotinamide-adenine-dinucleotide-phosphate; NDH – NADPH dehydrogenase; PC – plastocyanin; PQ – plastoquinone; POC – particulate organic carbon; PON – particulate organic nitrogen; PSI – photosystem 1; PSII – photosystem 2; PQ – plastocyanin; Q_A – Quinone A; Q_B – Quinone B; RubisCO – Ribulose-1,5-bisphosphat-carboxylase/-oxygenase; SDH – succinate-dehydrogenase; SOD – superoxide-dismutase.

2.4.2.1 Photosynthesis

The photosynthetic apparatus in photoauthotrophs consists of two photosystems (PSI and PSII). These photosystems are located in the thylakoid membrane, which is an invagination of the plasma membrane (Fig. 6). Light energy absorbed by chlorophyll and phycobilins in the light harvesting complexes (LHC) is transferred to specific chlorophylls of the reaction centre, causing the excitation of electrons. The PSII associated electrons of the reaction centre are donated to the electron acceptors of the photosynthetic electron transport chain (ETC). The "missing" electrons in the chlorophyll are replaced by the oxidation of a water molecule via the oxygen evolving complex.

In the ETC, electrons are further transported via the electron acceptors Q_A, Q_B, the plastoquinone-pool (PQ-pool) and the cytochrome b_6/f complex towards a mobile electron carrier, the plastocyanin (PC). The reduced PC can either donate the electron towards a cytochrome C oxidase, where O_2 is reduced to H_2O, or it is transferred to oxidized PSI. The latter is formed by light excitation of electrons and their subsequent transfer to ferredoxin (Fd). In the linear electron transport, Fd then binds to NADP reductase, forming the reductant $NADPH+H^+$. The described electron transfer drives a translocation of protons (H^+) through the membrane. Together with H^+ obtained from the water splitting process at PSII, a proton gradient across the thylakoid membrane is established. This gradient is used for the production of biochemical energy in form of adenosine-triphosphate (ATP) by the ATP synthase in the thylakoid membrane.

One important difference between cyanobacteria and eukaryotic photoautrophs is the PSI:PSII ratio. Cyanobacteria have high and variable ratios (Myers et al., 1980; Papageorgiou, 1996), so that in comparison with plants, PS II accounts for relatively little of the cellular chlorophyll. A high ratio favors the cyclic electron flow around PSI in which electrons cycle from PSI/Fd through the PQ-pool and the cytochrome b_6/f complex back to PSI. This cycling of electrons contributes to the proton gradient, increasing the ATP synthesis but does not lead to $NADPH+H^+$ production (Vermaas, 2001). Another reason for the relatively large amount of PSI in cyanobacteria is the reduction of the ETC by electrons originating from respiration. Specifically, the thylakoid-bound succinate dehydrogenase (SDH) of the tricarboxylic acid cycle introduces electrons into the PQ-pool (Schmetterer, 1994; Vermaas, 2001). In the dark, these electrons are donated to the thylakoid-bound cytochrome C oxidase (Schmetterer, 1994). In the light, however, the high abundance of PSI guarantees an oxidized PQ-pool which is important to minimize photodamage. Moreover, high PSI:PSII ratio may also serve to compete effectively

with the cytochrome C oxidase for electrons, thus maximizing the number of electrons that can be used for NADP reduction and reductive pathways like CO_2 and N_2 fixation.

In *Trichodesmium*, a distinct diurnal regulation of both, photosynthesis as well as respiration is known. This pattern involves a decline in O_2 production caused by a reversible down-regulation of PSII activity (Berman-Frank et al., 2001; Küpper et al., 2004). In terms of respiration, high rates were observed at the beginning of the photoperiod, which decline towards midday and evening (Berman-Frank et al., 2001). The diurnal pattern in photosynthesis and respiration was modulated by light (Breitbarth et al., 2008) and correlated with N_2 fixation activity (Berman-Frank et al., 2001).

2.4.2.2 Carbon acquisition

Most of the reductive power and biochemical energy generated in the light reactions of photosynthesis are allocated for uptake of inorganic carbon and its subsequent reduction into organic compounds (Falkowski and Raven, 2007). The rate of CO_2 fixation largely depends on the carboxylation efficiency of Ribulose-1,5-bisphosphate carboxylase/oxygenase (RubisCO). This ancient and highly conserved enzyme, which evolved at times of high CO_2 and low O_2 levels (Falkowski and Raven, 2007), is generally characterized by low affinities to CO_2, slow maximum turnover rates, as well as susceptibility to a competing and wasteful reaction with O_2 (photorespiration). As cyanobacterial RubisCO possesses one of the lowest CO_2 affinities among phytoplankton (K_M 105-185 μmol L^{-1} CO_2; Badger et al. 1998), a considerable amount of resources has to be invested to circumvent this bottleneck in photosynthesis. To achieve sufficient rates of C fixation, cyanobacteria as well as other phytoplankton groups operate so-called CO_2 concentrating mechanisms (CCMs) which enhance the CO_2 levels in the close proximity of RubisCO, thereby increasing the carboxylation reaction.

Cyanobacterial CCMs comprise several functional elements. In so-called carboxysomes, RubisCO is condensed and closely associated with carbonic anhydrase (CA). The latter enzyme accelerates the otherwise slow interconversion between CO_2 and HCO_3^-. Next to this structural characteristic for cyanobacteria, CCMs involve the active uptake and accumulation of CO_2 and/or HCO_3^- (Giordano et al., 2005). There are large species-specific differences but also within a single species, the CCM has been shown to vary depending on environmental conditions, for instance, changes in CO_2 supply (Ogawa and Kaplan, 2003; Giordano et al., 2005). For *Trichodesmium* IMS101, genomic analysis identified constituents of a beta type carboxysome as well as a Na^+-dependent HCO_3^- transporter (BicA) and the CO_2 transport system $NDH1_4$, which is located at the thylakoid membrane (Fig. 6). Genes encoding for external CA were not identified (Giordano et al., 2005).

The ability to take up HCO_3^- is advantageous since concentrations of HCO_3^- are an order of magnitude higher than concentrations of CO_2. Especially in cyanobacteria, HCO_3^- transport allows for high accumulation of inorganic carbon within the cell to compensate for the poor substrate affinities of RubisCO (Badger et al., 1998; Price et al., 2004). Uptake of CO_2, on the other hand, may be less costly than the ionic form HCO_3^- but its accumulation bears the risk of high CO_2 efflux (Price and Badger, 1989). Thus, CO_2 molecules entering the cell have to be converted to HCO_3^-, for which membranes are less permeable. This conversion is accomplished by a protein complex at the thylakoid membrane (NDH) and the reaction is thought to be catalyzed by electrons or $NADPH+H^+$ (Price and Badger, 1989; Friedrich and Scheide, 2000).

The characteristics of the CCM will partly determine whether and how *Trichodesmium* will respond to environmental changes like ocean acidification. The CCM of *Trichodesmium* has not yet been characterized, neither its regulation in response to changes in CO_2 supply. This information is urgently required as it may provide an explanation for responses of *Trichodesmium* to elevated CO_2.

2.4.2.3 N_2 FIXATION

As a diazotroph, *Trichodesmium* mainly fuels its N demand by N_2 fixation (Mulholland et al., 2004). The reduction of N_2 by the enzyme nitrogenase, which evolved under O_2-free conditions in the Archean (Falkowski, 1997; Falkowski and Raven, 2007), is highly energy-demanding and sensitive to O_2. Thus, photosynthetic energy generation and N_2 fixation within the same cell appear to be mutually exclusive processes (Falkowski, 1997). To circumvent this inhibitory effect, diazotrophs evolved biochemical as well as morphological adaptations to separate photosynthetic O_2 evolution and N_2 fixation in time and space. In this respect, *Trichodesmium* differs from other diazotrophs as it lacks the clear spatial (i.e. heterocysts) and temporal separation (day vs. night activity) of both processes. In *Trichodesmium*, nitrogenase is localized in subsets of neighboring cells, so-called diazocytes, which also contain photosynthetic components and comprise about 15 to 20 % cells within a trichome (Durner et al., 1996; Berman-Frank et al., 2003). To protect the nitrogenase from photosynthetic O_2 evolution, *Trichodesmium* has developed a distinct diurnal rhythm in photosynthesis and N_2 fixation (Lin et al., 1999; Berman-Frank et al., 2001). Also O_2-reducing mechanisms, like the Mehler reaction, have been proposed (Berman-Frank et al., 2001; Küpper et al., 2004). In the latter, electrons from the ETC are transferred to an O_2 molecule, forming superoxide radicals, which are disproportionate by superoxide dismutase to H_2O_2 and O_2. The H_2O_2 is rapidly detoxified to H_2O by the ascorbate peroxidase pathways.

Regarding energy requirements for N_2 fixation, the splitting of the triple-bond of N_2 to form NH_3 requires at least 16 ATP as well as 8 electrons (Kana, 1993; Milligan et al., 2007). ATP is proposed to be mainly supplied through linear, but also cyclic electron transport, while electrons are donated by reduced Fd. Since there is competition between N_2 fixation and C assimilation for energy and reductants, a concerted regulation of these processes is essential to survive, especially under oligotrophic conditions. To fully understand responses to environmental changes one therefore has to look at the interplay rather than the processes in isolation.

2.5 Outline of the thesis

This thesis investigates the response of the diazotroph *Trichodesmium* IMS101 to different environmental conditions with emphasis on ocean acidification. In dilute batch cultures, the effect of CO_2 concentration and light regime on growth, elemental composition and production rates is investigated. In addition to describe these responses, the study aim to understand the underlying metabolic processes, such as photosynthesis, carbon acquisition and N_2 fixation. Next to the influence of pCO_2 on ecophysiology of *Trichodesmium*, the effect of a bloom situation on carbonate chemistry is described. The findings of the different experiments will be used to make prediction about the fate of this important cyanobacterium.

Publication I compares the two most common approaches to quantify different aspects of carbon acquisition and tests their key assumption and reliability. The methods are applied on a range of different phytoplankton species from different taxa including *Trichodesmium*.

Publication II investigates the ecophysiological responses of *Trichodesmium* to different pCO_2 levels (150, 370 and 1000 µatm). To explain the observed CO_2-sensitivity in biomass production, the CCM and its regulation by CO_2 and diurnal changes are described.

Publication III examines the combined effect of light and CO_2 on *Trichodesmium*. To understand the strong CO_2-dependent ecophysiological responses and their modulation by light, gross photosynthesis, carbon acquisition, N_2 fixation and Mehler reaction are investigated in detail. Implications for biogeochemical cycles are discussed.

Publication IV describes the effect of a *Trichodesmium* bloom on carbonate chemistry under different availability of inorganic phosphorus. To explain the observed aragonite precipitation under P-depletion, changes in bulk carbonate chemistry are measured and additionally modeled for the diffusive boundary layer of *Trichodesmium* aggregates.

In a concluding discussion, main results of this study are summarized and evaluated in the context of physiology, ecology and biogeochemistry. At the end, perspectives are given for future research.

Publications

3 Publications

3.1 List of publications

This doctoral thesis is based on following publications and manuscripts:

Publication I: Rost B, Kranz SA, Richter K-U, Tortell PD (2007) Isotope disequilibrium and mass spectrometric studies of inorganic carbon acquisition by phytoplankton. Limnology and Oceanography: Methods 5: 328-337.

Publication II: Kranz SA, Sültemeyer D, Richter K-U, Rost B (2009) Carbon acquisition by *Trichodesmium*: the effect of pCO_2 and diurnal changes. Limnology and Oceanography 54: 548-559.

Publication III: Kranz SA, Levitan O, Prášil O, Richter K-U, Berman-Frank I, Rost B; Combined effects of CO_2 and light on the N_2 fixing cyanobacteria *Trichodesmium* IMS101: Physiological responses (submitted to Plant Physiology).

Publication IV: Kranz SA, Wolf-Gladrow D, Nehrke, G., Langer G, Rost B; Calcium carbonate precipitation induced by the growth of the marine cyanobacterium *Trichodesmium*
(submitted to Limnology and Oceanography)

Appendix I: Levitan O, Kranz SA, Spungin D, Prášil O, Rost B, Berman-Frank I; Combined effects of CO_2 and light on the N_2 fixing cyanobacteria *Trichodesmium* IMS101: A mechanistic view (submitted to Plant Physiology).

Appendix II: Ralph P, Wilhelm C, Lavaud J, Torsten J, Petrou K, Kranz SA; Fluorescence as an assay to understand aspects of the physiology of light regulation. In Advances in applied phycology (Book Series). Chapter 12. (Eds. D. Suggett & O. Prasil) (submitted Book chapter).

3.2 Declaration on the contribution of each publication

Publication I: Die Laborexperimente wurden in Zusammenarbeit mit Björn Rost geplant und durchgeführt. Ich habe einen maßgeblichen Anteil der Daten erhoben und ausgewertet. Das Manuskript wurde in Zusammenarbeit mit den Koautoren verfasst.

Publication II: Die Laborexperimente wurden von mir geplant und durchgeführt. Ich habe die Daten ausgewertet und das Manuskript in Zusammenarbeit mit den Koautoren verfasst.

Publication III: Die Laborexperimente wurden von mir geplant und durchgeführt. Ich habe die Daten ausgewertet und das Manuskript in Zusammenarbeit mit den Koautoren verfasst.

Publication IV: Die Laborexperimente wurden von mir geplant und durchgeführt. Ich habe die Daten ausgewertet und das Manuskript in Zusammenarbeit mit den Koautoren verfasst.

Publication I

LIMNOLOGY
and
OCEANOGRAPHY: METHODS

Limnol. Oceanogr.: Methods 5, 2007, 328–337
© 2007, by the American Society of Limnology and Oceanography, Inc.

Isotope disequilibrium and mass spectrometric studies of inorganic carbon acquisition by phytoplankton

Björn Rost[1], Sven A. Kranz[1], Klaus-Uwe Richter[1], and Philippe D. Tortell[2]*
[1]Alfred Wegener Institute for Polar and Marine Research, Am Handelshafen 12, 27570, Bremerhaven, Germany
[2]Department of Earth and Ocean Sciences, and Department of Botany, University of British Columbia, 6270 University Boulevard, Vancouver, British Columbia V6T 1Z4, Canada

Abstract

Given the need to assess potential effects of rising atmospheric CO_2 on aquatic primary productivity, many studies have investigated the physiological mechanisms of inorganic carbon acquisition by a variety of phytoplankton species. Membrane inlet mass spectrometry (MIMS) has become the preferred methodological approach for laboratory experiments, whereas the ^{14}C disequilibrium method has proven to be particularly useful for field studies. In the present investigation, we explicitly compare results of carbon acquisition measurements obtained with both of these approaches. Testing a range of phytoplankton species from different taxa, we show that both methods provide nearly identical results on the contribution of HCO_3^- and CO_2 relative to net carbon fixation. In contrast, although both approaches yielded highly reproducible estimates for extracellular carbonic anhydrase activity, the results differed significantly between the two methods. By directly comparing these two leading methods, we provide experimental confirmation of key assumptions used for data interpretation and discuss possible effects of assay conditions. Our analysis highlights the individual strengths and weaknesses of different approaches.

Over the past two decades, significant progress has been made toward understanding the physiological mechanisms of inorganic carbon (C_i) acquisition in marine and freshwater phytoplankton. This research recently has gained increased attention given the need to understand the potential effects of rising atmospheric CO_2 on marine primary production. While early studies suggested that phytoplankton could be growth-limited by the CO_2 supply in the ocean (e.g., Riebesell et al. 1993), subsequent laboratory and fieldwork has documented the existence of carbon concentrating mechanisms (CCM) in many phytoplankton species (Giordano et al. 2005 and references therein). The CCM – which functions to saturate C fixation by RubisCO – involves the active transport of CO_2 and/or HCO_3^-, as well as various isoforms of the enzyme carbonic anhydrase (CA) that catalyze the interconversion between these C_i species. The extent to which various taxa possess CCMs, and the relative efficiency of these C_i uptake mechanisms remain poorly understood. This information is needed to understand the effects of changing CO_2 levels on marine primary productivity and phytoplankton ecology (Giordano et al. 2005), and for the interpretation of ^{13}C signatures in marine organic matter (Laws et al. 2001 and references therein).

A variety of methods have been developed to examine C_i use by phytoplankton. Early work focused on kinetic approaches aimed at characterizing C_i affinities of cells and the O_2/CO_2 sensitivity of C_i fixation, providing evidence for the existence of C_4-like photosynthetic properties in phytoplankton (Graham and Whittingham 1968; Berry et al. 1976). Subsequent studies using silicone oil centrifugation methods (Badger et al. 1977, 1980; Kaplan et al. 1980) demonstrated that cells had the capacity to transport HCO_3^- and concentrate large intracellular C_i pools, whereas the activity of both intracellular and periplasmic carbonic anhydrase became apparent in a wide variety of phytoplankton taxa (Reed and Graham 1981; Aizawa and Miyachi 1986; Sültemeyer et al. 1993). More recently, the use of MIMS to study cellular CO_2 and O_2 fluxes has provided a new level of insight into C_i uptake by phytoplankton (Badger et al. 1994; Sültemeyer et al. 1995). In principle, MIMS can be used to measure intracellular C_i pool sizes,

*Alfred Wegener Institute for Polar and Marine Research, Am Handelshafen 12, 27515, Bremerhaven, Germany, Bjoern.Rost@awi.de

Acknowledgments

We thank Dieter Wolf-Gladrow, Lubos Polerecky, and two anonymous reviewers for constructive comments on the manuscript. This work is part of the multidisciplinary project BOOM (Biodiversity of Open Ocean Microcalcifiers), funded by the Institute Francais de la Biodiversité via the Agence National de la Recherche, grant ANR-05-BDIV-004. Funding for PDT was provided by the Natural Sciences and Engineering Council of Canada.

the kinetic properties of CO_2 and HCO_3^- transport, and the activities of intracellular and extracellular CA. This approach has proven extremely useful for integrated C_i uptake studies in phytoplankton, and, recently, has been successfully applied to a number of environmentally relevant marine species grown in laboratory cultures (Giordano et al. 2005). Although the MIMS is increasingly used in field studies (e.g., Tortell 2005; Tortell et al. 2006), the high cost and technical requirements for instrumentation remain a limitation. Moreover, MIMS analysis is not ideally suited for natural phytoplankton assemblages given the small net CO_2 and O_2 fluxes associated with many mixed autotrophic and heterotrophic communities.

Oceanographic field studies of C_i uptake by phytoplankton have thus far lagged behind laboratory work, and there have been relatively few published reports documenting the physiological mechanisms of C_i use by natural marine phytoplankton assemblages (Tortell et al. 2000; Tortell and Morel 2002; Cassar et al. 2004; Martin and Tortell 2006; Tortell et al. 2006). These studies have confirmed the existence of CCMs in situ, and demonstrated that HCO_3^- is a major source of inorganic C for photosynthesis in several ocean regions. For the most part, these field studies have relied on sensitive ^{14}C-based methods to estimate C_i uptake rates and the relative importance of extracellular CA activity. In particular, the isotope disequilibrium method (Espie and Coleman 1986; Elzenga et al. 2000) has proven to be useful for open ocean field work (Tortell and Morel 2002, Martin and Tortell 2006), and it is likely that this technique will be applied widely in future field studies of marine and freshwater phytoplankton assemblages.

As we progress in our understanding of C_i uptake by phytoplankton, it will become increasingly important to compare the results of laboratory and field experiments. This task is complicated by the different methods and protocols employed by various investigators. In most cases, independent methods are used to measure the same physiological parameters, yet the agreement between methods has not been explicitly examined. Moreover, each method has its own inherent assumptions that often are difficult to assess directly. A comparison of methods, therefore, is highly desirable. In this article, we present a comparison of two leading methods for C_i uptake measurements in phytoplankton. Using a range of phytoplankton taxa, we show that the isotope disequilibrium and MIMS methods provide very similar estimates of CO_2:HCO_3^- uptake ratios. In contrast, significant discrepancies exist in the estimates of extracellular CA activities. We discuss the individual strengths and weaknesses of the different approaches, and provide experimental confirmation of the key assumptions used for their interpretation.

Materials and procedures

Cultures conditions and sampling—For our method comparison, we chose to work with a variety of phytoplankton species (*Trichodesmium erythraeum* [IMS101], *Heterocapsa triquetra* [K-0481], *Emiliania huxleyi* [PML B92/11, highly calcifying strain], *Phaeodactylum tricornutum* [CCAP 1052/1A], *Thalassionema nitzschioides*, and *Phaeocystis globosa*) representing a wide range of taxonomic groups (cyanobacteria, dinoflagellate, coccolithophore, and diatoms) and functional modes of inorganic carbon acquisition. Cells were grown at 15°C in 0.2-μm-filtered seawater (salinity 34) enriched with nutrients according to f/2 medium (Guillard & Ryther 1962), except for *T. erythraeum*, which was grown at 25°C in artificial media YBCII (Chen et al. 1996). Acclimations were performed in dilute batch cultures (< 40 μg L^{-1} Chlorophyll *a*) under incident light intensities of 150 μmol photons m^{-2} s^{-1} and a light-dark cycle of 16:8 h, or 12:12 h in the case of *T. erythraeum*.

Cultures generally were sparged with air containing pCO_2 of 370 μatm (37.5 Pa) for all species except *P. tricornutum* which was cultured with 1800 μatm (182.4 Pa) CO_2 to minimize HCO_3^- use. Cultures of *H. triquetra* were not aerated as dinoflagellates are known to be negatively affected by the turbulence resulting from air bubbling (P.J. Hansen, pers. comm.). For this species, medium pH was adjusted to 8.0 and culture bottles closed with no headspace. Cultures in which the pH has shifted significantly from the target value (pH drift > 0.08) were excluded from further analysis. For all species, cells were acclimated to the respective carbonate chemistry for at least 5 d.

Prior to the measurements, cells were concentrated by gentle filtration onto polycarbonate membranes (pore size 3, 5, or 8 μm). During the filtration, culture media was exchanged with the respective assay buffer in a stepwise fashion maintaining the cells in suspension. Unless stated otherwise, cells were harvested simultaneously from the same culture flask and then were used in parallel assays (^{14}C versus MIMS). Both approaches yield estimates of the fraction of HCO_3^- versus CO_2 taken up by cells as well as the activity of extracellular carbonic anhydrase.

^{14}C disequilibrium measurements—The ^{14}C disequilibrium technique was developed to examine steady-state $^{14}CO_2$ and $H^{14}CO_3^-$ uptake by phytoplankton following a transient isotopic disequilibrium induced by the addition of a neutral pH $^{14}C_i$ spike into an alkaline pH cell suspension. The theory and methodology of this technique has been described extensively in several recent articles (Elzenga et al. 2000; Tortell and Morell 2002; Martin and Tortell 2006). Briefly, the method is based on the slow interconversion between HCO_3^- and CO_2, which allows differential labeling of these carbon species with ^{14}C over time periods of several minutes. In the C_i spike solution (pH 7.0) $^{14}CO_2$ represents 20% of the total DIC pool. In contrast, CO_2 accounts for only 0.4% of the total DIC in the cell suspension (pH 8.5) once equilibrium is reached. As a result, the specific activity (dpm mol^{-1}) of CO_2 in the $^{14}C_i$ spike solution is initially high, and it decays exponentially to an equilibrium value over the duration of the assay. If a phytoplankton species takes up CO_2 only, the ^{14}C incorporation rate should reflect these changes in the specific activity, i.e., high initial rates which decrease to lower values at equilibrium. The specific activity of $H^{14}CO_3^-/^{14}CO_3^{2-}$ (hereafter referred to as HCO_3^-) in the injected $^{14}C_i$ spike is close to its equilibrium

value and therefore remains nearly constant during the experiment. Consequently, species which use predominantly HCO_3^- as the carbon source show a near constant ^{14}C incorporation rate, i.e., a virtually linear time course of incorporation.

In practice, it is the accumulation of ^{14}C, rather than the instantaneous uptake rate which is measured in time-course experiments. As a result, the uptake curves are best modeled in their integral form (modified from Elzenga et al. 2000):

$$DPM_t = V_t(1\text{-}f)\ (\alpha_1 t + (\Delta SA_{CO2}/SA_{DIC})\ (1 - e^{-\alpha 1 t}))/\alpha_1 + V_t(f)\ (\alpha_2 t + (\Delta SA_{HCO3}/SA_{DIC})\ (1 - e^{-\alpha 2 t}))/\alpha_2 \quad (1)$$

V_t is the total rate of C_i uptake; f is the fraction of uptake attributable to HCO_3^-; α_1 and α_2 are the temperature-, salinity-, and pH-dependent first order rate constants for CO_2 and HCO_3^- hydration and dehydration, respectively (calculated as described by Espie and Colman 1986 with temperature and salinity corrections derived from Johnson 1982). Under the experimental conditions used for most experiments (15°C, salinity 34, pH 8.5) α_1 and α_2 are 0.0272 and 0.032 s^{-1}, respectively. For experiments conducted at 25°C, the constants were calculated as 0.0801 and 0.0977 s^{-1}, respectively. ΔSA_{CO2} and ΔSA_{HCO3} are the differences between the initial and equilibrium values of the specific activity of CO_2 and HCO_3^-; and SA_{DIC} is the specific activity of all inorganic carbon species at equilibrium. During steady-state photosynthesis, V_t and f are assumed to be constant so that changes in the instantaneous ^{14}C uptake rate reflect only changes in the specific activity of the two C_i species. The values of $\Delta SA_{CO2}/SA_{DIC}$ and $\Delta SA_{HCO3}/SA_{DIC}$ are set by the difference in pH between the ^{14}C spike and seawater buffer, with the values of 49 and –0.19, respectively.

In this study, we largely followed the experimental protocol described by Rost et al. (2006) with a few modifications. Concentrated cell suspensions were transferred into a cuvette (4 mL volume) with the respective media buffered at pH 8.5 (BICINE-NaOH, 20 mmol L^{-1}). After pre-incubation to 300 µmol photons m^{-2} s^{-1} for 6 min, a 10 µCi ^{14}C spike (37 MBq) of pH 7.0 (Amersham, CFA3, in HEPES, 50 mmol L^{-1}) was injected into the cell suspension. Afterwards, subsamples of 200 µL were withdrawn at short intervals and dispensed into 1.5ml of HCl (6 N) to stop C fixation. To remove residual $^{14}C_i$ (i.e., which was not fixed into acid-stable, photosynthetic products), samples were purged with air for at least 3 h. Following this, 10 mL scintillation cocktail (Packard, Ultima Gold AB) was added to the vials and the ^{14}C was measured by standard liquid scintillation procedures. To correct for any residual inorganic ^{14}C not removed by the degassing procedure, blanks consisting of spike added to cell-free buffer were measured and subtracted from all samples.

We ran the isotope disequilibrium experiments in two ways to examine CO_2:HCO_3^- uptake ratios and the importance of extracellular carbonic anhydrase activity. In the standard approach, potential eCA activity was eliminated by the presence of dextran-bound sulfonamide (DBS; Synthelec AB), a membrane-impermeable inhibitor of extracellular carbonic anhydrase. The inhibitor was added to a final concentration of 50 µmol L^{-1} at least 10 min prior to the experiments. In a modified approach (i.e., control experiments), incubations were also run without DBS in order to assess potential eCA activity in cells. For quantitative interpretation, the ^{14}C disequilibrium data were fit according to Eq. 1, using a Marqand-Levenberg non-linear regression algorithm. In the DBS run, the rate constants α_1 and α_2, were taken as the uncatalyzed values (see above), and the fraction of HCO_3^- take up by cells, f, was estimated (Elzenga et al. 2000) from the curve fitting procedure. In the control experiment, eCA activity was estimated from the data fits by allowing the rate constant, α_1, to vary as a model parameter whereas f was constrained to the value obtained in the DBS-treated sample (Martin and Tortell 2006). Values of α_2 can be calculated directly from α_1. Consequently, the modeled increase in the rate of HCO_3^-/CO_2 equilibration (hereafter referred to as α') was used to assess eCA expression. Extracellular CA activity (CA^{14C}) was expressed as:

$$CA^{14C} = (\alpha' - \alpha)/\alpha \quad (2)$$

MIMS: C_i flux measurements—The mass spectrometric technique uses the chemical disequilibrium between CO_2 and HCO_3^- during light-dependent C_i uptake to differentiate between CO_2 and HCO_3^- fluxes across the plasmalemma. Estimates of these fluxes were made using the equations of Badger et al. (1994). Briefly, C_i flux estimations are based on simultaneous measurements of O_2 and CO_2 during consecutive light and dark intervals. During dark intervals, known amounts of C_i are added prior to the initiation of the subsequent light interval. Rates of O_2 consumption in the dark and O_2 production in the light are used as direct estimates of respiration and net C fixation, respectively. Net CO_2 uptake is calculated from the steady-state rate of CO_2 depletion at the end of the light period, corrected for the CO_2/HCO_3^- interconversion in the medium. The HCO_3^- uptake is derived by a mass balance equation, i.e., the difference between net C fixation and net CO_2 uptake. As for all disequilibrium approaches, a lack of eCA activity is required, as this enzyme acts to rapidly dissipate CO_2/HCO_3^- disequilibrium in the cell boundary layer. The pseudo-first-order rate constant k_2 (formation of CO_2 from HCO_3^-) is determined experimentally from the initial slope of CO_2 evolution after injection of known amounts of HCO_3^- into CO_2-free buffered medium. The rate constant k_1 (formation of HCO_3^- from CO_2) is calculated from the product of k_2 and the ratio of CO_2 and HCO_3^- concentrations. Badger et al. (1994) provides more background on the numerical analysis of the data.

All MIMS measurements were carried out in an 8 mL thermostated cuvette, which was attached to a sectorfield multicollector mass spectrometer (Isoprime; GV Instruments) via a gas-permeable membrane (PTFE, 0.01 mm) inlet system. Prior to C_i flux measurements, the MIMS was calibrated for O_2 and CO_2 concentrations. Calibration for O_2 was achieved by measuring an air-equilibrated and oxygen-free assay buffer sample. The MIMS CO_2 signals were calibrated by injection of known amounts of $NaHCO_3^-$ into HCl (0.2 mmol L^{-1}). The CO_2 base-

line was determined by addition of 20 µL NaOH (10 mmol L^{-1}) into C_i-free media. Whereas the consumption of CO_2 by the MIMS is negligible, measured changes in O_2 signals were corrected for the O_2 consumption of the system. The simultaneously recorded background signal of argon, which is not affected by biological activities, was used to correct for small signal fluctuations in the oxygen signal. Assays were performed in the respective media, buffered with HEPES (50 mmol L^{-1}, pH 8.0). Light/dark intervals lasted 6 min and the incident photon flux density was 300 µmol photons m^{-2} s^{-1}. Concentration of DBS was 50 µmol L^{-1} to ensure the complete inhibition of any eCA activity.

MIMS: CA activity measurements—CA activity was determined from the ^{18}O depletion of doubly labeled aqueous $^{13}C^{18}O_2$ caused by several hydration and dehydration steps of CO_2 and HCO_3^- (Silverman 1982). This mass spectrometric procedure allows the determination of CA activity from intact cells under conditions similar to those during growth, and also can differentiate between intracellular and extracellular CA (eCA) activity (Palmqvist et al. 1994). Changes in the ion beam intensities corresponding to concentrations of the CO_2 isotopomers $^{13}C^{18}O^{18}O$ (m/z = 49), $^{13}C^{18}O^{16}O$ (m/z = 47) and $^{13}C^{16}O^{16}O$ (m/z = 45) were recorded continuously. The ^{18}O enrichment was calculated as:

$$^{18}O \log (\text{enrichment}) = \log((^{13}C^{18}O_2) \times 100)/\Sigma^{13}CO_2) = \log ((49 \times 100)/(45 + 47 + 49)) \quad (3)$$

CA assays were performed in f/2 medium, buffered with HEPES (50 mmol L^{-1}, pH 8.0) and were carried out in the dark. $NaH^{13}C^{18}O_3$ was added to a final concentration of 1 mmol L^{-1} and the uncatalyzed rate of ^{18}O loss was recorded for at least 8 min. Subsequently, 50-150 µL of cell suspension were added to yield a final Chl *a* concentration of 0.05-1.0 µg mL^{-1}. For the calculation of eCA activity (CA^{18O}), the linear rate of decrease in ^{18}O atom fraction after the addition of the cell suspension (S_2) was compared to the non-catalyzed decline (S_1) and normalized on Chl *a* basis:

$$CA^{18O} = (S_2 - S_1)/(S_1 \times \mu g \text{ Chl } a) \quad (4)$$

Assessment and discussion

The aim of this investigation was to compare different approaches for estimating CO_2 and HCO_3^- uptake and eCA activity in phytoplankton. We purposefully chose a diverse group of species with a wide range of carbon acquisition mechanisms and unique cellular architectures. As anticipated, we observed a large range in physiological characteristics among the species tested. For the purposes of this study, we shall not discuss these differences as they have been or will be addressed in other studies (Rost et al. 2003, 2006, Kranz et al. in prep.). Before comparing ^{14}C disequilibrium and MIMS results, it is important to summarize main assumptions underlying the calculations.

Assumptions of calculation—The interpretation of ^{14}C incorporation time-courses depends critically upon knowing the rate at which ^{14}C species approach equilibrium and the ratio

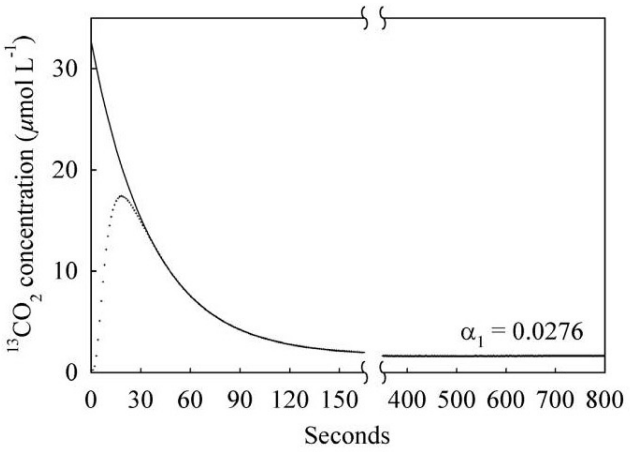

Fig. 1. Verification of theoretical rate constants from ^{14}C disequilibrium assay by MIMS measurements using ^{13}C as a tracer. At time zero, a $^{13}C_i$ spike (pH 7.0, HEPES, 50mM) was added into buffered media (pH 8.5, BICINE, 20mM) and the exponential decay of $^{13}CO_2$ into the HCO_3^- pool was monitored over time. Symbols represent measurements and the solid line represents a first order exponential decay fit to the data. The fit yielded a mean value for α_1 of 0.029 ± 0.004 s^{-1} (n = 6).

of CO_2 to HCO_3^- in the ^{14}C spike and seawater buffer. In previous studies, these values have been derived from thermodynamic and kinetic constants published in the literature (Johnson 1982; Espie and Colman 1986). Here we used the MIMS to check the values experimentally for our buffer solutions.

Central to the data analysis are the rate constants α_1 and α_2 that determine the time required for $^{14}CO_2$ / $H^{14}CO_3^-$ interconversion. In the absence of eCA activity, α_1 and α_2 are theoretically expected to be 0.0272 and 0.032 s^{-1}, respectively, under the experimental conditions used at 15°C. To verify these calculated values, the rate of C_i equilibration was measured under our assay conditions using ^{13}C as a tracer. For these tests, a $^{13}C_i$ spike solution (pH 7.0, HEPES, 50 mM) was added into buffered media (pH 8.5, BICINE, 20 mM) and the exponential decay of $^{13}CO_2$ into the HCO_3^- pool was monitored over time. In order to resolve the rate constants more precisely, the concentration of the C_i spike was twice as high as that used in the ^{14}C assay.

We found excellent agreement between theoretical and experimentally-derived rate constants. Figure 1 shows the time-course of $^{13}CO_2$ decay following the addition of the $^{13}C_i$ spike to the alkaline buffer at 15°C. The initial increase in signal intensity corresponds to the time required for homogeneous mixing and the response time of the sampling inlet and mass spectrometer. Beyond this initial rise, $^{13}CO_2$ concentrations subsequently decay exponentially as chemical equilibrium is approached. A first-order exponential decay fit to the data (ignoring the first ~ 30 seconds) yielded a rate constant (0.029 ± 0.004 s^{-1}; n = 6), which was practically identical to the theoretical calculations (0.0272 s^{-1}). It should be noted, how-

ever, that erroneous rate constants (resulting, for example, from small temperature shifts) cause a bias in *f* estimates. In species preferring CO_2 (*f* = 0.25), for instance, an overestimation in rate constants by about 10% would result in slightly higher estimates (*f* = 0.28) whereas estimates in HCO_3^- users (*f* = 0.75) are less sensitive to errors in the rate constants.

When the $^{13}CO_2$ decrease was extrapolated back to time zero, the predicted concentration added to the system was 33 μmol L^{-1}, a concentration that is very close to the theoretical value for a 20 μCi (74 MBq; SA ~ 55 mCi/mmol) spike into 4 mL assay media. Our calculations and experimental results (Fig. 1) indicate that $^{14}C_i$ additions greater than 10 μCi (37 MBq) under these conditions can introduce a significant perturbation in the carbonate system during the early part of the experiment, by elevating CO_2 levels. In contrast, the ^{14}C additions have only a minor (<5%) effect on total DIC concentrations in the seawater buffer.

In a second test, we used the MIMS to determine the relative proportions of CO_2 and HCO_3^- in our two experimental buffers (pH 7.0 and 8.5), as these ratios determine the initial and final conditions of the measurement. This was done by measuring the increase in CO_2 concentration upon additions of known amounts of C_i into the respective buffer. As with our determination of the rate constants, we also found excellent agreement between the expected and measured CO_2/DIC ratios. The measured values of 19.5% (± 1.5%; *n* = 4) in the pH 7.0 spike and 0.48% (± 0.11%; *n* = 6) in pH 8.5 media are not significantly different from those derived theoretically for use in our calculations (i.e., 19.5% and 0.4% CO_2 fraction, respectively). Thus, we are fully confident in the empirical constants used for our ^{14}C data analysis. Nevertheless, it should be noted that small changes in pH, both in the acidic spike and in the alkaline media, have large effects on the respective CO_2 fraction. The corresponding changes in ΔSA of the C_i species introduce an error in the *f* estimates derived from the model fit. In species preferring CO_2 (*f* = 0.25), for example, an overestimation of CO_2 fraction of the acidic spike by about 10% would cause the *f* estimate to be about 8% lower (*f* = 0.17) whereas *f* estimates in species preferring HCO_3^- are hardly affected.

The MIMS approach also relies on several key assumptions. The chemical disequilibrium between CO_2 and HCO_3^- during light-dependent C_i uptake is used to differentiate between CO_2 and HCO_3^- fluxes. O_2 fluxes are subsequently converted into carbon by applying a respiratory quotient (RQ) and photosynthetic quotient (PQ). Since the HCO_3^- uptake is derived from a mass balance between net CO_2 uptake and C_i fixation, the PQ directly affects the HCO_3^- uptake estimates. As in previous studies (e.g., Sültemeyer et al. 1995; Amoroso et al. 1998; Burkhardt et al. 2001), we applied values of 1.0 and 1.1 for the RQ and PQ, respectively. Underestimating the PQ would cause an overestimation of net C_i fixation and hence HCO_3^- contribution, whereas an overestimation in PQ would yield erroneously low HCO_3^- uptake.

The process of calcification (i.e., calcium carbonate production by cells like *E. huxleyi*) presents a further complicating factor for MIMS analysis. This process potentially affects the estimation of HCO_3^-/CO_2 uptake as an additional cellular C_i sink that is not accounted for in the calculations of Badger et al. (1994). However, since the HCO_3^- uptake is calculated from O_2-derived C_i uptake (i.e., photosynthetic C_i fixation) the influence of calcification on the calculations will only be small. The good agreement with HCO_3^-/CO_2 uptake estimates based on the ^{14}C method (see below), which is not affected by the photosynthetic quotient or the process of calcification, suggests that assumptions and calculations of the MIMS approach are robust.

Estimates for CO_2 and HCO_3^- uptake—Examples of ^{14}C incorporation time-courses by *P. tricornutum* and *T. nitzschioides* are given in Fig. 2. For *P. tricornutum*, identical time-courses were

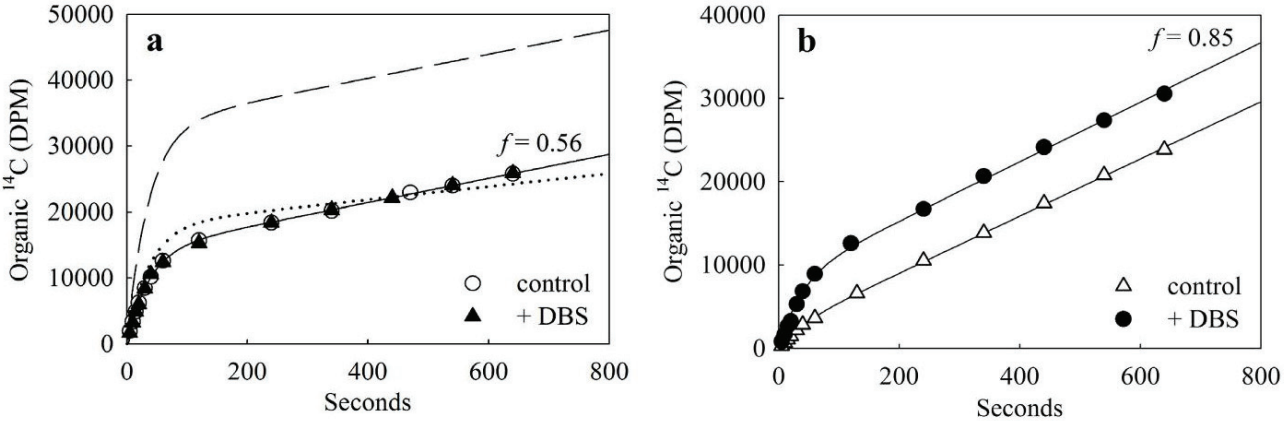

Fig. 2. Representative results from ^{14}C disequilibrium assays for *P. tricornutum* (a), and *T. nitzschioides* (b). Values of *f* shown on Fig. 2 represent the proportion of HCO_3^- uptake relative to net C fixation in DBS-treated cells (50 μmol L^{-1}), yielding values of 0.56, and 0.85 for the two species, respectively. The dashed lines represent best possible model fits with only CO_2 uptake, and the dotted curve in (a) represents the CO_2-only model fit constraining the final slope. Differences in ^{14}C incorporation between DBS and control, as seen in *T. nitzschioides*, were used to quantify eCA activities.

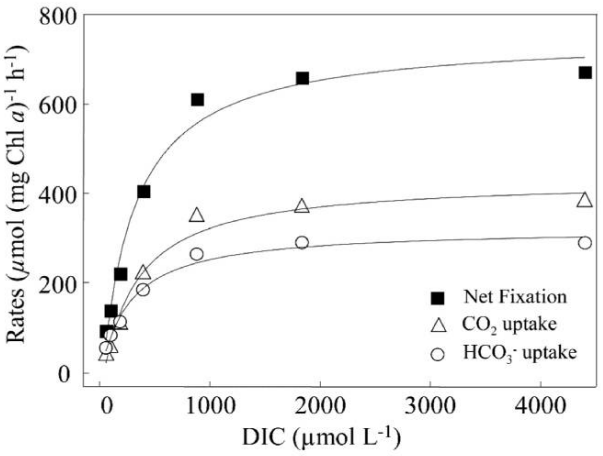

Fig. 3. Representative results from C_i flux assay showing Chl *a*-specific rates of net photosynthesis (squares), net CO_2 uptake (triangles), and HCO_3^- uptake (circles) as a function of DIC concentration in the assay medium for *P. tricornutum*. Curves were obtained from a Michaelis-Menten fit.

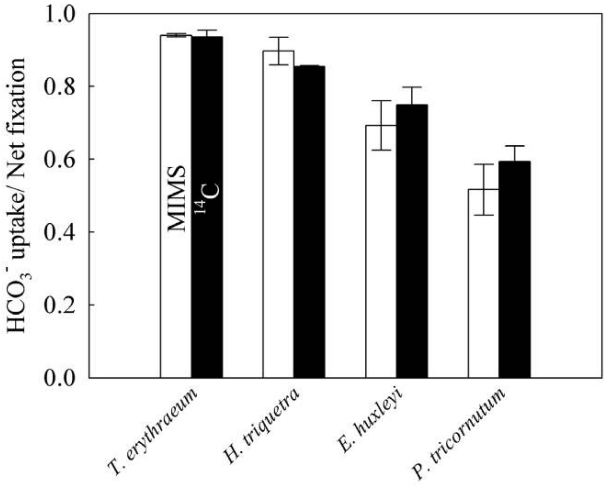

Fig. 4. Comparison of the HCO_3^- contribution relative to net C_i fixation obtained by C_i flux measurements (white columns) and ^{14}C disequilibrium technique (black columns) for the various phytoplankton species tested. Uptake ratios from MIMS measurements were based on the rates obtained at C_i concentrations of about 2 mmol L^{-1}. Values and standard deviations are based on at least triplicate measurements ($n \geq 3$) and the same culture was sampled for simultaneous measurements using both techniques.

obtained in the presence and absence of DBS, indicating a lack of eCA activity in this strain as noted in previous studies (Burkhardt et al. 2001). The ^{14}C incorporation time-course obtained for this species could not be fit using a CO_2-only model (i.e., $f = 0$). As is evident from respective dashed and dotted curve (Fig. 2a), the observed C_i uptake curves cannot be fit without including a substantial contribution of HCO_3^- uptake. This is particularly obvious when final slope (V_f) is constrained to fit the observed slope (dashed curve on Fig. 2a). Values of f (the proportion of HCO_3^- uptake relative to net C-fixation) in DBS-treated cells were 0.56. For *T. nitzschioides*, there was a substantial difference between the time-course data for control and DBS experiments, indicating the presence of eCA activity (see below). As with *P. tricornutum* however, the time-course data could not be fit using a CO_2-only uptake model. Indeed, HCO_3^- accounted for the large majority of C uptake in *T. nitzschioides* with an f value of 0.85.

Representative results for C_i flux assays are shown for *P. tricornutum* (Fig. 3). Rates of net photosynthesis, CO_2 and HCO_3^- uptake were calculated and expressed as a function of DIC concentration. In order to compare these results with those obtained from the ^{14}C experiments we estimated the HCO_3^- contribution relative to net C_i fixation at DIC concentrations at ~2 mmol L^{-1}. For the data shown in Figure 3, the contribution of HCO_3^- was 0.45 under this external DIC concentration.

Comparison of the HCO_3^- contribution estimated from isotope disequilibrium results and MIMS analysis (at 2 mmol L^{-1} external DIC) revealed excellent agreement between the two methods for all species tested (Fig. 4). The methods produced similar results for "HCO_3^- users" such as *T. erythraeum*, "CO_2 users" like *P. tricornutum* as well as the calcifying coccolithophore *E. huxleyi*. The largest discrepancy between methods was observed for *P. tricornutum*. In this species, the ^{14}C disequilibrium technique yielded HCO_3^- contributions of up to 10% higher than those derived by C_i flux measurements. This difference was, however, not statistically significant (*t* test, $P > 0.05$), given the relative error associated with each measurement.

Estimates for CA activity—Whereas the MIMS has been used to measure CA activities for more than two decades, the modified approach of the ^{14}C disequilibrium technique recently was described by Elzenga et al. (2000). Examples of ^{14}C incorporation time-courses by *T. nitzschioides* are given in Fig. 2b. In contrast to *P. tricornutum*, ^{14}C incorporation differed significantly between control and DBS-treated cells, indicating the presence of eCA activity in this species. We used the isotope disequilibrium data to estimate the rate of CO_2/HCO_3^- interconversion in the cell boundary layer. To quantify this, the data from control (i.e., no DBS) experiments were fit while constraining f to the value obtained in the DBS-treated sample, but allowing α to vary (Elzenga et al. 2000, Martin and Tortell 2006). In the control for *T. nitzschioides*, α' was estimated to equal 0.19 s^{-1}, which is approximately a 6-fold enhancement of the non-catalyzed rate constant ($\alpha = 0.0272$ s^{-1}).

Representative results from a mass spectrometric CA assay are shown for *T. nitzschioides* (Fig. 5). Changes in the ^{18}O-loss after the addition of cells compared to the spontaneous rate indicate significant eCA activity in this species. Activities for eCA by this approach are plotted together with those obtained

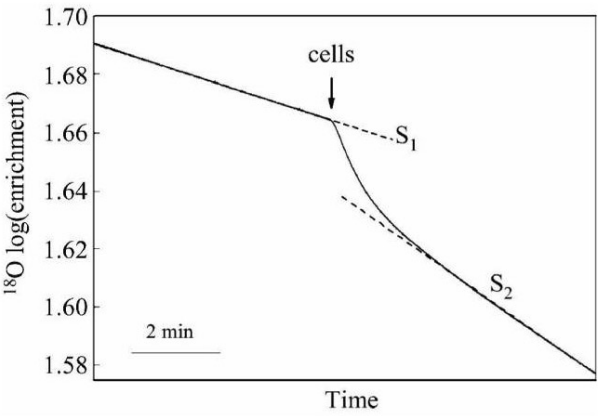

Fig. 5. Representative results for mass spectrometric CA assay with *T. nitzschioides*. Based on the concentrations of different CO_2 isotopomers $^{13}C^{18}O^{18}O$ (m/z 49), $^{13}C^{18}O^{16}O$ (m/z 47), and $^{13}C^{16}O^{16}O$ (m/z 45) the ^{18}O log(enrichment) is calculated. Activities of eCA are calculated by comparing the final linear rate of ^{18}O depletion (S_2) after the addition of cells with the initial linear slope (S_1), representing the uncatalyzed rate of ^{18}O exchange.

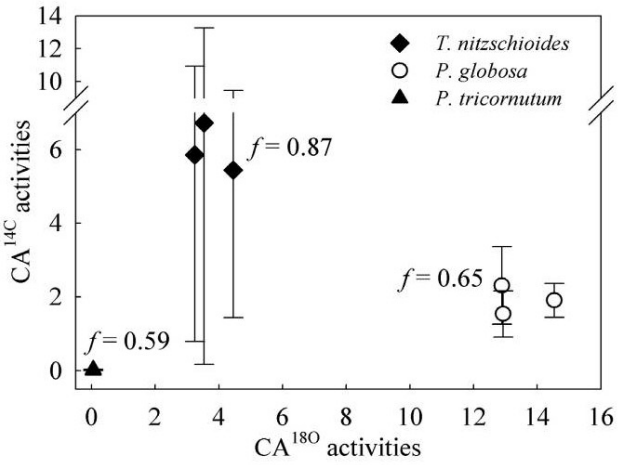

Fig. 6. Comparison of extracellular CA activities obtained by MIMS and ^{14}C disequilibrium technique with *T. nitzschioides*, *P. globosa*, and *P. tricornutum*. Values were estimated from control ^{14}C time course data, by fitting the data using Eq. 1, allowing α' to vary ($\alpha \geq 0.0272\ s^{-1}$), *f* was constrained to the value obtained in the DBS run. Activities obtained by MIMS were normalized to Chl *a* whereas activities obtained by ^{14}C were not normalized. Error bars represent standard error in α' estimates obtained by the model fit.

by ^{14}C technique in Figure 6, including also *P. globosa* and *P. tricornutum*. Both approaches yielded high eCA activities in *T. nitzschioides* and *P. globosa* and confirmed the lack of eCA in *P. tricornutum*. Unlike the estimation of *f*, however, the two methods yielded largely different values for activities, even when changes in α' were normalized to Chl *a* (data not shown). Moreover, errors in the ^{14}C derived CA estimates are much higher than those obtained by the MIMS approach. These findings can most likely be explained by inherent differences of the methods, which will be discussed below.

The ^{14}C disequilibrium technique assesses eCA activity by comparing the ^{14}C fixation modeled as an increase in α, hence by changes in the rate constants in the cell boundary layer. As a consequence, CA activity estimates reflect "effective activities" in the boundary layer and as such should be independent of the total biomass of plankton in the sample. In contrast, the MIMS approach quantifies bulk eCA activity in suspension by monitoring the changes in ^{18}O loss of doubly labeled HCO_3^-. These "quantitative activities" are clearly biomass-dependent and have to be normalized. In other words, whereas the MIMS measures eCA activities directly by its effect on the interconversion of CO_2 and HCO_3^-, the ^{14}C technique derives eCA activities indirectly by comparing the ^{14}C uptake kinetics in the absence and presence of DBS. Based on these considerations, one could expect that ^{14}C-based "boundary layer" estimates are higher than those ^{18}O-based "bulk" estimates of eCA activities. This is only true, however, for *T. nitzschioides* and not *P. globosa*. A further reason for the discrepancy may be the fact that eCA activities are measured in the dark for MIMS and in the light for the ^{14}C method. Potential light-activation of eCA, as has been suggested by Nimer et al. (1998), is consequently not accounted for by the MIMS approach.

Estimates for eCA activities by the ^{14}C approach showed high errors for *T. nitzschioides* whereas in *P. globosa* and *P. tricornutum* the errors in α were much smaller (Figure 6). To understand this result, we applied the model (Eq. 1) to a series of hypothetical ^{14}C time-course experiments with different *f* and α values (Martin and Tortell 2006). A random error of up to 5% was introduced to simulate experimental noise in the test data sets. The results given in Fig. 7 indicate that the curve-

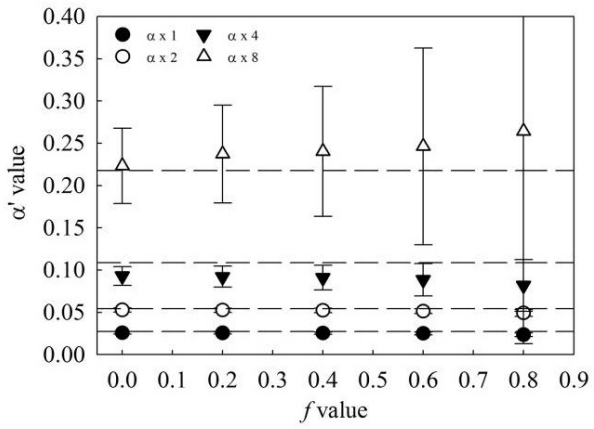

Fig. 7. Model calculations on α'estimates for a series of hypothetical ^{14}C time-course data with specified values of *f* and α (given by the dashed lines). A random error of up to 5% was introduced to simulate experimental noise to the test data set.

fitting algorithm does not provide accurate estimates of α at high contribution of HCO_3^- and high eCA activities (such as observed for *T. nitzschioides*). This occurs because the ^{14}C incorporation does not deviate strongly enough from a linear function. The errors in the model-derived α′ estimates are smaller, however, when the HCO_3^- contribution is lower and moderate or no eCA activity is present. This approach, therefore, provides a means to estimate eCA activities with reasonable precision, provided that cells are not predominant HCO_3^- users ($f < 0.7$) and possess moderate amounts of eCA ($CA^{18O} < 4$). Unfortunately, high proportion of HCO_3^- uptake is often accompanied by high levels of eCA activities, especially when cells were acclimated under low CO_2 levels (e.g., Rost et al. 2003).

Assay conditions and limitations—Despite the close agreement in CO_2/HCO_3^- uptake ratios obtained by the different approaches, assay conditions differ in some aspects from the conditions under which cells are cultured, and this could potentially introduce some bias into the results. As disequilibrium techniques, both MIMS and ^{14}C approaches require the lack of eCA activity. In the present study this was achieved by treating cells with dextran-bound sulfonamide (DBS), a membrane-impermeable inhibitor of eCA (Sültemeyer et al. 1990). Since DBS prevents CA-mediated HCO_3^- use, the proportion of direct HCO_3^- or CO_2 uptake could also be altered by this treatment. Whereas the presence of DBS most likely will not affect the estimates on HCO_3^-/CO_2 uptake in species lacking eCA, the contribution of direct CO_2 uptake may be higher in situ when cells express extracellular CA activity. Inhibitors for eCA may also have other effects than eliminating eCA activity. It has recently been argued that CA inhibitors like acetazolamide (AZ) affect photosynthesis non-specifically over and above the effects on eCA activity (Pollock and Colman 2001, Martin and Tortell 2006). We therefore tested the effect of DBS on photosynthesis by comparing the ^{14}C fixation with our control. Whereas DBS and control samples always yielded similar rates of photosynthesis (compare final ^{14}C incorporation rates given in Fig. 2), the presence of the inhibitor AZ often resulted in lower incorporation rates (data not shown). Martin and Tortell (2006) suggested that AZ may affect the HCO_3^- transport system directly, leading to an underestimation of the HCO_3^- contribution to total C_i uptake and thus experiments with AZ-treated cells should be interpreted with caution.

The methods tested here are also limited to a certain pH range, i.e., rather low values of 8.0 for the MIMS and higher values of 8.5 for the ^{14}C approach. Since the pH strongly alters the speciation between CO_2 and HCO_3^- in the media, assay pH may directly influence the uptake ratio of the respective carbon species. The higher pH of the ^{14}C experiments, may favor HCO_3^- uptake by cells compared to that seen at pH 8.0. In addition, results also may be altered by pH effects unrelated to carbonate chemistry, such as by differences in the energy requirement to maintain internal pH (Raven & Lucas 1985). In view of the similar results obtained by the different methods, this influence can be considered small, at least for those species investigated in our study.

For both approaches, it is important that cells are not affected negatively over the entire course of the experimental assay. For instance, cells can be damaged during the process of harvesting or as a result of turbulent shear stress in the stirred cuvette. Oxygen accumulation over the duration of the assays (as a byproduct of photosynthesis in a closed system) also can alter photosynthesis and hence cause bias in the results. In the ^{14}C disequilibrium technique, a progressive decrease in photosynthetic net fixation would increase the difference between initial and final slope of the ^{14}C uptake curve, yielding a higher apparent CO_2 contribution to total carbon fixation. In the MIMS assay, a decrease in photosynthetic activity with time will cause underestimation of net fixation, CO_2 and HCO_3^- uptake and consequently lower apparent half-saturation constants of these processes. This effect would not, however, specifically affect the relative contributions of CO_2 and HCO_3^- uptake.

C_i flux measurements usually are performed across a range of C_i concentrations to yield the kinetics of CO_2 and HCO_3^- uptake. Hence, these experiments typically last longer than the ^{14}C disequilibrium assays, and consequently are more prone to introducing physiological stress on cells. It is therefore advisable to test the constancy of cellular activity by monitoring photosynthetic O_2 evolution over the assay time range in all species. None of the species investigated here showed a decline in photosynthesis under assay condition (data not shown). Elevated O_2 concentrations during MIMS assays can be counteracted by purging with N_2, prolonging the dark phases, or by working with lower cell densities.

Comments and recommendations—Our comparison of the MIMS and ^{14}C disequilibrium technique demonstrate that reliable and comparable estimations of the ratio of photosynthetic CO_2 and HCO_3^- uptake can be obtained. This was true for a variety of phytoplankton species from different taxonomic groups. The ^{14}C method can be regarded as a robust and accurate method, easily adaptable for field applications. For more detailed carbon flux studies, the MIMS technique offers a powerful tool as it also provides uptake kinetics and changes therein. This information is needed to fully characterize the CCM in phytoplankton and assess the CO_2 sensitivity of photosynthesis and C_i uptake.

Assessing extracellular CA activities by the ^{14}C approach allows accurate estimates of the acceleration in rate constants provided that cells are not predominant HCO_3^- users and possess moderate amounts of eCA. For estimates of eCA activities, covering a range of activities in CO_2 as well as HCO_3^- users, the MIMS provides a more accurate approach. It should be noted that values for absolute eCA activities cannot be compared directly between approaches.

In view of the general goal of adapting methods to low cell concentrations (resembling conditions of the natural environment) the carbon flux measurements by MIMS are limited by

the need to create a measurable chemical disequilibrium in the bulk solution. In this respect, the ^{14}C approach in which an isotopic disequilibrium is induced has a significant advantage for field studies, as it allows experiments to be conducted with cell densities closer to in situ values.

References

Aizawa, K., and S. Miyachi. 1986. Carbonic anhydrase and CO_2 concentrating mechanism in microalgae and cyanobacteria. FEMS Microbiol. Rev. 39:215–233.

Amoroso, G., D. Sültemeyer, C. Thyssen, and H. P. Fock. 1998. Uptake of HCO_3^- and CO_2 in cells and chloroplasts from the microalgae *Chlamydomonas reinhardtii* and *Dunaliella tertiolecta*. Plant Physiol. 116:193–201.

Badger, M. R., A. Kaplan, and J. A. Berry. 1977. The internal CO_2 pool of *Chlamydomonas reinhardtii*: Response to external CO_2. Carnegie Institute Year Book 76:362–366.

———, A. Kaplan, and J. A. Berry. 1980. Internal inorganic carbon pool of *Chlamydomonas reinhardtii*. Evidence for a CO_2 concentrating mechanism. Plant Physiol. 66:407–413.

———, K. Palmqvist, and J.-W. Yu. 1994. Measurement of CO_2 and HCO_3^- fluxes in cyanobacteria and microalgae during steady-state photosynthesis. Physiol. Plant. 90:529–536.

Berry, J. A., J. Boynton, A. Kaplan, and M. R. Badger. 1976. Growth and photosynthesis of *Chlamydomonas reinhardtii* as a function of CO_2 concentration. Carnegie Institute Wash Year Book 75:423–432.

Burkhardt, S., G. Amoroso, U. Riebesell, and D. Sültemeyer. 2001. CO_2 and HCO_3^- uptake in marine diatoms acclimated to different CO_2 concentrations. Limnol. Oceanogr. 46(6): 1378–1391.

Cassar, N., E. A. Laws, R. R. Bidigare, and B. N. Popp. 2004. Bicarbonate uptake by Southern Ocean phytoplankton, GlobalBiogeochem. Cycles 18, GB2003, [doi:10.1029/ 2003GB002116].

Chen, Y.-B., J. P. Zehr, and M. Mellon. 1996. Growth and nitrogen fixation of the diazotrophic filamentous non-heterocystous cyanobacterium *Trichodesmium* sp. IMS 101 in defined media: Evidence for a circadian rhythm, J. Phycol. 32(6):916–923.

Elzenga, J. T. M., H. B. A. Prins, and J. Stefels. 2000. The role of extracellular carbonic anhydrase activity in inorganic carbon utilization of *Phaeocystis globosa* (Prymnesiophyceae): A comparison with other marine algae using the isotope disequilibrium technique. Limnol. Oceanogr. 45(2): 372–380.

Espie, G. S., and B. Colman. 1986. Inorganic carbon uptake during photosynthesis. I. A theoretical analysis using the isotope disequilibrium technique. Plant Physiol. 80:863–869.

Giordano, M., J. Beardall, and J. A. Raven. 2005. CO_2 concentrating mechanisms in algae: mechanisms, environmental modulation, and evolution. Annu. Rev. Plant Biol. 56:99–131.

Graham, D., and C. P. Whittingham. 1968. The path of carbon during photosynthesis in *Chlorella pyrenoidosa* at high and low carbon dioxide concentrations. Z. Pflanzenphysiol. 58: 418–427.

Guillard, R. R. L., and J. H. Ryther. 1962. Studies of marine planktonic diatoms. Can. J. Microbiol. 8:229–239.

Johnson, K. S. 1982. Carbon dioxide hydration and dehydration kinetics in seawater. Limnol. Oceanogr. 27:849–855.

Kaplan, A., M. R. Badger, and J. A. Berry. 1980. Photosynthesis and the intracellular inorganic carbon pool in the bluegreen alga *Anabaena variabilis*: Response to external CO_2 concentration. Planta 149:219–226.

Laws, E. A., B. N. Popp, R. R. Bidigare, U. Riebesell, S. Burkhardt, and S. G. Wakeham. 2001. Controls of the molecular distribution and carbon isotopic composition of alkenones in certain haptophyte algae, Geochem. Geophys. Geosyst. 2000GC000057.

Martin, C. L., and P. D. Tortell. 2006. Bicarbonate transport and extracellular carbonate anhydrase in Bering Sea phytoplankton assemblages: Results from isotopic disequilibrium experiments. Limnol. Oceanogr. 51(5):2111–2121.

Nimer, N. A., M. Warren, and M. J. Merrett. 1998. The regulation of photosynthetic rate and activation of extracellular carbonic anhydrase under CO_2-limiting conditions in the marine diatom *Skeletonema costatum*. Plant Cell Environ. 21:805–812.

Palmqvist, K., J.-W. Yu, and M. R. Badger. 1994. Carbonic anhydrase activity and inorganic carbon fluxes in low- and high-C_i cells of *Chlamydomonas reinhardtii* and *Scenedesmus obliquus*. Physiol. Plant. 90:537–547.

Pollock, S. V., and B. Colman. 2001. The inhibition of the carbon concentrating mechanism of the green alga *Chlorella saccharophila* by acetazolamide. Physiol. Planta 111: 527–532.

Raven, J. A., and W. J. Lucas. 1985. Energy costs of carbon acquisition. p. 305-324. *In* W. J. Lucas and J. A. Berry [eds], Inorganic Carbon Uptake by Aquatic Photosynthetic Organisms, The American Society of Plant Physiologists, Rockville, MD, USA.

Reed, M. L., and D. Graham. 1981. Carbonic anhydrase in plants: Distribution, properties and possible physiological roles, p 47–94. *In* L. Reinhold, J. B. Harborne and T. Swain [eds], Progress in Phytochemistry, v. 7, Pergamon Press, Oxford.

Riebesell, U., D. A. Wolf-Gladrow, and V. Smetacek. 1993. Carbon dioxide limitation of marine phytoplankton growth rates. Nature 361:249–251.

Rost, B., U. Riebesell, S. Burkhardt, and D. Sültemeyer. 2003. Carbon acquisition of bloom-forming marine phytoplankton. Limnol. Oceanogr. 48(1):55–67.

———, K.-U. Richter, U. Riebesell, and P. J. Hansen. 2006. Inorganic carbon acquisition in red tide dinoflagellates, Plant Cell Environ. 29:810–822.

Silverman, D. N. 1982. Carbonic anhydrase. Oxygen-18 exchange catalyzed by an enzyme with rate-contributing proton-transfer steps. Methods Enzymol. 87:732–752.

Sültemeyer, D. F., H. P. Fock, and D. T. Canvin. 1990. Mass spectrometric measurement of intracellular carbonic anhy-

drase activity in high and low C_i cells of *Chlamydomonas*. Plant Physiol. 94:1250–1257.

Sültemeyer, D., C. Schmidt, and H. P. Fock. 1993. Carbonic anhydrases in higher plants and aquatic microorganisms. Physiol. Plant. 88:179–190.

———, G. D. Price, J.-W. Yu, and M. R. Badger. 1995. Characterization of carbon dioxide and bicarbonate transport during steady-state photosynthesis in the marine cyanobacterium *Synechococcus* strain PCC7002. Planta 197:597–607.

Tortell, P. D. 2000. Evolutionary and ecological perspectives on carbon acquisition in phytoplankton. Limnol. Oceanogr. 45(3):744–750.

——— 2005. Dissolved gas measurements in oceanic waters made by membrane inlet mass spectrometry. Limnol. Oceanogr.: Methods 3:24–37.

———, and F. M. M. Morel. 2002. Sources of inorganic carbon for phytoplankton in the eastern Subtropical and Equatorial Pacific Ocean. Limnol. Oceanogr. 47(4):1012–1022.

———, C. L. Martin, and M. E. Corkum. 2006. Inorganic carbon uptake and intracellular assimilation by Pacific phytoplankton assemblages. Limnol. Oceanogr. 51(5):2102-2110.

Submitted 4 December 2006
Revised 6 July 2007
Accepted 25 July 2007

Publication II

Limnol. Oceanogr., 54(2), 2009, 548–559
© 2009, by the American Society of Limnology and Oceanography, Inc.

Carbon acquisition by *Trichodesmium*: The effect of pCO_2 and diurnal changes

Sven A. Kranz
Alfred Wegener Institute for Polar and Marine Research, Am Handelshafen 12, 27570 Bremerhaven, Germany

Dieter Sültemeyer
Fachbereich Biologie, Technische Universität Kaiserslautern, Postfach 3049, D-67653 Kaiserslautern, Germany

Klaus-Uwe Richter and Björn Rost
Alfred Wegener Institute for Polar and Marine Research, Am Handelshafen 12, 27570 Bremerhaven, Germany

Abstract

We investigated carbon acquisition by the N_2-fixing cyanobacterium *Trichodesmium* IMS101 in response to CO_2 levels of 15.1, 37.5, and 101.3 Pa (equivalent to 150, 370, and 1000 ppm). In these acclimations, growth rates as well as cellular C and N contents were measured. In vivo activities of carbonic anhydrase (CA), photosynthetic O_2 evolution, and CO_2 and HCO_3^- fluxes were measured using membrane inlet mass spectrometry and the ^{14}C disequilibrium technique. While no differences in growth rates were observed, elevated CO_2 levels caused higher C and N quotas and stimulated photosynthesis and N_2 fixation. Minimal extracellular CA (eCA) activity was observed, indicating a minor role in carbon acquisition. Rates of CO_2 uptake were small relative to total inorganic carbon (Ci) fixation, whereas HCO_3^- contributed more than 90% and varied only slightly over the light period and between CO_2 treatments. The low eCA activity and preference for HCO_3^- were verified by the ^{14}C disequilibrium technique. Regarding apparent affinities, half-saturation concentrations ($K_{1/2}$) for photosynthetic O_2 evolution and HCO_3^- uptake changed markedly over the day and with CO_2 concentration. Leakage (CO_2 efflux : Ci uptake) showed pronounced diurnal changes. Our findings do not support a direct CO_2 effect on the carboxylation efficiency of ribulose-1,5-bisphosphate carboxylase/oxygenase (RubisCO) but point to a shift in resource allocation among photosynthesis, carbon acquisition, and N_2 fixation under elevated CO_2 levels. The observed increase in photosynthesis and N_2 fixation could have potential biogeochemical implications, as it may stimulate productivity in N-limited oligotrophic regions and thus provide a negative feedback on rising atmospheric CO_2 levels.

Marine phytoplankton contribute up to 50% of global primary production (Falkowski et al. 1998) and influence Earth's climate by altering various biogeochemical cycles (Schlesinger 2005). In this respect, phytoplankton can be distinguished into so-called functional types, which affect these cycles differently. Next to diatoms (silicifiers) and coccolithophores (calcifiers), diazotrophic cyanobacteria (dinitrogen-fixers) contribute largely to overall marine primary production. The current increase in atmospheric CO_2 and rising sea-surface temperature are bound to affect phytoplankton communities in numerous ways (Boyd and Doney 2002). In view of potential ecological implications and feedbacks on climate, several studies have investigated CO_2 sensitivity in key phytoplankton species, mainly focusing on the groups of diatoms and coccolithophores (Nielsen 1995; Burkhardt and Riebesell 1997; Rost et al. 2003).

Diazotrophic cyanobacteria affect marine ecosystems by providing reactive nitrogen to otherwise nitrogen-limited regions. The filamentous nonheterocystous cyanobacterium *Trichodesmium* thrives in oligotrophic areas of tropical and subtropical seas. Forming large blooms, this species contributes about half of all marine N_2 fixation (Mahaffey et al. 2005). In contrast to other diazotrophs, *Trichodesmium* has evolved special features allowing N_2 fixation to occur during the photoperiod. To protect the oxygen-sensitive enzyme nitrogenase, which catalyzes the reduction of N_2 to NH_3, from photosynthetic O_2 evolution, this species has developed distinct diurnal rhythms in photosynthesis and N_2 fixation (Berman-Frank et al. 2001*b*). This intriguing species has been investigated by several studies focusing on the effects of phosphorus and iron limitations as well as temperature, salinity, and irradiance (Berman-Frank et al. 2001*a*; Fu and Bell 2003; Breitbarth et al. 2007). The potential influence of CO_2-induced changes in seawater chemistry, however, has been ignored until very recently.

Barcelos e Ramos et al. (2007), Levitan et al. (2007), and Hutchins et al. (2007) observed a strong increase in photosynthesis and N_2 fixation in *Trichodesmium* under elevated CO_2 levels. This trend is predominantly attributed to changes in cell division (Hutchins et al. 2007; Levitan et al. 2007) but also altered elemental ratios of carbon to nitrogen (Levitan et al. 2007) or nitrogen to phosphorus (Barcelos e Ramos et al. 2007). Despite differences in their findings, e.g., in terms of absolute rates or elemental ratios,

Acknowledgments

We thank Ilana Berman-Frank, Orly Levitan, Katherina Petrou, and two anonymous reviewers for their constructive comments on the manuscript. The research leading to these results has received funding from the European Research Council under the European Community's Seventh Framework Programme (FP7/2007-2013)/ERC grant agreement (205150).

the magnitudes of these CO_2 effects exceed those previously seen in other marine photoautotrophs. The underlying processes responsible for the strong CO_2 sensitivity in this important diazotroph are currently unknown.

Understanding CO_2 sensitivity in photosynthesis, which provides the energy for growth and any other downstream processes, requires information about modes of carbon uptake and fixation in phytoplankton. Most of the reductive power and energy generated in the light reactions of photosynthesis are allocated for assimilation of inorganic carbon (Ci) and subsequent reduction (Falkowski and Raven 2007). A large proportion of these costs is associated with the operation of so-called CO_2 concentrating mechanisms (CCMs), which function to increase the carboxylation reaction of ribulose-1,5-bisphosphate carboxylase/oxygenase (RubisCO). This enzyme evolved during times of elevated CO_2 levels and is characterized by very low affinity for its substrate CO_2, a slow maximum turnover rate, as well as a susceptibility to a competing reaction with O_2. Since cyanobacterial RubisCO has one of the highest half-saturation constants ever measured (K_M of 105–185 μmol L^{-1} CO_2; Badger et al. 1998), this group has to invest considerable resources into the CCM to avoid the risk of carbon limitation as well as the wasteful process of photorespiration. This CCM involves active uptake of CO_2 and/or HCO_3^- as well as carbonic anhydrase (CA), which catalyzes the otherwise slow conversion between HCO_3^- and CO_2. Processes that minimize the CO_2 efflux from the cell are also important components of an efficient CCM. To date, there are no physiological studies on these central processes in *Trichodesmium*.

In the present study, we investigated the physiological responses of *Trichodesmium* IMS101 to different CO_2 levels, comparing Last Glacial Maximum (15.1 Pa), present-day (37.5 Pa), and projected upper CO_2 values for the year 2100 (101.3 Pa; Raupach et al. 2007). To assess diurnal changes in these treatments, responses were generally measured at different time intervals over the photoperiod. In each CO_2 treatment, responses in growth rates, elemental ratios, and rates of photosynthesis and production of particulate organic nitrogen were measured. To develop a process-based understanding of responses in the incubations, different in vivo bioassays were applied. O_2 evolution under steady-state photosynthesis, quantified CO_2 and HCO_3^- uptake rates, as well as cellular leakage (CO_2 efflux : Ci uptake) were measured by the use of a membrane inlet mass spectrometer. Activities of external carbonic anhydrase (eCA) were determined by monitoring ^{18}O exchange from doubly labelled $^{13}C^{18}O_2$. As a second approach, short-term ^{14}C disequilibrium measurements were conducted to estimate CA activities and distinguish the carbon source taken up.

Methods

Culture conditions—Stock cultures of *Trichodesmium erythraeum* IMS101 (isolated by Prufert-Bebout et al. 1993) were grown at 25°C in a 12 : 12 h light : dark (LD) cycle at 150 μmol photons m^{-2} s^{-1} in 0.2-μm-filtered unbuffered YBCII media (Chen et al. 1996). For experiments, semicontinuous batch cultures were grown in 1-liter custom-made cylinder flasks (diameter 7 cm) at the same temperature and light regime. Air containing three different CO_2 partial pressures (pCO_2) of 15.1, 37.5, and 101.3 Pa (equivalent to 150, 370, and 1000 ppm) was sparged continuously through the cultures. CO_2 gas mixtures were generated with gas-mixing pumps (Digamix 5KA18/8-F and 5KA36/8-F, Woesthoff GmbH), using CO_2-free air (Nitrox CO_2RP280; Domnick Hunter GmbH), pure CO_2 (Air Liquide Deutschland GmbH), or ambient air. Regular dilution with fresh, pre-acclimated media ensured that the carbonate chemistry remained constant and that the cells stayed in the midexponential growth phase. Cultures in which the pH had shifted in comparison to cell-free media at the respective pCO_2 (pH drift >0.06) were excluded from further analysis. Total alkalinity was measured in duplicate by potentiometric titration and calculated from linear Gran Plots (Gran 1952). The carbonate system was calculated from total alkalinity (TA), pCO_2, phosphate, temperature, and salinity using the program CO2Sys (Lewis and Wallace 1998). Equilibrium constants of Mehrbach et al. (1973) refitted by Dickson and Millero (1987) were chosen. Carbonate chemistry for the respective pCO_2 treatments is given in Table 1.

Table 1. Parameters of the seawater carbonate system calculated from pCO_2, alkalinity, pH, phosphate, temperature, and salinity using the CO2Sys program (Lewis and Wallace 1998) (n=3; ±SD).

pCO_2 (Pa)	pH (NBS)	CO_2 (μmol L^{-1})	DIC (μmol L^{-1})	TA (μEq L^{-1})
15.1	8.56±0.03	3.9±0.3	1879±24	2535±12
37.5	8.26±0.03	9.9±0.7	2113±20	2535±12
101.3	7.89±0.03	27.2±1.9	2322±16	2535±12

Growth, elemental composition, and fixation rates—Cultures were acclimated to the respective pCO_2 for at least 14 d (>5 generations) before measuring. In general, samples were taken at the beginning of the photoperiod to account for diurnal changes. Cell densities were determined using an inverted microscope (Zeiss, Axiovert 200) by measuring the number of filaments, length, and cell size in a Sedgwick-Rafter Cell (S50, Graticules). The average cell size for each pCO_2 treatment was estimated based on the length of individual filaments and corresponding cell counts (>10,000 individual counts). Samples for chlorophyll *a* (Chl *a*) measurements were filtered onto cellulose nitrate filters (Sartorius) and stored at −80°C. Chl *a* was subsequently extracted in 5–10 mL acetone (overnight in darkness, at 4°C) and determined with a fluorometer (Turner Designs).

Samples for particulate organic carbon (POC) and nitrogen (PON) were filtered onto precombusted (500°C; 9 h) GFF filters and stored in precombusted (500°C; 9 h) petri dishes at −20°C. Prior to analysis, filters were treated with 200 μL HCl (0.1 μmol L^{-1}) to remove all inorganic carbon. POC and PON were subsequently measured in duplicate on an EA mass spectrometer (ANCA-SL 2020).

Growth rates were determined based on changes in cell density, Chl *a* concentration, as well as POC and PON, respectively, and are given as mean values. Growth rates (μ) were calculated as:

$$\mu(\mathrm{d}^{-1}) = \frac{\ln(N_1) - \ln(N_0)}{\Delta t} \quad (1)$$

where N_0 and N_1 are concentration of cells, Chl *a*, POC, or PON at time t_0 and t_1, respectively, and Δt is the time between sampling intervals. Production rates of PON (P_N) and POC (P_C) per day were calculated according to the following equations:

$$P_N = \mu \times \mathrm{PON} \times (\mathrm{Chl}\ a)^{-1} \quad (2)$$

$$P_C = \mu \times \mathrm{POC} \times (\mathrm{Chl}\ a)^{-1} \quad (3)$$

Determination of CA activity—After a minimum of 14 d acclimation to the respective pCO_2, cells were concentrated by gentle filtration over a membrane filter (pore size 8 μm; Isopore, Millipore). The culture media was stepwise exchanged with the respective assay medium, and CA activities were determined using a membrane inlet mass spectrometer (MIMS). The system consisted of a temperature-controlled cuvette, a membrane-inlet (polytetrafluoroethylene membrane, 0.01 mm), and a sectorfield multicollector mass spectrometer (Isoprime; GV Instruments). Gas molecules dissolved in solution permeated through the membrane and were ionized, and, depending on their mass : charge ratio (*m*/*z*), ions were then separated and detected.

CA activity was determined from the ^{18}O depletion of doubly labelled $^{13}C^{18}O_2$ in water caused by several hydration and dehydration steps of CO_2 and HCO_3^- (Silverman 1982). The reaction sequence of ^{18}O loss from initial $^{13}C^{18}O^{18}O$ (m/z = 49) via the intermediate $^{13}C^{18}O^{16}O$ (m/z = 47) to the final isotopomer $^{13}C^{16}O^{16}O$ (m/z = 45) was recorded simultaneously. The ^{18}O enrichment was calculated as:

$$\log(\text{enrichment}) = \log\frac{(^{13}C^{18}O_2) \times 100}{^{13}C^{16}O_2 + {}^{13}C^{18}O^{16}O + {}^{13}C^{18}O_2} = \log\frac{(m/z\,49) \times 100}{(m/z\,45) + (m/z\,47) + (m/z\,49)} \quad (4)$$

CA measurements were performed in 8 mL of YBCII medium buffered with 2-(4-[2-hydroxyethyl]-1-piperazinyl)ethanesulfonic acid (HEPES, 50 mmol L^{-1}, pH 8.00) at 25°C. If not stated otherwise, all measurements were carried out in the dark to avoid interference with light-dependent carbon uptake by the cells. Bicarbonate was added (1 mmol L^{-1} $NaH^{13}C^{18}O$), and once the chemical equilibrium was reached, the uncatalyzed rate of ^{18}O loss was recorded for at least 5 min. Subsequently, 100–200 μL of concentrated cell suspension were added to the media to yield a final Chl *a* concentration of 0.5–2.5 μg mL^{-1}. For calculation of extracellular CA activities (eCA), the increasing rate of ^{18}O depletion after addition of the cells (S_2) was compared to the uncatalyzed reaction (S_1) and normalized on a Chl *a* basis (Badger and Price 1989):

$$U = \frac{(S_2 - S_1) \times 100}{S_1 \times \mu\mathrm{g\ Chl}\ a} \quad (5)$$

Consequently, 100 units (U) correspond to an enhancement in the interconversion between HCO_3^- and CO_2 relative to the spontaneous rate by 100% per μg Chl *a*. Following the eCA measurements, light was added (300 μmol photons m^{-2} s^{-1}) to monitor light-induced changes in the ^{18}O exchange. This method is indicative of active transport of Ci, as there will be an enhanced influx of labelled Ci into the cell to the active site of internal CA, resulting in an increase of the ^{18}O loss (Badger and Price 1989).

Intracellular CA (iCA) activity was determined in the presence of 50 μmol L^{-1} dextran-bound sulfonamide (DBS), a membrane-impermeable inhibitor of eCA. The activity of iCA was estimated from the rapid decline in log (enrichment) upon the injection of cells, defined as Δ, and calculated according to Palmqvist et al. (1994). Values of Δ are expressed per μg Chl *a*.

Determination of photosynthesis and Ci fluxes—The O_2 and Ci fluxes were determined during steady-state photosynthesis with the same MIMS as for the CA measurements. The method established by Badger et al. (1994) is based on simultaneous measurements of O_2 and CO_2 during consecutive light and dark intervals. Known amounts of inorganic carbon were added to measure photosynthesis and carbon uptake rates as a function of CO_2, HCO_3^-, or dissolved inorganic carbon (DIC) concentrations. Photosynthesis, CO_2 uptake, and HCO_3^- uptake were calculated according to the equations of Badger et al. (1994). Cells were harvested in the same manner as for the CA measurements using CO_2-free YBCII medium (50 mmol L^{-1} HEPES, pH 8.00) and transferred into the cuvette before DBS was added (final concentration of 50 μmol L^{-1}). Light and dark intervals during the assay lasted 6 and 5 min, respectively. The incident photon flux density was 300 μmol photons m^{-2} s^{-1}. Chl *a* concentrations in the assay ranged from about 0.5 to 4 μg mL^{-1}. Further details on the method and calculations are given in Badger et al. (1994) and Rost et al. (2007).

^{14}C disequilibrium method—Cells were concentrated via gentle filtration in the same manner as for the MIMS assays, but they were washed and resuspended with buffered YBCII media (BICINE-NaOH, 20 mmol L^{-1}, pH 8.50). Afterward, cells were transferred into a cuvette (4 mL volume) and pre-incubated to 300 μmol photons m^{-2} s^{-1} for 6 min. The ^{14}C disequilibrium technique makes use of the transient isotopic disequilibrium upon an acidic ^{14}C spike into cell suspension at high pH to determine whether CO_2 or HCO_3^- is the preferred carbon species for photosynthesis (Espie and Colman 1986; Elzenga et al. 2000). This approach also provides semi-quantitative estimates of external CA activity. In the

present study, we followed the protocol described by Rost et al. (2007).

Results

Growth, elemental ratios, and fixation rates—To assess the overall sensitivity of *Trichodesmium* to different CO_2 levels (15.1, 37.5, and 101.3 Pa), responses in growth rates, elemental ratios, rates of photosynthesis, and production rates of particulate organic nitrogen were measured. Growth rates were determined during mid-exponential growth phase based on cell counts, Chl *a*, POC, and PON. The mean growth rate was 0.31 ± 0.04 d^{-1} (Fig. 1a) and did not differ significantly between pCO_2 treatments ($p = 0.378$; one way ANOVA). The C : N ratios (4.6 ± 0.1) and Chl *a* : cell ratios (1.0 ± 0.2) did not differ between the treatments. However, POC and PON increased from 4.1 ± 0.6 pmol C $cell^{-1}$ and 0.9 ± 0.1 pmol N $cell^{-1}$ at 37.5 Pa to 5.4 ± 0.6 pmol C $cell^{-1}$ and 1.2 ± 0.1 pmol N $cell^{-1}$ at 101.3 Pa CO_2 (Figs. 1b,c). The corresponding POC and PON production rates increased from 51.7 ± 8.0 to 67.6 ± 7.4 μmol C (mg Chl *a*)$^{-1}$ h^{-1} and from 11.4 ± 2.2 to 14.9 ± 1.8 μmol N (mg Chl *a*)$^{-1}$ h^{-1}, representing a stimulation in carbon and nitrogen fixation by almost 40%.

In terms of diurnal changes, carbon and nitrogen contents per cell showed distinct patterns leading to strong changes in C : N ratios (Fig. 2a). During the course of the day, the C : N ratio increased from 4.76 ± 0.04 at the onset of the photoperiod to 4.91 ± 0.04 around midday (09:00 h–12:00 h). It decreased to 4.48 ± 0.08 during the afternoon (12:00 h–17:00 h) and subsequently increased to 4.95 ± 0.09 toward the scotoperiod (21:00 h). This diurnal variation in the C : N ratio indicates distinct differences in the patterns of carbon or nitrogen fixation over the day. Rates of photosynthesis and respiration (based on O_2 evolution) as determined by MIMS also showed pronounced diurnal changes in all acclimations (Fig. 2b). Rates of photosynthesis decreased by 48% during the first 3 h of the photoperiod, while dark respiration increased by 102%. After reaching lowest and highest rates around midday, respectively, this pattern reversed, and photosynthesis increased while dark respiration decreased toward the end of the photoperiod (Fig. 2b).

Carbonic anhydrase activities—External CA activity determined by MIMS directly reflects the acceleration in the conversion between CO_2 and HCO_3^- relative to the spontaneous rate. In *Trichodesmium*, eCA activities were about 50 ± 10 units (μg Chl *a*)$^{-1}$, and they neither varied between treatments nor over the photoperiod (data not shown). The activity of internal CA remained constant in all acclimations and was near the detection limit, i.e., Δ values were about 0.25 ± 0.08 (μg Chl *a*)$^{-1}$ following calculations of Palmqvist et al. (1994).

The ^{18}O exchange technique can provide information about active Ci transport systems. As shown in Fig. 3, illumination resulted in an enhanced uptake of ^{18}O-labelled $^{13}CO_2$ (*m*/*z* 49 and 47) and a large efflux of unlabelled $^{13}CO_2$ (*m*/*z* 45), leading to a light-dependent decrease in log

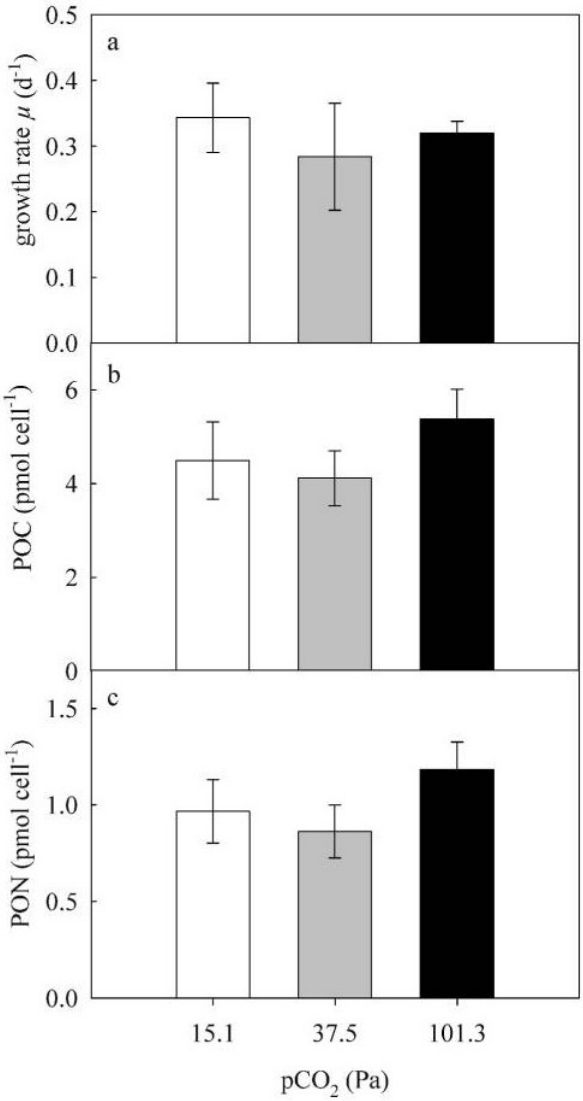

Fig. 1. (a) Mean growth rates of *Trichodesmium* based on changes in cell density, Chl *a*, POC, PON (b) content of POC per cell, and (c) content of PON per cell in different acclimations of 15.1 Pa, 37.5 Pa, and 101.3 Pa pCO_2. Data present mean values ($n \geq 3$; ±SD).

(enrichment). Similar patterns were observed in all acclimations and throughout the photoperiod.

Photosynthetic O_2 evolution and carbon fluxes—Photosynthesis and Ci uptake are shown as functions of CO_2 and HCO_3^- concentration measured during steady-state conditions (Fig. 4) by MIMS. Maximum rates of photosynthesis (V_{max}) and half-saturation concentrations ($K_{1/2}$) were obtained from a Michaelis–Menten fit and are summarized for all pCO_2 treatments in Table 2. Kinetics for photosynthetic O_2 evolution were affected both by pCO_2 and photoperiod. While V_{max} differed only slightly between pCO_2 treatments, diurnal variations were pronounced

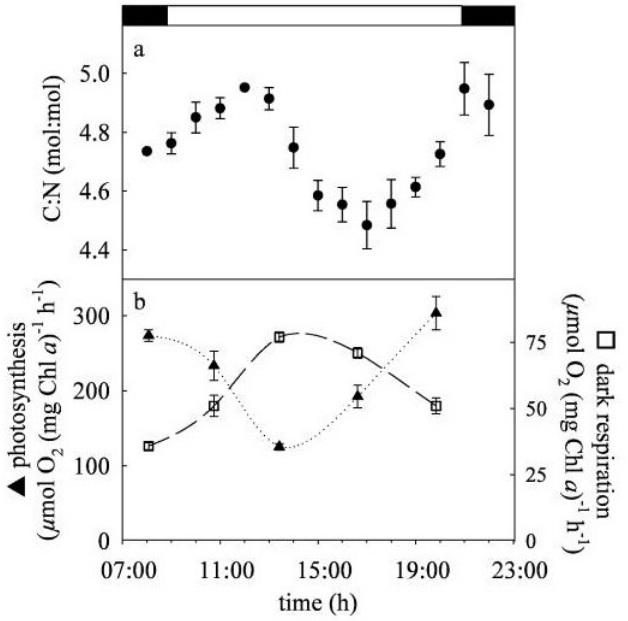

Fig. 2. (a) Diurnal variations in C : N ratios of the 37.5 Pa acclimation in *Trichodesmium*. Symbols represent average values ($n \geq 2 \pm$ SD). (b) Pattern of photosynthesis and dark respiration as measured during carbon flux measurements in light and dark cycles, respectively. Data present mean values ($n \geq 3$; ±SD).

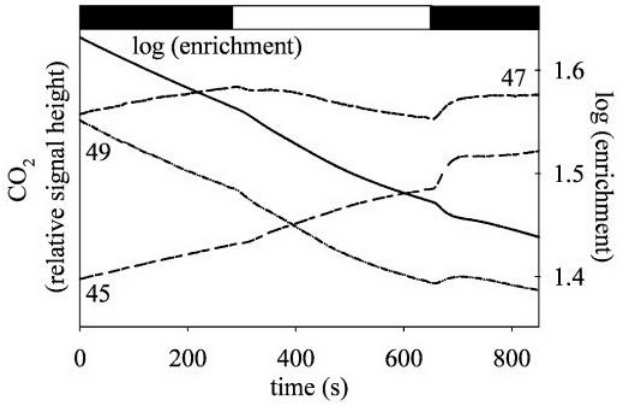

Fig. 3. Time course of changes in log (enrichment) and the CO_2 isotopomers $^{13}C^{18}O_2$ (*m/z* 49), $^{13}C^{16}O^{18}O$ (*m/z* 47), $^{13}C^{16}O_2$ (*m/z* 45) by cells of *Trichodesmium* acclimated to 37.5 Pa CO_2 measured at 15:00 h. The eCA inhibitor DBS (50 mmol L^{-1}) was applied during the assay. Black and white bars at the top indicate the dark and light period, respectively.

(Fig. 5a; Table 2). Minimum values were obtained about 3 h after illumination (125 to 170 μmol O_2 [mg Chl *a*]$^{-1}$ h^{-1}), and increased by nearly twofold toward the end of the photoperiod (303 to 330 μmol O_2 [mg Chl *a*]$^{-1}$ h^{-1}). As indicated by the $K_{1/2}$ (DIC) values, affinities differed significantly between pCO_2 acclimations and also showed a strong diurnal pattern, with highest values around midday (Fig. 5b; Table 2). $K_{1/2}$ (CO_2) values for photosynthesis ranged between 0.9 and 13.6 μmol L^{-1} CO_2 (data not shown).

In terms of carbon fluxes, *Trichodesmium* showed a preference for HCO_3^- as a carbon source for photosynthesis (Fig. 4; Table 3). The high HCO_3^- contribution to net fixation was verified by the ^{14}C disequilibrium method (*see* below). The $K_{1/2}$ values for HCO_3^- uptake and diurnal variability therein strongly increased from low to the high pCO_2 acclimation (Table 2), ranging between 40 and 100 μmol DIC L^{-1} in the low pCO_2 treatment and 85 and 520 μmol DIC L^{-1} in the high pCO_2 treatment. This CO_2 effect on affinities persisted despite the large diurnal variations in $K_{1/2}$, being most pronounced during midday and lowest at the beginning of the photoperiod. Rates for CO_2 uptake were very low in all acclimations and throughout the photoperiod (Table 2). In terms of gross CO_2 uptake, $K_{1/2}$ and V_{max} remained unaffected by pCO_2 in the acclimation as well as over the photoperiod. $K_{1/2}$ values ranged between 3.3 and 6.1 μmol L^{-1} CO_2, and V_{max} ranged between 51 and 114 μmol CO_2 (mg Chl *a*)$^{-1}$ h^{-1}. Net CO_2 flux was often negative, showing lowest values between 12:00 h and 15:00 h, which made it impossible to calculate $K_{1/2}$ values. These rates reflect the CO_2 efflux that occurs during steady-state photosynthesis. The proportion of Ci efflux compared to gross Ci uptake, i.e., cellular leakage, was estimated by MIMS from the CO_2 efflux observed directly upon darkening. Independent of the pCO_2 acclimation, *Trichodesmium* showed large variations in leakage during the photoperiod, and the highest ratio (~0.5) occurred at 12:00 h (Fig. 6).

^{14}C disequilibrium method—Figure 7 shows an example of the ^{14}C incorporation of a culture acclimated to 101.3 Pa CO_2. Monitoring the ^{14}C incorporation for more than 12 min, i.e., well into equilibrium, yielded a high level of precision for determining the carbon sources. In measurements of the same culture without DBS (control), similar rates of ^{14}C incorporation were obtained, indicating a lack of significant eCA activity. The ratio of HCO_3^- to net fixation did not significantly differ between the acclimations or throughout the photoperiod; values ranged between 0.86 and 0.95 (Table 3).

Discussion

This study assessed the sensitivity of *Trichodesmium erythraeum* (IMS101) to changes in CO_2 concentration by measuring responses to the different acclimations (e.g., growth, elemental ratios, fixation rates) and by describing the modes of carbon acquisition (e.g., CA activities, O_2 evolution, carbon fluxes). Cells were acclimated in unbuffered artificial seawater and maintained at low cell densities to match the natural environment in nonbloom situations as closely as possible. *Trichodesmium* showed no responses in growth rate, but particulate organic carbon and nitrogen production rates increased strongly at elevated pCO_2 (Fig. 1) The apparent $K_{1/2}$ values for photosynthetic O_2 evolution were significantly lower than values known for RubisCO (Badger et al. 1998), demonstrating the operation of a CCM in this species. *Trichodesmium* showed a strong

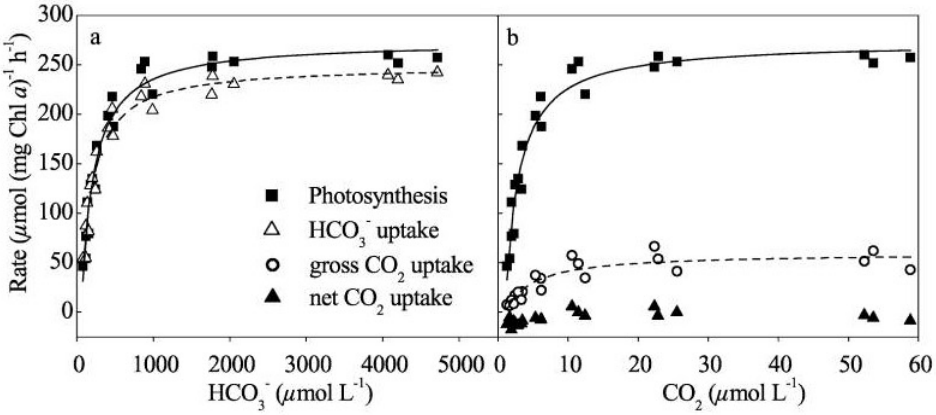

Fig. 4. Chl *a*–specific rates of (a) photosynthesis and HCO_3^- uptake and (b) photosynthesis and gross as well as net CO_2 uptake and is a function of HCO_3^- and CO_2 concentration in the assay media. The given examples show results from cells acclimated to 101.3 Pa CO_2 and were measured at 07:00 h. Curves were obtained from a Michaelis–Menten fit.

preference for HCO_3^- as a carbon source, which did not change with CO_2 availability or over the diurnal cycle. In terms of CO_2 and HCO_3^- affinities, however, cells showed strong responses to CO_2 treatments and photoperiod.

Growth, elemental ratios, and production rates—Previous studies have observed CO_2 effects on growth (Riebesell et al. 1993), photosynthesis (Nielsen 1995; Rost et al. 2003), and elemental ratios (Burkhardt and Riebesell 1997) in diatoms and coccolithophores. Large responses in growth, photosynthesis, and elemental ratios with respect to changes in pCO_2 have recently been found in the diazotrophic species *Trichodesmium* (Barcelos e Ramos et al. 2007; Hutchins et al. 2007; Levitan et al. 2007). It should be noted that all these studies, including the present one, have used the same *Trichodesmium* isolate from the Atlantic Ocean (IMS101).

Our findings indicate no sensitivity in growth rates over the tested CO_2 range (15.1 to 101.3 Pa CO_2), but they do show CO_2-dependent changes in the elemental composition of *Trichodesmium* (Fig. 1a). In comparison to the previously published data, growth rates (μ = 0.32) are slightly higher than those obtained by Levitan et al. (2007; μ = 0.27) and lower than those from Barcelos e Ramos et al. (2007; μ = 0.45) under high CO_2. For low CO_2 levels, our data do not agree with the diminished rates observed by Levitan et al. (2007; μ = 0.12) and Barcelos e Ramos et al. (2007; μ = 0.15 to 0.3) or the absence of growth observed by Hutchins et al. (2007). According to the latter study, *Trichodesmium* cannot thrive under the CO_2 levels that

Table 2. $K_{1/2}$ and V_{max} of photosynthesis, HCO_3^- uptake, and gross CO_2 uptake over a diurnal cycle and acclimated to 15.1, 37.5, and 101.3 Pa pCO_2. The photoperiod started at 09:00 h and ended at 21:00 h. Kinetic parameters were calculated from a Michaelis–Menten fit to the combined data of several ($n \geq 3$; ±SD) independent measurements. Values for $K_{1/2}$ and V_{max} are given in μmol L^{-1} and μmol (mg Chl *a*)$^{-1}$ h^{-1}, respectively.

		Photosynthesis		HCO_3^- uptake		Gross CO_2 uptake	
Time (h)	pCO_2 (Pa)	$K_{1/2}$ (DIC)	V_{max} (DIC)	$K_{1/2}$ (HCO_3^-)	V_{max} (HCO_3^-)	$K_{1/2}$ (CO_2)	V_{max} (CO_2)
07:00	15.1	61±24	233±14	63±25	242±15	4±1	88±7
	37.5	126±13	219±7	111±9	213±4	6±1	56±3
	101.3	214±18	274±8	190±16	250±7	5±1	60±5
09:30	15.1	40±11	187±9	41±11	232±11	4±1	82±7
	37.5	72±12	207±6	27±8	219±9	4±1	73±6
	101.3	85±33	233±20	52±23	226±18	6±2	56±6
12:00	15.1	102±33	147±9	30±6	199±6	3±2	67±10
	37.5	286±96	171±16	112±29	198±11	4±1	60±3
	101.3	519±54	125±4	111±23	150±7	7±1	51±2
15:00	15.1	54±12	298±12	25±6	266±9	3±1	90±8
	37.5	94±29	270±20	51±11	232±9	3±1	97±10
	101.3	443±105	192±15	188±38	206±10	5±1	64±2
18:00	15.1	25±35	319±21	30±8	248±9	4±1	92±4
	37.5	112±25	330±16	61±15	284±13	4±2	114±13
	101.3	257±70	303±22	181±56	274±20	5±1	90±7

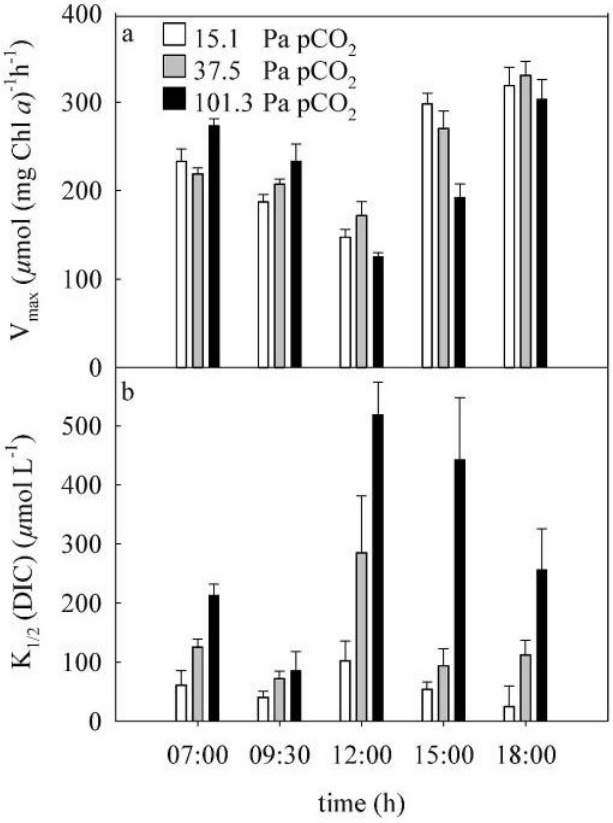

Fig. 5. Maximum rates (V_{max}) and half-saturation concentrations ($K_{1/2}$) of photosynthesis over a diurnal cycle acclimated to different pCO_2 conditions. Kinetic parameters were calculated from a Michaelis–Menten fit to the combined data of several independent measurements. Error bars denote ±SD.

Table 3. Contribution of HCO_3^- uptake relative to net C fixation. Values of MIMS measurement were obtained at 2 mmol L^{-1} DIC. Values of ^{14}C were obtained by fitting the ^{14}C incorporation pattern. Values represent the mean of three independent measurements ($n \geq 3$; ±SD).

		HCO_3^- uptake : C fixation	
Time (h)	pCO_2 (Pa)	MIMS	^{14}C disequilibrium
07:00	15.1	1.02±0.20	–
	37.5	1.01±0.08	–
	101.3	0.98±0.11	0.94±0.01
09:30	15.1	1.08±0.28	0.94±0.01
	37.5	1.02±0.19	0.95±0.01
	101.3	1.02±0.22	0.92±0.01
12:00	15.1	1.11±0.35	0.93±0.01
	37.5	1.09±0.31	0.93±0.01
	101.3	1.13±0.38	0.90±0.01
15:00	15.1	0.99±0.19	0.92±0.02
	37.5	0.98±0.15	0.93±0.01
	101.3	1.06±0.27	0.87±0.02
18:00	15.1	0.99±0.17	–
	37.5	1.01±0.24	–
	101.3	1.02±0.35	0.92±0.02

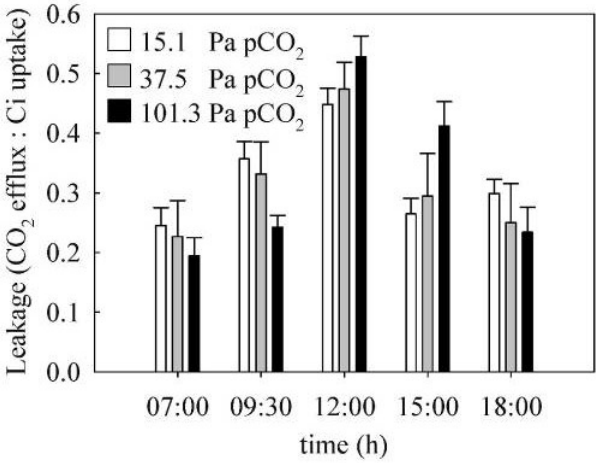

Fig. 6. Ratio of CO_2 efflux : gross Ci uptake in *Trichodesmium* at different acclimations over a day. Values indicate leakage measured with MIMS method calculated for the CO_2 concentrations in the acclimation. Data present mean values ($n \geq 3$; ±SD).

prevailed during glacial times and commonly occur under bloom conditions. Some of the strong CO_2 dependence observed by Barcelos e Ramos et al (2007) is also caused by reduced growth rates in the low pCO_2 range, which furthermore shows significant variability.

The carbon and nitrogen contents per cell increased at high pCO_2 compared to the lower pCO_2 acclimations (Figs. 1b,c) while the C : N ratios remained constant at ~4.6 (obtained at the beginning of the photoperiod). Measured carbon quotas and elemental ratios are comparable with those obtained by Hutchins et al. (2007) and similar to C : N ratios reported for the low pCO_2 acclimation by Barcelos e Ramos et al. (2007). However, in their study, the cell quotas for C and N decreased with increasing pCO_2, which is the opposite to the trend

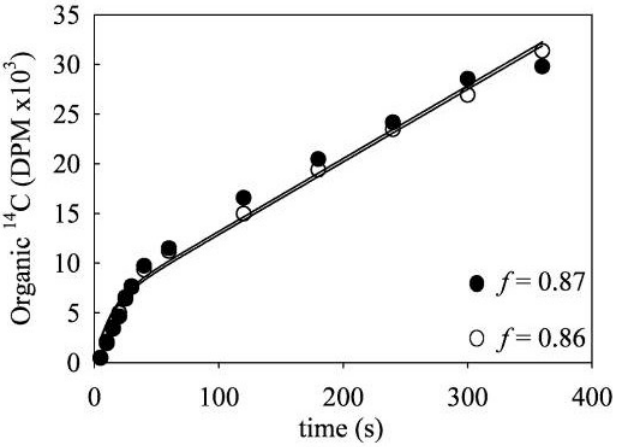

Fig. 7. Examples of disintegrations per minute (DPM) of ^{14}C during a short-term incubation of cells acclimated to 101.3 Pa CO_2 and measured at 15:00 h. Values of f in DBS-treated cells (closed symbols) and the control (open symbols) represent the proportion of HCO_3^- uptake relative to net C fixation.

observed by Levitan et al. (2007), who found an increase in C and N quota as well as the respective ratio under elevated pCO_2. In all studies, the observed magnitude in CO_2 sensitivity to carbon and N_2 fixation differed strongly. Using the acetylene reduction assay, Barcelos e Ramos et al. (2007) and Levitan et al. (2007) observed stimulation in N_2 fixation by approximately 40% and even up to 400%, while Hutchins et al. (2007) obtained stimulation by up to 35% over the respective CO_2 range. In our study, we assessed the process of N_2 fixation by measuring the production of particulate organic nitrogen. The results show a 40% increase in the production rates under high pCO_2 (Fig. 1c) as well as elevated C fixation (Fig. 1b). Both processes were equally stimulated, which is reflected by the constant C : N ratios. These findings are consistent with Barcelos e Ramos et al. (2007) and Hutchins et al. (2007), while in Levitan et al. (2007), C : N ratios increased with CO_2.

The discrepancy between studies may be attributed to differences in methodology (e.g., midexponential growth versus late stationary phase) or growth conditions (light intensities). Preliminary data (S. Kranz and O. Levitan unpubl. data) showed that light levels strongly influenced CO_2 dependency of growth as well as C and N quotas in *Trichodesmium*. Responses consistent within all mentioned studies on *Trichodesmium* show that elevated CO_2 stimulates both C and N_2 fixation rates

Diurnal variations in photosynthesis and N_2 fixation—Diazotrophic organisms have developed numerous strategies to fix N_2 efficiently (Berman-Frank et al. 2007). Nitrogenase, the enzyme that catalyzes the reduction of atmospheric N_2 to ammonia, is inhibited by O_2, and thus N_2 fixation has to be separated from photosynthetic O_2 evolution. In the nonheterocystous *Trichodesmium*, a distinct diurnal pattern of N_2 fixation and O_2 evolution has been observed (Berman-Frank et al. 2001*b*; Milligan et al. 2007). Our study verifies these diurnal rhythms, finding a pronounced decrease in photosynthesis and increased dark respiration during midday (Fig. 2b). The concomitant decrease in C : N ratio during that time also reflects increasing rates of N_2 fixation (Fig. 2a). Additionally, the Mehler reaction appears to be involved in light-dependent O_2 uptake during N_2 fixation (Kana 1993; Milligan et al. 2007). The inverse correlation between photosynthesis and respiration observed in the present and previous studies is caused by the fact that both processes share the same protein complex in the electron transport chain. Consequently, the increase in dark respiration results in a down-regulation of the water splitting in Photosystem II (PSII) due to a negative feedback reaction in the electron transport chain (Milligan et al. 2007).

Due to high adenosine triphosphate (ATP) and electron requirements, N_2 fixation is among the most costly processes for the cell next to carbon assimilation (Falkowski and Raven 2007). However, this process occurs during midday when photosynthesis is down-regulated and hence the ATP and nicotinamide adenine dinucleotide phosphate (NADPH) supply is low. The way in which *Trichodesmium* copes with this shortage in energy supply is not yet fully understood. Another enigma relates to CO_2 sensitivity in photosynthetic carbon assimilation and N_2 fixation, as both processes compete for ATP and reductants provided by the light reaction of photosynthesis. While external CO_2 levels could affect the C fixation directly by controlling the carboxylation efficiency of RubisCO or indirectly by modifying the energy costs of their CCM, there are currently no CO_2-related processes known to directly influence nitrogenase activities. The strong effects of CO_2 as well as diurnal changes in C and N fixation observed in this and previous studies must be reflected in the modes of carbon acquisition of *Trichodesmium*. In the following, we will characterize the CCM of *Trichodesmium*, the diurnal changes, and regulation with respect to CO_2 availability.

Carbonic anhydrase activities—External CA (eCA), which accelerates the interconversion between HCO_3^- and CO_2 at the cell surface, has been found to increase in response to decreasing CO_2 supply in various microalgal species (Berman-Frank et al. 1995; Rost et al. 2003). It is a common notion that eCA is involved in indirect HCO_3^- utilization by converting HCO_3^- to CO_2, which could then diffuse into the cell or be actively transported through the plasma membrane and subsequently used for photosynthesis (Sültemeyer et al. 1998; Elzenga et al. 2000). External CA activity in *Trichodesmium* was low—values of about 50 units per μg Chl *a*—and did not change with CO_2 supply (data not shown). In species that express significant quantities of eCA, activity is usually an order of magnitude higher (Rost et al. 2003; Trimborn et al. 2008). Moreover, there was no stimulation of photosynthesis by the addition of bovine CA (data not shown). The lack of significant eCA activity was further verified by the ^{14}C disequilibrium method (Elzenga et al. 2000), which yielded similar ^{14}C incorporation patterns in the presence and absence of DBS (Fig. 7). Consequently, the low activity and the lack of induction under low CO_2 supply indicate that eCA does not play an important, if any, role in the carbon acquisition by *Trichodesmium*.

Internal carbonic anhydrase (iCA) in cyanobacteria is required for the rapid conversion from HCO_3^- to CO_2 prior to the fixation by RubisCO. When interpreting iCA activity, as defined according to Palmqvist et al. (1994), one has to bear in mind that Δ values are in vivo estimates, which depend not only on the rate of intracellular ^{18}O depletion (i.e., CA activity) but also on the diffusive influx of doubly labelled CO_2 and, thus, on the diffusive properties of cyanobacterial membranes and cell shape. Therefore, despite being semiquantitative estimates, Δ values are still appropriate for direct comparison between treatments within the same species. Internal CA in *Trichodesmium* is presumably located in the carboxysome to operate near RubisCO (Price et al. 2008). These data show that *Trichodesmium* possesses low iCA activity, which is constitutively expressed. The iCA activity observed, despite being low, possibly reflects the CA activity inside the carboxysome catalyzing the interconversion between HCO_3^- and CO_2 (Price et al. 2008). In addition, the CO_2 uptake system in *Trichodesmium*, located

at the thylakoid membrane, functions like CA by accelerating the conversion of CO_2 into HCO_3^- (Price et al. 2008). However, this function may only play a role under illumination when electrons and NAD(P)H are available to drive this process.

Using the ^{18}O exchange technique, we examined the presence of light-dependent Ci transport systems. In the case of active Ci uptake, a decline in log (enrichment) during illumination would be expected as a result of an enhanced uptake of ^{18}O-labelled CO_2 and HCO_3^- into the cells, increased ^{18}O exchange catalyzed by internal CA, and subsequent efflux of ^{18}O-unlabelled CO_2 (Badger and Price 1989; Palmqvist et al. 1994). Such a net CO_2 efflux from photosynthetically active cells can only be explained by an active accumulation of Ci and the presence of iCA within the cells. As shown in Fig. 3, illumination resulted in a decrease of $^{13}C^{18}O_2$ ($m/z = 49$) due to uptake of labelled carbon species and an increase in $^{13}C^{16}O_2$ ($m/z = 45$) as a result of efflux of the latter. The consequent decrease in log (enrichment) was accompanied by an increase in oxygen production (data not shown). These patterns were measured in all acclimations throughout the photoperiod and are indicative of the presence of a CCM.

Photosynthetic O_2 evolution—Early studies demonstrated a CO_2-dependent regulation of the CCM of cyanobacteria (Kaplan et al. 1980). More recent studies have shown that the apparent affinity for Ci increases strongly with decreasing Ci availability in the culture medium (Woodger et al. 2003; Price et al. 2004). These studies typically compared present-day (i.e., ~37.5 Pa) with unnaturally high CO_2 levels (i.e., 2000–5000 Pa), and it is therefore not yet fully understood to what extent this regulation occurs under environmentally relevant CO_2 concentrations. In the present study, photosynthetic O_2 evolution as a function of CO_2 concentration was monitored to gain information about the overall efficiency and regulation of carbon acquisition in *Trichodesmium*. Half-saturation constants were generally lower (0.9–13.6 μmol L^{-1} CO_2) than those reported for cyanobacterial RubisCO (105–185 μmol L^{-1} CO_2; Badger et al. 1998). Moreover, we observed a gradual regulation by pCO_2 in the acclimations. While we obtained lowest apparent affinities for Ci at high pCO_2, maximum photosynthetic O_2 evolution rates were not affected in the bioassays (Fig. 5a; Table 2). The high apparent affinities, as well as the CO_2-dependent changes therein, demonstrate the operation of a CCM for *Trichodesmium*, and these findings are consistent with kinetics observed in other cyanobacteria (Sültemeyer 1998; Price et al. 2004).

The strongest variation in the CCM was, however, observed over the diurnal cycle. As an example, $K_{1/2}$ for photosynthetic O_2 evolution varied between 85 and 520 μmol L^{-1} DIC in the 101.3 Pa CO_2 treatment (Fig. 6b). This up- and down-regulation of the CCM is most likely associated with the diurnal pattern of N_2 fixation. During midday, when N_2 fixation is greatest, the apparent affinities as well as maximum rates for photosynthetic O_2 evolution are down-regulated. The down-regulation of the CCM and the up-regulation of dark- and light-dependent respiration (*see* previous discussion) result in lower net O_2 evolution, which is a prerequisite for efficient N_2 fixation, as shown previously (Berman-Frank et al. 2001*b*; Milligan et al. 2007). The trigger for this diurnal CCM regulation may be changes in the redox state of the photosynthetic electron chain, which could result from lower PSII activity in line with higher respiration in *Trichodesmium* and/or the concentration of photorespiratory metabolites (Kaplan et al. 2001).

Although the CO_2 dependence of O_2 evolution provides information about the efficiency and regulation of carbon acquisition, it cannot provide any details about the underlying mechanisms. To get a process-based understanding, we therefore have to look at the carbon source(s) and respective uptake kinetics.

Carbon source and uptake kinetics—An essential component of a CCM is the active uptake of inorganic carbon and its accumulation within the cell. Several methods have been employed to distinguish between CO_2 and HCO_3^- uptake in microalgae and cyanobacteria. In this study, estimates of CO_2 and HCO_3^- uptake were obtained by means of mass spectrometry (Badger et al. 1994) and the ^{14}C disequilibrium technique (Espie and Colman 1986; Elzenga et al. 2000). This is the first time such techniques have been applied to *Trichodesmium*.

Rates of CO_2 uptake determined by MIMS were very low in *Trichodesmium*, representing generally less than 10% relative to net carbon fixation (Table 2). Net CO_2 fluxes were low, even negative under some conditions, reflecting higher CO_2 efflux than uptake. Since the CO_2 uptake could not support the observed rates of photosynthesis, most of the inorganic carbon was taken up as HCO_3^- (Table 3). In the instances when net fluxes of CO_2 were negative, HCO_3^- uptake exceeded net fixation (Badger et al. 1994). The strong preference for HCO_3^- in *Trichodesmium* did not change with CO_2 treatments or photoperiod. These findings were confirmed by the ^{14}C disequilibrium method (Espie and Colman 1986; Elzenga et al. 2000), which showed on average 92% contribution of HCO_3^- uptake relative to net carbon fixation. Please note that the contribution of HCO_3^-, as determined by ^{14}C disequilibrium approach, can never exceed net fixation (Elzenga et al. 2000). These results are consistent with previous studies showing that CCMs in cyanobacteria are generally based on active HCO_3^- uptake (Price et al. 2008). With respect to the high accumulation of Ci necessary to compensate for their low-affinity RubisCO, cyanobacteria may prefer HCO_3^- over CO_2 because of the higher equilibrium concentration of HCO_3^- in marine systems. Moreover, as a charged molecule, HCO_3^- can be accumulated more efficiently in the cytoplasm than CO_2 (Price and Badger 1989).

The apparent affinities of the HCO_3^- uptake systems differed among CO_2 treatments and over the photoperiod. With decreasing CO_2 availability, apparent affinity for HCO_3^- uptake increased (Table 2), and this trend generally persisted throughout the photoperiod. Various studies have shown that changes in apparent affinity can be accomplished by expression of high versus low affinity transporters (Omata et al. 1999; Price et al. 2004) or by post-translational modifications of existing transport proteins,

e.g., by phosphorylation (Sültemeyer et al. 1998). For *Trichodesmium*, deoxyribonucleic acid (DNA) sequence analysis indicates the presence of one medium and/or low affinity HCO_3^- transporter (BicA) and a low-affinity NDH-1_4 CO_2 uptake system (Price et al. 2004, 2008). The observed $K_{1/2}$ values for HCO_3^- uptake and the low contribution of CO_2 to the overall uptake observed in our study support the findings from these molecular studies.

The uptake kinetics for HCO_3^- varied strongly over the photoperiod, although they were less pronounced than variations in photosynthetic O_2 evolution (Table 2). Apparent affinities for HCO_3^- were highest at the beginning of the photoperiod, with $K_{1/2}$ values between ~25 and 50 μmol L^{-1} HCO_3^-, and lowest during and following N_2 fixation, with $K_{1/2}$ values up to 190 μmol L^{-1} HCO_3^-. These diurnal variations in HCO_3^- transport efficiency occurred in all treatments but were more distinct under high pCO_2.

Changes in uptake kinetics, as in the HCO_3^- uptake system, may be caused by variations in the reductive state of photosynthetic electron transport carriers, which affect the balance between cyclic and linear electron transport and thus the energy supply for transporters (Li and Canvin 1998). With respect to diurnal changes in *Trichodesmium*, the electron flow can also be altered by the up-regulation of the Mehler reaction (Kana 1993; Milligan et al. 2007). As an O_2-consuming process, it can additionally effect the $[O_2]:[CO_2]$ ratio in the proximity of RubisCO, which has been suggested to be another trigger for the regulation of CCMs (Kaplan et al. 2001). Consequently, changes in the redox state of the photosynthetic electron transport carriers as well as the low $[O_2]:[CO_2]$ ratios during midday could have contributed to the observed down-regulation of the HCO_3^- uptake efficiency. The highly induced HCO_3^- uptake systems at the beginning of the photoperiod may have been triggered by light and the excess of electrons. An up-regulated CCM and consequently efficient Calvin cycle provides the best mechanism to drain electrons (photochemical quenching) and avoid photodamage, similar to the response observed in *Chlamydomonas reinhardtii* (Marcus et al. 1986). The frequently excessive HCO_3^- uptake observed may further provide a means to efficiently dissipate excess light energy (Tchernov et al. 1997). These and possibly other quenching mechanisms are important for *Trichodesmium*, since it thrives in low latitudes close to the surface, with high average irradiance.

Leakage—The efficiency of a CCM not only depends on the kinetics of the active carbon uptake systems but also on the loss of Ci via efflux. Leakage (ratio of Ci efflux to total Ci uptake) will increase the energetic costs of a CCM and/or decrease its capability to reach carbon saturation (Raven and Lucas 1985). Consequently, to increase the overall CCM efficiency, it is necessary to minimize the leakage. Following the approach by Badger et al. (1994), the MIMS was used to estimate leakage.

The MIMS approach yielded similar estimates for leakage in all pCO_2 treatments, yet the photoperiod imposed strong changes in leakage, with values as high as 0.55 during midday (Fig. 6). These high values were the result of increasing efflux combined with the down-regulation of total Ci uptake (Fig. 5; Table 2). As argued already, such high leakage might help to dissipate excess energy at times when PSII and Calvin cycle activity are down-regulated in *Trichodesmium*. Such modification of leakage will most likely be associated with a CO_2-trapping mechanism. It has been suggested that CO_2 efflux from the carboxysome is converted back to HCO_3^- by the PSII-associated NDH-CO_2 uptake system (Price et al. 2008). The diurnal changes in PSII activity (Berman-Frank et al. 2001*b*) may therefore directly regulate the effective leakage of the cell and thus explain most of the diurnal variation we observed in *Trichodesmium*. It should be noted, however, that the CO_2 efflux estimated according to Badger et al. (1994) is based on the assumptions that the rate of diffusive CO_2 efflux in the light is well represented by the first seconds upon darkening. Despite shortcomings in methodology, our data indicate that higher leakage, for instance during midday, reflect a down-regulation of the overall CCM activity, which is consistent with the lower affinities of the Ci uptake system during these times (Table 2; Fig. 5).

Ecological and biogeochemical implications—Diazotrophic cyanobacteria like *Trichodesmium* support a large fraction of biological productivity in tropical and subtropical areas and exert, over long timescales, a significant influence on global carbon cycles by providing a major source of reactive N to the water column (Falkowski and Raven 2007). Despite its global importance, studies have only recently begun to investigate the effect of elevated CO_2 on species such as *Trichodesmium* (Barcelos e Ramos et al. 2007; Hutchins et al. 2007; Levitan et al. 2007). This study, consistent with previous investigations, showed a strong increase in photosynthesis and N_2 fixation under elevated CO_2 levels. To the extent that we can extrapolate these laboratory experiments to the real ocean, the marine N_2 fixation by *Trichodesmium* could increase from present-day to future pCO_2 level by 40% (the present study) or even up to 400% (Levitan et al. 2007). Similarly, high sensitivity to changes in carbonate chemistry has been observed in photosynthesis (Barcelos e Ramos et al. 2007; Hutchins et al. 2007; Levitan et al. 2007; present study).The magnitude of these CO_2 effects would, if representative for the natural environment, have large implications for the future ocean.

The relevance of marine N_2 fixation is also expected to increase owing to the projected expansion of oligotrophic regions to higher latitudes as a result of surface ocean warming and increased stratification (Boyd and Doney 2002; Breitbarth et al. 2007). Elevated N_2 fixation in a future ocean will likely influence phytoplankton in terms of productivity and species composition, and thereby alter the microbial food web (Mulholland et al. 2006). In summary, CO_2-related effects on photosynthesis and N_2 fixation as well as the overall changes in the ecosystem would provide a negative feedback on the increase in atmospheric CO_2. Significant uncertainties remain, however, as to the degree of sensitivity to CO_2 and the modification of these responses by other environmental factors (e.g., P or Fe limitation). Moreover, it is still unknown whether the

observed responses in *Trichodesmium* can be generalized to include other important diazotrophic cyanobacteria.

The present study has taken a first step toward understanding the underlying processes behind strong CO_2 sensitivity by photosynthesis and N_2 fixation in *Trichodesmium*. This diazotrophic organism was found to operate an efficient CCM based almost entirely on direct HCO_3^- uptake. Consequently, a direct effect of elevated CO_2 on RubisCO carboxylation efficiency is unlikely (i.e., higher active or diffusive CO_2 uptake would increase internal CO_2/O_2 concentrations) or at least not the main reason for the CO_2 sensitivity observed. Instead, owing to the observed plasticity in CCM regulation, *Trichodesmium* may be able to optimize the allocation of resources (e.g., ATP and NADPH) between the CCM and other processes like N_2 fixation. Such a resource allocation would explain the influence of CO_2 on nitrogenase activity. In view of the potential ecological and biogeochemical implications, investigation into the regulation of photosynthesis, CCMs, and N_2 fixation in *Trichodesmium* and other important diazotrophs is clearly a research priority.

References

BADGER, M. R., T. J. ANDREWS, S. M. WHITNEY, M. LUDWIG, D. C. YELLOWLEES, W. LEGGAT, AND G. D. PRICE. 1998. The diversity and coevolution of Rubisco, plastids, pyrenoids, and chloroplast-based CO_2-concentrating mechanisms in algae. Can. J. Bot. **76:** 1052–1071.

———, K. PALMQVIST, AND J.-W. YU. 1994. Measurement of CO_2 and HCO_3^- fluxes in cyanobacteria and microalgae during steady-state photosynthesis. Physiol. Plant. **90:** 529–536.

———, AND G. D. PRICE. 1989. Carbonic anhydrase activity associated with the cyanobacterium *Synechococcus* PCC7942. Plant Physiol. **89:** 51–60.

BARCELOS E RAMOS, J., H. BISWAS, K. G. SCHULZ, J. LA ROCHE, AND U. RIEBESELL. 2007. Effect of rising atmospheric carbon dioxide on the marine nitrogen fixer *Trichodesmium*, Glob. Biogeochem. Cy. **21:** GB2028, doi:10.1029/2006GB002898.

BERMAN-FRANK, I., J. T. CULLEN, Y. SHAKED, R. M. SHERRELL, AND P. G. FALKOWSKI. 2001a. Iron availability, cellular iron quotas and nitrogen fixation in *Trichodesmium*. Limnol. Oceanogr. **46:** 1249–1260.

———, A. KAPLAN, T. ZOHARY, AND Z. DUBINSKY. 1995. Carbonic anhydrase activity in a natural bloom forming dinoflagellate. J. Phycol. **31:** 906–913.

———, P. LUNDGREN, Y. CHEN, H. KÜPPER, Z. KOLBER, B. BERGMAN, AND P. G. FALKOWSKI. 2001b. Segregation of nitrogen fixation and oxygenic photosynthesis in the marine cyanobacterium *Trichodesmium*. Science **294:** 1534–1537.

———, A. QUIGG, Z. V. FINKEL, A. J. IRWIN, AND L. HARAMATY. 2007. Nitrogen-fixation strategies and Fe requirements in cyanobacteria. Limnol. Oceanogr. **52:** 2260–2269.

BOYD, P. W., AND S. C. DONEY. 2002. Modelling regional responses by marine pelagic ecosystems to global climate change. Geophys. Res. Let. **29:** 1806, doi:10.1029/2001GL014130.

BREITBARTH, E., A. OSCHLIES, AND J. LA ROCHE. 2007. Physiological constraints on the global distribution of *Trichodesmium*—effect of temperature on diazotrophy. Biogeosciences **4:** 53–61.

BURKHARDT, S., AND U. RIEBESELL. 1997. CO_2 availability affects elemental composition (C : N : P) of the marine diatom *Skeletonema costatum*. Marine Ecology Progress Series **155:** 67–76.

CHEN, Y. B., J. P. ZEHR, AND M. MELLON. 1996. Growth and nitrogen fixation of the diazotropic filamentous nonheterocystous cyanobacterium *Trichodesmium* sp. IMS101 in defined media: Evidence for a circadian rhythm. J. Phycol. **32:** 916–923.

DICKSON, A. G., AND F. J. MILLERO. 1987. A comparison of the equilibrium constants for the dissociation of carbonic acid in seawater media. Deep-Sea Res. **34:** 1733–1743.

ELZENGA, J. T. M., H. B. A. PRINS, AND J. STEFELS. 2000. The role of extracellular carbonic anhydrase activity in inorganic carbon utilization of *Phaeocystis globosa* (Prymnesiophyceae): A comparison with other marine algae using the isotope disequilibrium technique. Limnol. Oceanogr. **45:** 372–380.

ESPIE, G. S., AND B. COLMAN. 1986. Inorganic carbon uptake during photosynthesis. A theoretical analysis using the isotope disequilibrium technique. Plant Physiol. **80:** 863–869.

FALKOWSKI, P. G., R. BARBER, AND V. SMETACEK. 1998. Biogeochemical controls and feedbacks on ocean primary production. Science **281:** 200–206.

———, AND J. A. RAVEN. 2007. Aquatic photosynthesis. Blackwell.

FU, F. X., AND P. R. F. BELL. 2003. Effect of salinity on growth, pigmentation, N_2-fixation and alkaline phosphatase activity of cultured *Trichodesmium* sp. Mar. Ecol. Prog. Ser. **257:** 69–76.

GRAN, G. 1952. Determinations of the equivalence point in potentiometric titrations of seawater with hydrochloric acid. Oceanol. Acta **5:** 209–218.

HUTCHINS, D. A., F.-X. FU, Y. ZHANG, M. E. WARNER, Y. FENG, K. PORTUNE, P. W. BERNHARDT, AND M. R. MULHOLLAND. 2007. CO_2 control of *Trichodesmium* N_2 fixation, photosynthesis, growth rates and elemental ratios: Implications for past, present and future ocean biogeochemistry. Limnol. Oceanogr. **52:** 1293–1304.

KANA, T. M. 1993. Rapid oxygen cycling in *Trichodesmium thiebautii*. Limnol. Oceanogr. **38:** 18–24.

KAPLAN, A., M. R. BADGER, AND J. A. BERRY. 1980. Photosynthesis and the intracellular inorganic carbon pool in the blue green alga *Anabaena variabilis*: Response to external CO_2 concentration. Planta **149:** 219–226.

———, Y. HELMAN, D. TCHERNOV, AND L. REINHOLD. 2001. Acclimation of photosynthetic microorganisms to changing ambient CO_2 concentration. Proc. Natl. Acad. Sci. USA **98:** 4817–4818.

LEVITAN, O., G. ROSENBERG, I. SETLIK, E. SETLIKOVA, J. GRIGEL, J. KLEPETAR, O. PRASIL, AND I. BERMAN-FRANK. 2007. Elevated CO_2 enhances nitrogen fixation and growth in the marine cyanobacterium *Trichodesmium*. Global Change Biol. **13:** 531–538.

LEWIS, E., AND D. W. R. WALLACE. 1998. Program developed for CO_2 system calculations. ORNL/CDIAC-105. Carbon Dioxide Information Analysis Center, Oak Ridge National Laboratory, U.S. Dept. Energy.

LI, Q. L., AND D. T. CANVIN. 1998. Energy sources for HCO_3^- and CO_2 transport in air-grown cells of *Synechococcus* UTEX 625. Plant Physiol. **116:** 1125–1132.

MAHAFFEY, C., A. F. MICHAELS, AND D. G. CAPONE. 2005. The conundrum of marine N_2 fixation. Am. J. Sci. **305:** 546–595.

MARCUS, Y., G. SCHUSTER, S. MICHAELS, AND A. KAPLAN. 1986. Adaptation to CO_2 level and changes in the phosphorylation of thylakoid proteins during the cell cycle of *Chlamydomonas reinhardtii*. Plant Physiol. **80:** 604–607.

MEHRBACH, C., C. CULBERSON, J. HAWLEY, AND R. PYTKOVICZ. 1973. Measurement of the apparent dissociation constants of carbonic acid in seawater at atmospheric pressure. Limnol. Oceanogr. **18:** 897–907.

MILLIGAN, A. J., I. BERMAN-FRANK, Y. GERCHMAN, G. C. DISMUKES, AND P. G. FALKOWSKI. 2007. Light-dependent oxygen consumption in nitrogen-fixing cyanobacteria plays a key role in nitrogenase protection. J. Phycol. **43:** 845–852.

MULHOLLAND, M. R., C. A. HEIL, D. A. BRONK, AND M. O. O'NEIL. 2006. Nitrogen fixation and release of fixed nitrogen by *Trichodesmium* sp. in the Gulf of Mexico. Limnol. Oceanogr. **51:** 1762–1776.

NIELSEN, M. V. 1995. Photosynthetic characteristics of the coccolithophorid *Emiliania huxleyi* (Prymnesiophyceae) exposed to elevated concentrations of dissolved inorganic carbon. J. Phycol. **31:** 715–719.

OMATA, T., G. D. PRICE, M. R. BADGER, M. OKAMURA, S. GOHTA, AND T. I. OGAWA. 1999. Identification of an ATP-binding cassette transporter involved in bicarbonate uptake in the cyanobacterium *Synechococcus* sp. strain PCC 7942. Proc. Natl. Acad. Sci. USA **96:** 13571–13576.

PALMQVIST, K., J.-W. YU, AND M. R. BADGER. 1994. Carbonic anhydrase activity and inorganic carbon fluxes in low- and high-Ci cells of *Chlamydomonas reinhardtii* and *Scenedesmus obliquus*. Physiologia Plantarum **90:** 537–547.

PRICE, G. D., AND M. R. BADGER. 1989. Expression of human carbonic anhydrase in the cyanobacterium *Synechococcus* PCC7942 creates a high CO_2–requiring phenotype: Evidence for a central role for carboxysomes in the CO_2-concentrating-mechanism. Plant Physiol. **91:** 505–513.

———, M. R. BADGER, F. J. WOODGER, AND B. M. LONG. 2008. Advances in understanding the cyanobacterial CO_2-concentrating-mechanism (CCM): Functional components, Ci transporters, diversity, genetic regulation and prospects for engineering into plants. J. Exp. Bot. **59:** 1441–1461.

———, F. J. WOODGER, M. R. BADGER, S. M. HOWITT, AND L. TUCKER. 2004. Identification of a SulP-type bicarbonate transporter in marine cyanobacteria. Proc. Natl. Acad. Sci. USA **101:** 18228–18233.

PRUFERT-BEBOUT, L., H. W. PAERL, AND C. LARSEN. 1993. Growth, nitrogen fixation, and spectral attenuation in cultivated *Trichodesmium* species. Appl. Environ. Microbiol. **59:** 1367–1375.

RAUPACH, M. R., G. MARLAND, P. CIAIS, C. LE QUÉRÉ, J. G. CANADELL, G. KLEPPER, AND C. B. FIELD. 2007. Global and regional drivers of accelerating CO_2 emissions. Proc. Natl. Acad. Sci. USA **104:** 10288–10293, doi:10.1073/pnas.0700609104.

RAVEN, J. A., AND W. J. LUCAS. 1985. Energy costs of carbon acquisition, p. 305–324. *In* W. J. Lucas and J. A. Berry [eds.], Inorganic carbon uptake by aquatic photosynthetic organisms. American Society of Plant Physiologists.

RIEBESELL, U., D. A. WOLF-GLADROW, AND V. SMETACEK. 1993. Carbon dioxide limitation of marine phytoplankton growth rates. Nature **361:** 249–251.

ROST, B., S. A. KRANZ, K.-U. RICHTER, AND P. TORTELL. 2007. Isotope disequilibrium and mass spectrometric studies of inorganic carbon acquisition by phytoplankton. Limnol. Oceanogr. Methods **5:** 328–337.

———, U. RIEBESELL, S. BURKHARDT, AND D. SÜLTEMEYER. 2003. Carbon acquisition of bloom-forming marine phytoplankton. Limnol. Oceanogr. **48:** 55–67.

SCHLESINGER, W. H. 2005. Biogeochemistry. Elsevier.

SILVERMAN, D. N. 1982. Carbonic anhydrase. Oxygen-18 exchange catalyzed by an enzyme with rate contributing proton-transfer steps. Methods Enzymol. **87:** 732–752.

SÜLTEMEYER, D. 1998. Carbonic anhydrase in eukaryotic algae: Characterization, regulation, and possible function during photosynthesis. Can. J. Bot. **76:** 962–972.

———, B. KLUGHAMMER, M. R. BADGER, AND G. D. PRICE. 1998. Protein phosphorylation and its possible involvement in the induction of the high-affinity CO_2-concentrating mechanism in cyanobacteria. Can. J. Bot. **76:** 954–961.

TCHERNOV, D., M. HASSIDIM, B. LUZ, A. SUKENIK, L. REINHOLD, AND A. KAPLAN. 1997. Sustained net CO_2 evolution during photosynthesis by marine microorganisms. Curr. Biol. **7:** 723–728.

TRIMBORN, S., N. LUNDHOLM, S. THOMS, K.-U. RICHTER, B. KROCK, P. J. HANSEN, AND B. ROST. 2008. Inorganic carbon acquisition in potentially toxic and non-toxic diatoms: The effect of pH-induced changes in the seawater carbonate chemistry. Physiologia Plantarum **133:** 92–105, doi:10.1111/j.1399-3054.2007.01038.x.

WOODGER, F. J., M. R. BADGER, AND G. D. PRICE. 2003. Inorganic carbon limitation induces transcripts encoding components of the CO_2-concentrating mechanism in *Synechococcus* sp. PCC7942 through a redox-independent pathway. Plant Physiol. **133:** 2069–2080.

Edited by: John Albert Raven

Received: 23 June 2008
Amended: 04 December 2008
Accepted: 05 December 2008

Publication III

Combined effects of CO_2 and light on the N_2 fixing cyanobacteria *Trichodesmium* IMS101: Physiological responses

Sven A. Kranz[1], Orly Levitan[2], Klaus-Uwe Richter[1], Ondřej Prášil[3], Ilana Berman-Frank[2] and Björn Rost[1]

[1] Alfred Wegener Institute for Polar and Marine Research, 27570 Bremerhaven, Germany
[2] Mina and Everard Goodman Faculty of Life Sciences, Bar Ilan University, Ramat-Gan, Israel
[3] Institute of Microbiology ASCR, Laboratory of Photosynthesis, Třeboň, Czech Republic

Abstract:

Recent studies on the diazotrophic cyanobacteria *Trichodesmium erythraeum* (IMS101) showed that increasing pCO_2 availability enhances N fixation and growth. Significant uncertainties remain as to the degree of the sensitivity to pCO_2, its modification by other environmental factors, and underlying processes causing these responses. To address these questions we examined the responses of *Trichodesmium* IMS101 grown under a matrix of low and high levels of pCO_2 (150 and 900 µatm) and irradiance (50 and 200 µmol photons m^{-2} s^{-1}). Growth rates as well as cellular C and N content increased with increasing pCO_2 and light levels in the cultures. The pCO_2-dependent stimulation in organic C and N production was highest under low-light. High pCO_2 stimulated rates of N_2 fixation and prolonged the duration while high light affected maximum rates only. Gross photosynthesis increased with light, but did not change with pCO_2. HCO_3^- was identified as the predominant carbon source taken up in all treatments. Inorganic carbon fluxes increased with light, but only gross CO_2 uptake was enhanced under high pCO_2. Light-dependent O_2 uptake was only detected under low pCO_2 combined with high-light or when low-light-acclimated cells were exposed to high-light, indicating that Mehler reaction functions also as a photo-protective mechanism in *Trichodesmium*. Our data confirm the pronounced pCO_2 effect on nitrogen fixation and growth in *Trichodesmium* and further show a strong modulation of these effects by light intensity. We attribute these responses to changes in the allocation of photosynthetic energy between carbon acquisition and the assimilation of C and N under elevated pCO_2. These findings are supported by a complementary study (Levitan et al, this issue), looking at photosynthetic fluorescence parameters of PSII, photosynthetic units stoichiometry (PSI:PSII) and pool sizes of key proteins in the carbon and nitrogen acquisition.

Introduction:

Human-induced climate change will significantly alter the marine environment within the next century and beyond. Future scenarios predict an increase from currently ~380 to about 750-1000 µatm pCO_2 in the atmosphere until the end of this century (Raven et al., 2005; Raupach et al., 2007). As the ocean takes up this anthropogenic pCO_2, the dissolved inorganic carbon (DIC) in the surface ocean increases while the pH decreases (Wolf-Gladrow et al., 1999). Rising global temperatures will increase surface ocean stratification, which may affect the light regime in the upper mixed layer as well as nutrient input from deeper waters (Doney, 2006). Uncertainties remain regarding both the magnitude of the physico-chemical changes and the biological responses of organisms including species and populations of the oceanic primary producers at the foundation of the food webs.

In view of potential ecological implications and feedbacks on climate, several studies have examined pCO_2 sensitivity in phytoplankton key species (Burkhardt and Riebesell, 1997; Riebesell et al., 2000; Rost et al., 2003; Tortell et al., 2008). Pronounced responses to elevated pCO_2 were observed in N_2 fixing cyanobacteria (Barcelos é Ramos et al., 2007; Hutchins et al., 2007; Levitan et al., 2007; Fu et al., 2008; Kranz et al., 2009), which play a vital role in marine ecosystems by providing a new source of biologically available nitrogen-species to otherwise nitrogen-limited regions. Recent studies focused on the impact of different environmental factors on the filamentous *Trichodesmium spp.*, which is known for high abundances and the formation of massive blooms in the tropical and subtropical areas (Capone et al., 2005; Mahaffey et al., 2005). Higher pCO_2 levels stimulated growth rates, biomass production and N_2 fixation (Hutchins et al., 2007; Levitan et al., 2007; Kranz et al., 2009) and affected inorganic carbon acquisition of the cells (Kranz et al., 2009). While elevated sea surface temperatures is predicted to shift the spatial distribution of *Trichodesmium spp*. towards higher latitudes (Breitbarth et al., 2007), the combined effects of pCO_2 and temperature may favor this species and extend its niche even farther (Hutchins et al., 2007). An increase in the average light intensity, caused by the predicted shoaling of the upper mixed layer, may further stimulate both growth and N_2 fixation of *Trichodesmium* (Breitbarth et al., 2008). Combined effects of light and pCO_2 have to our knowledge, not been studied yet, although these environmental factors are likely to influence photosynthesis and other key processes in *Trichodesmium*.

To understand the responses of an organism to changes in environmental conditions, metabolic processes must be studied. In *Trichodesmium*, photosynthetically generated energy (ATP and NADPH) is primarily used for the fixation of CO_2 in the Calvin-Benson cycle. A large

proportion of this energy is, however, also required for the process of N_2 fixation via nitrogenase and for the operation of a CO_2-concentrating mechanism (CCM). The latter involves active uptake of inorganic carbon, which functions to increase the rate of carboxylation reaction mediated by RubisCO. This ancient and highly conserved enzyme is characterized by low affinities for its substrate CO_2 and a susceptibility to a competing reaction with O_2, which initiates photorespiration (Badger et al., 1998). As cyanobacterial RubisCO possesses one of the lowest CO_2 affinities among phytoplankton (Badger et al., 1998), a considerable amount of resources have to be invested to achieve sufficient rates of C fixation and to avoid photorespiration. A first step towards a mechanistic understanding of responses in *Trichodesmium* has been taken by Levitan et al. (2007), focusing on pCO_2-dependency of nitrogenase activity and photosynthesis. Subsequently, Kranz et al. (2009) described variations in CCM efficiency with pCO_2 and suggested that the observed plasticity in CCM regulation allowed energetic re-allocation under high pCO_2 which may explain the observed pCO_2-dependent changes in nitrogenase activity, growth, and elemental composition (Barcelos é Ramos et al., 2007; Hutchins et al., 2007; Levitan et al., 2007).

In the present study, we measured growth responses as well as metabolic key processes in *Trichodesmium* IMS101 under environmental conditions that likely alter the energy budget and/or energy allocation of the cell. Cultures were acclimated to a matrix of low and high pCO_2 (150 and 900 µatm) at two different light intensities (50 and 200 µmol photons m^{-2} s^{-1}). For each of the four treatments, changes in growth rates, elemental ratios and the accumulation of elemental C and N were measured. Metabolic processes (gross photosynthesis, CCM activity, C fixation and O_2 uptake) were obtained by means of membrane-inlet mass spectrometry (MIMS) while N_2 fixation was detected by gas chromatography. As these processes may vary over the diurnal cycle in *Trichodesmium* (Berman-Frank et al., 2001; Kranz et al., 2009) measurements were performed in the morning and around midday. The results on metabolic processes were accompanied by measurements on fluorescence of PSII, ratios of the photosynthetic units (PSI:PSII), and pool sizes of key proteins involved in the C and N fixation as well as assimilation (Levitan et al., same issue).

Material and Methods:

Culture conditions

Cultures of *Trichodesmium sp*. IMS 101 (originally isolated by Prufert-Bebout et al., 1993) were grown at 25°C in 0.2 μm-filtered unbuffered N-free YBCII media (Chen et al., 1996). All cells were cultured as single filaments, grown in 1-liter cylindrical glass flasks (diameter 7 cm) and incubated at a "12:12 h light:dark" cycle with light provided by white fluorescence bulbs (Osram, BIOLUX) at two different light intensities (50 and 200 µmol photons m^{-2} s^{-1}). Cultures were continuously bubbled with air containing different CO_2 partial pressures (pCO_2) of 150 and 900 µatm. The bubbling was sufficient to avoid aggregate formation, but did not alter the integrity of the filaments. CO_2 gas mixtures were generated with gas-mixing pumps (Digamix 5KA18/8-F and 5KA36/8-F, Woesthoff GmbH), using CO_2-free air (Nitrox CO_2RP280; Domnick Hunter) and pure CO_2 (Air Liquide Deutschland). Dilute batch cultivation, i.e. regular dilution with fresh, pre-equilibrated media, ensured that the carbonate chemistry remained constant and cells stayed in the mid-exponential growth phase. Cultures in which the pH shifted (pH shift >0.06) in comparison to a reference (i.e. cell-free media at the respective pCO_2 levels) were excluded from further analysis.

Seawater carbonate chemistry

Samples for total alkalinity (TA) were taken from the cultures filtrate (Whatman GFF filter; ~0.6 µm), stored in 100 ml borosilicate bottles at room temperature, and measured by potentiometric titration (Brewer et al., 1981) with an average precision of ±10 µmol kg^{-1}. TA was calculated from linear Gran Plots (Gran, 1952). TA measurements were calibrated with certified reference material (Dr. Andrew Dickson; Scripps Institution of Oceanography). The pH_{NBS} was determined every morning, using a pH/ion meter (model 713 pH Meter, Metrohm). The carbonate system was calculated from TA, pH_{NBS}, temperature, salinity and phosphate using CO2Sys (Lewis and Wallace, 1998). Equilibrium constants of Mehrbach et al. (1973) refitted by Dickson and Millero (1987) were chosen. Carbonate chemistry for the respective pCO_2 treatments are given in Table I.

Elemental composition, growth, and production rates

Cells were acclimated to the respective pCO_2 and light levels for at least 30 days (>10 generations) prior to harvesting. In all acclimations, samples for growth responses were taken simultaneously at the beginning of the photoperiod to account for diurnal changes. Cell densities

were determined using an inverted microscope (Zeiss, Axiovert 200) by measuring the number and the length of filaments as well as the cell size in a Sedgwick-Rafter Cell (S50, Graticules).

Samples for particulate organic carbon (POC), nitrogen (PON) and phosphorus (PP) were filtered onto precombusted (500°C; 9 h) glass fibre filters (GFF) and stored in precombusted (500°C; 9 h) petri dishes at -20°C. Prior to analysis, filters for POC were treated with 200 μL HCl (0.1 N) to remove all inorganic carbon. POC and PON filters were measured in duplicate with an EA mass spectrometer (ANCA-SL 2020), with an average precision of ± 1 µg C and ± 0.5 µg N, respectively. Particulate P was measured photometrically by using a modified version of the ALOHA protocol (Hawaii Institute of Marine Biology, Analytical Services laboratory at the University of Hawaii).

Growth, POC and PON production rates were determined based on changes in cell density, chlorophyll *a* (chl *a*), as well as POC and PON. Growth rates (μ) were calculated according to the following equation:

$$\mu[\mathrm{d}^{-1}] = \frac{\ln(N_1) - \ln(N_0)}{\Delta t} \quad (1)$$

where N_0 and N_1 are concentrations (cell, chl *a,* POC, PON) at the beginning (t_o) and the end of sampling (t_1), and Δt is the time between sampling intervals. Production rates of POC and PON were calculated according to the following equations:

$$\text{POC production} = \mu \times \text{POC cell}^{-1} \quad (2)$$

$$\text{PON production} = \mu \times \text{PON cell}^{-1} \quad (3)$$

Samples for chl *a* were filtered on GF/filters and immediately stored at -80°C. Chl *a* was subsequently extracted in 5-10 mL 90% acetone (overnight in darkness, at 4°C) and determined with a fluorometer (Turner Designs) by measuring non-acidified and acidified fluorescence.

N_2 fixation

Rates of N_2 fixation were estimated using the acetylene reduction assay (Capone, 1993). The samples (concentrations between 0.02 and 0.08 µg chl *a* ml^{-1}) were spiked with acetylene (20% of headspace volume) and incubated for 1 h at acclimation light and temperature with gentle continuous shaking of the bottles to avoid aggregation or settlement. The rate of acetylene reduction to ethylene was measured using a gas chromatograph with a flame-ionization detector (Thermo Finnigan Trace GC) and quantified relative to an ethylene standard. Rates were normalized to chl *a* and a conversion factor of "4:1" (Capone and Montoya, 2001) was applied to convert ethylene production to N_2 fixation rates. Results were then normalized to chl *a*. To

account for the diurnal patterns, nitrogen fixation rates were measured every 2 hours from the onset of light until 2 hours after dark.

Photosynthetic O_2 evolution, O_2 uptake and C fixation

Rates of gross and net O_2 production, O_2 uptake and C fixation were measured by membrane-inlet mass spectrometry (MIMS). All MIMS measurements were carried out in an 8 mL thermostated cuvette, which was attached to a sectorfield multicollector mass spectrometer (Isoprime; GV Instruments) via a gas-permeable membrane (PTFE, 0.01 mm) inlet system. O_2 evolving and O_2 consuming processes can be separated in the light by measuring $^{16}O_2$ evolution from water-splitting and $^{18}O_2$ uptake from the medium. To this end, the media was initially bubbled with nitrogen to remove all the $^{16}O_2$ and then enriched with $^{18}O_2$, ensuring that mainly $^{18}O_2$ is taken up by O_2 consuming processes. For further details on the calculations of O_2 fluxes the reader is referred to Peltier and Thibault (1985) and Fock and Sültemeyer (1989). Rates of net C fixation and respiration were deduced from changes in CO_2 concentrations in the media, using the pH-dependent CO_2/DIC ratios determined as part of the daily calibration. Rates of gross C fixation were calculated by adding rates of respiration to net C fixation.

Assays were performed in YBCII media buffered with HEPES (50 mM, pH 7.8) or BICINE (50 mM, pH 8.4) depending on the respective pCO_2 of the acclimation. To obtain assay conditions, the medium was purged with N_2 overnight, subsequently sealed in 40 ml glass bottles, and spiked with 20-40 µl $^{18}O_2$ to yield air-equilibrated O_2 concentrations (i.e. 21%). For measurements, cells were concentrated by gentle filtration (8 µm; Isopore, Millipore). The culture medium was exchanged stepwise with the $^{18}O_2$-enriched assay media and cells were subsequently transferred to the MIMS cuvette.

Measurements were performed at acclimation light (50 and 200 µmol photons m^{-2} s^{-1}) and DIC levels (~1900 and 2300 µmol DIC) if not mentioned otherwise. Light and dark intervals lasted 6 min to obtain O_2 and C fluxes under steady-state conditions. DIC concentrations were adjusted by addition of a 1 M HCO_3^- solution prior to measurements. The required equilibrium in the carbonate system, a prerequisite to convert CO_2 traces into C fixation and respiration, was ensured by adding carbonic anhydrase (20 µM bovine CA, Sigma). To differentiate between photosynthetic and respiratory electron transport, DCMU, an inhibitor of PSII, was added to a final concentration of 2.5 µM to block photosynthetic electron flow and thus O_2 evolution during the measurement.

Inorganic carbon acquisition and leakage

Uptake of inorganic carbon sources for photosynthesis were determined by MIMS measurements. This approach is based on simultaneous measurements of O_2 and CO_2 during consecutive light and dark intervals at steady-state photosynthesis. Net photosynthesis, CO_2 uptake, and HCO_3^- uptake were calculated according to the equations of Badger et al. (1994). For measurements, cells were concentrated in the same manner as for the O_2 flux measurements, exchanging growth media with assay media (pH 7.8 and 8.4) containing air-equilibrated O_2 levels. Light and dark intervals during the assay lasted 6 min. Light was adjusted to the respective photon flux densities in the acclimation (50 and 200 µmol photons m^{-2} s^{-1}). To completely inhibit external carbonic anhydrase activity, dextrane-bound sulphonamide (DBS) was added to a final concentration of 50 μmol L^{-1}. Results were normalized to chl *a* (concentration in the assay ranged from 0.5 to 2 μg chl *a* mL^{-1}). Further details on the method and calculations are given in Badger et al. (1994) and Rost et al. (2007).

Isotopic composition was determined by EA-mass spectrometry (ANCA-SL 2020) to obtain information about inorganic carbon leakage (CO_2 efflux:C uptake) following the approach by Rost et al.(2006). Values for isotopic composition of POC ($\delta^{13}C_{POC}$) are reported relative to the Pee Dee Belemnite standard (PDB) in ‰. Isotopic fractionation during POC formation (ε_p) was calculated relative to the isotopic composition of CO_2 ($\delta^{13}C_{CO2}$) in the medium. To determine the isotopic composition of DIC ($\delta^{13}C_{DIC}$), 8 mL of the culture medium was fixed with $HgCl_2$ (~110 mg L^{-1} final concentration). Extractions and measurements were performed in the laboratory of H. J. Spero (University of California, Davis) with a precision of ± 0.11‰. The isotopic composition of CO_2 ($\delta^{13}C_{CO2}$) was calculated from $\delta^{13}C_{DIC}$, following a mass balance equation (Zeebe and Wolf-Gladrow, 2007).

Isotopic fractionation is driven by the intrinsic discrimination of ^{13}C by RubisCO (ε_f), setting the upper most values for ε_P. Variations in fractionation are principally determined by changes in leakage as well as carbon source taken up (Sharkey and Berry, 1985):

$$\varepsilon_P = a \times \varepsilon_s + L \times \varepsilon_f \quad (4)$$

where ε_f is assumed to be ~25‰ (Guy et al., 1993), ε_s represents the equilibrium fractionation between CO_2 and HCO_3^-, and *a* is the fractional contribution of HCO_3^- to total C uptake. Since HCO_3^- is about 9‰ enriched in ^{13}C relative to CO_2 (Zeebe and Wolf-Gladrow, 2007), an increasing proportion of HCO_3^- uptake reduces the ε_P value, which is defined relative to CO_2 as the carbon source. If there is no change in carbon source, ε_P increases with increasing leakage.

Results:

Elemental composition, growth and production rates

Cellular quotas of POC and PON increased with both pCO_2 and light, while PP quotas remained constant in all treatments (P >0.05 One-way ANOVA for PP) (Table II). POC quota ranged between 3.79 ±0.09 and 4.51 ±0.21 pmol $cell^{-1}$ under low-light and 4.60 ±0.46 and 5.02 ±0.57 pmol $cell^{-1}$ under high-light. Elevated pCO_2 significantly increased the POC $cell^{-1}$ by 19% at low-light (P=0.001; t-test,) and by 9%, although not significant, at high-light treatments (P=0.226; t-test), respectively (Table II). PON quotas exhibited similar patterns, with values ranging from 0.59 ±0.03 to 0.88 ±0.06 pmol $cell^{-1}$ under low-light and 0.86 ±0.08 to 1.04 ±0.09 pmol $cell^{-1}$ under high-light at low and high pCO_2, respectively (Table II). The pCO_2-dependent changes in PON quota were even larger than those of the POC, with a significant increase by 47% under low-light (P<0.001, t-test) and 21% under high-light (P<0.05, t-test). Respective C to N ratios decreased from 6.41 ±0.39 to 5.04 ±0.15 under low-light (P<0.05 One-way ANOVA followed by a post doc test) and from 5.25 ±0.19 to 4.85 ±0.10 under high-light (P=0.09 One-way ANOVA followed by a post doc test)with increasing pCO_2 (Table II). Chlorophyll (chl *a* $cell^{-1}$) did not differ significantly between treatments, excluding cells grown under low-light and low pCO_2 (P<0.001, One-way ANOVA followed by a post hoc test, Table II).

Growth increased significantly with both elevated pCO_2 and higher light (P<0.001, One-way ANOVA followed by a post hoc, Table II). There was no difference between growth rate estimates whether based on changes in cell densities, chl *a*, POC or PON and thus were reported as mean values. Doubling times ranged between 0.15 ±0.03 and 0.24 ±0.03 d^{-1} at low-light and from 0.38 ±0.02 to 0.42 ±0.02 d^{-1} at high-light (Table II, Fig 1A). Elevated pCO_2 increased growth rates by 60% under low-light and by 11% under the high-light treatment. Rates of POC production also increased significantly under elevated pCO_2 (P<0.001, t-test), ranging between 0.57 ±0.11 and 1.10 ±0.17 pmol C $cell^{-1}$ d^{-1} under low-light and 1.76 ±0.26 and 2.12 ±0.34 pmol C $cell^{-1}$ d^{-1} under high-light (Fig. 1B, Table II). The PON production increased under elevated pCO_2 (P<0.001, t-test), ranging between 0.09 ±0.02 and 0.21 ±0.04 pmol N $cell^{-1}$ d^{-1} under low-light and 0.33 ±0.05 and 0.44 ±0.06 pmol N $cell^{-1}$ d^{-1} under high-light (Fig. 1B, Table II). Notably, at low-light, elevated pCO_2 caused the strongest relative increase in POC and PON production, being 93% and 133% higher than under low pCO_2, respectively.

N_2 fixation

Both the diurnal pattern and the rates of N_2 fixation responded strongly to pCO_2 and light (Fig. 2). For the low-light acclimations, N_2 fixation peaked 3 hours after the beginning of the photoperiod with maximum rates, which range between 1.61 ±0.51 to 3.03 ±0.56 nmol N_2 chl a^{-1} h^{-1} for low and high pCO_2, respectively. Under high-light, both pCO_2 acclimations peaked about 5 hours after the onset of light and maximum rates were 15.45 ±1.29 and 19.21 ±6.48 nmol N_2 chl a^{-1} h^{-1} for the low and high pCO_2 treatments, respectively (Fig. 2). Elevated pCO_2 increased maximum rates about 2-fold under low-light, while maximum rates appear not to differ at high-light. More prominently, under high-light, elevated pCO_2 yielded in a prolonged phase with high N_2 fixation rates, that lasted until the end of the photoperiod. This pCO_2 effect on the diurnal cycle was also present but less pronounced under low-light. N_2 fixation during the dark period was absence in all acclimations. As a result of the higher fixation rates and the prolonged N_2 fixation under elevated pCO_2, the integrated diurnal values of N_2 fixation increased by 199% and 112% under low and high-light, respectively.

Photosynthetic O_2 evolution, O_2 uptake and C fixation

Gross O_2 evolution increased with light but was neither affected by pCO_2 nor varied between measurements performed about 2-3 hours (morning) and 6-7 hours (midday) after the beginning of the photoperiod (Fig 3A, Table III). O_2 evolution ranged between 119 ±22 and 156 ±4 µmol O_2 µg chl a^{-1} h^{-1} at low-light and 432 ±153 and 534 ±51 µmol O_2 µg chl a^{-1} h^{-1} at high-light (Fig. 3a, Table III). Oxygen uptake in the light was present in all treatments (Fig. 3B), yet rates were not significantly enhanced ($P > 0.05$, t-test) compared to those determined in the dark in all, except the 150 µatm pCO_2 at 200 µmol photons m^{-2} s^{-1} treatment (Table III). In the latter, O_2 uptake significantly exceeded dark respiration by about 140% ($P<0.001$, t-test) in the morning and about 70% during midday ($P<0.001$, t-test) (Table III), showing light-dependent O_2 uptake. Light-dependent O_2 uptake was also induced when 50 µmol photons m^{-2} s^{-1} acclimated cells were exposed to 200 µmol photons m^{-2} s^{-1} during the measurements, irrespective of the pCO_2 level of the acclimation (Table III). Such instantaneous effects were also observed in the gross O_2 evolution, i.e. low-light acclimated cells exposed to high-light yielded rates similar to cells that had been acclimated to high-light. Gross C fixation rates ranged between 145 ±22 and 324 ±112 µmol C µg chl a^{-1} h^{-1} in the low-light and 487 ±192 and 582 ±94 µmol C µg chl a^{-1} h^{-1} in the high-light acclimated cells and did not vary with pCO_2 or over the day.

Inorganic carbon acquisition and leakage

HCO_3^- was the major inorganic carbon source taken up by *Trichodesmium* under all acclimations, while CO_2 contributed only a minor fraction. Rates of HCO_3^- uptake were affected by both light and pCO_2, ranging from 82 ±19 to 121 ±25 µmol HCO_3^- chl a^{-1} h^{-1} in low-light and from 196 ±29 to 287 ±50 µmol HCO_3^- chl a^{-1} h^{-1} in high-light at low and high pCO_2, respectively (Table III). Under low-light, HCO_3^- uptake slightly decreased, although not significantly ($P>0.05$, One-way ANOVA followed by a post hoc Holm-Sidak test), when cultures were acclimated to high pCO_2. Under high-light, HCO_3^- uptake remained relatively stable at both pCO_2 levels. Rates of gross CO_2 uptake were affected by both light and pCO_2, ranging between 10 ±1 and 53 ±9 µmol CO_2 chl a^{-1} h^{-1} in low-light and 59 ±6 and 147 ±31 µmol CO_2 chl a^{-1} h^{-1} at high-light at low and high pCO_2 respectively (Table III). Gross CO_2 uptake rates were significantly enhanced by 50 to 210% in the high compared to the low pCO_2 acclimation ($P<0.001$, t-test). To illustrate the contribution of each carbon species to the total carbon uptake, the ratio of HCO_3^- uptake to gross CO_2 uptake (HCO_3^-:CO_2) was calculated (Figure 4). Ratios ranged between 2 and 10, reflecting that HCO_3^- was the major carbon species taken up in all treatments. The increased relevance of CO_2 uptake was indicated by the declining HCO_3^- to CO_2 ratios under elevated pCO_2 and high-light. Rates of net O_2 evolution obtained in these assays (data not shown) were similar to those obtained in the assays on O_2 fluxes (Tab. III).

The cellular leakage, i.e., the ratio between the C efflux and total C uptake, was estimated from ^{13}C fractionation (Sharkey and Berry, 1985; Rost et al., 2006). Under low pCO_2, isotopic fractionation (ε_p) was relatively low with values of 12.94 ±0.78‰ and 7.19 ±0.58‰ at low and high-light, respectively (Fig. 5). Higher ε_p values were observed under elevated pCO_2, being 15.69 ±1.12‰ and 16.54 ±0.10‰ at low and high-light, respectively. In the low pCO_2 acclimation, the calculated leakage of CO_2 ranged between 0.57 ±0.01 at high-light and 0.84 ±0.01 at low-light, and was ~0.90 ±0.01 in both high pCO_2 acclimations (Fig. 5).

Discussion:

The results of our study confirm the pronounced pCO_2 effect on nitrogen fixation and growth in *Trichodesmium* and further show a strong modulation of these effects by irradiance. Cellular gas exchange measurements revealed pCO_2-dependent changes in rates of N_2 fixation over the

course of the photoperiod, as well as in modes of C acquisition. Taken together, our results indicate the reallocation of photosynthetic energy between both processes. Further evidence for this is presented in our complementary study (Levitan et al., same issue).

Elemental ratios, growth and production rates

Trichodesmium spp. demonstrates high plasticity in growth and/or elemental composition with changing levels of pCO_2 (Barcelos é Ramos et al., 2007; Hutchins et al., 2007; Levitan et al., 2007; Kranz et al., 2009) and light (Breitbarth et al., 2008). The observed responses to these abiotic factors provide *prima facie* evidence for increasing importance of *Trichodesmium spp*. in future oceans. In our study, the combined effect of pCO_2 and light, two factors that are predicted to change in the future ocean, were studied on *Trichodesmium* IMS101 and are discussed on an ecophysiological level.

The elemental composition of *Trichodesmium* cells showed an increase in POC and PON quotas with enhanced pCO_2 concentrations (Fig. 1; Table II), a finding consistent with Kranz et al. (2009) but contradicting Barcelos é Ramos et al. (2007), who reported decreasing POC and PON quotas with elevated pCO_2. No pCO_2-dependent changes in elemental stoichiometry of C to N were observed in previous studies with light intensities >100 µmol photons m^{-2} s^{-1} (Barcelos é Ramos et al., 2007; Hutchins et al., 2007; Levitan et al., 2007; Kranz et al., 2009). However, under 50 µmol photons m^{-2} s^{-1} lower C to N ratios were obtained under elevated pCO_2 (Table II), reflecting a greater pCO_2 effect on the PON than on the POC quota under low light. Cell quotas for PP did not differ between acclimations (Table II), a finding that disagrees with decreasing organic phosphorus quotas under elevated pCO_2 observed by (Barcelos é Ramos et al., 2007). The observed increase in C to P and/or N to P ratios in our and previous studies imply that more biomass can be produced per available P.

The observed increase in growth rates under elevated pCO_2 is consistent with previous findings from *Trichodesmium* (Barcelos é Ramos et al., 2007; Hutchins et al., 2007; Levitan et al., 2007). Yet, the magnitude in pCO_2-dependent stimulation differed strongly between studies and is probably associated with the different light intensities applied (~80 to 150 µmol photons m^{-2} s^{-1} (Barcelos é Ramos et al., 2007; Hutchins et al., 2007; Levitan et al., 2007; Kranz et al., 2009). As our study focused on different pCO_2 levels in combination with low and high-light, we could indeed verify that light levels strongly modify the responses of *Trichodesmium* to pCO_2 (Fig. 1). As for the responses in elemental composition, the relative changes in growth rates to elevated pCO_2 were largest under low-light.

Due to the described effects on elemental composition and growth rates, the buildup of biomass in *Trichodesmium* increased strongly under elevated pCO_2 (Fig. 1). The pCO_2-dependent stimulation was highest under low-light with 93% increase for POC production and 133% increase for PON production relative to low pCO_2. Although not directly comparable, Hutchins et al. (2007) measured ^{14}C incorporation over 24h, an approach comparable to POC production rates in our study, and observed a 40-50% increase in C fixation when elevating the pCO_2 from 380 to 750 µatm pCO_2. Such responses in growth or POC production rates to elevated pCO_2 exceed those reported for other important marine phytoplankton groups such as diatoms and coccolithophores (e.g. Burkhardt et al., 1999; Zondervan et al., 2002; Langer et al., 2006) and demonstrate the exceptionally high sensitivity of *Trichodesmium* to pCO_2.

The strong responses in growth, POC and PON production rates, corroborate previous publications stating that central physiological processes are pCO_2 sensitive. While processes like CCMs and C fixation are intrinsically CO_2-dependent (Giordano et al., 2005), a direct CO_2 effect on processes like N_2 fixation appeared unlikely. Further, the observation that the pCO_2-sensitivity of POC and PON production rates is altered by light levels hints to an essential role of energy availability and allocation that we subsequently explored by measuring metabolic processes like N_2 fixation, gross photosynthetic O_2 evolution, CCM and C fixation, as well as Mehler reaction. Our complementary study focuses on these processes by measuring respective protein pools (Levitan et al., same issue).

N_2 fixation

Since *Trichodesmium* cultures were grown in N-free medium and thus had to acquire all nitrogen for growth by fixation of dissolved atmospheric N_2, the differences in PON production between treatments must be associated with respective changes in N_2 fixation. Under both low-light acclimations (50 µmol photons $m^{-2}s^{-1}$), N_2 fixation peaked about 3 hours after onset of the light, and showed reduced activities over midday until the end of the photoperiod (Fig. 2A). This atypical diurnal pattern may be caused by an energy shortage imposed by the low-light levels, which first and foremost affects energy-demanding processes such as N_2 fixation. Despite energy shortages under low-light, elevated pCO_2 highly stimulated N_2 fixation rates, which implies that more energy is available for this process. Under high-light (200 µmol photons $m^{-2}s^{-1}$), maximum rates of N_2 fixation rates were more than 6-fold higher than in the low-light acclimations (Fig. 2A) and peaked during midday (5 hours after onset of the light), as typically reported for *Trichodesmium* (e.g. Berman-Frank et al., 2001). While under low pCO_2, N_2 fixation rates declined after the midday peak, high pCO_2 levels resulted in a prolonged N_2

fixation until the end of the photoperiod. Such combined effects by light and pCO_2 on the diurnal patterns have not previously been reported and may indicate extended resource and energy availability for N_2 fixation and a change in regulation of nitrogenase (see Levitan et al., same issue).

As a consequence of the changes in rates and patterns of N_2 fixation under high-light and elevated pCO_2, integrated N_2 fixation rates over the day increased by 199% at low-light and 112% under high-light (Fig. 2B). N_2 fixation by nitrogenase should be coupled to PON production since N_2 is the only N source available (Fig. 1C). While both approaches indeed confirm the strong pCO_2-sensitivity in *Trichodesmium*, the relative stimulation by elevated pCO_2 was larger for the integrated N_2 fixation rates than those of the daily PON production (Figs. 1C and 2B). This apparent difference between measurements could be explained by the loss of previously reduced N_2 as DON (Capone et al., 1994; Glibert and Bronk, 1994) or ammonia (Mulholland et al., 2004) to the media. Under the applied continuous air bubbling of the culture, ammonia may be stripped from the culture medium and thus cannot be entirely used for PON production.

Fixation of N_2 and production of PON differ in their demand for energy and resources. Thus, pCO_2-dependent changes in the availability of energy and resources may affect both processes differently. While N_2 fixation by nitrogenase is mainly controlled by the availability of energy and electrons provided by the photosynthetic and respiratory pathways (a minimum of 16 ATP, 8 electrons and 8 protons are required to reduce N_2 into NH_4^+), the PON accumulation is regulated by glutamine synthetase (GS) and glutamine oxoglutarate aminotransferase (GOGAT), called the GS/GOGAT pathway. The primary substrates for the GS/GOGAT are NH_4^+ and α-ketoglutarate, a respiratory intermediate of the citric acid cycle within respiration and requires relatively little energy (1 ATP, 1 $NADPH+H^+$, and 2 protons to form one glutamate). For a mechanistic understanding of these findings, it is therefore important to look at possible regulations of key proteins in N metabolism (Levitan et al., same issue).

Where does the additional energy and resources result from to support the observed stimulation in N_2 fixation and PON production under elevated pCO_2? To answer this question we compared the changes of energy generated in photosynthesis and energy consumed by processes involved in C metabolism.

Gross photosynthesis

Photosynthesis generates energy and reductants that maintain metabolic processes such as N_2 fixation, carbon assimilation and biomass buildup in *Trichodesmium*. In this study, direct

measurements of O_2 evolution from water splitting (gross photosynthesis) yielded rates of photosynthetic electron generation, providing estimations about energy and reductant production of the culture. Regardless of pCO_2, gross photosynthesis was greatly stimulated by light (Fig. 3). Thus, the enhanced N_2 fixation and PON production rates under high-light (Fig. 1, Fig. 2) can be explained by a higher supply of energy and reductants. Gross photosynthesis was insensitive to the applied pCO_2 levels (Fig. 3). This is comparable with results obtained by Levitan et al. (2007), who found no change in O_2 evolution at three different pCO_2 acclimations. The production of energy and reductants is not only set by electron generation at PSII, but strongly controlled by the down-stream processes along the electron transport chain. For example, rapid cyclic electron transport around PSI would yield higher ATP production at the expense of NADPH or N_2 fixation. We examined these light/pCO_2 effects in more detail at the level of the core proteins of PSII and PSI and their ratio (see Levitan et al., same issue). Our findings here show that elevated pCO_2 did not alter the supply of energy provided by gross photosynthesis. Thus, energy-demanding processes related to C metabolism must have been down-regulated to explain the strong stimulation in N metabolism under elevated pCO_2.

Inorganic C acquisition and fixation

Active carbon acquisition is a mandatory process for the subsequent C fixation in the Calvin-Benson cycle. For the operation of these so-called CO_2-concentrating mechanisms, cyanobacteria like *Trichodesmium* need to invest a large amount of energy, which is primarily required due to its poor substrate affinity of RubisCO (Badger et al., 1998). *Trichodesmium* IMS101 operates an active CCM based predominantly on the uptake of HCO_3^- (Kranz et al., 2009). The relative HCO_3^- contribution to the total carbon fixation was about 90% and remained rather constant under all applied pCO_2 concentrations (150-1000 μatm) (Kranz et al., 2009). In the present study, HCO_3^- was also the preferred C species in all treatments (Fig. 4, Table III). These results concur with studies showing that CCMs in marine cyanobacteria are generally based on the transport and accumulation of HCO_3^- within the cell (Price et al., 2008). In some cyanobacteria, internal pools of inorganic carbon were up to 1000-fold higher than ambient concentrations (Kaplan et al., 1980), emphasizing the generally high energetic costs of their CCMs.

Despite the predominance of HCO_3^- transport, gross CO_2 uptake rate increased under elevated CO_2 (Fig. 4, Table III). Genome analysis identified the $NDH1_4$, a CO_2 uptake system located at the thylakoid membrane (Ohkawa et al., 2001), to be present in *Trichodesmium spp.*. This complex is considered to catalyze the conversion from CO_2 to HCO_3^- (Badger et al., 2006)

by utilizing reductants or electrons provided mostly by electron transport (Friedrich and Scheide, 2000; Price et al., 2002; Price et al., 2008), and may generate extra ATP by shuffling protons through the Q-cycle of the thylakoid membrane (Friedrich and Scheide, 2000; Price et al., 2002). HCO_3^- uptake on the other hand is mediated by BicA transporters that are located in the plasma membrane and function as Na^+/HCO_3^- symporters (Price et al., 2004), which are indirectly energized by ATP hydrolysis. Consequently, the changes in HCO_3^- and CO_2 uptake observed in our study (Fig. 4) may reflect changes in the activity of the CCM components and the availability and/or utilization of ATP and NADPH. Furthermore, the changes in uptake ratios may indicate a shift between linear versus cyclic electron transport (Li and Canvin, 1998).

The high energetic costs, associated with the operation of a CCM (Raven and Lucas, 1985), play a central role in the overall energy budget of the cell. Kranz et al. (2009) observed a high plasticity of CCM regulation, for instance in DIC affinities, in response to changes in pCO_2 concentrations and over the photoperiod. Regulation of DIC affinities, for example, will likely alter the energy allocation between the CCM and other metabolic processes. The ability of *Trichodesmium* to down-regulate its DIC affinities under elevated pCO_2 (Kranz et al., 2009) and the observed up-regulation in the CO_2 uptake system (Fig. 4, Table III) could therefore provide the energetic "surplus" to explain the stimulation in N metabolism and/or organic carbon production.

Although the POC production rates increased significantly under elevated pCO_2 (Fig. 1B), rates of C fixation in the MIMS assays were not stimulated in the high pCO_2 treatment (Table III). Part of this apparent contradiction may result from the fact that POC production rates cover several generations including dark and light phases, while C fixation is based on "instantaneous" measurements at specific time intervals during the photoperiod. Such discrepancies between direct measurements of C fixation and daily POC turnover rates in *Trichodesmium spp*. were also reported for field populations (Mulholland et al., 2006). As *Trichodesmium* IMS101 was able to saturate C fixation in the assays at pCO_2 concentrations of the respective acclimations (data not shown; (Kranz et al., 2009), we conclude that the observed changes in POC production rates cannot be caused by direct effects on the carboxylation efficiency of RubisCO but are rather due to changes in energy-availability for down-stream processes. Additional information on RubisCO quantities, energy requirements and availability will be provided by Levitan et al. (same issue).

Leakage

In addition to the processes involved in C uptake and accumulation, the ability to reach high rates of C fixation also depends on the loss of C via leakage (C efflux : total C uptake). In the present study, ^{13}C fractionation data (ε_P) were used to assess changes in leakage between the different acclimations. A positive correlation between ε_P and pCO_2 concentration was obtained under both light levels. This increase in ε_P under elevated pCO_2 may partly result from the decrease in the contribution of HCO_3^- to total C uptake under elevated pCO_2 (see Eq. 4), since more of the isotopically-lighter CO_2 is taken up. At high-light, the change in HCO_3^- to CO_2 ratio (Fig. 4, Table III) can explain only about 1‰ differences in ε_P while both pCO_2-treatments differ by more than 9‰. Alternatively, most of the variations in ε_P must result from changes in the leakage. To quantify these changes, Eq. 4 was applied to our data (i.e., measured ε_P and a). Leakage was generally higher under elevated pCO_2 compared to low pCO_2 acclimations (Fig. 6). The estimated leakage indicates rather high permeability for CO_2 that appears counterintuitive for cells operating a CCM. High membrane permeability may however be beneficial for other reasons, e.g., it will prevent a build-up of gases like O_2 or NH_3 within the cell.

Irrespective of the actual values of leakage, which are prone to errors in assumptions (e.g. the intrinsic fractionation of RubisCO), the trends in ε_P indicate that elevated pCO_2 causes higher leakage ($P<0.001$, One-way ANOVA followed by a post hoc test). These changes in leakage may be linked to the NDH-1_4-CO_2 uptake complex in *Trichodesmium*. The higher leakage observed at low-light may therefore reflect a reduction in the hydration of CO_2 due to a lower reductant availability caused by low photosynthetic electron transport.

At high-light and low-pCO_2 levels, HCO_3^- uptake sustains most of the C uptake (Fig. 4, Table III) while the CO_2 uptake system may be used primarily as a CO_2 scavenging mechanism (Fridlyand et al., 1996), supported by high reductant availability, which in turn could explain the lower leakage here. High pCO_2, on the other hand, leads to a higher CO_2 diffusion to the proximity of the $NDH1_4$, which under these conditions may function as a system for CO_2 uptake rather than prevention of CO_2 efflux. Further investigations on the dynamics of leakage and possible regulations by $NDH1_4$ in *Trichodesmium* have to be conducted to understand this essential process within its CCM.

Light-dependent O_2 uptake

Processes that reduce the O_2 concentration within the cell may play an important function in supporting and protecting nitrogenase in *Trichodesmium* from oxidative degradation (Kana, 1993; Berman-Frank et al., 2001; Milligan et al., 2007). In particular, the photo-reduction of O_2

by the Mehler reaction catalyzes the conversion of O_2 to H_2O. Changes in this O_2 scavenging process could therefore influence N_2 fixation rates. The Mehler reaction was also identified to be involved in photo-protection in other photoautotrophic species (Osmond and Grace, 1995; Osmond et al., 1997; Asada, 1999; Foyer and Noctor, 2000). To test for the presence and role of Mehler reaction in our different acclimations, light-dependent O_2 uptake was measured.

In low-light acclimated cells, *in situ* rates of O_2 uptake in the light were similar to the rates measured in the dark (Fig. 3B; Table III). In addition, the O_2 uptake rates were unaffected by the inhibition of PSII activity using DCMU (3-(3,4-dichlorophenyl)-1,1-dimethylurea). Both observations indicate that the Mehler reaction was not present when *Trichodesmium* IMS101 was grown under low-light, regardless of pCO_2. Moreover, it indicates that the respiratory O_2 uptake via the terminal oxidase is not repressed during illumination. These findings provide an additional perspective to the current understanding of the Mehler reaction and the terminal oxidase activity in *Trichodesmium* (Milligan et al., 2007). It is likely that under the low-light levels applied here (50 µmol photons m^{-2} s^{-1}), Mehler reaction may not be beneficial as it competes for the "scarce" electrons and its operation would decrease the energy supply for C and N fixation. In addition, the need for O_2 scavenging under low-light is reduced because of low photosynthetic O_2 production and respiratory O_2 uptake occurring in the light.

In high-light acclimated cells, Mehler reaction was only detected under low pCO_2 where the electrons generated at PSII may not be drained sufficiently to processes like NADP reduction or N_2 fixation. The Mehler reaction may therefore act as a shunt for routing excess electrons, thereby avoiding an over-reduction and damage of the photosynthetic compartments. After DCMU addition, the rates of O_2 uptake were similar to those obtained in the dark, confirming terminal oxidase activity during illumination. In high-light acclimated cells, grown at elevated pCO_2, light-dependent O_2 uptake was not detected. Under these conditions, the observed stimulation in N_2 fixation, POC and PON production as well as gross CO_2 uptake (i.e. $NDH1_4$ activity) may provide sufficient electron sinks, thereby reducing the need for the Mehler reaction.

Short-term exposure of the 50 µmol photons $m^{-2}s^{-1}$ acclimated cells to 200 µmol photons $m^{-2}s^{-1}$ (6 min) resulted in strong increase in light-dependent O_2 uptake, irrespective of the applied pCO_2 levels (Table III). The apparent operation of the Mehler reaction under these conditions may reduce the sudden electron flux within the ETC, which otherwise may causes photodamage Furthermore, the Mehler reaction may compensate for some of the light-stimulated O_2 evolution and thus act as a protection mechanism for nitrogenase. Such a relationship between Mehler reaction and N_2 fixation was observed for *Trichodesmium* in several studies (Kana, 1993;

Milligan et al., 2007). However, different growth conditions and the use of significantly higher light levels during the assays could also be a reason for the detection of Mehler reaction in previous studies.

Under the applied conditions in this study, Mehler reaction does not contribute to the observed stimulation in N_2 fixation under elevated pCO_2. Our findings suggest, however, that the Mehler reaction in *Trichodesmium* is more involved in photo-protection than in O_2 scavenging. This proposed role may be advantageous in view of the high and variable light levels typical for the natural environments of *Trichodesmium* (La Roche and Breitbarth, 2005).

Conclusion

Our data on production rates and elemental composition bear important implications for future changes in the relevant biogeochemical cycles. The pCO_2-dependent stimulation in the rate of biomass production may increase the CO_2 drawdown in the upper mixed layer and affect the vertical transport of organic matter. This "fertilization" effect on *Trichodesmium* may also expand to other phytoplankton as this important diazotroph fixes N_2 into particulate and dissolved compounds, thus providing a major source of bio-available N to oligotrophic oceans (Capone et al., 2005). In addition to the rate of production, biomass buildup is ultimately limited by the availability of other nutrients such as P. Consequently, the observed increase in C to P and/or N to P under elevated pCO_2 (Barcelos é Ramos et al., 2007; Levitan et al., in press) may imply that more biomass can be produced per available P, for instance over the course of a *Trichodesmium* bloom. In terms of the light-dependent changes in CO_2-sensitivity, the rise in pCO_2 may have a stronger effect on *Trichodesmium* thriving in deeper waters than for cells close to the surface. Furthermore, new information about metabolic key pathways and related proteins involved in C and N metabolism are provided within this and our complementary study (Levitan et al., same issue). Although *Trichodesmium* can saturate carbon fixation even at low pCO_2 levels by operating an efficient CCM, this comes at an energetic costs and competes with other energy-demanding processes like N_2 and C fixation. The observed responses to elevated pCO_2 could not be attributed to enhanced energy generation via gross photosynthesis. Instead, energetic costs of the CCM were reduced under high pCO_2, providing a surplus of energy and reductants that in turn enabled higher rates of N_2 fixation, PON and POC production and growth.

References:

Asada K (1999) The water-water cycle in chloroplasts: scavenging of active oxygens and dissipation of excess photons. Annu Rev Plant Physiol Plant Mol Biol **50:** 601–639

Badger MR, Andrews TJ, Whitney SM, Ludwig M, Yellowlees DC (1998) The diversity and co-evolution of Rubisco, plastids, pyrenoids and chloroplast-based CO_2-concentrating mechanisms in the algae. Can. J. Bot **76:** 1052

Badger MR, Palmqvist K, Yu JW (1994) Measurement of CO_2 and HCO_3^- fluxes in cyanobacteria and microalgae during steady-state photosynthesis. Physiol. Plant. **90:** 529

Badger MR, Price GD, Long BM, Woodger FJ (2006) The environmental plasticity and ecological genomics of the cyanobacterial CO_2 concentrating mechanism. J. Exp. Bot. **57:** 249-265

Barcelos é Ramos J, Biswas H, Schulz KG, LaRoche J, Riebesell U (2007) Effect of rising atmospheric carbon dioxide on the marine nitrogen fixer *Trichodesmium*. Global Biogeochem. Cycles **21:** -

Berman-Frank I, Lundgren P, Chen YB, Küpper H, Kolber Z, Bergman B, Falkowski P (2001) Segregation of nitrogen fixation and oxygenic photosynthesis in the marine cyanobacterium *Trichodesmium*. Science **294:** 1534-1537

Breitbarth E, Oschlies A, LaRoche J (2007) Physiological constraints on the global distribution of *Trichodesmium* – effect of temperature on diazotrophy. Biogeosciences **4:** 53–61

Breitbarth E, Wohlers J, Kläs J, LaRoche J, Peeken I (2008) Nitrogen fixation and growth rates of *Trichodesmium* IMS-101 as a function of light intensity. Mar Ecol Prog Ser **359:** 25-36

Brewer PG, Bradshaw AL, Williams RT (1981) Measurements of total carbon dioxide and alkalinity in the North Atlantic Ocean. *In* JR Trabalka, DE Reichle, eds, The changing carbon cycle: A global analysis. Springer, New York, pp 348–370

Burkhardt S, Riebesell U (1997) CO_2 availability affects elemental composition (C:N:P) of the marine diatom *Skeletonema costatum*. Marine Ecology Progress Series **155:** 67-76

Burkhardt S, Riebesell U, Zondervan I (1999) Stable carbon isotope fractionation by marine phytoplankton in response to daylength, growth rate, and CO_2 availability. Mar Ecol Prog Ser. **184:** 31-41

Capone DG (1993) Determination of nitrogenase activity in aquatic samples using the acetylene reduction procedure. *In* PF Kemp, B Sherr, E Sherr, J Cole, eds, Handbook of Methods in Aquatic Microbial Ecology. Lewis Publishers, New York, pp 621–631

Capone DG, Burns JA, Montoya JP, Subramaniam A, Mahaffey C, Gunderson T, Michaels AF, Carpenter EJ (2005) Nitrogen fixation by *Trichodesmium spp.*: An important source of new nitrogen to the tropical and subtropical North Atlantic Ocean. Global Biogeochem. Cycles **19:** GB2024, 2010.1029/2004GB002331

Capone DG, Ferrier MD, Carpenter EJ (1994) Cycling and release of glutamate and glutamine in colonies of the marine planktonic cyanobacterium, *Trichodesmium thiebautii*. Appl. Environ. Microbiol. **60:** 3989-3995

Capone DG, Montoya JP (2001) Nitrogen fixation and denitrification. Methods in Microbiology **30:** 501-515

Chen Y-B, Zehr JP, Mellon M (1996) Growth and nitrogen fixation of the diazotrophic filamentous nonheterocystous cyanobacterium *Trichodesmium* sp. IMS 101 in defined media: evidence for a circadian rhythm. Journal of Phycology **32:** 916-923

Dickson AG, Millero FJ (1987) A comparison of the equilibrium constants for the dissociation of carbonic acid in seawater media. Deep Sea Research Part A. Oceanographic Research Papers **34:** 1733-1743

Doney SC (2006) Oceanography: Plankton in a warmer world. Nature **444:** 695-696

Fock HP, Sültemeyer DF (1989) O_2 evolution and uptake measurements in plant cells by mass spectrometer. *In* HF Liskens, JF Jackson, eds, Modern Methods of Plant Analysis Vol 9. Springer-Verlag, Heidelberg, Germany, pp 3–18

Foyer CH, Noctor G (2000) Oxygen processing in photosynthesis: regulation and signaling. New Phytol **146:** 359-388

Fridlyand L, Kaplan A, Reinhold L (1996) Quantitative evaluation of the role of a putative CO_2-scavenging entity in the cyanobacterial CO_2-concentrating mechanism. Biosystems **37:** 229-238

Friedrich T, Scheide D (2000) The respiratory complex I of bacteria, archaea and eukarya and its module common with membrane-bound multisubunit hydrogenases. FEBS Letters **497:** 1-5

Fu F-X, Mulholland MR, Garcia NS, Beck A, Bernhardt PW, Warner ME, Sanudo-Wilhelmy SA, Hutchins DA (2008) Interactions between changing pCO_2, N_2 fixation, and Fe limitation in the marine unicellular cyanobacterium *Crocosphaera*. Limnol. Oceanogr. **53:** 2472–2484

Giordano M, Beardall J, Raven JA (2005) CO_2 Concentrating Mechanisms in Algae: Mechanisms, Environmental Modulation, and Evolution. Annual Review of Plant Biology **56:** 99-131

Glibert PM, Bronk DA (1994) Release of dissolved organic nitrogen by marine diazotrophic cyanobacteria, *Trichodesmium spp*. Appl. Environ. Microbiol **60:** 3996–4000

Gran G (1952) Determination of the equivalence point in potentiometric titrations. Part II. The Analyst **77:** 661

Guy RD, Fogel ML, Berry JA (1993) Photosynthetic fractionation of stable isotopes of oxygen and carbon. Plant Physiol. **101:** 37-47

Hutchins DA, Fu F-X, Zhang Y, Warner ME, Feng Y, Portune K, Bernhardt PW, Mulholland MR (2007) CO_2 control of *Trichodesmium* N_2 fixation, photosynthesis, growth rates and elemental ratios: Implications for past, present and future ocean biogeochemistry. Limnol. Oceanogr. **552:** 1293–1304

Kana TM (1993) Rapid oxygen cycling in *Trichodesmium thiebautii*. Limnol. Oceanogr. **38:** 18–24

Kaplan A, Badger MR, Berry JA (1980) Photosynthesis and the intracellular inorganic carbon pool in the blue green alga *Anabaena variabilis*: Response to external CO_2 concentration. Planta **149:** 219-226

Kranz SA, Sueltemeyer D, Richter K-U, Rost B (2009) Carbon acquisition in *Trichodesmium*: the effect of pCO_2 and diurnal changes. Limnology and Oceanography **54:** 548-559

La Roche J, Breitbarth E (2005) Importance of the diazotrophs as a source of new nitrogen in the ocean. Journal of Sea Research **53:** 67-91

Langer G, Gussone N, Nehrke G, Riebesell U, Eisenhauer A, Kuhnert H, Rost B, Trimborn S, Thoms S (2006) Coccolith strontium to calcium ratios in Emiliania huxleyi: The dependence on seawater strontium and calcium concentrations. Limnol. Oceanogr. **51:** 310–320

Levitan O, Rosenberg G, Setlik I, Setlikova E, Grigel J, Klepetar J, Prasil O, Berman-Frank I (2007) Elevated CO_2 enhances nitrogen fixation and growth in the marine cyanobacterium *Trichodesmium*. Global Change Biology **13:** 531-538

Lewis E, Wallace DWR (1998) Program developed for CO_2 system calculations. ORNL/CDIAC-105. *In*. (Carbon Dioxide Information Analysis Center, Oak Ridge National Laboratory, US Department of Energy, Oak Ridge, Tennessee, 1998).

Li QL, Canvin DT (1998) Energy sources for HCO_3^- and CO_2 transport in air-grown cells of *Synechococcus* UTEX 625. Plant Physiol. **116:** 1125–1132

Mahaffey C, Michaels AF, Capone DG (2005) The conundrum of marine N_2 fixation. Am J Sci **305:** 546-595

Mehrbach C, Culberson CH, Hawley JE, Pytkowicz RM (1973) Measurement of the Apparent Dissociation Constants of Carbonic Acid in Seawater at Atmospheric Pressure. Limnology and Oceanography **18:** 897-907

Milligan AJ, Berman-Frank I, Gerchman Y, Dismukes GC, Falkowski PG (2007) Light-dependent oxygen consumption in nitrogen-fixing cyanobacteria plays a key role in nitrogenase protection. Journal of Phycology **43:** 845-852

Mulholland MR, Bronk DA, Capone DG (2004) Dinitrogen fixation and release of ammonium and dissolved organic nitrogen by *Trichodesmium* IMS101. Aquatic Microbial Ecology **37:** 85-94

Mulholland MR, Heil CA, Bronk DA, O'Neil MO (2006) Nitrogen fixation and release of fixed nitrogen by *Trichodesmium* sp. in the Gulf of Mexico. Limnol. Oceanogr. **51:** 1762-1776

Ohkawa H, Sonoda M, Shibata M, Ogawa T (2001) Localization of NAD(P)H dehydrogenase in the cyanobacterium *Synechocystis* sp strain PCC 6803. Journal of Bacteriology **183:** 4938-4939

Osmond CB, Badger MR, Maxwell K, Bjoerkman O, Leegood RC (1997) Too many photons: photorespiration, photoinhibition and photooxidation. Trends Plant Sci. **2:** 119-121

Osmond CB, Grace SC (1995) Perspectives on photoinhibition and photorespiration in the field: quintessential inefficiencies of the light and dark reactions of photosynthesis? Journal of Experimental Botany **46:** 1351-1362

Peltier G, Thibault P (1985) O_2 uptake in the light in *Chlamydomonas* - evidence for persistent mitochondrial respiration. Plant Physiology and Biochemistry **79:** 225-230

Price GD, Badger MR, W. FJ, Long BM (2008) Advances in understanding the cyanobacterial CO_2-concentrating-mechanism (CCM): functional components, Ci transporters, diversity, genetic regulation and prospects for engineering into plants. J. Exp. Bot. **59:** 1441-1461

Price GD, Maeda S-I, T. O, M.R. B (2002) Modes of inorganic carbon uptake in the cyanobacterium *Synechococcus* sp. PCC7942. Functional Plant Biology **29:** 131-149

Price GD, Woodger FJ, Badger MR, Howitt SM, Tucker L (2004) Identification of a SulP-type bicarbonate transporter in marine cyanobacteria. Proc. Natl. Acad. Sci. USA. **101:** 18228-18233

Prufert-Bebout L, Paerl HW, Lassen C (1993) Growth, Nitrogen Fixation, and Spectral Attenuation in Cultivated *Trichodesmium* Species. Appl. Environ. Microbiol. **59:** 1367-1375

Raupach MR, Marland G, Ciais P, Le Quere C, Canadell JG, Klepper G, Field CB (2007) Global and regional drivers of accelerating CO_2 emissions. PNAS **104:** 10288-10293

Raven J, Caldeira K, Elderfield H, Hoeg-Guldberg Oea (2005) Ocean acidification due to increasing atmospheric carbon dioxide. Policy Document 12/05, The Royal Society, London. Available at: www.royalsoc.ac.uk

Raven JA, Lucas WJ (1985) Energy costs of carbon acquisition. *In* WJ Lucas, JA Berry, eds, Inorganic carbon uptake by aquatic photosynthetic organisms. Americam Society of Plant Physiologists, Rockville, MD, pp 305–324

Riebesell U, Zondervan I, Rost B, Tortell PD, Zeebe E, Morel FMM (2000) Reduced calcification in marine plankton in response to increased atmospheric CO_2. Nature **407:** 634-637

Rost B, Kranz SA, Richter K-U, Tortell PD (2007) Isotope disequilibrium and mass spectrometric studies of inorganic carbon acquisition by phytoplankton. Limnol. Oceanogr. Methods **5:** 328-337

Rost B, Richter K-U, Riebesell U, Hansen PJ (2006) Inorganic carbon acquisition in red-tide dinoflagellates. Plant, Cell and Environment **29:** 810-822

Rost B, Riebesell U, Burkhardt S, Sueltemeyer D (2003) Carbon acquisition of bloom-forming marine phytoplankton. Limnol. Oceanogr. **48:** 55

Sharkey TD, Berry JA (1985) Carbon isotope fractionation of algae influenced by an inducible CO_2-concentrating mechanism. *In* WJ Lucas, JA Berry, eds, Inorganic carbon uptake by aquatic photosynthetic organisms. American Society of Plant Physiologists, Rockville., pp 389-401

Tortell PD, Payne CD, Li Y, Trimborn S, Rost B, Smith WO, Riesselman C, Dunbar R, Sedwick P, DiTullio G (2008) The CO_2 response of Southern Ocean phytoplankton. Geophys. Res. Lett. **35:** L04605

Wolf-Gladrow DA, Bijma J, Zeebe RE (1999) Model simulation of the carbonate chemistry in the microenvironment of symbiont bearing foraminifera. Marine Chemistry **64:** 181-198

Zeebe RE, Wolf-Gladrow DA (2007) CO_2 in seawater: equilibrium, kinetics, isotopes. Elsevier Science B.V., Amsterdam

Zondervan I, Rost B, Riebesell U (2002) Effect of CO_2 concentration on the PIC/POC ratio in the coccolithophore *Emiliania huxleyi* grown under light-limiting conditions and different daylengths. Journal of Experimental Marine Biology and Ecology **272:** 55-70

Acknowledgements:

The research leading to these results has received funding from the European Research Council under the European Community's Seventh Framework Programme (FP7/2007-2013) / ERC grant agreement [205150]. O. Levitan was founded by the DAAD (Deutscher Akademischer Auslandsdienst). O. Prášil was supported by GACR 206/08/1683 and AV0Z50200510. This research was also supported by BMBF-MOST (GR1950) to I. Berman-Frank and a MOST fellowship to O. Levitan.

Tables:

Table I: Parameters of the seawater carbonate system: calculated from TA, pH, phosphate, temperature and salinity using the CO2Sys program (Lewis and Wallace 1998). Errors are ±1, SD (n > 3).

pCO_2 (µatm)	CO_2 (μmol kg^{-1})	TA (μEq kg^{-1})	pH (NBS)	DIC (μmol kg^{-1})
150	3.8 ± 0.3	2487 ± 9	8.57 ± 0.03	1841 ± 19
900	23.3 ± 1.5	2470 ± 14	7.94 ± 0.03	2240 ± 17.9

Table II: Growth rates, cellular elemental quotas and C and N production rates of *Trichodesmium* IMS101 under a matrix of pCO_2 and light. Values represent the mean of triplicate cultures, sampled over several days, all within exponential phase. Errors are ±1 SD

	acclimation			
	low-light (50 µmol photons $m^{-2}s^{-1}$)		high-light (200 µmol photons $m^{-2}s^{-1}$)	
	150 µatm pCO_2	900 µatm pCO_2	150 µatm pCO_2	900 µatm pCO_2
growth µ [d^{-1}] [A,C, E]	0.15 ±0.03	0.24 ±0.03	0.38 ±0.02	0.42 ±0.02
POC [pmol C $cell^{-1}$] [A,D]	3.79 ±0.09	4.51 ±0.21	4.60 ±0.46	5.02 ±0.57
PON [pmol N $cell^{-1}$] [A,D]	0.59 ±0.03	0.88 ±0.06	0.86 ±0.08	1.04 ±0.09
PP [nmol P $cell^{-1}$] [A]	73 ±9	78 ±9	70 ±14	71±4
C : N [mol:mol] [A,C,E]	6.41±0.39	5.04 ±0.15	5.25 ±0.19	4.85 ±0.10
chl *a* [pg $cell^{-1}$] [A,C]	0.47 ±0.04	0.72 ±0.05	0.67 ±0.14	0.69 ±0.08
POC production rates [pmol C $cell^{-1}$ d^{-1}] [A,C,D]	0.57 ±0.11	1.10 ±0.17	1.76 ±0.26	2.12 ±0.34
PON production rates [pmol N $cell^{-1}$ d^{-1}] [A,C,D]	0.09 ±0.02	0.21 ±0.04	0.33 ±0.05	0.44 ±0.06

[A] (n>10)

[B] (n=6)

[C] t-test: significant difference between low-light acclimations

[D] t-test: significant difference between high-light acclimations

[E] One Way ANOVA: significant difference between all acclimations

Table III: Rates of metabolic processes in *Trichodesmium* IMS101. Values represent rates measured 3-4 hours (am) and 6-7 hours (pm) after begin of the photoperiod. Blanks denote no measurement or only 1 replicate. Errors are ±1 SD (n>3).

	assay condition		acclimation			
			low-light (50 µmol photons $m^{-2}s^{-1}$)		high-light (200 µmol photons $m^{-2}s^{-1}$)	
			150 µatm pCO_2	900 µatm pCO_2	150 µatm pCO_2	900 µatm pCO_2
gross O_2 evolution [µmol O_2 chl a^{-1} h^{-1}]	low-light	am	143 ±16	119 ±22	/	±/
		pm	156 ±4	135 ±17	/	/
	high-light	am	453	538 ±70	454 ±28	534 ±51
		pm	612	429 ±42	486 ±81	432 ±153
O_2 uptake [µmol O_2 chl a^{-1} h^{-1}]	low-light	am	81 ±21	46 ±18	/	/
		pm	27 ±12	23 ±23	/	/
	high-light	am	200	137 ±33	254 ±49	117 ±42
		pm	81	83 ±62	115 ±57	123 ±27
	dark	am	115 ±10	83 ±11	106 ±44	126 ±30
		pm	25 ±8	24 ±7	67 ±13	111 ±24
C fixation [µmol CO_2 chl a^{-1} h^{-1}]	low-light	am	277 ±1	157 ±31	/	/
		pm	324 ±112	145 ±22	/	/
	high-light	am	437	489 ±116	536 ±243	519 ±91
		pm	344	508 ±48	582 ±94	487 ±192
C respiration [µmol CO_2 chl a^{-1} h^{-1}]	acclimation light	am	97 ±16	163 ±141	122 ±210	189 ±87
		pm	237 ±69	373 ±18	191 ± 96	296 ±159
HCO_3^- uptake [µmol HCO_3^- chl a^{-1} h^{-1}]	acclimation light	am	105 ±8	82 ±19	196 ±29	224 ±30
		pm	121 ±25	98 ±8	287 ±50	282 ±28
CO_2 uptake [µmol CO_2 chl a h^{-1}]	acclimation light	am	10 ±1	22 ±10	59 ±6	90 ±19
		pm	17 ±5	53 ±9	61 ±8	147 ±31

Figure legends:

Fig 1: Responses of *Trichodesmium* IMS101 to different light (50 and 200 µmol photons m^{-2} s^{-1}) and pCO_2 levels (150 and 900 µatm pCO_2): A) growth rates, B) production rates of particulate organic carbon (POC), C) production rates of particulate organic nitrogen (PON). Numbers in parenthesis denote the relative increase from low to high pCO_2 levels. Errors are ±1 SD (n≥10). Asterisks between bars indicate significant difference between low to high pCO_2 levels (t-test, $P<0.05$).

Fig. 2: A) Diurnal cycle of nitrogen fixation of *Trichodesmium* IMS101 at the different light and pCO_2 acclimations. Measurements were obtained from duplicate cultures. Errors are ±1 SD The black and white areas in the figure head corresponds to the dark and light period of the diurnal cycle. B) Integrated diurnal N_2 fixation rate from Fig. 2A. Numbers in parenthesis denote the relative increase from low to high pCO_2 levels. Errors are ±1 SD (n≥2).

Fig. 3: Oxygen fluxes of *Trichodesmium* IMS101 measured 3-4 hours (am; bright bars) and 6-7 hours (pm; striped bars) after the beginning of the photoperiod. A. Gross O_2 evolution rate. B. O_2 uptake in the light rates. Errors are ±1 SD (n≥2).

Fig. 4: HCO_3^-:CO_2 ratio in *Trichodesmium* IMS101 obtained from HCO_3^- and gross CO_3 uptake rate (Table III) measured 3-4 hours (am; bright bars) and 6-7 hours (pm; striped bars) after the beginning of the photoperiod. Errors are ±1 SD (n≥3).

Fig 5: Leakage of CO_2 in *Trichodesmium* IMS101 at different acclimations calculated according to Sharkey and Berry (1985). Dotted lines denote the 0 and 1 level of α (HCO_3^- uptake : Ci uptake). Open and grey symbols represent the 150 µatm and 900 µatm pCO_2 acclimations, respectively. Triangles: 200 µmol photons $m^{-2}s^{-1}$; Squares: 50 µmol photons $m^{-2}s^{-1}$. Errors are ±1 SD (n>3).

Figures:

Figure 1:

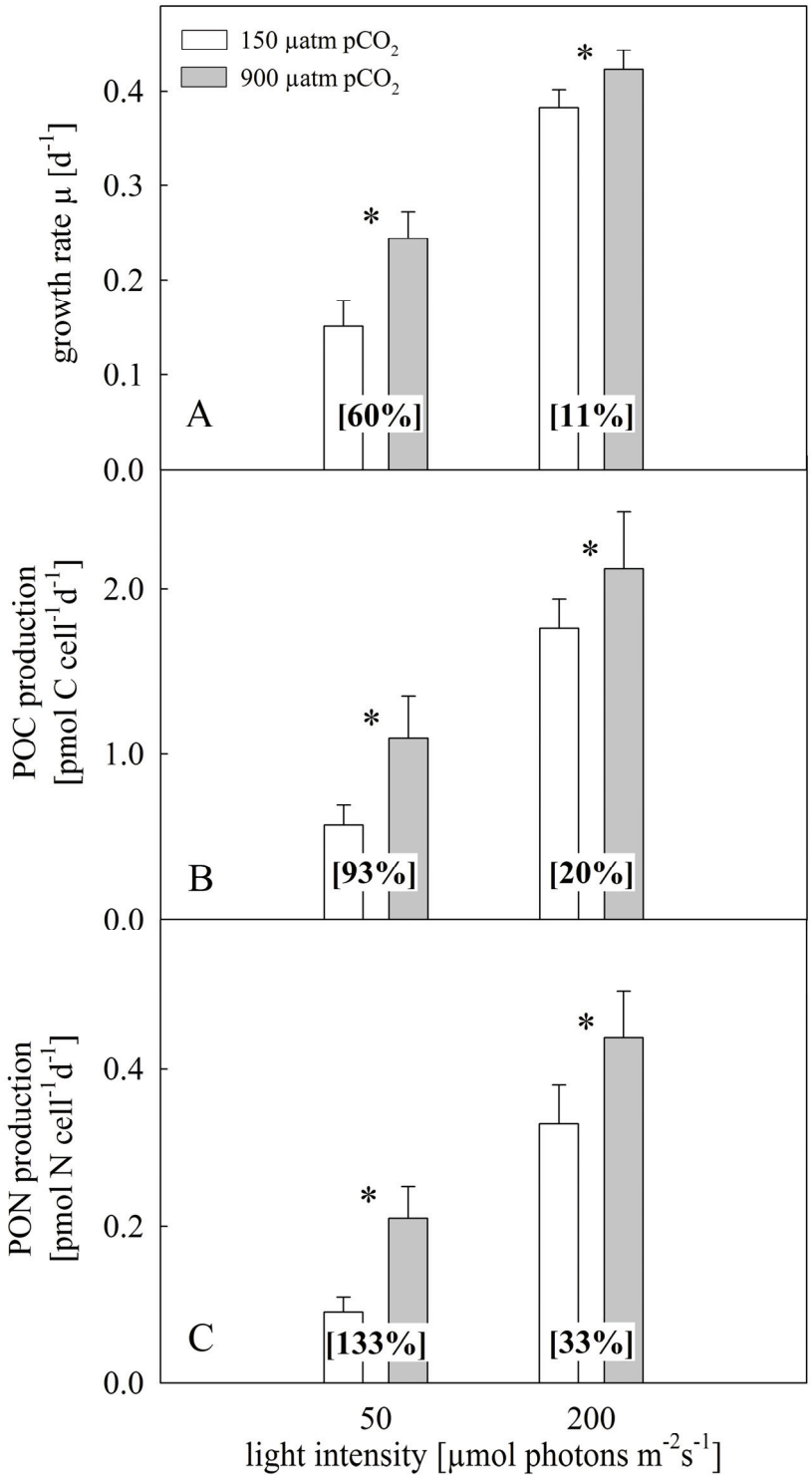

Figure 2:

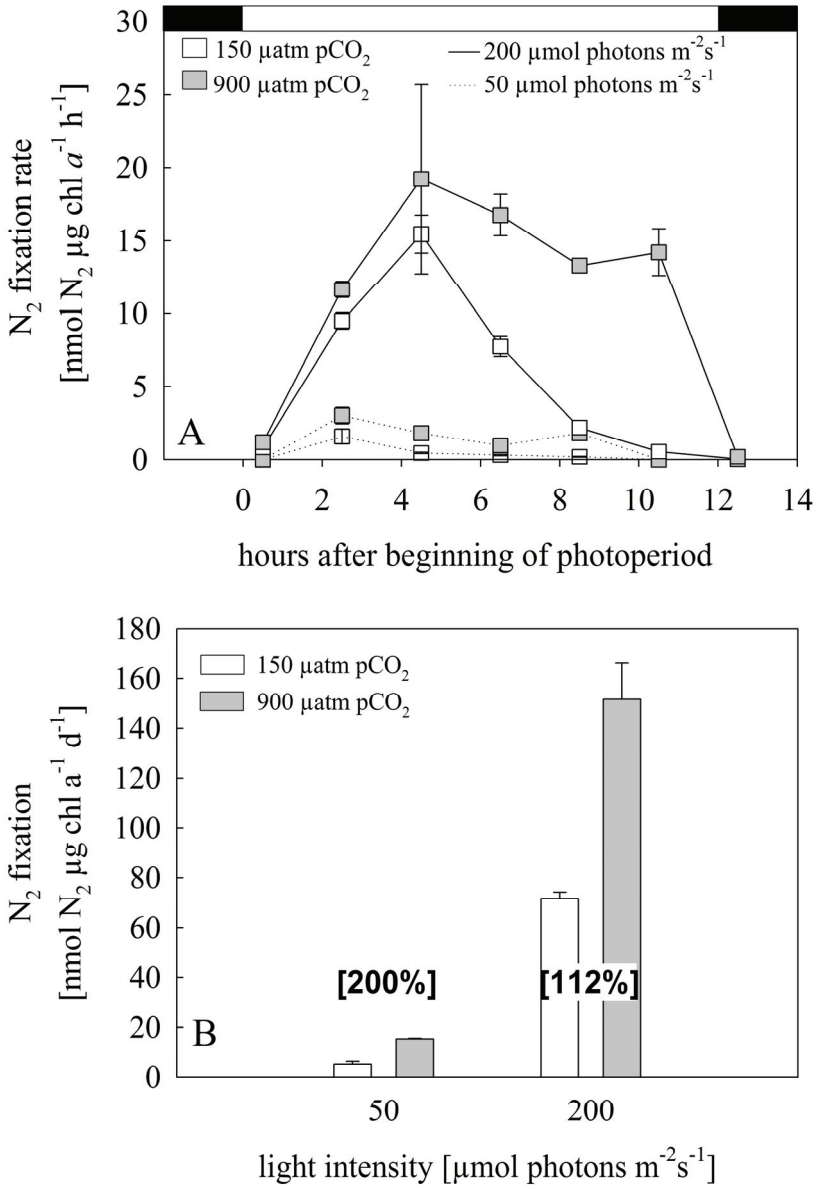
150 µatm pCO2
900 µatm pCO2
200 µmol photons m-2s-1
50 µmol photons m-2s-1
N2 fixation rate
[nmol N2 µg chl a-1 h-1]
A
hours after beginning of photoperiod
150 µatm pCO2
900 µatm pCO2
N2 fixation
[nmol N2 µg chl a-1 d-1]
[200%]
[112%]
B
light intensity [µmol photons m-2s-1]

Figure 3:

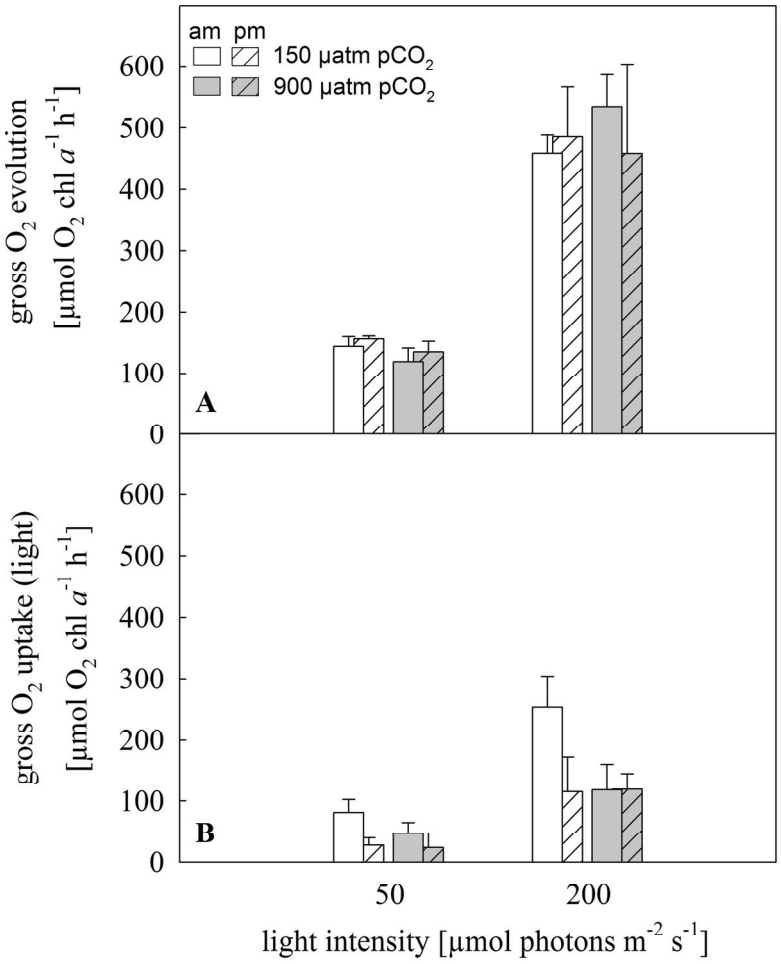
am pm
150 µatm pCO2
900 µatm pCO2
gross O2 evolution
[µmol O2 chl a-1 h-1]
A
gross O2 uptake (light)
[µmol O2 chl a-1 h-1]
B
0
100
200
300
400
500
600
50
200
light intensity [µmol photons m-2 s-1]

Figure 4:

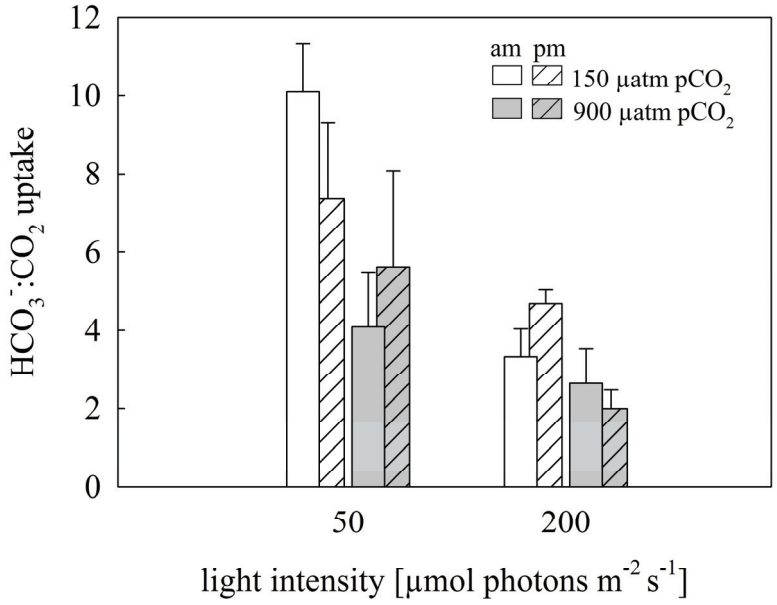
12
10
8
6
4
2
0
HCO_3^-:CO_2 uptake
am pm
150 µatm pCO_2
900 µatm pCO_2
50
200
light intensity [µmol photons m^{-2} s^{-1}]

Figure 5:

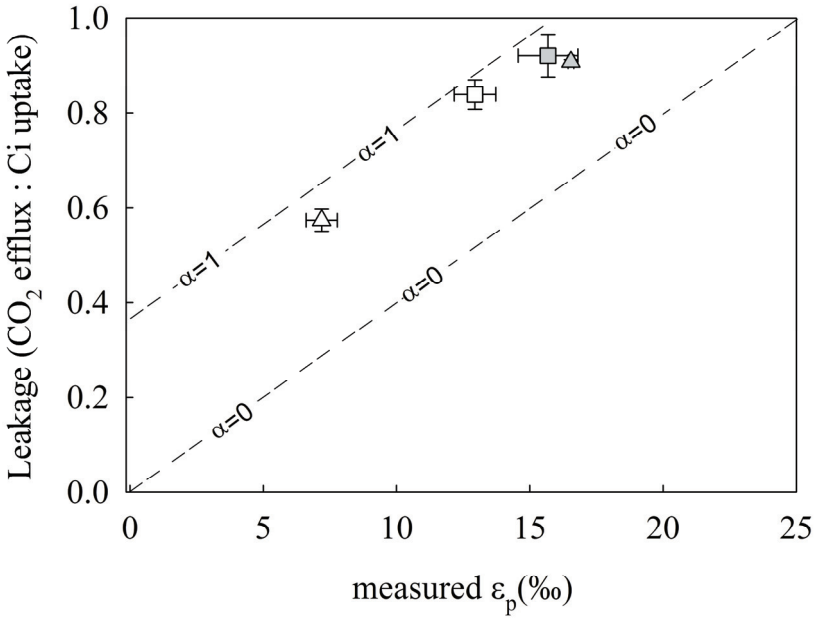
1.0
0.8
0.6
0.4
0.2
0.0
0
5
10
15
20
25
Leakage (CO_2 efflux : Ci uptake)
measured ε_p(‰)
α=1
α=1
α=0
α=0

Publication IV

Calcium carbonate precipitation induced by the growth of the marine cyanobacteria *Trichodesmium*

Sven A. Kranz[1]; Dieter Wolf-Gladrow[1]; Gernot Nehrke[1]; Gerald Langer[2], Björn Rost[1]

[1] Alfred Wegener Institute for Polar and Marine Research, 27570 Bremerhaven, Germany

[2] ICTA, Autonomous University of Barcelona (UAB), 08193 Bellaterra, Spain

Abstract:

Cyanobacteria are important primary producers of the contemporary oceans and have affected global biogeochemical cycles over geological timescales. The diazotrophic *Trichodesmium spp*, are known for their large scale blooms and substantial input of 'reactive nitrogen' to the oligotrophic subtropical and tropical areas. In this laboratory study, we monitored the buildup of biomass and concomitant shift in seawater carbonate chemistry over the course of a *Trichodesmium* bloom under different phosphorus (P) availability. During exponential growth, dissolved inorganic carbon (DIC) decreased while pH increased until maximum cell densities were reached. Once P became depleted, DIC decreased even further and total alkalinity (TA) dropped, which was accompanied by precipitation of aragonite. Under P-replete conditions, DIC increased and TA remained constant in the post bloom phase. A diffusion-reaction model was employed to estimate changes in carbonate chemistry of the diffusive boundary layer. The data presented here demonstrate the capability of *Trichodesmium* to induce precipitation of aragonite from seawater.

Introduction:

Phytoplankton plays a vital role in geochemical cycling of biogenic elements and has influenced Earth's climate over geological timescales. These photoautotrophic organisms fix carbon dioxide (CO_2) in the upper mixed layer of the ocean and subsequently drive the vertical export of particulate organic carbon (POC). In the water column, remineralisation and respiration releases organically-bound CO_2, which then accumulates in deeper layers. This process, termed *organic carbon pump*, causes a net drawdown of CO_2 from the atmosphere into the ocean. In contrast, precipitation of calcium carbonate ($CaCO_3$) by various groups of organisms provide a CO_2 source for the atmosphere. This counterintuitive effect of the so-called *carbonate pump* is caused by consumption of dissolved inorganic carbon (DIC) and total alkalinity (TA) in a 1:2 ratio during the process of calcification.

Marine productivity is typically driven by diatoms, coccolithophores, dinoflagellates and cyanobacteria. As the most ancient group, cyanobacteria were responsible for the original oxidization of the Earth's atmosphere and dominated elemental cycles over geological timescales (Des Marais 2000). In the Cretaceous, this group was also known to play an important role in the buildup of immense carbonate sediments (Riding 2006). Nowadays, $CaCO_3$ production by cyanobacteria seems to be more or less restricted to specific environments like hard water lakes, stromatolites or biological crusts (Pentecost and Riding 1986). In contemporary oceans, cyanobacteria are mostly considered in view of their ability to provide new nitrogen by N_2 fixation.

The bloom-forming filamentous diazotroph *Trichodesmium* plays a vital role for primary productivity in the tropical and subtropical oceans (Capone et al. 2005; Mulholland et al. 2006). In contrast to non-diazotrophic species, the development of a bloom is therefore often controlled by the availability of phosphorus (P) and/or iron rather than 'reactive N' (e.g. nitrate, nitrite, ammonium, urea). As described in several studies on phytoplankton bloom dynamics, the buildup of biomass is typically accompanied by a decrease in DIC and increase in pH (Holligan et al. 1993; Arrigo et al. 1999). To our knowledge, there are no data on changes in carbonate chemistry over the course of a *Trichodesmium* bloom. Yet, high biomasses observed in *Trichodesmium* blooms (La Roche and Breitbarth 2005) imply large alteration in the carbonate chemistry.

In this study, we investigated the bloom development of *Trichodesmium* under different P availability and monitored corresponding changes in carbonate chemistry. In addition to a strong shift in carbonate chemistry, $CaCO_3$ was formed under P-deplete conditions. Possible

explanations for this precipitation process are provided and consequences for biogeochemistry are discussed.

Material and Methods:

Cultures of *Trichodesmium erythraeum* IMS101 (CCMP1985) were grown at 26°C in 0.2 μm-filtered artificial seawater based on YBCII media (Chen et al. 1996; Table 1). A light intensity of 200 μmol photons m^{-2} s^{-1} was provided in a 12:12 h light to dark cycle. Experiments were carried out in sterile 20 L polycarbonate Nalgene bottles. To keep cells in suspension, bottles were placed on an orbital shaker. The headspace was continuously exchanged via a membrane pump with 0.2 µm-filtered ambient air (~380 µatm CO_2). For each treatment, cells from a preculture were inoculated into two 15 L culture media. In one treatment, the P concentration was kept between 2.5 and 6 µmol PO_4^{3-} by repeated addition (P-replete), while in the other culture, the P was allowed to be fully consumed by the cells (P-deplete). Inorganic phosphorus was measured colourimetrically on a daily basis using a continuous flow analyzer (Evolution III, Aliance Intruments).

To monitor the carbonate chemistry of the media, DIC and TA were measured every day. Samples for TA were filtered through glass-fibre filters (GFF, nominal pore size ~0.6 µm) and stored in 100 ml borosilicate bottles at room temperature until potentiometric titration with an average precision of ±7 µmol kg^{-1}. TA was calculated from linear Gran Plots (Gran 1952). DIC samples were sterile-filtered (cellulose acetate filters, pore size 0.2 µm) and stored in 5 ml borosilicate flasks without headspace at 4°C. DIC was measured using an Technicon TRAACS 800 (Stoll et al. 2001) with a precision of ±5 µmol kg^{-1}. TA and DIC measurements were calibrated using certified reference seawater standards (CRM standards, supplied by Dr. Andrew Dickson, Scripps Institution of Oceanography). The carbonate system (pH_{tot}; Ω_{Ar}) was calculated from TA, DIC, temperature, salinity and phosphate concentration using CO2Sys (Lewis and Wallace 1998). Equilibrium constants of (Mehrbach et al. 1973) refitted by (Dickson and Millero 1987) were chosen.

Samples for chl *a* analysis were filtered onto glass fibre filters (GFF) and stored at -80°C. Chl *a* was subsequently extracted in 5-10 mL acetone (overnight in darkness, at 4°C) and determined with a fluorometer (Turner Designs) according to the JGOFS chl *a* protocol (http://ocean.stanford.edu/cal/JGOFS_chla.pdf). Samples for POC were filtered onto

precombusted (500°C; 9 h) GFF filters and stored in precombusted (500°C; 9 h) petri dishes at -20°C. Prior to analysis, filters were treated with 200 μL HCl (0.1 N) to remove all inorganic carbon. Subsequently, POC was measured on an EA mass spectrometer (ANCA-SL 2020) with a precision of ~1% of the total carbon (C) amount. Growth rates (μ) within the exponential growth phase were calculated as:

$$\mu(\mathrm{d}^{-1}) = \frac{\ln(N_1) - \ln(N_0)}{\Delta t} \quad (1)$$

where N_0 and N_1 are concentration of chl *a* at time t_0 and t_1, respectively, and Δt is the time between sampling intervals.

At the end of the post-bloom phase, the particulate fraction of the residual medium was harvested via centrifugation (5000 g, 10 min) and subsequently analyzed using scanning electron microscopy (SEM) and Raman spectroscopy. These samples were filtered onto polycarbonate filters (Nucleopore, pore size 0.2 μm), dried for 3 h at 50 °C and stored in a desiccator. Samples for SEM were finally sputter-coated with gold-palladium and morphology was examined by means of SEM (Philips XL-30). Samples for Raman spectroscopy were additionally washed in acetone to remove organics. For phase identification of the precipitate, a confocal Raman microscope (WITec, Ulm, Germany) with a diode laser (785 nm), having an excitation energy of 20 mW at the sample surface (determined with a Coherent LaserCheck powermeter) and a Nikon 100x (NA 0.95) objective was used.

Results:

Cell growth was initiated at chl *a* concentrations of 0.6 and 1.4 μg L^{-1} and monitored over the duration of 25 days. After inoculation, cells did not exhibit a lag-phase and started to grow exponentially for 13 to 14 days before reaching maximum chl *a* densities, followed by a post-bloom phase (Fig. 1A). In one treatment, cells were allowed to consume P entirely (P-deplete; Fig. 1B), reaching PO_4^{3-} levels below 0.1 μM after day 11. In the other treatment, PO_4^{3-} concentrations maintained between 2.5 and 6 μM (P-replete; Fig. 1B). Specific growth rates during the exponential phase, determined by changes in chl *a* concentration (Fig. 1A), were similar for all cultures and ranged between 0.51 and 0.58 d^{-1}. Maximum values for chl *a* varied between 0.52 and 0.55 mg L^{-1} in the P-deplete culture and between 0.46 and 0.50 mg L^{-1} in P-replete cultures.

The carbonate chemistry showed similar patterns during early and mid exponential growth phase in both P-replete and P-deplete cultures, but started to deviate strongly in terms of DIC and TA at the end of the exponential phase (day 13 and 14; Fig. 2A and B). In the P-replete cultures, the DIC decreased from an initial concentration of 2150 µmol kg^{-1} to a minimum of about 1500 µmol kg^{-1} at the end of the exponential phase (Fig. 2A). During the post bloom phase, DIC increased again to values slightly lower than initial concentrations. The pH_{tot} increased with increasing cell densities, from initial values of 8.0 up to 8.81 (day 13-15; Fig. 2C). A decline in pH was observed during the post bloom phase, reaching values between 8.15 and 8.30 (Fig. 2C). TA remained relatively constant with a mean of 2447 ±16 µmol kg^{-1} over the duration of the experiment (Fig. 2B). The calculated aragonite saturation state (Ω_{Ar}; $[Ca^{2+}]$ $[CO_3^{2-}]$ / solubility product of aragonite) increased with increasing pH and decreasing DIC from initial values of 3.3 ±0.0 up to 9.9 ±0.2 (Fig. 2D).

In the P-deplete cultures, DIC decreased from initial concentrations of 2160 µmol kg^{-1} to about 1000 µmol kg^{-1}, much lower than in the P-replete cultures, and values remained low until the end of the experiment (Fig. 2A). The pH_{tot} increased from initial values of 7.95 to 8.76 (on day 13 and 14) with a subsequent decline to values of about 7.90 (Fig. 2C). TA values remained relatively constant at 2447 ±12 µmol kg^{-1} until the transition to the post-bloom phase, when TA started to drop quickly and leveled off to about 1400 µmol kg^{-1} (Fig. 2B). The calculated Ω_{Ar} increased from initial 3.1 ±0.2 to about 9.1 ±0.6 (Fig. 2C). After TA dropped, white precipitates were observed and further analyzed.

The investigation of the precipitate by means of SEM showed particles which can be described best as aggregates of fibers having a length of about 20 µm (Fig. 3A and B). The Raman spectra (Fig. 3C) of the samples and two references (natural calcite and aragonite) show the typical vibration modes ν_1 (1085 cm^{-1} calcite and aragonite) and ν_4 (711 cm^{-1} calcite and 705 cm^{-1} aragonite) for CO_3 in a crystal lattice (Behrens et al. 1995). The precipitate can unambiguously identified as aragonite using the lattice vibrations between 100 and 400 cm^{-1} wave numbers. Calcite and aragonite both show a strong peak at ~153 cm^{-1} (155 cm^{-1} calcite and 152 cm^{-1} aragonite) but show unique peaks at 282 cm^{-1} (calcite) and 206 cm^{-1} aragonite). Raman spectra determined at 20 different positions chosen randomly across the precipitate showed no other carbonate phase than aragonite to be present.

Discussion:

Bloom events by *Trichodesmium* are often associated with highly stratified waters (Gianesella-Galvao et al. 1995; Siqueira et al. 2006) and low inorganic nutrient availability (Capone and Carpenter 1982), conditions which were mimicked within our laboratory study. The pattern and rate in the buildup of biomass (Fig. 1A) is consistent with the findings of previous studies on bloom dynamics of *Trichodesmium* (Berman-Frank et al. 2004; La Roche and Breitbarth 2005). Maximum cell densities obtained in this study (~5.5×10^9 cells L^{-1}; calculated using a chl *a* quota by Kranz et al. 2009), are within the range of cell concentrations reported for blooms in the ocean (up to 6.6×10^9; La Roche and Breitbarth 2005). The observed termination of the bloom, even under P-repletion, might be explained by an autocatalyzed cell death in *Trichodesmium* (Berman-Frank et al. 2004).

During bloom development, the DIC drawdown by photosynthetic carbon uptake exceeds the slow re-equilibration with the atmosphere, causing chemical speciation of the DIC pool to shift towards higher CO_3^{2-} concentration and pH. Upper pH values in our study are comparable to those observed during phytoplankton blooms (Hansen 2002), but such data on *Trichodesmium* blooms are scarce. Satpathy et al. (2007) observed pH values of 8.3 within a *Trichodesmium* bloom, yet the biomass in this field study was orders of magnitude lower (~4×10^6 cells L^{-1}) than the one in our and other studies (~5.7×10^9 cells L^{-1}; Suvapepun 1992). Next to the total biomass build up, weather conditions and mixing will also determine the magnitude in carbonate chemistry shift. In calm and highly stratified waters, a large shift in the carbonate system of the bulk seawater can be expected. The overall changes in carbonate chemistry due to photosynthetic carbon uptake are however largest in the close proximity of the cells, the diffusive boundary layer (Wolf-Gladrow et al. 1999; Ploug 2008).

The deviation in carbonate chemistry between cell surface and bulk critically depends on the C uptake, rate as well as speciation, and the surface-to-volume ratio (Wolf-Gladrow and Riebesell 1997). *Trichodesmium* operates an efficient carbon concentrating mechanism (CCM) primarily based on direct HCO_3^- uptake (Kranz et al. 2009). Owing to high affinities for HCO_3^-, *Trichodesmium* can maintain high rates of carbon uptake even at low DIC concentrations. As filaments of *Trichodesmium* tend to form aggregates, so-called ‘puffs’ and ‘tufts’ often being >500 µm in diameter (La Roche and Breitbarth 2005), the surface-to-volume ratio is significantly smaller than for single filaments. Both, high rates of C uptake in combination with the large size of aggregates imply that carbonate chemistry at the cell surface largely deviates from the situation in bulk water.

To estimate the carbonate chemistry in the microenvironment of a *Trichodesmium* aggregate, a diffusion-reaction model has been applied (Wolf-Gladrow and Riebesell 1997). Carbon fixation was approximated from growth rates (0.31 d^{-1}) and POC quotas (5 pmol cell^{-1}) in the late exponential phase. HCO_3^- contribution (80% of total C uptake) were taken from Kranz et al. (2009). For model calculations, a spherical aggregate (diameter 700 µm) with 15000 cells were used. Calculations for pH and Ω_{Ar} at the aggregate surface yielded significantly higher values than measured for the bulk media (Fig. 4). This finding supports our hypothesis that the impact on carbonate chemistry of a natural *Trichodesmium* bloom, which is dominated by aggregates (Taboada et al. 2010), is comparable or even more pronounced than in our study (Fig. 2).

This is the first study reporting the precipitation of aragonite induced by *Trichodesmium* (Fig. 3A and B). As discussed above, the photosynthetic activity of *Trichodesmium* can shift the carbonate system towards high pH within the bulk and even further in the boundary layer. The concomitant increase in Ω_{Ar} to values as high as ~10 (Fig. 2C) likely triggers the aragonite formation observed in the P-deplete cultures. As $CaCO_3$ precipitation by cyanobacteria occurs at the cell sheath (Obst et al. 2009), it is strongly influenced by ambient conditions and thus, despite high supersaturation with respect to aragonite, may be hindered by interfering ions like PO_4^{3-} (House 1987; Lin and Singer 2005). This may explain that no aragonite precipitation occurred in the P-replete cultures. Consequently, late bloom situations with typically high Ω_{Ar} and low PO_4^{3-} concentrations like in our study (Fig. 1B and 2C) favor the precipitation of aragonite.

Marine calcification by the filamentous cyanobacteria *Girvanella* were responsible for the formation of immense carbonate sediments about 750-700 Myr ago (Riding 2006). In the Paleozoic and Mesozoic, several $CaCO_3$ precipitation events were triggered by a diverse cyanobacterial flora (Riding 2006). In the Cenozoic, calcification events by cyanobacteria became scarce and thus less important for sediment formation (Riding 2006). It was proposed, that the oceanic carbonate chemistry over the Cenozoic changed so that calcification by cyanobacteria became less favorable (Riding 1982; Pentecost and Riding 1986). Nonetheless, there is evidence for calcification induced by cyanobacteria in marine systems today (Golubic and Campbell 1981; Yates and Robbins 1995), e.g. at the Great Bahama Bank (Robbins et al. 1996) where also *Trichodesmium* occur (Carpenter et al. 1987). Field observations are needed to verify the potential of *Trichodesmium* to induce $CaCO_3$ precipitation and to judge possible implications for biogeochemical cycling.

References:

Arrigo KR, Robinson DH, Worthen DL, Dunbar RB, DiTullio GR, VanWoert M, Lizotte MP (1999) Phytoplankton Community Structure and the Drawdown of Nutrients and CO_2 in the Southern Ocean. Science **283:** 365-367

Behrens G, Kuhn LT, Ubic R, Heuer AH (1995) Raman Spectra of Vateritic Calcium Carbonate. Spectroscopy Letters **28:** 983-995

Berman-Frank I, Bidle KD, Haramaty L, Falkowski PG (2004) The demise of the marine cyanobacterium, *Trichodesmium spp*., via an autocatalyzed cell death pathway. Limnol. Oceanogr. **49:** 997-1005

Capone DG, Burns JA, Montoya JP, Subramaniam A, Mahaffey C, Gunderson T, Michaels AF, Carpenter EJ (2005) Nitrogen fixation by *Trichodesmium spp*.: An important source of new nitrogen to the tropical and subtropical North Atlantic Ocean. Global Biogeochem. Cycles **19:** GB2024, 2010.1029/2004GB002331

Capone DG, Carpenter EJ (1982) Nitrogen Fixation in the Marine Environment. Science **217:** 1140-1142

Carpenter EJ, Scranton MI, Novelli PC, Michaels A (1987) Validity of N_2 fixation rate measurements in marine *Oscillatoria* (*Trichodesmium*). J. Plankton Res. **9:** 1047-1056

Chen Y-B, Zehr JP, Mellon M (1996) Growth and nitrogen fixation of the diazotrophic filamentous nonheterocystous cyanobacterium *Trichodesmium* sp. IMS 101 in defined media: evidence for a circadian rhythm. J. Phycol. **32:** 916-923

Des Marais DJ (2000) Evolution: When Did Photosynthesis Emerge on Earth? Science **289:** 1703-1705

Dickson AG, Millero FJ (1987) A comparison of the equilibrium constants for the dissociation of carbonic acid in seawater media. Deep Sea Res. Part I-Ocean. Res. Papers **34:** 1733-1743

Gianesella-Galvao SMF, Costa MPF, Kutner MB (1995) Bloom de *Oscillatoria* (*Trichodesmium*) *erythraea* (Ehr.) Kutz. in coastal waters of the Southweast Atlantic. Publ. Esp. Inst. Oceonograf. **11:** 133-140

Golubic S, Campbell S (1981) The relationship between blue-green algae and carbonate deposits. *In* N Carr, BA Whitton, eds, Phanerozoic Stromatolites. Springer, Berlin, pp 209-229

Gran G (1952) Determination of the equivalence point in potentiometric titrations. Part II. The Analyst **77:** 661

Hansen PJ (2002) Effect of high pH on the growth and survival of marine phytoplankton: implications for species succession. Aquat. Microb. Ecol. **28:** 279-288

Holligan PM, Fernandez E, Aiken J, Balch WM, Boyd P, Burkill PH, Finch M, Groom SB, Malin G, Muller K, Purdie DA, Robinson C, Trees CC, Turner SM, Vanderwal P (1993) A biogeochemical study of the coccolithophore, *Emiliania huxleyi,* in the North-Atlantic. Glob. Biogeochem. Cycles **7:** 879-900

House WA (1987) Inhibition of calcite crystal growth by inorganic phosphate. J. Coll. Interf. Science **119:** 505-511

Kranz SA, Sueltemeyer D, Richter K-U, Rost B (2009) Carbon acquisition in *Trichodesmium*: the effect of pCO_2 and diurnal changes. Limnol. Oceanogr. **54:** 548-559

La Roche J, Breitbarth E (2005) Importance of the diazotrophs as a source of new nitrogen in the ocean. J. Sea Res. **53:** 67-91

Lewis E, Wallace DWR (1998) Program developed for CO_2 system calculations. ORNL/CDIAC-105. *In*. (Carbon Dioxide Information Analysis Center, Oak Ridge National Laboratory, US Department of Energy, Oak Ridge, Tennessee, 1998).

Lin Y-P, Singer PC (2005) Inhibition of calcite crystal growth by polyphosphates. Water Research **39:** 4835-4843

Mehrbach C, Culberson CH, Hawley JE, Pytkowicz RM (1973) Measurement of the Apparent Dissociation Constants of Carbonic Acid in Seawater at Atmospheric Pressure. Limnol. Oceanogr. **18:** 897-907

Mulholland MR, Heil CA, Bronk DA, O'Neil MO (2006) Nitrogen fixation and release of fixed nitrogen by *Trichodesmium* sp. in the Gulf of Mexico. Limnol. Oceanogr. **51:** 1762-1776

Obst M, Wehrli B, Dittrich M (2009) $CaCO_3$ nucleation by cyanobacteria: laboratory evidence for a passive, surface-induced mechanism. Geobiol. **7:** 324-347

Pentecost A, Riding R (1986) Calcifcation in cyanobacteria. *In* BSC Leadbeater, R Riding, eds, Biomineralization in Lower Plants and Animals. Clarendon Press, Oxford., pp 914-921

Ploug H (2008) Cyanobacterial surface blooms formed by *Aphanizomenon* sp. and *Nodularia spumigena* in the Baltic Sea: Small-scale fluxes, pH, and oxygen microenvironments. Limnol. Oceanogr. **53:** 914-921

Riding R (1982) Cyanophyte calcification and changes in ocean chemistry. Nature **299:** 814-815

Riding R (2006) Cyanobacterial calcification, carbon dioxide concentrating mechanisms, and Proterozoic-Cambrian changes in atmospheric composition. Geobiol. **4:** 299-316

Robbins LL, Yates KK, Shinn G, Blackwelder P (1996) Whiting on the great Bahama bank: a microscopic solution to a macroscopic mystery. Bahm. J. Science **4:** 2-7

Satpathy KK, Mohanty AK, Sahu G, Prasad VMR, Venkatesan R, Natesan U, Rajan M (2007) On the occurrence of *Trichodesmium erythraeum* (Ehr.) bloom in the coastal waters of Kalpakkam, east coast of India. Indian J.Sci.Technol. **1:** 1-9

Siqueira A, Kolm HE, Brandini FP (2006) Offshore distribution patterns of the cyanobacterium *Trichodesmium erythraeum* ehrenberg and associated phyto- and bacterioplankton in the southern Atlantic coast (Paraná, Brazil). Braz. Arch. Biol. Technnol. **49:** 323-337

Stoll MHC, Bakker K, Nobbe GH, Haese RR (2001) Continuous-Flow Analysis of Dissolved Inorganic Carbon Content in Seawater. Anal. Chem. **73:** 4111-4116

Suvapepun S (1992) *Trichodesmium* blooms in the Gulf of Thailand. *In* EJ Carpenter, DG Capone, JG Rueter, eds, Marine Pelagic Cyanobacteia: *Trichodesmium* and Other Diazotrophs. Kluwer Academic, Dordrecht, p 343

Taboada FG, Gil RG, Hofer J, Gonzalez S, Anadon R (2010) *Trichodesmium spp.* population structure in the eastern North Atlantic subtropical gyre. Deep Sea Res. Part I-Ocean. Res. Papers **57:** 65-77

Wolf-Gladrow D, Riebesell U (1997) Diffusion and reactions in the vicinity of plankton: A refined model for inorganic carbon transport. Mar. Chem. **59:** 17-34

Wolf-Gladrow DA, Bijma J, Zeebe RE (1999) Model simulation of the carbonate chemistry in the microenvironment of symbiont bearing foraminifera. Mar. Chem. **64:** 181-198

Yates KK, Robbins LL (1995) Experimental evidence for a $CaCO_3$ precipitation mechanism for marine *Synechocystis*. Bull. Instit. oceanogr. Monaco Sp. Ed. **14:** 51–59

Acknowledgements:

The research leading to these results has received funding from the European Research Council under the European Community's Seventh Framework Programme (FP7/2007-2013) / ERC grant agreement [205150]. Financial support was also provided by the Federal Ministry of Education and Research (BMBF, FKZ 03F0608 A03F0608B) and this research contributes to the "European Project on Ocean Acidification" (EPOCA) under grant agreement n°211384. G. Langer acknowledges financial support by the Spanish Ministry of Education (Juan de la Cierva programme) co-funded by the European Social Fund and Ministry of Science and Innovation. We thank Klaus-Uwe Richter and Ulrike Richter for laboratory assistance.

Tables:

Table 1: modified YBC II media

	[mmol L^{-1}]		[µmol L^{-1}]
NaCl	420	$FeCl_3$	0.41
KCl	10	Na_2-EDTA	2
$MgCl_2$	20	Biotin	0.002
$CaCl_2$	10	Vitamin B_{12}	0.004
$MgSO_4$	25	Thiamine-HCl	0.3
KBr	1	$MnCl_2$	0.02
H_3BO_3	0.58	$ZnSO_4$	0.004
$SrCl_2$	0.07	$CoCl_2$	0.003
NaF	0.07	Na_2MoO_4	0.011
LiCl	0.03	$CuSO_4$	0.001
$NaHCO_3$	2.2	KH_2PO_4	5

Figure legends:

Figure 1: Changes in concentrations of (A) Chl *a*, (B) PO_4^{3-} over the course of a bloom. Grey diamonds present the P-deplete, black circles present the P-replete cultures. The vertical dotted line represents the transition phase between exponential and post bloom phase. The grey area represents the range of PO_4^{3-} concentrations in the P-replete culture.

Figure 2: Changes in (A) DIC, (B) TA, (C) pH_{tot} and (D) Ω_{Ar} over the course of a bloom. Grey diamonds present the P-deplete, black circles present the P-replete cultures. The vertical dotted line represents the transition phase between exponential and post bloom phase.

Figure 3: (A, B) SEM pictures and (C) Raman Spectra of the precipitate found in the P-deplete cultures: (A) Precipitate show needle type aragonitic crystals. Size bars are given in the picture. (C) Raman spectra of reference material (calcite, aragonite) and the sample. Calcite and aragonite both show a strong peak at ~153 cm^{-1} (155 cm^{-1} calcite and 152 cm^{-1} aragonite) but show unique peaks at 282 cm^{-1} (calcite) and 206 cm^{-1} aragonite), using the lattice vibrations between 100 and 400 cm^{-1} wave-numbers. Raman spectra were determined at 20 different positions chosen randomly across the crystal and showed no other carbonate phase than aragonite to be present.

Figure 4: Modelled profiles of pH and Ω_{Ar} and DIC for a *Trichodesmium* aggregate as a function of the distance from the surface of the aggregate. Solid line denote pH_{tot}, dashed line Ω_{Ar} and dotted line DIC.

Figures:

Figure 1:

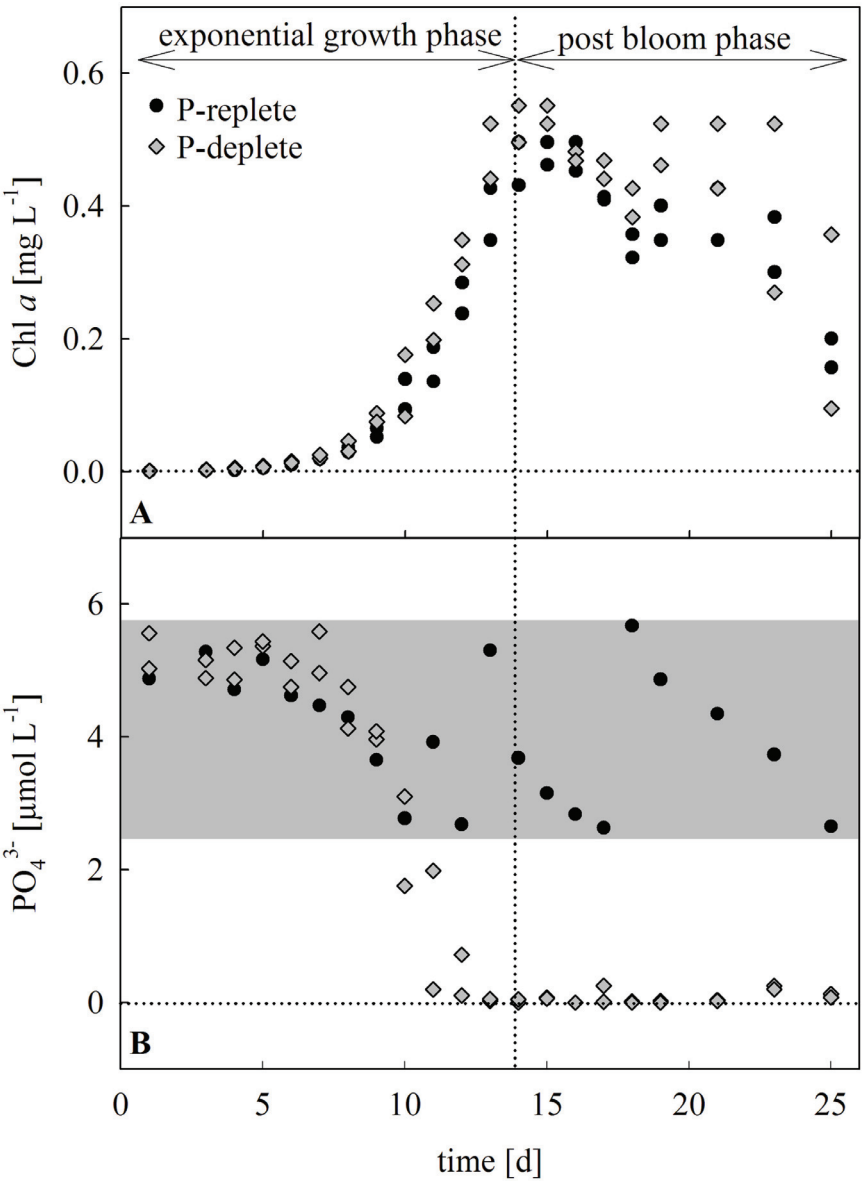

Figure 2:

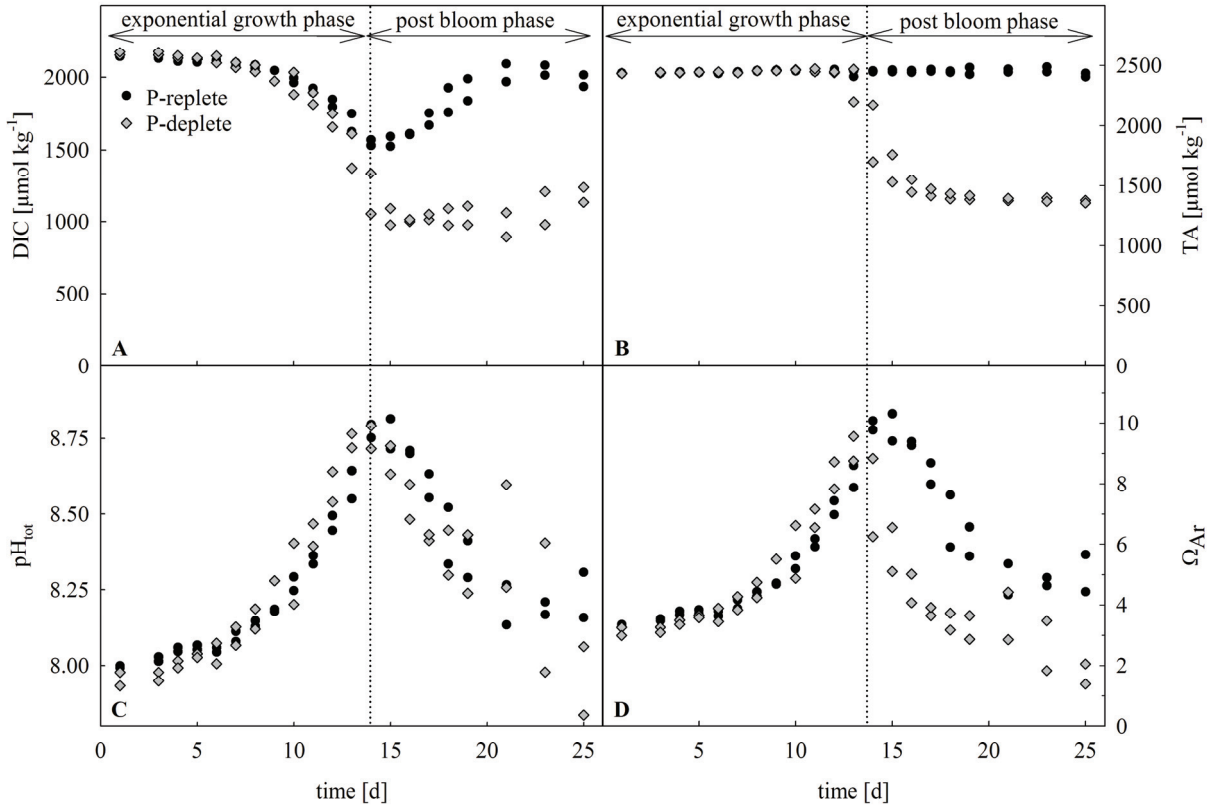
exponential growth phase
post bloom phase
exponential growth phase
post bloom phase
P-replete
P-deplete
DIC [µmol kg-1]
TA [µmol kg-1]
pHtot
ΩAr
A
B
C
D
time [d]
time [d]

Figure 3:

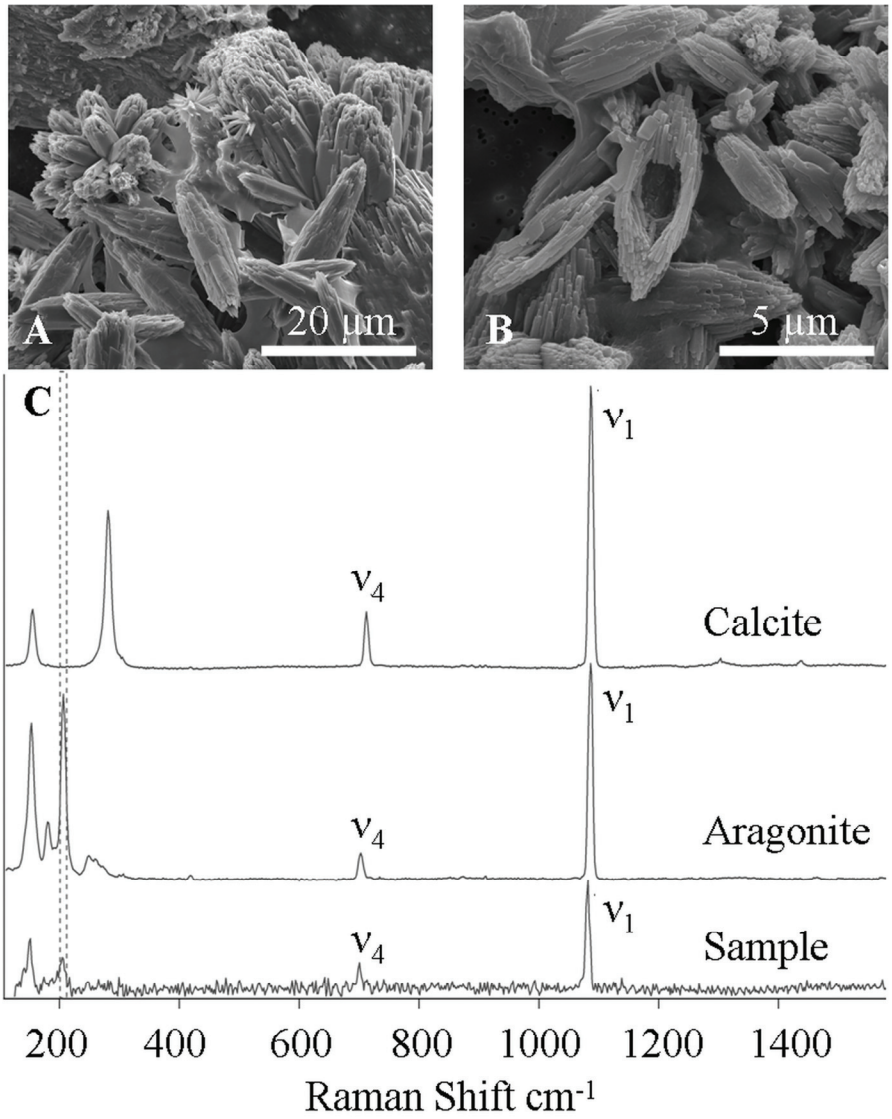
A
20 µm
B
5 µm
C
ν1
ν4
Calcite
ν1
ν4
Aragonite
ν1
ν4
Sample
200
400
600
800
1000
1200
1400
Raman Shift cm-1

Figure 4:

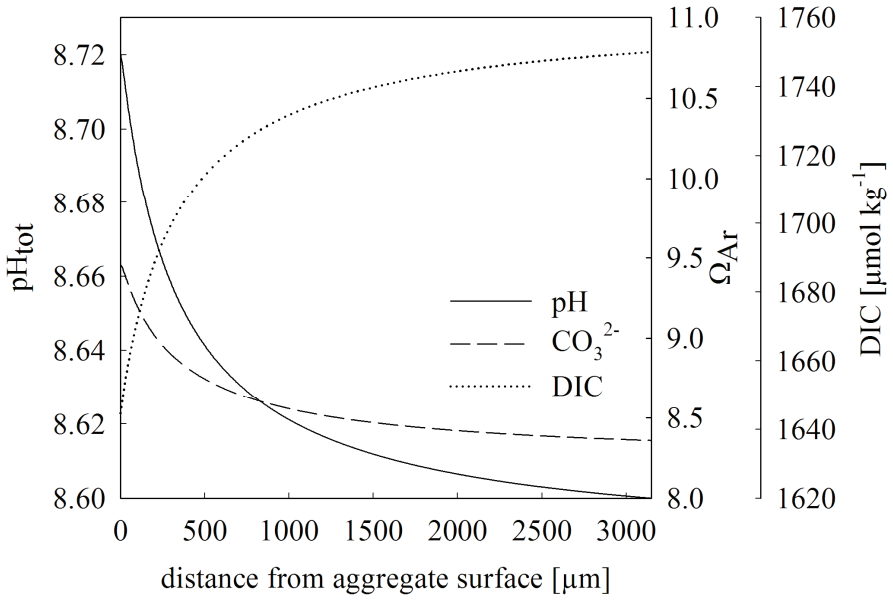
8.72
8.70
8.68
8.66
8.64
8.62
8.60
pHtot
11.0
10.5
10.0
9.5
9.0
8.5
8.0
ΩAr
1760
1740
1720
1700
1680
1660
1640
1620
DIC [µmol kg-1]
pH
CO3 2-
DIC
0
500
1000
1500
2000
2500
3000
distance from aggregate surface [µm]

General discussion

4 General discussion

Trichodesmium spp. challenged scientists for decades since Dugdale et al. (1961) reported the fixation of N_2 by this species. It became of particular interest for biogeochemistry when its contribution to the overall N_2 fixation in the tropical and subtropical areas was estimated (Carpenter and McCarthy, 1975). Several studies henceforward postulated a significant influence of *Trichodesmium* on the global carbon and nitrogen cycles (Falkowski, 1997; Gruber and Sarmiento, 1997). Considering the current increase in atmospheric CO_2 as well as global temperatures and their effects on the marine environment (Solomon et al., 2007), it is necessary to elucidate *Trichodesmium*'s response to those changes. This thesis describes the effects of different CO_2 levels on the ecophysiology of the diazotroph *Trichodesmium erythraeum* and investigates potential underlying processes. In the following, the main conclusions are summarized and discussed in terms of consequences for ecology and biogeochemistry. Finally, perspectives for future research are outlined.

4.1 Ecophysiology and underlying processes

Responses of *Trichodesmium erythraeum* were assessed in different CO_2 perturbation experiments. In these acclimations, *Trichodesmium* showed increased production of POC and PON under CO_2 levels predicted for the future ocean (Publication II). Further investigations showed that light levels strongly modify CO_2-sensitivity in POC and PON production as well as cell division rates (Publication III), observing the highest stimulation by CO_2 under limiting light conditions. Such responses in growth and production rates due to elevated pCO_2 exceed those reported for other important marine phytoplankton functional groups such as diatoms and coccolithophores (Burkhardt et al., 1999; Zondervan et al., 2002; Langer et al., 2006) and demonstrate an exceptionally high CO_2-sensitivity of *Trichodesmium*. Similar responses were also found in other studies on *Trichodesmium* (Hutchins et al., 2007; Levitan et al., 2007), for which various reasons have been discussed, including CO_2 limitation of photosynthetic C fixation. Since cyanobacteria possess a RubisCO with one of lowest CO_2-affinities among phytoplankton, strong changes in C fixation with increasing CO_2 levels can be expected, especially when cells depend on diffusive CO_2 uptake.

To understand the observed CO_2 effects on growth, elemental composition and production rates (Publication II & III), information about modes of C acquisition in *Trichodesmium* is required. These processes have been increasingly studied in marine phytoplankton as they were identified to explain CO_2 effects on marine primary productivity and phytoplankton ecology (Giordano et al., 2005). A variety of methods to examine these processes have been used, but as

they differ in concepts and protocols, obtained results and interpretations may not match. In Publication I, ^{14}C and MIMS-based approaches were applied to quantify the uptake of CO_2 and/or HCO_3^- as well as CA activities for several phytoplankton species including *Trichodesmium*. The ^{14}C disequilibrium technique was confirmed as a robust and accurate method to differentiate between CO_2 and HCO_3^- as inorganic carbon source. Although data from this technique lack central information on C acquisition, e.g. affinities, one can quantify species-specific differences in the preference for CO_2 and HCO_3^- or assess changes in the use of carbon sources under different conditions. Being easily adaptable, the approach is ideal for field applications, especially in combination with other ^{14}C-based incubations (Tortell et al., 2008).

A more precise characterization of cellular carbon fluxes, such as rates and affinities for CO_2 and HCO_3^- uptake, can only be obtained by the instrumentally more sophisticated MIMS approach. Such detailed data are needed to fully describe the acclimation responses in photosynthetic C acquisition to ocean acidification. Although based on different assumptions, both approaches yield comparable estimates on the relative contribution of CO_2 versus HCO_3^- uptake. Regarding estimates for activity of extracellular carbonic anhydrase (eCA), results differed significantly between the two approaches. Assessing eCA activities by the ^{14}C approach was found to be only applicable when cells take up mainly CO_2 and possess only low activities of eCA. For more precise estimates, covering a range of activities in CO_2 as well as HCO_3^- users, MIMS provides the ideal tool. This method comparison provided experimental confirmation of key assumptions and demonstrated strengths and weaknesses of the different approaches, which were further considered for the detailed characterization of the CCM in *Trichodesmium* (Publication II & III).

Data in Publication II & III clearly demonstrated the presence of a CCM in *Trichodesmium*, primarily based on HCO_3^- uptake. The uptake and accumulation of HCO_3^- allows *Trichodesmium* to saturate its RubisCO, even under low DIC concentrations. Consequently, a direct effect of CO_2 on the carboxylation efficiency of RubisCO, as suggested by Hutchins et al. (2007), can be excluded as main reason for the CO_2-sensitivity observed for *Trichodesmium*. Despite the predominance of HCO_3^- transport, the gross CO_2 uptake rate increased under elevated CO_2 (Publication III). Due to the high CO_2 permeability of membranes, uptake and accumulation of this carbon species do not appear efficient for *Trichodesmium*. To prevent diffusive CO_2 loss, cyanobacteria typically convert CO_2 to HCO_3^- at the thylakoid membrane by the $NDH1_4$ complex utilizing reductants from cyclic or linear electron transport (Friedrich and Scheide, 2000; Badger et al., 2006). Changes in uptake kinetics found for the HCO_3^- transport at the different CO_2 levels (Publication II) as well as the changes in the CO_2 to HCO_3^- uptake

ratios (Publication III) may be caused by variations in the reductive state of the electron transport chain. This in turn will affect the balance between cyclic and linear electron transport and thus alter the energy supply for transporters (Li and Canvin, 1998). Post-translational modification of the transport proteins may also be a cause for changes in the transport affinities (Sueltemeyer et al., 1998). Underlying mechanisms for affinity changes have, however, not been investigated to this level in this study.

In addition to direct uptake of HCO_3^-, extracellular carbonic anhydrase (eCA) may represent another important component of the CCM. This enzyme accelerates the chemical equilibrium between HCO_3^- and CO_2 and thus replenishes the inorganic carbon species mainly taken up. In diatoms, Trimborn et al. (2008) found high eCA activities to be correlated with high HCO_3^- uptake. The authors suggested that eCA converts effluxing CO_2 to HCO_3^-, subsequently being transported back into the cell via the HCO_3^- transporter. Such a C recycling mechanism would be most efficient when CA-mediated conversion is localized to the periplasmic space, i.e. in close vicinity of the HCO_3^- transporter. Despite being a HCO_3^- user, *Trichodesmium* showed only low eCA activities (Publication II). In contrast to eukaryotic phytoplankton, cyanobacteria like *Trichodesmium* have developed other strategies that do not involve eCA. In analogy to the proposed role of eCA in HCO_3^- users by Trimborn et al. (2008), $NDH1_4$ functions to convert CO_2 to HCO_3^- in cyanobacteria. As this process is located at the thylakoid membrane, it seems to be involved in the prevention of CO_2 loss rather than its uptake.

The CO_2 efflux is important to consider, as the CCM efficiency not only depends on the uptake kinetics but also on the loss of inorganic carbon. In Publication II & III, MIMS and the interpretation of ^{13}C fractionation patterns were used to assess information on cellular leakage (i.e. C efflux/gross C uptake). Although approaches attained different absolute values, which can partly be attributed to differences in concepts (e.g. instantaneous versus integrated estimates), both indicated CO_2- and/or light-dependent regulations within this parameter. Based on ^{13}C fractionation, estimated leakage was found to increase with pCO_2 as well as light availability (Publication III). The higher leakage under these conditions can partly be explained by the increasing overall C uptake relative to C fixation under high CO_2 levels. Since CO_2 efflux is the key driver for changes in leakage, the underlying biochemical explanation may rest upon the function of $NDH1_4$. While at high-light and low CO_2 levels, $NDH1_4$ may be used primarily as a CO_2-scavenging mechanism (consistent with the observed low leakage), high CO_2 levels may lead to a higher CO_2 diffusion to the proximity of the $NDH1_4$ when it maily functions as a system for CO_2 uptake (consistent with high rates of CO_2 uptake). As $NDH1_4$ is proposed to be driven by reductants from cyclic or linear electron transport, this protein complex may represent

a switch for the regulation of reductant-demanding metabolic processes. Further investigations on leakage and possible regulations by $NDH1_4$ in *Trichodesmium* have to be conducted, but in view of the current uncertainties in leakage estimates, new approaches are required to assess this essential process within CCMs.

As discussed above, various aspects of the CCM in *Trichodesmium* were regulated as a function of pCO_2. Equally or even more pronounced changes in the CCM were observed over the diurnal cycle (Publication II). Apparent affinities for HCO_3^- uptake as well as leakage changed markedly over the day. Lower overall CCM efficiency was found to be correlated with highest activities of the nitrogenase during midday (Publication II & III). In addition to this typical diurnal pattern in N_2 fixation (Berman-Frank et al., 2001; Mulholland et al., 2004; Milligan et al., 2007) observed under low and ambient CO_2 levels, high CO_2 resulted in a prolonged high N_2 fixation and low CCM efficiency until the end of the photoperiod (Publication II & III). Such CO_2-dependent changes in diurnal patterns as well as the light-dependent changes in CO_2 effects suggest altered energy allocation to be the key to the strong CO_2-sensitivity in *Trichodesmium*.

To investigate the energy budget and energy allocation, Publication III assessed major energy sources and sinks such as gross photosynthesis, nitrogenase activity, carbon acquisition and Mehler reaction simultaneously. Data presented in Publication III showed that the CO_2 effects on growth, POC and PON production could not be attributed to changes in gross photosynthesis (i.e. energy generation via linear electron transport). This finding supports the hypothesis that CO_2 effects are caused by improved energy allocation (Publication II). The high energetic costs associated with the operation of a CCM represent a large fraction of the overall energy budget in *Trichodesmium*. The ability to regulate the CCM activity to its actual demand reduces the energetic costs and allows reallocation of energy to N_2 and C fixation. Moreover, enhanced cyclic electron transport around PS I, as indicated by the high PSI:PSII ratio at high CO_2 (Appendix I), suggest an increased ATP production (Wolk, 1982). Overall, the high CO_2-sensitivity in *Trichodesmium* is not caused by a direct CO_2 effect on the carboxylation efficiency of RubisCO (Publication II), but rather can be attributed to CO_2-dependent reallocation of resources between the CCM, N_2 fixation, the Calvin cycle (Publication III).

The allocation of electrons to O_2 via pseudocyclic electron transport was often discussed as another way to enhance N_2 fixation. This photocatalyzed reduction of O_2 via the so-called Mehler reaction can scavenge O_2 and thus protect the O_2-sensitive nitrogenase. For *Trichodesmium*, Mehler reaction has been observed especially during N_2 fixation (Kana, 1993; Milligan et al., 2007). In Publication III, Mehler reaction was not correlated with N_2 fixation but

mainly found to be induced when cells were exposed to high light. These results contradict with the proposed function and rather hint to a photo-protective mechanism under high light. This process may be advantageous in view of the high and variable light levels typical for the natural environments of *Trichodesmium* (La Roche and Breitbarth, 2005).

Although having added another piece to the metabolic jigsaw of the diazotroph *Trichodesmium*, many uncertainties remain regarding the interdependent regulation of different metabolic pathways. Nontheless, data presented provide the potential to predict how this organism will thrive in the future ocean.

4.2 Implications for ecology and biogeochemistry

As elevated CO_2 yield in increasing growth, improved N_2 fixation and C acquisition as well as P utilization (Publication II & III), this sensitivity is likely to increase the competitive fitness of *Trichodesmium*. Consequently, "CO_2-fertilization" may increase the performance and dominance of *Trichodesmium* in the oligotrophic tropical and subtropical areas. The resulting "N-fertilization" may in turn be advantageous for cells like picocyanobacteria and nanoflagellates specialized for the uptake of NH_4^+ (Hutchins et al., 2009). Even though the increased N_2 fixation may alleviate the effect of an enhanced stratification on productivity caused by global warming (Doney, 2006), it will shift areas typically N-limited to be limited by inorganic phosphorus (P) and/or iron (Fe) in the future. As global warming will also result in an expansion of oligotrophic areas, a wider distribution of *Trichodesmium* can generally be expected (Breitbarth et al., 2007; Carpenter and Capone, 2008). In view of consequences on higher trophic levels, the increased C:P ratio under elevated pCO_2 (Publication III) may reduce the nutritional value of the produced organic matter (Boersma, 2000; Sterner and Elser, 2002; Van de Waal et al., 2009). As *Trichodesmium* is hardly grazed by heterotrophic eukaryotes (La Roche and Breitbarth, 2005), the lower nutritional values will mostly impact on bacterial production. In summary, the findings within this thesis and other recent studies on *Trichodesmium* (Barcelos é Ramos et al., 2007; Hutchins et al., 2007; Levitan et al., 2007) suggest this genus to be among the "winners" of global change. The consequences for the ecosystem structure and functioning, e.g. shift in species dominance or interactions within the food web, remain uncertain.

The changes in production rates (Publication II & III) and a possible increase in dominance of *Trichodesmium*, will have severe implications for future marine elemental cycling and climate feedback. Assuming that the CO_2-dependent increase in biomass and N_2 fixation can be scaled up to the ocean, the potential increase in new N inputs by *Trichodesmium* can be calculated for

the future. The current annual N_2 fixation by *Trichodesmium spp.* has been estimated to be around 60 Tg N yr^{-1} (Mahaffey et al., 2005). Data on CO_2-dependency in N_2 fixation rates obtained within this thesis and recent publications (see Hutchins et al., 2009 for review) suggest that N_2 fixation by *Trichodesmium spp.* might increase by 30 to 120 % to around 80 to 130 Tg N yr^{-1} until the end of this century. With respect to global N_2 fixation, *Trichodesmium spp.* would increase its contribution from about 25 to about 50 % (Galloway et al., 2004), which underline the role of *Trichodesmium* in the current and future global N budget. The high variability in estimates may be attributed to differences in methodology or growth conditions in the laboratory studies. Publication III explains part of these discrepancies as CO_2-effects were found to be strongly modulated by light.

In terms of vertical transport of organic matter, a fraction of senescent *Trichodesmium* sinks and contributes to the biological carbon pump. As enhanced pCO_2 results in higher production of biomass (Publication II & III), a correspondingly larger amount is expected to sink down to the oceans interior in the future. The CO_2 effect on the biological carbon pump may expand to other phytoplankton as more N become available via N_2 fixation by *Trichodesmium*. Moreover, exudation of transparent exopolymeric particles (TEP) was observed for senescent *Trichodesmium* cells (Berman-Frank et al., 2007). Assuming that CO_2 would not only stimulate the production of POC but also TEP (Engel et al., 2004), especially at the end of a bloom, relatively more biomass may sink to depth caused by TEP-mediated aggregate formation. But not only the amount and the sinking velocity of particulate organic material impact the efficiency of the biological pump, also the C:N:P stoichiometry is important to consider. The observed increase in C:P (Publication III) may increase the remineralization depth and thus the export of organic material. Since only a few measurements of sedimentation rates have been performed to date in order to quantify the vertical flux of material produced by *Trichodesmium* (Karl et al., 1997), sinking and sedimentation rates are poorly constrained. Nonetheless, the observed CO_2-dependency in POC production, C:N:P stoichiometry, and possibly TEP formation will increase the CO_2 drawdown in *Trichodesmium*-dominated areas.

While most experiments in this thesis are concerned with the effect of carbonate chemistry on *Trichodesmium*, working in dilute semi-continuous cultures, Publication IV monitored the effect of biomass buildup on carbonate chemistry in a *Trichodesmium* bloom. The observed DIC decrease and pH increase during exponential growth of *Trichodesmium* was comparable to those variations in natural phytoplankton bloom events (Arrigo et al., 1999; Watson et al., 2000). A diffusion-reaction model has been applied, demonstrating, that the carbonate chemistry at the cell surface of a *Trichodesmium* aggregate largely deviated from the situation in bulk water.

Such changes in DIC and pH alter the CO_2 availability for photosynthesis and thus may impose restriction on bloom development (Hansen et al., 2007; Hansen, 2002). The CCM activity in *Trichodesmium* (Publication II), however, enables the cells to perform high photosynthetic rates even under low DIC and CO_2 availability and thus circumvent limitation effects. Unexpected changes in carbonate chemistry were observed at the transition from exponential to stationary phase once P was consumed. The observed drop in TA could be explained by the precipitation of inorganic carbon in form of aragonite. This phenomenon demonstrates the capability of *Trichodesmium* to induce precipitation of $CaCO_3$, a process known for cyanobacteria in the past oceans (Riding, 2006). If this aragonite precipitation by *Trichodesmium* also occurs in the natural environment, this bears new implications for the biogeochemical role of this cyanobacterial species, as it may alter vertical profiles of TA and DIC in the oligotrophic ocean. If aragonite formation is a typical phenomenon at the end of a *Trichodesmium* bloom, it may act as ballast material and increase the export of organic matter (Armstrong et al., 2002; Klaas and Archer, 2002).

In this thesis, potential changes on future C and N cycling were discussed based on the stimulation in POC and PON production in *Trichodesmium* (Publication II & III). In order to get a more general view on the marine N budget, one also has to look at nitrification as well as denitrification and how these processes may be affected by ocean acidification. Nitrification is driven by organisms such as proteobacteria like *Nitrosomas*, *Nitrosococcus* (NH_3-oxidizing) and *Nitrobacter*, *Nitrospina* (NO_2-oxidizing). Since these bacteria are autotrophs, they depend on CO_2 fixation by RubisCO and thus may benefit from elevated pCO_2. Investigations on responses of these organisms to ocean acidification indicated, however, a reduction in the global ammonium oxidation rate in the surface ocean (Huesemann et al., 2002; Blackford and Gilbert, 2007; Yool et al., 2007). This scenario would ultimately reduce surface ocean nitrate concentrations and thus nitrate-supported primary production. The marine denitrification may be indirectly affected from ocean acidification as more organic matter may reach deeper waters (Riebesell et al., 2007) and cause O_2 minimum zones to expand. This decline on O_2 concentration in turn favors denitrification by bacteria likes *Pseudomonas* or anammox by *Scalindua*-related species (Kuypers et al., 2003), resulting in the production of gaseous N species. In summary, the overall marine N inventory and thus primary productivity will critically depend on whether the N gain via N_2 fixation will be larger than the N loss via denitrification and anammox.

4.3 Perspectives for future research

The results obtained in this thesis provide new information on ecophysiological responses of *Trichodesmium erythraeum* to variations in CO_2 availability and give details on underlying processes. Several questions for future research arise from the findings presented here. As shown in Publication II and III, growth and primary production of the non-heterocystous filamentous *Trichodesmium* was stimulated by increasing CO_2 levels, which in turn will have large implications on the future marine C and N cycle. Significant uncertainties remain, whether the observed responses of this diazotroph can be generalized to other important cyanobacteria like filamentous heterocyst-containing or unicellular diazotrophic as well as endosymbiontic species associated to e.g. diatoms. To assess the full diversity in responses of marine N_2 fixers to climate change, species like marine *Anabaena*, *Synecchocystis* or *Richelia* should be included in future surveys.

Most studies investigated CO_2 effects in isolation from other environmental factors. Publication III found strong modulation in CO_2-sensitivity under different light levels. This illustrates the need to look at multiple variables in combination with CO_2. The availability of nutrients generally has strong effect on the physiology of phytoplankton and thus will most likely alter the CO_2-sensitivity. Future CO_2 perturbation experiments on diazotrophs should for instance address the availability of iron, as this micro-nutrient is highly required for their nitrogenase enzyme as well as the photosynthetic apparatus and often limits growth in the natural environment. As P-limitation in oligotrophic areas is expected to intensify in the future, CO_2 effects should be investigated under different P availability. Experiments may also investigate the effect of different nitrogen sources like nitrate or ammonia, as eutrophication in coastal areas may reduce the competitiveness of diazotrophs.

Likewise to the approach taken in this thesis, future studies should go beyond the descriptive level and unravel the underlying mechanisms for the observed responses. Such process-understanding will allow for extrapolation to other species or growth conditions. To improve our knowledge about metabolic key processes, methods have to be developed or optimized. In comparison to the indirect approaches to assess N_2 fixation by acetylene-reduction, a MIMS-based method to directly measure N_2 fixation would improve our estimates for this important process. Additionally, these measurements could be combined with C and O_2 fluxes, allowing for the characterization of key processes in *Trichodesmium* and their regulation under different growth conditions.

Regarding the uncertainties in photosynthetic and respiratory electron transport, fluorescence methods should be coupled with MIMS-based approaches. This combination provides a new tool to investigate CO_2 leakage and the function of $NDH1_4$ (Publication III) in cyanobacteria but also

more general aspects of the electron transport. Additionally, processes like the Mehler reaction and photorespiration could be quantified with these methods by the use of specific inhibitors. A first step towards this combined approach has been taken with the review on "Fluorescence as an assay to understand aspects of the physiology of light regulation" (Appendix II). In this book chapter, different inhibitors and their function to quantify electron flux in phytoplankton are presented.

Future experiments should be expanded to the level of gene and proteins expression of key enzymes (Appendix I). Those data on the molecular level in combination with ecophysiological studies will maximize our current understanding of the CO_2-sensitivity in this intriguing group of cyanobacteria. Laboratory experiments shall ideally be complemented by field studies. These may cover different perturbation experiments (CO_2, N, P, Fe) during cruises or at field stations like TENATSO on Cape Verde Islands. Data from this thesis as well as future projects shall be exploited to develop cell models and to improve the parameterization of ecosystem and biogeochemical models. The anticipated results from these models will significantly improve our predictive capabilities on how the marine biosphere will respond to future environmental changes.

5 References

Armstrong RA, L. C, Hedges JI, Honjo S, S.G. W (2002) A new, mechanistic model for organic carbon fluxes in the ocean based on the quantitative association of POC with ballast minerals. Deep Sea Research Part II: Topical Studies in Oceanography **49:** 219 - 236

Arrigo KR, Robinson DH, Worthen DL, Dunbar RB, DiTullio GR, VanWoert M, Lizotte MP (1999) Phytoplankton Community Structure and the Drawdown of Nutrients and CO_2 in the Southern Ocean. Science **283:** 365-367

Badger MR, Andrews TJ, Whitney SM, Ludwig M, Yellowlees DC (1998) The diversity and co-evolution of Rubisco, plastids, pyrenoids and chloroplast-based CO_2-concentrating mechanisms in the algae. Can. J. Bot **76:** 1052

Badger MR, Price GD, Long BM, Woodger FJ (2006) The environmental plasticity and ecological genomics of the cyanobacterial CO_2 concentrating mechanism. J. Exp. Bot. **57:** 249-265

Barcelos é Ramos J, Biswas H, Schulz KG, LaRoche J, Riebesell U (2007) Effect of rising atmospheric carbon dioxide on the marine nitrogen fixer *Trichodesmium*. Global Biogeochem. Cycles **21:** doi:10.1029/2006GB002898

Berman-Frank I, Lundgren P, Chen Y-B, Kuepper H, Kolber Z, Bergman B, Falkowski P (2001) Segregation of Nitrogen Fixation and Oxygenic Photosynthesis in the Marine Cyanobacterium *Trichodesmium*. Science **294:** 1534-1537

Berman-Frank I, Lundgren P, Chen YB, Küpper H, Kolber Z, Bergman B, Falkowski P (2001) Segregation of nitrogen fixation and oxygenic photosynthesis in the marine cyanobacterium *Trichodesmium*. Science **294:** 1534-1537

Berman-Frank I, Lundgren P, Falkowski P (2003) Nitrogen fixation and photosynthetic oxygen evolution in cyanobacteria. Res Microbiol. **154:** 157-164

Berman-Frank I, Rosenberg G, Levitan O, Haramaty L, Mari X (2007) Coupling between autocatalytic cell death and transparent exopolymeric particle production in the marine cyanobacterium *Trichodesmium*. Environmental Microbiology **9:** 1415-1422

Blackford JC, Gilbert FJ (2007) pH variability and CO_2 induced acidification in the North Sea. Journal of Marine Systems **64:** 229-241

Blankenship RE (2001) Molecular evidence for the evolution of photosynthesis. Trends in Plant Science **6:** 4-6

Boersma M (2000) The nutritional quality of P-limited algae for *Daphnia*. Limnology and Oceanography **45:** 1157-1161

Breitbarth E, Oschlies A, LaRoche J (2007) Physiological constraints on the global distribution of *Trichodesmium* – effect of temperature on diazotrophy. Biogeosciences **4:** 53–61

Breitbarth E, Wohlers J, Kläs J, LaRoche J, Peeken I (2008) Nitrogen fixation and growth rates of *Trichodesmium* IMS-101 as a function of light intensity. Marine Ecology Progress Series **359:** 25-36

Burkhardt S, Riebesell U, Zondervan I (1999) Stable carbon isotope fractionation by marine phytoplankton in response to daylength, growth rate, and CO_2 availability. Marine Ecology Progress Series **184:** 31-41

Capone DG (2000) The marine nitrogen cycle. *In* D Kirchman, ed, Microbial Ecology of the Ocean. Wiley-Liss, New York, pp 455-493

Capone DG (2001) Marine nitrogen fixation: what 's the fuss? Curr. Opin. Microbiol. **4:** 341–348

Capone DG, Knapp AN (2007) Oceanography: A marine nitrogen cycle fix? Nature **445:** 159-160

Capone DG, Subramaniam A, Montoya JP, Voss M, Humborg C, Johansen AM, Siefert RL, Carpenter EJ (1998) An extensive bloom of the N_2-fixing cyanobacterium *Trichodesmium erythraeum* in the central Arabian Sea Marine Ecology Progress Series **172:** 281-292

Capone DG, Zehr JP, Paerl H, Bergman B, Carpenter EJ (1997) *Trichodesmium*, a Globally Significant Marine Cyanobacterium. Science **276:** 1221-1229

Carpenter EJ, Capone DG (2008) Nitrogen fixation. *In* DG Capone, DA Bronk, MR Mulholland, EJ Carpenter, eds, Nitrogen in the Marine Environment, Ed 2nd. Elsevier Press, Amsterdam, pp 141-198

Carpenter EJ, McCarthy JJ (1975) Nitrogen Fixation and Uptake of Combined Nitrogenous Nutrients by *Oscillatoria* (*Trichodesmium*) *thiebautii* in the Western Sargasso Sea. Limnology and Oceanography **20:** 389-401

Codispoti LA, Brandes JA, Christensen JP, Devol AH, Naqvi SWA, Paerl HW, T. Y (2001) The oceanic fixed nitrogen and nitrous oxide budgets: Moving targets as we enter the anthropocene? Scientia Marina **65:** doi:10.3989/scimar.2001.3965s3285

Des Marais DJ (2000) EVOLUTION: When Did Photosynthesis Emerge on Earth? Science **289:** 1703-1705

Devol AH (2003) Nitrogen cycle: Solution to a marine mystery. Nature **422:** 575-576

Dickson AG (1981) An Exact Definition of Total Alkalinity and a Procedure for the Estimation of Alkalinity and Total Inorganic Carbon from Titration Data. Deep-Sea Research Part A - Oceanographic Research Papers **28:** 609-623

Doney SC (2006) Oceanography: Plankton in a warmer world. Nature **444:** 695-696

Doney SC, Mahowald N, Lima I, Feely RA, Mackenzie FT, Lamarque JF, Rasch PJ (2007) Impact of anthropogenic atmospheric nitrogen and sulfur deposition on ocean acidification and the inorganic carbon system. Proceedings of the National Academy of Sciences of the United States of America **104:** 14580-14585

Durner J, Bohm I, Knorzer OC, Boger P (1996) Proteolytic degradation of dinitrogenase reductase from *Anabaena variabilis* (ATCC 29413) as a consequence of ATP depletion and impact of oxygen. Journal of Bacteriology **178:** 606–610

Dyhrman ST, Chappell PD, Haley ST, Moffett JW, Orchard ED, Waterbury JB, Webb EA (2006) Phosphonate utilization by the globally important marine diazotroph *Trichodesmium*. Nature **439:** 68-71

Ehrenberg CG (1830) Neue Beobachtungen über blutartige Erscheinungen in Ägypten, Arabien und Sibirien, nebst einer Übersicht und Kritik der früher bekannten. Poggend. Annal. **18:** 476-514

Engel A, Thoms S, Riebesell U, Rochelle-Newall E, Zondervan I (2004) Polysaccharide aggregation as a potential sink of marine dissolved organic carbon. Nature **428:** 929-932

Falkowski PG (1997) Evolution of the nitrogen cycle and its influence on the biological sequestration of CO_2 in the ocean. Nature **387:** 272-275

Falkowski PG, Raven JA (2007) Aquatic Photosynthesis. Blackwell Publishers.

Farquhar J, Bao H, Thiemens M (2000) Atmospheric Influence of Earth's Earliest Sulfur Cycle. Science **289:** 756-758

Field CB, Behrenfeld MJ, Randerson JT, Falkowski P (1998) Primary Production of the Biosphere: Integrating Terrestrial and Oceanic Components. Science **281:** 237-240

Friedrich T, Scheide D (2000) The respiratory complex I of bacteria, archaea and eukarya and its module common with membrane-bound multisubunit hydrogenases. FEBS Letters **497:** 1-5

Galloway JN, Dentener FJ, Capone DG, Boyer EW, Howarth RW, Seitzinger SP, Asner GP, Cleveland CC, Green PA, Holland EA, Karl DM, Michaels AM, Porter JH, Townsend AR, C.J. V (2004) Nitrogen cycles: Past, present, and future. Biogeochemistry **70:** 153-226

Giordano M, Beardall J, Raven JA (2005) CO_2 Concentrating Mechanisms in Algae: Mechanisms, Environmental Modulation, and Evolution. Annual Review of Plant Biology **56:** 99-131

Gruber N (2005) Oceanography: A bigger nitrogen fix. Nature **436:** 786-787

Gruber N, Sarmiento J (1997) Global patterns of marine nitrogen fixation and denitrification. Glob Biogeochem Cycles **11:** 235-266

Hansen PJ (2002) Effect of high pH on the growth and survival of marine phytoplankton: implications for species succession. Aquat. Microb. Ecol. **28:** 279-288

Hansen PJ, Lundholm N, Rost B (2007) Growth limitation in marine red-tide dinoflagellates: effects of pH versus inorganic carbon availability. Marine ecology progress series **334:** 63-71

Hawser SP, O'Neil JM, Roman MR, Codd GA (1992) Toxicity of blooms of the cyanobacterium *Trichodesmium* to zooplankton. J. Appl. Phycol. **4:** 79-86

Holland HD (1984) The chemical evolution of the atmosphere and the oceans. Princeton University Press, Princeton

Huesemann MH, Skillman AD, Crecelius EA (2002) The inhibition of marine nitrification by ocean disposal of carbon dioxide. Marine Pollution Bulletin **44:** 142-148

Hutchins DA, Fu F-X, Zhang Y, Warner ME, Feng Y, Portune K, Bernhardt PW, Mulholland MR (2007) CO_2 control of *Trichodesmium* N_2 fixation, photosynthesis, growth rates and elemental ratios: Implications for past, present and future ocean biogeochemistry. Limnol. Oceanogr. **552:** 1293–1304

Hutchins DA, Mulholland MR, Fu F (2009) Nutrient cycles and marine microbes in a CO_2-enriched ocean. Oceanography **22:** 128-145

Javaux EJ, Knoll AH, Walter MR (2001) Morphological and ecological complexity in early eukaryotic ecosystems. Nature **412:** 66-69

Johnson PW, Sieburth JM (1979) Chroococcoid Cyanobacteria in the Sea: A Ubiquitous and Diverse Phototrophic Biomass. Limnology and Oceanography **24:** 928-935

Kana TM (1993) Rapid oxygen cycling in *Trichodesmium thiebautii*. Limnol. Oceanogr. **38:** 18–24

Karl D, Letelier R, Tupas L, Dore J, Christian J, Hebel D (1997) The role of nitrogen fixation in biogeochemical cycling in the subtropical North Pacific Ocean. Nature **388:** 533-538

Karl D, Michaels A, Bergman B, Capone D, Carpenter E, Leetelier R, Lipschultz F, Paerl H, Sigman D, Stal L (2002) Dinitrogen fixation in the world's oceans. Biogeochemistry **57/58:** 47–98

Kasting JF, Siefert JL (2002) Life and the Evolution of Earth's Atmosphere. Science **296:** 1066-1068

Kasting JF, Toon OB, J.B. P (1988) How climate evolved on the terrestrial planets. Sci. Am. **258:** 90-97

Klaas C, Archer DE (2002) Association of sinking organic matter with various types of mineral ballast in the deep sea: Implications for the rain ratio. Global Biogeochem. Cycles **16:** 1116

Küpper H, Ferimazova N, Setlik I, Berman-Frank I (2004) Traffic Lights in *Trichodesmium*. Regulation of Photosynthesis for Nitrogen Fixation Studied by Chlorophyll Fluorescence Kinetic Microscopy. Plant Physiol. **135:** 2120-2133

Kuypers MMM, G. L, Woebken D, Schmid M, Fuchs BM, Amann R, Jorgensen BB, Jetten MSM (2005) Massive nitrogen loss from the Benguela upwelling system through anaerobic ammonium oxidation. Proc Natl Acad Sci USA **102:** 6478–6483

Kuypers MMM, Sliekers AO, Lavik G, Schmid M, Jorgensen BB, Kuenen JG, Damste JSS, Strous M, Jetten MSM (2003) Anaerobic ammonium oxidation by anammox bacteria in the Black Sea. Nature **422:** 608-611

La Roche J, Breitbarth E (2005) Importance of the diazotrophs as a source of new nitrogen in the ocean. Journal of Sea Research **53:** 67-91

Langer G, Gussone N, Nehrke G, Riebesell U, Eisenhauer A, Kuhnert H, Rost B, Trimborn S, Thoms S (2006) Coccolith strontium to calcium ratios in Emiliania huxleyi: The dependence on seawater strontium and calcium concentrations. Limnol. Oceanogr. **51:** 310–320

Levitan O, Rosenberg G, Setlik I, Setlikova E, Grigel J, Klepetar J, Prasil O, Berman-Frank I (2007) Elevated CO_2 enhances nitrogen fixation and growth in the marine cyanobacterium *Trichodesmium*. Global Change Biology **13:** 531-538

Li QL, Canvin DT (1998) Energy sources for HCO_3^- and CO_2 transport in air-grown cells of *Synechococcus* UTEX 625. Plant Physiol. **116:** 1125–1132

Lin S, Henze S, Lundgren P, Bergman B, Carpenter EJ (1999) Whole-cell immunolocalization of nitrogenase in marine diazotrophic cyanobacteria *Trichodesmium spp*. Appl.Environ. Microbiol **64:** 3052–3064

Mahaffey C, Michaels AF, Capone DG (2005) The conundrum of marine N_2 fixation. Am J Sci **305:** 546-595

Margulis L (1971) Symbiosis and evolution. Sci Am. **225:** 49–57

Margulis L (1996) Archaeal-eubacterial mergers in the origin of Eukarya: phylogenetic classification of life. Proc Natl Acad Sci **93:** 1071-1076

Mereschkowsky C (1905) Über Natur und Ursprung der Chromatophoren im Pflanzenreiche. Biol. Centralbl **25:** 593–604

Milligan AJ, Berman-Frank I, Gerchman Y, Dismukes GC, Falkowski PG (2007) Light-dependent oxygen consumption in nitrogen-fixing cyanobacteria plays a key role in nitrogenase protection. J. Phycol. **43:** 845–852

Mulholland MR, Bronk DA, Capone DG (2004) Dinitrogen fixation and release of ammonium and dissolved organic nitrogen by *Trichodesmium* IMS101. Aquatic Microbial Ecology **37:** 85-94

Myers J, Graham JR, Wang RT (1980) Light harvesting in *Anacystis nidulans* studied in pigment mutants. Plant Physiol.**:** 1144-1149

Ogawa T, Kaplan A (2003) Inorganic Carbon Acquisition Systems in Cyanobacteria. Photosynth Res. **77:** 105-115

Paerl HW (1994) Spatial segregation of CO_2-fixation in *Trichodesmium spp*.: Linkage to N_2-fixation potential. J Phycol. **30:** 790-799

Paerl HW, Bebout BM (1988) Direct Measurement of O_2-Depleted Microzones in Marine Oscillatoria: Relation to N_2 Fixation. Science **241:** 442-445

Paerl HW, Bebout BM (1992) Oxygen dynamics in *Trichodesmium* spp. dynamics. *In* EJ Carpenter, DG Capone, JG Rueter, eds, Marine Pelagic Cyanobacteria: *Trichodesmium* and Other Diazotrophs. Kluwer Academic, Dordrecht, Netherlands, pp 43-59

Papageorgiou GC (1996) The photosynthesis of cyanobacteria (blue bacteria) from the perspective of signal analysis of chlorophyll alpha fluorescence. Journal of Scientific & Industrial Research **55:** 596-617

Partensky F, Hess WR, Vaulot D (1999) *Prochlorococcus*, a marine photosynthetic prokaryote of global significance. Microbiol Mol Biol Rev **63:** 106-127

Price GD, Badger MR (1989) Expression of human carbonic anhydrase in the cyanobacterium *Synechococcus* PCC7942 creates a high CO_2-requiring phenotype. Evidence for a central role for carboxysomes in the CO_2 concentrating mechanism. Plant Physiol. **91:** 505

Price GD, Woodger FJ, Badger MR, Howitt SM, Tucker L (2004) Identification of a SulP-type bicarbonate transporter in marine cyanobacteria. Proc. Natl. Acad. Sci. USA. **101:** 18228-18233

Rai AN, Soderback E, B. B (2000) Tansley Review No. 116. Cyanobacterium-Plant Symbioses. New Phytologist **147:** 449-481

Raven J, Caldeira K, Elderfield H, Hoeg-Guldberg Oea (2005) Ocean acidification due to increasing atmospheric carbon dioxide. Policy Document 12/05, The Royal Society, London. Available at: www.royalsoc.ac.uk

Riding R (2006) Cyanobacterial calcification, carbon dioxide concentrating mechanisms, and Proterozoic-Cambrian changes in atmospheric composition. Geobiology **4:** 299-316

Riebesell U, Schulz KG, Bellerby RGJ, Botros M, Fritsche P, Meyerhofer M, Neill C, Nondal G, Oschlies A, Wohlers J, Zollner E (2007) Enhanced biological carbon consumption in a high CO_2 ocean. Nature **450:** 545-U510

Rost B, Zondervan I, Wolf-Gladrow D (2008) Sensitivity of phytoplankton to future changes in ocean carbonate chemistry: Current knowledge, contradictions and research directions. Marine ecology progress series **373:** 227-237

Rye R, Holland HD (1998) Paleosols and the evolution of atmospheric oxygen; a critical review. Am J Sci **298:** 621-672

Sarmiento JL, Dunne J, Gnanadesikan A, Key RM, Matsumoto K, Slater R (2002) A new estimate of the $CaCO_3$ to organic carbon export ratio. Global biogeochemical cycles **16:** 54.51-54.11

Sarmiento JL, R. M, C. LQ (1995) Air-sea CO_2 transfer and the carbon budget of the North Atlantic. Philos T Roy Soc B **348:** 211-219

Sato S, Paranagua MN, Eskinazi E (1966) On the mechanism of red tide of *Trichodesmium* in Recife, northeastern Brazil, with some considerations of the relation to the human disease Tamandare fever. Trabalhos do Instituto Oceanografico da Universidade de Recife **5/6:** 7–49

Schmetterer G (1994) Cyanobacterial respiration. *In* DA Bryant, ed, The Molecular Biology of Cyanobacteria. Kluwer Academic Publishers, Dordrecht, The Netherlands., pp 409–435

Solomon S, Qin M, Manning Z, Chen M, Marquis, Averyt KB, Tignor M, Miller HL (2007) Climate Change 2007: The Physical Science Basis. Contribution of Working Group I to the

Fourth Assessment Report of the Intergovernmental Panel on Climate Change. Cambridge University Press, Cambridge, United Kingdom and New York, NY, USA.

Sournia A, Chrdtiennot-Dinet M-J, Ricard M (1991) Marine phytoplankton: how many species in the world ocean? J. Plankton Res. **13:** 1093-1099

Sterner RW, Elser JJ (2002) Ecological stoichiometry. The biology of elements from molecules to the biosphere. Princeton University Press, Princeton; NJ

Subramaniam A, Carpenter EJ, Karentz D, Falkowski PG (1999) Bio-optical properties of the marine diazothrophic cyanobacteria *Trichodesmuim spp*. I. Absorption and photosynthetic action spectra. Limnol. and Oceanogr. **44:** 608-617

Sültemeyer D, Klughammer B, Badger MR, Price GD (1998) Fast induction of high-affinity HCO_3^- transport in cyanobacteria. Plant Physiol **116:** 183

Suvapepun S (1992) *Trichodesmium* blooms in the Gulf of Thailand. *In* EJ Carpenter, DG Capone, JG Rueter, eds, Marine Pelagic Cyanobacteia: Trichodesmium and Other Diazotrophs. Kluwer Academic, Dordrecht, p 343

Tett P, Barton ED (1995) Why are there about 5000 species of phytoplankton in the sea? J. Plankton Res. **17:** 1693-1704

Tortell PD, Payne CD, Li Y, Trimborn S, Rost B, Smith WO, Riesselman C, Dunbar R, Sedwick P, DiTullio G (2008) The CO_2 response of Southern Ocean phytoplankton. Geophys. Res. Lett. **35:** L04605

Trimborn S, Lundholm N, Thoms Sa, Richter K-U, Krock B, Hansen PJ, Rost B (2008) Inorganic carbon acquisition in potentially toxic and non-toxic diatoms: the effect of pH-induced changes in seawater carbonate chemistry. Physiologia Plantarum **133:** 92-105

Van de Waal DB, Verschoor AM, Verspagen JMH, Van Donk E, Huisman J (2009) Climate-driven changes in the ecological stoichiometry of aquatic ecosystems. Frontiers in Ecology and the Environment

Vermaas WF (2001) Photosynthesis and respiration in cyanobacteria. *In* Encyclopedia of Life Sciences. Nature Publishing Group, London, pp 1-7

Villareal TA, Carpenter EJ (1990) Diel buoyancy regulation in the marine diazotrophic cyanobacterium *Trichodesmium thiebautii*. Limnology and Oceanography **35 (8):** 1832-1837

Volk T, Hoffert MI (1985) Ocean carbon pumps: analysis of relative strengths and efficiencies in ocean-driven atmospheric CO_2 changes. *In* ET Sunquist, WS Broecker, eds, The carbon cycle and atmospheric CO_2: natural variation archean to present, Vol 32. American Geophysical Union, Geophysical Monographs, Washington, D.C, pp 99-110

Waterbury JB (2005) Little Things Matter A Lot Overlooked in the ocean until the 1970s, cyanobacteria are among Earth's most important organisms. Oceanus, Woods Hole Oceanographic Institution

Waterbury JB, Watson SW, Guillard RRL, Brand LE (1979) Widespread occurrence of a unicellular, marine, planktonic, cyanobacterium. Nature **277:** 293-294

Watson AJ, Bakker DCE, Ridgwell AJ, Boyd PW, Law CS (2000) Effect of iron supply on Southern Ocean CO_2 uptake and implications for glacial atmospheric CO_2. Nature **407:** 730-733

Wolf-Gladrow DA, Bijma J, Zeebe RE (1999) Model simulation of the carbonate chemistry in the microenvironment of symbiont bearing foraminifera. Marine Chemistry **64:** 181-198

Wolf-Gladrow DA, Zeebe RE, Klaas C, Koertzinger A, Dickson AG (2007) Total alkalinity: The explicit conservative expression and its application to biogeochemical processes. Marine Chemistry **106:** 287-300

Wolk CP (1982) Heterocysts. *In* NG Carr, W B.A., eds, The Biology of Cyanobacteria. Blackwell Scientific Publishers, Oxford, pp 359-368

Xiong J, Fischer WM, Inoue K, Nakahara M, Bauer CE (2000) Molecular Evidence for the Early Evolution of Photosynthesis. Science **289:** 1724-1730

Yool A, Martin AP, Fernandez C, Clark DR (2007) The significance of nitrification for oceanic new production. Nature **447:** 999-1002

Zeebe RE, Wolf-Gladrow DA (2007) CO_2 in seawater: equilibrium, kinetics, isotopes. Elsevier Science B.V., Amsterdam

Zehr JP, Ward BB (2002) Nitrogen cycling in the ocean: New perspectives on processes and paradigms. Applied and Environmental Microbiology **68:** 1015-1024

Zondervan I, Rost B, Riebesell U (2002) Effect of CO_2 concentration on the PIC/POC ratio in the coccolithophore *Emiliania huxleyi* grown under light-limiting conditions and different daylengths. Journal of Experimental Marine Biology and Ecology **272:** 55-70

Appendix I

The combined effects of pCO_2 and light on the N_2 fixing cyanobacteria *Trichodesmium* IMS101: A mechanistic view

Orly Levitan[1], Sven A. Kranz[2], Dina Spungin[1], Ondrej Prasil[3], Björn Rost[2] and Ilana Berman-Frank[1]

[1] The Mina and Everard Goodman Faculty of Life Sciences, Bar Ilan University, Ramat-Gan, 52900 Israel

[2] Alfred Wegener Institute for Polar and Marine Research, 27570 Bremerhaven, Germany

[3] Institute of Microbiology MBU AVCR, Trebon and Institute of Physical Biology, University of South Bohemia, Nove Hrady, Czech Republic

Abstract:

The marine diazotroph cyanobacterium *Trichodesmium* responds to elevated atmospheric pCO_2 with higher N_2 fixation and growth rates. To unveil the underlying mechanisms we examined the influence of pCO_2 (150 and 900 μatm) and light (50 and 200 μmol photons m^{-2} s^{-1}) on *Trichodesmium* IMS101. We expand on Kranz et al. (this volume), and focus on photosynthetic fluorescence parameters of PSII, ratios of the photosynthetic units (PSI:PSII), and on the pool sizes of key proteins involved in the fixation of carbon and nitrogen, and their subsequent assimilation. We show that fluxes related to PSII electron transfer, O_2 evolution and carbon fixation increased mainly as a response to high light and not to changes in pCO_2. Changes in pCO_2 and light decoupled the activity of proteins from their pool size and controlled the operation of the carbon concentrating mechanism (CCM). Elevated pCO_2 and high light led to lower amounts of several key proteins (NifH, PsbA, and PsaC) while amounts of AtpB and RbcL did not significantly change. The reduced investment in protein synthesis freed up energy that could be reallocated to increase N_2 fixation and growth at elevated pCO_2 while supporting similar photosynthetic fluxes. We suggest that the high flexibility in resources and energy in *Trichodesmium* is mediated by changes in the redox state of the photosynthetic electron transport chain and by post-translational regulation of key proteins. Thus, *Trichodesmium* is expected to flourish in the future surface oceans characterized by elevated pCO_2, higher temperatures and high light.

Introduction:

The marine filamentous nitrogen fixing (diazotroph) cyanobacteria *Trichodesmium* spp. blooms extensively in areas corresponding to almost half of the Earth's surface (Carpenter and Capone, 2008). *Trichodesmium* contributes 25 to 50% of the estimated rates of N_2 fixation in the oligotrophic subtropical and tropical oceans where these new nitrogen inputs stimulate carbon and nitrogen cycling (Capone and Subramaniam, 2005; Mahaffey et al., 2005). The increases in atmospheric pCO_2, and the subsequent impacts on ocean acidification, are also predicted to influence diazotrophs and specifically *Trichodesmium* for which elevated pCO_2 significantly increased growth and N_2 fixation rates (Hutchins et al., 2007, Levitan et al., 2007; in press, Ramos et al, 2007).

The reported sensitivity of *Trichodesmium* to changes in pCO_2 prompted further investigation into the organismal responses and its underlying mechanisms, specifically when combined with other environmental parameters such as temperature, nutrient availability, and light. Increased N_2 fixation and growth rates, changes in inorganic carbon acquisition, limited flexibility of C:N ratios, and conservation of photosynthetic activities with increased pCO_2, suggested that ATP and reductants (electrons, NAD(P)H) are reallocated in the cells (Levitan et al. 2007; in press, Kranz et al, 2009, Kranz et al. this volume).

In *Trichodesmium,* as in all cyanobacteria, different metabolic pathways such as respiration and photosynthetesis share several cellular complexes/proteins such as the plastoquinone (PQ) pool, succinate dehyrogenase (SDH) and ferredoxin (Fd) (Fig 1). Energetic currencies (electrons, ATP, NAD(P)H) are also shared and can be allocated/utilized according to cellular requirements. N_2 fixation by nitrogenase and the subsequent assimilation of NH_4^+ by glutamine synthetase (GS) requires C-skeletons from the tri-carboxylic acid (TCA) reactions (Fig 1). Moreover, linear and pseudocyclic photosynthesis can also generate additional ATP and reductants essential for N_2 fixation.

To understand the regulation of these metabolic pathways in *Trichodesmium* under varying pCO_2 levels, we designed an experiment to characterize changes in the fluxes of carbon, nitrogen, and oxygen, their related protein pool sizes, and in PSII variable fluorescence parameters. The experiment was performed with *Trichodesmium* IMS101 cultures acclimated to past and future pCO_2 levels (150 and 900 μatm) at high and low light (50 and 200 μmol photons m^{-2} s^{-1}).

In the first part of this combined report (Kranz et al., this volume) we examined the physiological responses to the different acclimation conditions. Elevated pCO_2 and light

enhanced the production of particulate organic carbon and nitrogen (POC and PON) production as well as growth rates. The relative stimulation by pCO_2 of these processes was higher in cultures acclimated to low light. This was reflected also in other measured physiological parameters, particularly the diel patterns of N_2 fixation and the integrated rates over the day. At high light, elevated pCO_2 extended the period of high N_2 fixation which lasted from 5 h after onset of light throughout the end of the photoperiod. Light, but not pCO_2, influenced gross photosynthesis as measured by PSII O_2 evolution. To supply the Calvin cycle with sufficient CO_2, *Trichodesmium* possess a carbon concentrating mechanism (CCM) mainly based on HCO_3^- uptake (Kranz et al., 2009, Kranz et al., this volume). When *Trichodesmium* was acclimated to higher pCO_2 (900 µatm) a decline in the cellular affinity to DIC was observed (Kranz et al. 2009) while the specific uptake of CO_2(aq) increased (Kranz et al. this volume – Fig 5).

Key protein pool sizes and photosystem physiology are fundamental cellular infrastructure that influence the underlying mechanisms subsequently reflected in the cells' physiology. In this study we extend the experimental results presented in Kranz et al. (part I, this volume) by examining the influence of pCO_2 at different light regimes on the photosynthetic fluorescence parameters of PSII, and on the pool sizes of key proteins involved in the carbon and nitrogen fixation and assimilation processes.

Materials and Methods:

Culture conditions and carbonate chemistry

Semi-continuous dilute batch cultures of *Trichodesmium sp*. IMS101 (originally isolated by Prufert-Bebout et al., 1993) were grown at 25 °C in 0.2 μm-filtered unbuffered N-free YBCII media (Chen et al., 1996). Cultures were grown as single filaments in 1 L cylindrical glass flasks (diameter 7 cm) in pCO_2 pre acclimated YCBII media. Light regime was 12:12 h light:dark cycle, at two different light intensities, 50 µmol photons m^{-2} s^{-1} (low light) and 200 µmol photons m^{-2} s^{-1} (high light). 200 µmol photons m^{-2} s^{-1} was chosen for saturating but not photodamaging irradiance according to Breitbarth et al., (2008). Light was supplied using white fluorescence bulbs (Osram, BIOLUX). Cultures were continuously bubbled with air containing different CO_2 partial pressures of 150 and 900 µatm. The gentle bubbling was sufficient to prevent formation of aggregates but did not cause high turbulence that could harm the integrity of the filaments. CO_2 gas mixtures were generated using gas-mixing pumps (Digamix 5KA18/8-

F and 5KA36/8-F, Woesthoff GmbH), CO_2-free air (Nitrox CO_2RP280; Domnick Hunter GmbH) and pure CO_2 (Air Liquide Deutschland GmbH).

Cultures were acclimated to experimental conditions at least 2 months prior to measurements. While species acclimate differently to changes in growth conditions, it is generally assumed that >10 generations are sufficient (MacIntyre and Cullen, 2005). Cultures were unialgal and at exponential growth bacterial biomass was not observed under light microscopy (X400 magnification).

Use of dilute batch cultures with experiments performed at the mid-exponential growth of the cells retained the carbonate chemistry constant. The pH was determined every morning, using a pH/ion meter (model 713 pH Meter, Metrohm). Cultures in which the pH had shifted (pH shift >0.06) in comparison to a reference (cell-free YBCII at the respective CO_2 levels) were excluded from further analysis. The carbonate system was calculated from total alkalinity (TA), pH, temperature, salinity and phosphate using CO2Sys (Lewis and Wallace 1998). Carbonate chemistry parameters for the respective CO_2 treatments are supplied in Kranz et al. this volume, Table I.

Sample collection for proteins

Samples of *Trichodesmium* IMS101 were collected 1 and 5 h after the onset of light by gentle filtration on 5 µm pore size polycarbonate filters (13 mm diameter, Osmonics) in the dark. Filtration volumes were 25-70 ml (depending on acclimation and culture biomass) and lasted ~1-3 minutes. Filters were placed in sterile DNase and RNase free centrifuge tubes and directly frozen with liquid nitrogen and subsequently stored at -80 °C.

Total protein extraction and quantification

Trichodesmium filters were resuspended in 250 µL 1X denaturing extraction buffer, containing 140 mM Tris base, 105 mM Tris–HCl, 0.5 mM ethylenediaminetetraacetic acid (EDTA), 2% lithium dodecyl sulfate (LDS), 10% glycerol, 0.1 mg/mL PefaBloc SC (AEBSF) protease inhibitor (Roche). Samples were sonicated until thawed using a Fisher Scientific Model 100 Sonic dismembrator with a microtip attachment at a setting of 30%. To avoid overheating, samples were then refrozen immediately in liquid N_2. Two cycles of freezing followed by thawing by sonication yielded maximal protein extraction with minimal degradation of representative membranes and soluble proteins (Brown et al., 2008). Following disruption, samples were centrifuged for 3 min at 10,000 g to remove insoluble material and unbroken cells.

The total protein concentration was measured with a modified Lowry assay (Bio-Rad DC) using bovine gamma globulin as a comparative protein standard.

Target protein quantification

Key proteins quantification was performed using standards (AgriSera, Sweden) and followed the procedure described in Brown et al., (2008) and Levitan et al. (in press). Primary antibodies (AgriSera, Sweden) were used at a dilution of 1:40,000 in 2% ECL advance blocking reagent in TBS-T for: NifH (Fe protein of the nitrogenase), GlnA (a subunit of glutamine synthetase), PsbA (D1 protein of PSII), PsaC (core subunit of PSI), AtpB (the CF_1 subunit of ATP synthase) and RbcL (the large subunit of the RubisCo). Blots were incubated for 1 h with horseradish peroxidase conjugated rabbit anti chicken secondary antibody (Abcam) for the NifH, GlnA, AtpB and RbcL primary antibodies, and with horseradish peroxidase conjugated chicken anti rabbit secondary antibody (Abcam) for the PsbA and PsaC primary antibodies, diluted to 1:40,000 in 2% ECL Advance blocking reagent in TBS-T. Blots were developed with ECL Advance detection reagent (Amersham Biosciences, GE healthcare) using a CCD imager (DNR, M-ChemiBIS). Protein levels on immunoblots were quantitated using Quantity One software (Bio-Rad) and calculated from standard curves (for each blot), for estimating the amounts of protein in experimental samples (after Brown et al., 2008).

PSII variable chlorophyll fluorescence

Photosystem II (PSII) fluorescence parameters of *Trichodesmium* IMS101 were measured twice a day, 1 and 5 hours after the onset of light using a Fluorescence Induction and Relaxation System (FIRe, Satlantic, Halifax, Canada) (Falkowski et al., 2004). This instrument is based on the same biophysical principles as the FRRF (Kolber et al., 1998) with LED excitation at 450 ± 30 nm and emission detected using a >678 nm long pass filter.

Parameters measured were: Fo – intrinsic fluorescence (arbitrary units, a.u.), Fm- maximal fluorescence (a.u.), Fv – variable fluorescence (Fv=Fm-Fo, a.u.), Fv/Fm – PSII photochemical quantum yield, σ_{PSII} – effective absorbance cross section of PSII ($Å^2$) and τ_{Qa} – the relaxation time of the Qa^- (μs). All parameters were measured after acclimation to dark (15 min), so that all PSII reaction centers are photochemically reduced. Additional measurements were performed under growth light irradiance (50 or 200 μmol photons m^{-2} s^{-1}) with an ambient light source (ALS, Satlantic). Blanks were prepared by filtering each sample using of 0.2 μm sterile Minisert filters (Sartorius) and blank traces were subtracted for each measurement.

For the Fo, Fm, Fv, Fv/Fm and σ_{PSII} parameters, data analysis was performed using a Matlab code (http://sourceforge.net/projects/fireworx) written by Ms. Audrey Burnett from John Cullen's laboratory (Department of Oceanography at Dalhousie University, Halifax, Canada) in coordination with Satlantic. Fo and F, values were normalized to the cultures chlorophyll values (Campbell et al., 1998). For the τ_{QA} analysis we have used the FIRePro software provided by Satlantic.

Calculation of open PSII Reaction centers and PSII Electron transfer rate

The number of open PSII reaction centers ($PSII_{OPEN}$) and electron transfer rate of PSII (ETR_{PSII}) were calculated using values from the photosynthetic fluorescence analysis and the amount of PsbA per cell calculated from the quantitative Western blots.

$PSII_{OPEN}$ was calculated according to equation 1 (van Kooten and Snel, 1990, MacKenzie et al. 2004):

$$PSII_{OPEN} = \frac{Fm' - Fs}{Fm' - Fo} \quad (1)$$

where Fm' is the maximum fluorescence in light acclimated cultures, Fs is the steady-state fluorescence level in the respective growth irradiance, and Fo is the minimum fluorescence level measured in the dark (Krause and Weis, 1991).

ETR_{PSII} was calculated according to equation 2 (MacKenzie et al. 2005, modified from Falkowski and Raven, 1997):

$$ETR_{PSII} = (E \times PSII_{OPEN} \times \sigma_{PSII} \times \frac{PSII}{cell}) \quad (2)$$

where E is the photon flux density of the illumination, $PSII_{OPEN}$ is the ratio of the photochemically reduced (open) PSII reaction centers, σ_{PSII} is the effective absorbance cross section of PSII and PSII $cell^{-1}$is the number of PSII reaction centers in a cell. Since cultures were growing under acclimated, non-photoinhibitory conditions, the PSII per cell was asstimated according to the number of D1 (PsbA) protein subunit, to reflect the number of PSII reaction centers (Burns et al., 2006).

Relative abundance of photosystems

The relative abundance of the two photosystems (PSI and PSII), was determined from emission spectra at 77 K. Samples were collected on a 13 mm GF/F, placed on sample holders in a quartz Dewar filled with liquid nitrogen. The spectra were determined on an AB2 Aminco spectrofluorometer using 435nm excitation and the resulting peaks were analyzed with PeakFit 4 software (PeakFit, Systat, Richmond, CA, USA). Peaks with maxima in the 680–695 nm regions

were assigned to PSII and 710–730 nm to PSI. Samples were taken from each treatment during 1 and 5 h after the onset of light.

Statistical analysis

Protein and most fluorescence data were analyzed by 3-Way ANOVA (pCO_2, light and time, $p<0.05$) with interactions. Analysis of Qa^- re-oxidation was done using 3-Way ANOVA (pCO_2, acclimation irradiance, ambient light, $p<0.05$). For finding significant difference between 4-8 groups (treatments and time of day) we used One-Way ANOVA ($p<0.05$) followed by a Scheffe Post-Hoc. For all Scheffe Post Hoc tests, different letters represent significant difference. For verifying significant different between the different pCO_2 and light conditions we used T-test for independent variables ($p<0.05$ or $p<0.01$). All data are presented as average values of independent replicates with ±1 standard deviation. Numbers of independent replicates (n=3 to 10) are presented for each figure in the figure legend.

Results:

We quantified amounts of key protein subunits involved in N_2 fixation and assimilation, energy production, and photosynthesis. The amounts (pmol μg protein^{-1}) of these proteins (NifH, GlnA, AtpB, PsbA, PsaC, and RbcL), at the two sampling points (1 and 5 h after the onset of light) are presented in Table I. All protein subunits are normalized to total protein amounts. The amount of total protein per cell was similar for all acclimations measured, and ranged between 8.36 ng and 14.3 ng in total protein cell^{-1} (One Way ANOVA, $p<0.05$, Scheffe post hoc test, data not shown).

Nitrogen fixation and assimilation

The Fe-protein subunit of nitrogenase (NifH) was significantly influenced by pCO_2 and time (3-Way ANOVA, $p<0.05$, Fig. 2, Table I). Although light itself did not distinctly influence NifH amounts, the interactions of pCO_2 and light significantly affected the protein pool size ($p<0.05$). At low light (50 μmol photons m^{-2} s^{-1}), pCO_2 concentrations (150 and 900 μatm) did not influence the amount of NifH that was higher at 5 h after the onset of light, relative to 1 h after the onset of light. At high light (200 μmol photons m^{-2} s^{-1}), pCO_2 concentrations significantly influenced both the amount and the pattern of NifH abundance. Low pCO_2 / high light acclimated cultures had high NifH protein amounts (0.302 ± 0.068 pmol μg protein^{-1}) which

differed from all other treatments (0.169 ± 0.033 to 0.217 ± 0.072 pmol μg protein^{-1}, One Way ANOVA, Scheffe post hoc test, $p<0.05$, n=3). At high pCO_2 / high light the NifH amounts remained constant for both time points measured (0.173 ± 0.03 and 0.167 ± 0.04 pmol μg protein^{-1}) and were as low as the NifH amounts measured 1 h after light for both low light acclimations (Fig. 2).

GlnA is a subunit of the decamer glutamine synthetase (GS) which is the first enzyme incorporating the NH_4^+ produced by the nitrogenase into an organic compound. Both pCO_2 and light affected GlnA amounts (3-Way ANOVA, $p<0.05$), with no significant interactions between them ($p<0.05$, Fig. 3A, Table I). The low pCO_2 / high light acclimation had the highest GlnA amounts (0.134 ± 0.007 pmol μg protein^{-1}) than all other acclimations (0.093 ± 0.005 - 0.116 ± 0.006), parallel to high amounts of NifH under the same acclimation (Figs. 2 and 3A, One Way ANOVA, Scheffe post hoc test, $p<0.05$, n=6).

ATPase abundance

AtpB, a subunit of the ATP synthase, was not influenced by either pCO_2 or light, with no significant interactions between them (3-Way ANOVA, $p<0.05$, Fig. 3A, Table I). Elevated pCO_2 had no pronounced effect on the amount of the AtpB between both light intensities (Fig. 3B, One Way ANOVA, Scheffe post hoc test, $p<0.05$, n=6). Time-dependency was observed only for the low light acclimations (3-Way ANOVA, T-test, $p<0.05$, n=3), but did not influence the One Way ANOVA results (n=3).

Abundance of photosynthetic units

PsbA (D1 protein of PSII) abundance exhibited sensitivity to pCO_2 and light with no significant interactions between them (3-Way ANOVA, $p<0.05$, Fig. 4A, Table I). Elevated pCO_2 lowered the amount of PsbA at both light intensities. A significant decrease of the PsbA amount was observed between low pCO_2 / low light (0.085 ± 0.015 pmol μg protein^{-1}) and high pCO_2 / high light (0.048 ± 0.014 pmol μg protein^{-1}) acclimations (One Way ANOVA, Scheffe post hoc test, $p<0.05$, n=6).

Light was the only notably influencing factor for changes in the amount of PsaC, a core subunit of PSI, (3-Way ANOVA, $p<0.05$, Fig. 4B, Table I), with no significant interactions between the three variables ($p<0.05$). While pCO_2 did not influence the PsaC pool size at both light intensities (One Way NOVA, $p<0.05$, Scheffe post hoc test), the subunit's pool size increased by ~150% at low irradiance (Fig. 4B, T-test, $p<0.05$, n=12). High pCO_2 / low light acclimation increased the PsaC amount (0.128 ± 0.013 pmol μg protein^{-1}) from that measured

for the high pCO_2 / high light acclimation (0.087 ± 0.010 pmol µg protein^{-1}, One Way ANOVA, $p<0.05$, Scheffe post hoc test).

The relative abundance of the two photosystems, PSI:PSII was calculated using two methods: the ratio of PsaC:PsbA protein pools (data from Table I. Fig. 5A) and deconvolution of the emission spectra at 77 K (Fig. 5B). Despite the different sensitivity of the two methods to our variables, both revealed similar patterns. Light, and the interaction of light and pCO_2, distinctly modulated PsaC: PsbA ratios (3-Way ANOVA, $p<0.05$, Fig. 5A). For the 77K emission spectra, pCO_2 was the only influencing factor (3-Way ANOVA, $p<0.05$, Fig. 5B), with no significant interactions between the three factors. Nevertheless, the average values from the 77K measurements supported the observed increase in the PSI:PSII ratio when comparing the low pCO_2 / low light (2.844 ± 0.588, Fog 5B) and the high pCO_2 / high light (3.895 ± 0.531) acclimations (One Way ANOVA, $p<0.05$, Scheffe post hoc test, n=7-10).

Ribulose-1,5-bisphosphate Carboxylase Oxygenase (RubisCO)

In our experiment, neither pCO_2 nor light significantly influenced the amount of the large subunit of the RubisCO, RbcL (Fig. 6A, Table I, One Way ANOVA, Scheffe post hoc test, $p<0.05$, n=6). This was further supported by 3-Way ANOVA ($p<0.05$, Fig. 6A).

RbcL:PsbA ratio was influenced only by pCO_2 (3-Way ANOVA, $p<0.05$, Fig. 6B, data from Table I), with no significant interactions between the variables. Elevated pCO_2 increased the ratio of RbcL:PsbA at both light intensities (Fig. 6B). Nevertheless, RbcL:PsbA ratio was ~2-fold higher for the high pCO_2 / high light acclimation in comparison with the low pCO_2 / low light acclimation (One Way ANOVA, Scheffe post hoc test, $p<0.05$, n=6).

Both pCO_2 and light influenced the ratio of the two primary assimilatory enzymes, RbcL (Fig. 6A) and GlnA (Fig. 3A, data from Table I), with no significant interactions between the variables (3-Way ANOVA, $p<0.05$, Fig. 6C). While high light resulted in a 23 % decrease in the RbcL:GlnA ratio in comparison to low light acclimations (T-test<0.01, n=12, data from Table I), pCO_2 did not appreciably change the RbcL:GlnA ratio in both light acclimations (Fig. 6C, One Way ANOVA, Scheffe post hoc test, $p<0.05$, n=6).

PSII variable chlorophyll fluorescence

The PSII variable fluorescence was measured twice a day, 1 and 5 hours after the onset of light (Fig. 7, n=9). pCO_2 concentrations influenced the intrinsic (Fo) and maximal (Fm) fluorescence of PSII (3-Way ANOVA , $p<0.05$, Fig. 5A and B). While light and time did not affect Fo and Fm, the interaction of light and time significantly influenced both parameters (3-Way ANOVA,

$p<0.05$). However, no significant differences were found for both parameters (Fo and Fm) between all our acclimations (Fig. 7A and B, One Way ANOVA, Scheffe post hoc test, $p<0.05$, n=9).

Both variable fluorescence (Fv) and photochemical quantum yield of PSII (Fv/Fm) were significantly influenced by pCO_2, light and time (3-Way ANOVA, $p<0.05$, Fig. 7C and D). Fv exhibited pCO_2-sensitivity at both light intensities, and declined at 5 h after the onset of light in all acclimation, excluding the high pCO_2/ low light acclimation (Fig. 7C, One Way ANOVA, Scheffe post hoc test, $p<0.05$, n=9). Fv was also notably influenced by the interaction of light and time (as were Fo and Fm), but no significant interactions were found for Fv/ Fm (3-Way ANOVA , $p<0.05$). In all our measurments, Fv/Fm was more affected by light and time of day than by pCO_2 level (Fig. 7D, One Way ANOVA, Scheffe post hoc test, $p<0.05$, n=9).

Both light and time of day (but not pCO_2) influenced the effective absorbance cross section of PSII ($\sigma_{PSII,}$) (3-Way ANOVA, $p<0.05$, Fig. 7D, n=9), although all values averaged between ~200 and ~250 $Å^2$. σ_{PSII} revealed a significant difference only for the high pCO_2 / high light acclimation at 5 h after the onset of light measurement (One way ANOVA, $p<0.05$, Scheffe post hoc test), however, it was still in the 200-250 $Å^2$ range.

The re-oxidation of the Qa^-, primary electron acceptor of PSII (τ_{Qa}, dark and light acclimated samples) was generally slower in the dark (Fig. 8). At 1h after the onset of light, only ambient light notably affected re-oxidation time (3-Way ANOVA, $p<0.05$), with no significant interaction between the three variables. During this time point, re-oxidation times ranged between 500 and 1000 μs, with no detectable effect of either pCO_2 or acclimation irradiance on the different acclimations (Fig. 8A, One Way ANOVA, $p<0.05$, n=3). At 5 h after the onset of light, both acclimation irradiance and ambient light affected τ_{Qa}, with a significant interaction between them (3-Way ANOVA, $p<0.05$). During midday, re-oxidation of Qa^- in the dark was slower (τ_{Qa} > 1000 μs) for all low light acclimated cultures, indicating a more reduced PQ pool in the dark (Fig. 8B). The low pCO_2 / high light acclimation was the only one for which the time for Qa^- re-oxidation did not increase in the dark (Fig. 8B).

Electron transfer in PSII

The number of open PSII is the fraction of the PSII reaction centers that are available to perform photochemistry. This fraction, calculated from the fluorescence parameters measured at given growth irradiances and in the dark, was not influenced by any of the tested variables or by their interactions (3-Way ANOVA, $p<0.05$). In addition, no significant differences were found between our acclimations (Fig. 9A, One Way ANOVA, Scheffe post hoc test, $p<0.05$, n=6).

pCO_2, light and the interaction between them influences the electron transfer rate of PSII (ETR) (3-Way ANOVA, $p<0.05$, Fig. 9B). Generally, the ETR decreased with pCO_2 elevation. This trend appears to be statistically significant only for the high light acclimations, but it is also observed for the low light acclimations (One Way ANOVA, Scheffe post hoc test, $p<0.05$, $n=6$). Although the One Way ANOVA indicated that the low pCO_2 / high light acclimation had the only significantly different ETR, the high pCO_2 / high light treatment was notably different from both low light acclimations (T-test, $p<0.01$, Fig. 9B, marked with an asterisk).

Discussion:

Our study provides information on the acclimation of essential metabolic processes in *Trichodesmium* IMS101 to changes in pCO_2 (150 and 900 µatm) and their modification by light (50 and 200 µmol photons m^{-2} s^{-1}). The first part of this combined study (Kranz et al., this volume) focused on quantifying fluxes of cellular O_2 evolution, light-dependent O_2 uptake, nitrogen acquisition and the uptake and fixation of inorganic carbon. Here we provide further mechanistic insights by examining activity of PSII and changes in protein amounts of major photosynthetic and nitrogen metabolism complexes (Fig. 10).

One of the most notable results we observed was the uncoupling between protein amounts and their functional activities. In fact, for some proteins, highest rates (Kranz et al. this volume) were often observed at the lowest protein amounts (Table I). In view of the integrated N_2 fixation rates (Kranz et al., this volume- Fig. 2), this reveals that under high light, elevated pCO_2 enabled a 112% increase in the integrated diel N_2 fixation rates at 50-66% of the NifH amount (Figs. 2 and 10, Table I). A similar behavior was observed for low light acclimated cultures. Here, elevated pCO_2 supported a 200% increase in N_2 fixation for the same amount of NifH (Table I, Kranz et al. this volume, Fig 2).

A prolonged period of N_2 fixation from midday until the scotoperiod was detected for the high pCO_2 / high light acclimation, while under low light N_2 fixation rates were markedly reduced with a narrow peak of activity 3 h into the light and a subsequent quick decline (Kranz et al., this volume- Fig 2). We suspect that at low irradiance, this decline results from a lack of energy available for N_2 fixation at midday so that maximal N_2 fixation rates are observed earlier in the day. Both high light acclimations demonstrated the typical N_2 fixation trend whereby rates increased from early morning towards midday (high N_2 fixation). NifH amounts also

exhibited the expected increase at midday for all acclimations but the high pCO_2 / high light (Fig. 2) (Chen et al., 1998). At high pCO_2 / high light, NifH amounts were similar for the two time points measured and were as low as the early morning values of all other acclimations (Fig 2) (Levitan et al., in press). This emphasizes the regulation of nitrogenase activity by changes in environmental conditions, and possibly indicates post-translational regulation (Levitan et al., in press). Post-translational regulation of the nitrogenase activity by a reversible ADP ribosylation of the dinitrogenase reductase (NifH) is known for other diazotrophs. In *Azospirillum brasilense*, post-translational modifications occur when the cells are shifted to anaerobic conditions or upon addition of NH_4^+ (Zhang et al., 1993). The same mechanism, controlled by NH_4^+ availability and light level, was observed for the phototrophic purple bacterium *Rhodobacter capsulatus* (Masepohl et al., 2002). Thereby, post-translational regulation could be one mechanism enabling changes in the diurnal pattern of the N_2 fixation rates in *Trichodesmium*.

Glutamine synthetase is responsible for the assimilation of NH_4^+ produced during N_2 fixation. The amount of the GlnA subunit was significantly higher at low pCO_2 / high light acclimation (Fig. 3A). This correlates with the higher amounts of the NifH protein under the same acclimation (Fig. 3A, Fig. 2). Thus, to obtain high N_2 fixation and assimilation rates under low pCO_2 and high light, higher amounts of core proteins (NifH, GlnA) are required.

The influence of light energy on photosynthesis and photosynthetic protein complexes is well known. Acclimation of phytoplankton to high irradiance can reduce the number of photosynthetic units and also result in higher maximal photosynthetic rates per unit chlorophyll (Sukenik et al., 1987 and references within, Behrenfeld et al. 1998, MacKenzie et al., 2004). Our results show that the amount of PsbA (D1 protein, a core subunit of PSII) decreased with elevation of both pCO_2 and light (Fig. 4A). The corresponding O_2 evolution and consumption rates were significantly influenced only by light but not by pCO_2 (Kranz et al., this volume-Fig. 3). This demonstrates that *Trichodesmium* can support higher metabolic rates despite lower protein amounts when acclimated to elevated pCO_2 and light, similar to the changes observed for NifH (Fig. 10).

PSII fluorescence measurements can be used to understand the efficiency and kinetics of electron transport in the thylakoid membrane and to provide information on the redox state of Qa and the PQ pool (Figs. 1 and 7). Our results exhibit no significant change in the maximal photochemical quantum yield of PSII (Fv/Fm) under different pCO_2 levels (Fig. 7B), in agreement with previously published data (Levitan et al., 2007). Higher irradiance caused a significant decrease in the Fv/Fm of *Trichodesmium* cultures that was paralleled by a decline in PsbA amounts.

Irradiance and not pCO_2 influenced the amounts of the PSI core protein PsaC (Fig. 4B). At high light, PsaC amounts decreased as observed for the cyanobacterium *S. elongatus* under replete inorganic carbon concentrations (MacKenzie et al., 2004). This can result from parallel decrease of PSII amount and/or from translation or post-translational regulation of PSI due to changes in the redox status of the electron transport components (Fujita, 1997). Higher PSI amounts may enable a higher electron flow through linear photosynthesis. This will lead to the reduction of ferredoxin and could enable enhanced N_2 fixation and/or NADPH production. Alternatively, relatively higher PSI can increase cyclic electron flow around PSI, supporting the activation of the NDH-1_4 as a leakage prevention mechanism (Kranz et al., this volume) and higher ATP production (Figs. 1 and 10).

Acclimation of cyanobacteria to different light intensities is often mediated by changes in the stoichiometry of the two photosystems, PSI:PSII, (Fig. 4B; Fujita, 1997, Mackenzie et al., 2004), and in phycobilisome assembly. Flexible photosystem stoichiometry is essential for controlling the absorption of light energy, influencing the production of ATP, reductants, and for reducing photodamage (Fujita, 1997). PSI:PSII ratios were higher at elevated pCO_2 and further influenced by high light. This indicates a preference towards higher PSI relative to PSII under elevated pCO_2, leading to higher N_2 fixation and growth rates (Figs. 4 and 5).

Photosynthetically generated reductants are used by the RubisCO enzyme in the Calvin cycle to reduce inorganic carbon to carbohydrates. RbcL is the large-subunit of RubisCO and its transcripts and activity are known to be light-insensitive (Falkowski and Raven, 2007). In our experiment, neither pCO_2 nor light influenced RbcL amounts for all the acclimations (Fig. 6A). The RbcL:PsbA ratio reflects the light saturation index for photochemistry, Ek (Fig. 6B, Suggett et al., 2006, Brown et al. 2008). We found higher RbcL:PsbA ratios when increasing pCO_2 and/or light. This is in agreement with Sukenik et al. (1987) reporting stable amounts of RubisCO relative to downstream complexes of the electron transfer chain which declined as irradiance increased. In our experiments, lower RbcL:PsbA ratios obtained for cultures acclimated to low light supported O_2 evolution rates similar to high light cclimations immediately when transferred to high light, regardless of pCO_2 (Kranz et al., this volume, Table 3). Thus, our results corroborate previous findings that light saturated photochemistry is limited by carbon fixation, and not by electron transfer from PSII (Sukenik et al., 1987, Falkowski, 1992).

We suggest that the observed changes in PsbA and PsaC are not a consequence of photosynthetic stress (limitation) but rather an acclimation strategy. Under elevated pCO_2 and light, the ability of *Trichodesmium* to reduce its investment in expensive protein synthesis and

repair, allows for increased N_2 fixation, improved carbon uptake and enhanced growth (Fig. 10). Further evidence for this strategy can be seen by examining the ratio of the two primary enzymes in C and N assimilation pathways, RbcL:GlnA. RbcL amounts were constant for all acclimations, yet at high light a lower RbcL:GlnA ratio was measured, indicating that *Trichodesmium* invest more in the nitrogen assimilation complexes, relative to the carbon assimilation complexes.

In photoautotrophic cyanobacteria lacking cellular compartmentalization, energy demanding and energy producing processes share the same complexes and pathways. Neither pCO_2 nor light significantly influenced the amount of the AtpB, the CF_1 subunit of ATP synthase, the major protein responsible for cellular energy production, (Fig. 3B). ATP production via ATP synthase depends on a cross membrane proton gradient of the thylakoid membrane, generated by complexes of the respiratory and photosynthetic pathways (Falkowski and Raven 2007). Increased respiration or faster photosynthetic electron transfer rates (ETR), both linear and cyclic, can enhance the proton gradient and subsequent production of ATP via the ATPase. Thus, increased ETR (Fig. 9B) detected under high light, could support higher ATP production. Also, cyclic photosynthesis around PSI and Q-cycle activation, i.e. due to NDH-1_4 activity, can enlarge the proton gradient and ATP production. ATP synthase activity is controlled at the protein level and by the redox state of the electron transport chain - allowing up to an order of magnitude increase in catalytic activity (Falkowski and Raven, 2007). Therefore, the same amount of AtpB (Fig. 3B) may support higher ATP production under different environmental conditions.

ATP is required for both carbon and N_2 fixation. Calculations by Brown et al., (2008) indicate that a ratios of RbcL:AtpB > 2.8 denote under-saturation of ATP for the Calvin cycle. In all the acclimations measured the RbcL:AtpB exceeded 2.8 (data from table I), indicating that under these conditions the RubisCO was energetically under saturated. Hence, the additional energy for metabolic processes such as N_2 fixation and growth must originate either from processes upstream to the RubisCO or from reduced requirements for protein biosynthesis (Fig. 10).

The efficiency of the photosynthetic ETR is affected by the redox state of the electron acceptors. For example, the primary electron acceptor of PSII (Qa) and factors downstream to Qa which can be additionally affected by the respiratory pathway (Suggett et al., 2006). A high ETR indicates an efficient generation of electrons by PSII and reduced energy dissipation due to heat or fluorescence production. The fraction of open PSII (at ambient irradiance) the PSII reaction centers that are available to perform photochemistry, did not change for any of our acclimations (Fig. 9A). A high flexibility in the ETR, utilizing an equal fraction of open PSII,

could account for the cells' ability to rapidly adjust to differing light regimes as we observed (Kranz et al. this volume-Fig. 3) and is typical for *Trichodesmium* in the upper ocean (Behrenfeld et al., 1998). Moreover, this strategy may also serve as a shunting valve for excess energy (Campbell et al., 1998, MacKenzie et al., 2004).

Discrepancies between ETR and O_2 evolution rates were observed for the low pCO_2 / high light acclimation (Fig 9B, Kranz et al., this volume). This may result from an excess supply of electrons used in the Mehler reaction that was detected only for this acclimation (Kranz et al., - this issue). At high light conditions, Mehler activity has been observed when ETR was decoupled from photosynthesis (Suggett et al. 2006). Also, both low light acclimations exhibited Mehler activity immediately when transferred from low to high light. This suggests that Mehler reaction, acting as an energy dissipating mechanism, decouple ETR from photosynthetic O_2 evolution and carbon fixation (Kranz et al., this volume-Table III).

Our results exhibit constant σ_{PSII} (excited by blue light) values of ~200-250 $Å^2$, which correspond with the typically low σ_{PSII} found in cyanobacteria (Suggett et al., 2006) and with previously measured σ_{PSII} of *Trichodesmium* (Küpper et al., 2008, Berman-Frank I. and Levitan, O., unpublished, Fig. 7E). Maintaining a relatively constant σ_{PSII} while changing the number ("n") of the PSII reaction centers (RC, represented by the amount of PsbA) characterizes a strategy termed "n-type" light acclimation (Falkowski and Owens, 1980). This strategy is also correlated with changes in RbcL:PsbA ratio (Fig. 6B), as also described for natural populations of *Trichodesmium* in the Gulf of Mexico (Brown et al., 2008). In cyanobacteria the absorbance cross section is also a function of the phycobillisomes content (Falkowski and Raven, 2007). It possible that under both light intensities applied in our study, no major changes occur in PSII antenna. This is in contrast to observed phycobillisomes changes when *Trichodesmium* was grown at much higher irradiance of 1000 μmol photons m^{-2} s^{-1} (Andresen et al., 2010). A strategy of keeping a small σ_{PSII} while changing the amount of RCs protein complexes was postulated for natural phytoplankton populations of the upper water column, as a means to manage PSII in case of photodamage (Behrenfeld et al. 1998). Since *Trichodesmium* spp. are often found near the surface, an n-type acclimation is advantageous.

In our experiments the periods for Qa^- re-oxidation, τ_{Qa}, under actinic irradiances were found to be ~500 μs, matching previous published values for phytoplankton (Falkowski et al., 1986; Falkowski and Raven, 2007). The difference between the re-oxidation time in dark versus light acclimated cultures indicates the extent and activity of processes that reduce the PQ pool in the dark (Fig 1). An example for such process is reported for *Synechocystis* sp. strain PCC 6803, where succinate dehydrogenase (SDH) contributes more to the redox state of the PQ pool in the

thylakoid then photosynthetic linear electron transfer and NADPH dehydrogenase (NDH, Cooley et al., 2000, Cooley and Vermaas, 2001). Yet, the slower dark Qa^- re-oxidation observed for the low pCO_2 / high light acclimation was not paralleled by an increase in measured C-respiration rates (Fig. 8B; Kranz et al. this volume- Table III).

The low CO_2 / high light acclimation revealed unique characteristics. This was the only acclimation for which NifH and GlnA amount were notably high (Figs. 2 and 3) and light-dependent O_2 uptake (Mehler reaction) was detected (Kranz et al., this volume – Table 3). In addition, light and dark Qa^- re-oxidation times were the same during midday (Fig. 8). This could result from a more reduced PQ pool that prevents faster re-oxidation rates to occur in the light (Fig. 1). The reduced PQ pool can be a consequence of higher ETR detected for this acclimation (Fig. 9B), which can generate more electrons for PSI and cyclic electron flow via the NDH-1_4 that acts as a CO_2 leakage prevention mechanism. This shows that although *Trichodesmium* mainly relies on bicarbonate as its major inorganic carbon source (Kranz et al., 2009), the pCO_2 contribution is important even when enough energy is supplied in the form of light. All of the above suggest that the combination of low pCO_2 with high light may decouple processes that are primarily activated by light. Such processes could meet their metabolic balance by using environmental regulatory signals like pCO_2.

Our study shows that for *Trichodesmium*, elevated pCO_2 and light led to lower amounts of several key proteins while increasing their metabolic fluxes (Fig. 10). We show that cells can reduce energetic and resource requirements for protein synthesis and can divert this "excess" to N_2 fixation and growth. We suggest that the flexible metabolism in *Trichodesmium* is mediated by changes in the redox state of the photosynthetic electron transport chain (i.e. Fig. 8) and by post-translational regulation of key proteins (i.e. Figs. 2, 3B, and 4) . This strategy maintains balanced growth and retains the known range for *Trichodesmium* C:N ratios. The changes in the CCM operation and Ci-uptake under high pCO_2 (Kranz et al. 2009, this volume-Table 3) can provide further energy and resources to support higher metabolic throughput and growth.

It has already been suggested that *Trichodesmium* spp. will thrive in the future acidified oceans (Hutchins et al., 2007, 2010, Kranz et al., 2009, Levitan et al., 2007, in press, Ramos et al., 2007). Here we show the mechanistic flexibility in cellular resources which enables this ancient cyanobacterium to adapt to changing conditions of pCO_2 and energy (Fig. 10). Moreover, our results imply that this acclimation strategy would facilitate bloom expansion under elevated pCO_2 combined with higher irradiance and temperatures (Levitan et al., in press).

References:

Andresen E, Lohscheider J, Setlikova E, Adamska I, Simek M, Küpper H (2010) Acclimation of *Trichodesmium erythraeum* ISM101 to high and low irradiance analysed on the physiological, biophysical and biochemical level. New Phytol **185:** 173-188

Behrenfeld MJ, Prasil O, Kolber ZS, Babin M, Falkowski PG (1998) Compensatory changes in Photosystem II electron turnover rates protect photosynthesis from photoinhibition. Photosynthesis Research **58:** 259-268

Breitbarth E, Wohlers J, Klas J, LaRoche J, Peeken I (2008) Nitrogen fixation and growth rates of *Trichodesmium* IMS101 as a function of light intensity. Marine Ecology Progress Series **359:** 25-36

Brown CM, MacKinnon JD, Cockshutt AM, Villareal TA, Campbell D (2008) Flux capacities and acclimation costs in *Trichodesmium* from the Gulf of Mexico. Marine Biology **154:** 413-422

Burns RA, MacKenzie DB, Campbell D (2006) Inorganic carbon repletion constrains steady-state light acclimation in the cyanobacteria *Synechococcus elongatus*. Journal of Phycology **42:** 610-621

Campbell D, Hurry V, Clarke AK, Gustafsson P, Oquist G (1998) Chlorophyll fluorescence analysis of cyanobacterial photosynthesis and acclimation. Microbiology and molecular Biology reviews **62:** 667-683

Capone DG, Subramaniam A (2005) Seeing microbes from space - Remote sensing is now a critical resource for tracking marine microbial ecosystem dynamics and their impact on global biogeochemical cycles. Asm News **71:** 179-196

Carpenter EJ, Capone DG (2008) Nitrogen Fixation in the Marine Environment. *In* Nitrogen in the Marine Environment (2nd Edition). Academic Press, San Diego, pp 141-198

Chen YB, Dominic B, Mellon MT, Zehr JP (1998) Circadian rhythm of nitrogenase gene expression in the diazotrophic filamentous nonheterocystous Cyanobacterium *Trichodesmium* sp strain IMS101. Journal of Bacteriology **180:** 3598-3605

Chen YB, Zehr JP, Mellon M (1996) Growth and nitrogen fixation of the diazotrophic filamentous nonheterocystous cyanobacterium *Trichodesmium* sp IMS 101 in defined media: Evidence for a circadian rhythm. Journal of Phycology **32:** 916-923

Cooley JW, Howitt CA, Vermaas WFJ (2000) Succinate : quinol oxidoreductases in the cyanobacterium *Synechocystis* sp strain PCC 6803: Presence and function in metabolism and electron transport. Journal of Bacteriology **182:** 714-722

Cooley JW, Vermaas WFJ (2001) Succinate dehydrogenase and other respiratory pathways in thylakoid membranes of *Synechocystis* sp strain PCC 6803: Capacity comparisons and physiological function. Journal of Bacteriology **183:** 4251-4258

Falkowski PG (1992) Phytoplankton photosynthesis in the ocean in relation to the global carbon cycle. Photosynthesis Research **34:** 108-108

Falkowski PG, Koblizek M, Gorbunov M, Kolber Z (2004) Development and application of variable chlorophyll fluorescence techniques in marine ecosystems. *In* G Papageorgiou, Govindjee, eds, Chlorophyll a Fluoerescence: Signature of Photosynthesis, 1st Ed Vol 19. Springer, pp 757-778

Falkowski PG, Owens TG (1980) Light-shade adaptation - 2 strategies in marinephytoplankton. Plant Physiology **66:** 592-595

Falkowski PG, Raven JA (1997) aquatic photosynthesis, 1st Ed. Blackwell science

Falkowski PG, Raven JA (2007) Aquatic photosynthesis, 2nd Ed. Princeton University Press, New Jersey

Falkowski PG, Wyman K, Ley AC, Mauzerall DC (1986) Relationship of steady-state photosynthesis to fluorescence in eukaryotic algae. Biochimica Et Biophysica Acta **849:** 183-192

Fujita Y (1997) A study on the dynamic features of photosystem stoichiometry: Accomplishments and problems for future studies. Photosynthesis Research **53:** 83-93

Hutchins DA, Fu FX, Zhang Y, Warner ME, Portune K, Bernhardt PW, Mulholland MR (2007) CO_2 control of *Trichodesmium* N_2 fixation, photosynthesis, growth rates, and elemental ratios: Implications for past, present, and future ocean biogeochemistry. Limnology and Oceanography **52:** 1293-1304

Hutchins DA, Mulholland MR, Fu FX (2010) Nutrient Cycles and Marine Microbes in a CO2 Enriched Ocean. Oceanography and marine biology: an annual review **22:** 128-145

Kolber Z, Prasil O, Falkowski PG (1998) Measurements of variable chlorophyll fluorescence using fast repetition rate techniques: defining methodology and experimental protocols. Biochimica Et Biophysica Acta-Bioenergetics **1367:** 88-106

Kranz S, Sültemeyer D, Richter K-U, Rost B (2009) Carbon acquisition by *Trichodesmium*: the effect of pCO_2 and diurnal changes. Limnology and Oceanography **54:** 548-559

Krause GH, Weis E (1991) Chlorophyll fluorescence and photosynthesis - the basics. Annual Review of Plant Physiology and Plant Molecular Biology **42:** 313-349

Küpper H, Setlik I, Seibert S, Prasil O, Setlikova E, Strittmatter M, Levitan O, Lohscheider J, Adamska I, Berman-Frank I (2008) Iron limitation in the marine cyanobacterium *Trichodesmium* reveals new insights into regulation of photosynthesis and nitrogen fixation. New Phytologist **179:** 784-798

Levitan O, Brown C, Sudhaus S, Campbell D, LaRoche J, Berman-Frank I (in press) Regulation of Nitrogen Metabolism in the Marine Diazotroph *Trichodesmium* IMS101 under Varying Temperatures and Atmospheric CO_2 Concentrations. *In* Environmental Microbiology ,

Levitan O, Rodsenberg G, Setlik I, Setlikova E, Grigel J, Klepetar J, Prasil O, Berman-Frank I (2007) Elevated CO_2 enhances nitrogen fixation and growth in the marine cyanobacterium *Trichodesmium*. Global Change Biology **13:** 1-8

Lewis E, Wallace DWR (1998) Developed for CO_2 system calculations. ORNL/CDIAC-105. *In*. Carbon Dioxide Information Analysis Center, Oak Ridge National Laboratory, US Department of Energy, Oak Ridge, Tennessee, 1998

MacIntyre HL, Cullen JJ (2005) Sing cultures to investigate the physiological ecology of microalgae. *In* RA Anderson, ed, Algal Culturing Techniques. Elsevier Academic Press, Massachusetts, pp 287-326

MacKenzie TDB, Burns RA, Campbell D (2004) Carbon status constrains light acclimation in the cyanobacterium *Synechococcus elongatus*. Plant Physiology **136:** 3301-3312

MacKenzie TDB, Johnson JM, Campbell D (2005) Dynamics of fluxes through photosynthetic complexes in response to changing light and inorganic carbon acclimation in *Synechococcus elongatus*. Photosynthesis Research **85:** 341-357

Mahaffey C, Michaels AF, Capone DG (2005) The conundrum of marine N_2 fixation. American Journal of Science **305:** 546-595

Masepohl B, Drepper T, Paschen A, Gross S, Pawlowski A, Raabe K, Riedel KU, Klipp W (2002) Regulation of nitrogen fixation in the phototrophic purple bacterium *Rhodobacter capsulatus*. Journal of Molecular Microbiology & Biotechnology. **4:** 243-248

Ramos BJ, Biswas H, Schulz K, LaRoche J, Riebesell U (2007) Effect of rising atmospheric carbon dioxide on the marine nitrogen fixer *Trichodesmium*. Global biogeochemical cycles **21**

Suggett DJ, Moore CM, Maranon E, Omachi C, Varela RA, Aiken J, Holligan PM (2006) Photosynthetic electron turnover in the tropical and subtropical Atlantic Ocean. Deep-Sea Research Part II-Topical Studies in Oceanography **53:** 1573-1592

Sukenik A, Bennett J, Falkowski PG (1987) Light saturated photosynthesis - Limitation by electron transport or carbon fixation? Biochimica et Biophysica Acta (BBA) - Bioenergetics **891:** 205-215

Kooten O, Snel JFH (1990) The use of chlorophyll fluorescence nomenclature in plant stress physiology. Photosynthesis Research **25:** 147-150

Zhang YP, Burris RH, Ludden PW, Roberts GP (1993) Posttranslational regulation of nitrogenase activity by anaerobiosis and ammonium in *azospirillum brasilense*. Journal of Bacteriology **175:** 6781-6788

Acknowledgments: We wish to thank Klaus-Uwe Richter from the Alfred Wegener Institute for Polar and Marine Research, 27570 Bremerhaven, Germany, for technical support during the experiments. We also thank Chris M. Brown from the Institute of Marine & Coastal Sciences for his kind and helpful advice regarding all protein work, Dr. Noga Stambler and Prof. Douglas Campbell for their criticism and advice. Statistical analysis was preformed with help from Dr. Rahcel S. Levy-Drummer, from the Mina and Everard Goodman Faculty of Life Sciences, Bar Ilan University, Ramat-Gan, 52900 Israel. This work is in partial fulfillment of the requirements for a PhD thesis for O. Levitan at Bar Ilan University. O. Levitan was supported by a Reiger Fellowship for Environmental Studies, the DAAD (Deutscher Akademischer Auslandsdienst) and an Eshkol Fellowship from the Israeli Ministry of Science. S.A. Kranz and B. Rost were founded by the European Research Council under the European Community's Seventh Framework Programme (FP7/2007-2013) / ERC grant agreement [205150]. O. Prášil was supported by GACR 206/08/1683 and AV0Z50200510. This research was also supported by BMBF-MOST (GR1950) to I. B.F.

Tables:

Table I: Average amounts (pmol μg protein^{-1}) of all measured protein subunits. (A and B) Results are presented as the averages for 1 h (A) and 5 h (B) after the onset of light (n=3). (C) Average value of the two sampling points (n=6). The proteins measured were PsbA (D1 protein of PSII), PsaC (core subunit of PSI), RbcL (the large subunit of the RubisCo), NifH (Fe protein of the nitrogenase) and GlnA (a subunit of glutamine synthetase).

A.

Protein amount – 1 h after the onset of light (pmol μg protein^{-1})	**50 μmol photons m^{-2} s^{-1}**		**200 μmol photons m^{-2} s^{-1}**	
	150 μatm	**900 μatm**	**150 μatm**	**900 μatm**
PsbA	0.083 ± 0.02	0.065 ± 0.02	0.061 ± 0.01	0.040 ± 0.00
PsaC	0.113 ± 0.01	0.136 ± 0.01	0.098 ± 0.01	0.092 ± 0.02
RbcL	0.504 ± 0.06	0.600 ± 0.09	0.625 ± 0.05	0.553 ± 0.07
AtpB	0.103 ± 0.02	0.114 ± 0.02	0.137 ± 0.02	0.116 ± 0.06
NifH	0.165 ± 0.02	0.163 ± 0.03	0.255 ± 0.06	0.173 ± 0.03
GlnA	0.111 ± 0.01	0.097 ± 0.01	0.129 ± 0.01	0.107 ± 0.01

B.

Protein amount- 5 h after the onset of light (pmol μg protein^{-1})	**50 μmol photons m^{-2} s^{-1}**		**200 μmol photons m^{-2} s^{-1}**	
	150 μatm	**900 μatm**	**150 μatm**	**900 μatm**
PsbA	0.088 ± 0.01	0.075 ± 0.01	0.068 ± 0.02	0.056 ± 0.02
PsaC	0.123 ± 0.02	0.120 ± 0.01	0.087 ± 0.01	0.084 ± 0.01
RbcL	0.683 ± 0.08	0.709 ± 0.07	0.563 ± 0.05	0.529 ± 0.06
AtpB	0.214 ± 0.03	0.142 ± 0.01	0.159 ± 0.06	0.128 ± 0.04
NifH	0.256 ± 0.01	0.270 ± 0.06	0.349 ± 0.04	0.167 ± 0.04
GlnA	0.120 ± 0.00	0.090 ± 0.02	0.139 ± 0.01	0.108 ± 0.00

C.

Protein amount –Average of both time points (pmol μg protein^{-1})	**50 μmol photons m^{-2} s^{-1}**		**200 μmol photons m^{-2} s^{-1}**	
	150 μatm	**900 μatm**	**150 μatm**	**900 μatm**
PsbA	0.085 ± 0.015	0.070 ± 0.017	0.064 ± 0.014	0.048 ± 0.014
PsaC	0.118 ± 0.015	0.128 ± 0.013	0.092 ± 0.011	0.087 ± 0.010
RbcL	0.593 ± 0.115	0.655 ± 0.091	0.594 ± 0.054	0.541 ± 0.059
AtpB	0.158 ± 0.079	0.128 ± 0.019	0.148 ± 0.016	0.122 ± 0.008
NifH	0.201 ± 0.051	0.217 ± 0.072	0.302 ± 0.068	0.169 ± 0.033
GlnA	0.116 ± 0.006	0.093 ± 0.005	0.134 ± 0.007	0.108 ± 0.000

Figure legends:

Fig. 1: Schematic representation of major cellular complexes involved in energy flow (electron, ATP, NAD(P)H, organic skeletons) in *Trichodesmium* IMS101. Dashed arrows represent movement direction of electrons while straight arrows represent directions of protons, ATP, NAD(P)H, and carbon skeletons. Measured proteins subunits are represented by grey diamonds.

Fig. 2: Changes in the amount of the nitrogenase Fe protein, NifH, (pmol μg^{-1}) in response to different light (50 and 200 µmol photons m^{-2} s^{-1}) and CO_2 levels (150 and 900 µatm pCO_2). For each light level, white bars represent 150 µatm CO_2 and grey bars represent 900 µatm CO_2. Open and coarse bars represent values measured at 1 and 5 h after the onset of light, respectively. Errors are ±1 standard deviation. (n=3). Significance between groups were determined by One-Way ANOVA ($p<0.05$) followed by a Scheffe Post Hoc test. Different letters represent significant differences between groups.

Fig. 3: Changes in the average amount of: A. Glutamine synthetase subunit, Glna A (pmol μg^{-1}), B. ATP synthetase, AtpB (pmol μg^{-1}), in response to different light (50 and 200 µmol photons m^{-2} s^{-1}) and CO_2 levels (150 and 900 µatm pCO_2). For each light level, white bars represent 150 µatm CO_2 and grey bars represent 900 µatm CO_2. Errors are ±1 standard deviation (n=6). Significance between groups were determined by One-Way ANOVA ($p<0.05$) followed by a Scheffe Post Hoc test. Different letters represent significant differences between groups.

Fig. 4: Changes in the average amount of photosynthetic proteins in response to different light (50 and 200 µmol photons m^{-2} s^{-1}) and CO_2 levels (150 and 900 µatm pCO_2). A. photosystem II (PSII) protein, PsbA (D1, pmol μg^{-1}), B. Photosystem I (PSI) protein, PsaC (pmol μg^{-1}). For each light level, white bars represent 150 µatm CO_2 and grey bars represent 900 µatm CO_2. Errors are ±1 standard deviation (n=6). Significance between groups were determined by One-Way ANOVA ($p<0.05$) followed by a Scheffe Post Hoc test. Different letters represent significant differences between groups.

Fig. 5: Changes in the average relative abundance of photosystem I (PSI) and photosystem II (PSII), in response to different light (50 and 200 µmol photons m^{-2} s^{-1}) and CO_2 levels (150 and 900 µatm pCO_2). A. Based on the quantification of the proteins sub complexes PsaC:PsbA (pmol:pmol, n=6). B. Based on 77K emission spectra (n=7-10). For each light level, white bars represent 150 µatm CO_2 and grey bars represent 900 µatm CO_2. Errors are ±1 standard deviation. Significance between groups were determined by One-Way ANOVA ($p<0.05$) followed by a Scheffe Post Hoc test. Different letters represent significant differences between groups.

Fig. 6: The influence of different light (50 and 200 µmol photons m^{-2} s^{-1}) and CO_2 levels (150 and 900 µatm pCO_2) on the: A. Average (1 and 5 h after light) amount of RubisCOs' large subunit as measured by quantifying RbcL (pmol μg^{-1}). B. The average ratio of RbcL to the PSII subunit PsbA (pmol:pmol). C. The average ratio of RbcL to the glutamine synthetase subunit, GlnA (pmol:pmol). For each light level, white bars represent 150 µatm CO_2 and grey bars represent 900 µatm CO_2. Errors are ±1 standard deviation (n=6). Significances between groups were determined by One-Way ANOVA ($p<0.05$) followed by a Scheffe Post Hoc test. Different letters represent significant differences between groups.

Fig. 7: The influence of different light (50 and 200 µmol photons m^{-2} s^{-1}) and CO_2 levels (150 and 900 µatm pCO_2) on photosystem II (PSII) parameters, measured by PSII fluorescence. A. intrinsic fluorescence (Fo, a.u.). B. maximal fluorescence (Fm. a.u.). C. variable fluorescence (Fv=Fm-Fo, a.u.). D. PSII photochemical quantum yield (Fv/Fm). E. the effective absorbance cross section of PSII (σ_{PSII} , $Å^2$). For each light level, white bars represent 150 µatm CO_2 and grey bars represent 900 µatm CO_2. Open and coarse bars represent values at 1 and 5 h after the onset of light, respectively. Errors are ±1 standard deviation (n=9). Significances between groups were determined by One-Way ANOVA ($p<0.05$) followed by a Scheffe Post Hoc test. Different letters represent significant differences between groups.

Fig. 8: The influence of different light (50 and 200 µmol photons m^{-2} s^{-1}) and CO_2 levels (150 and 900 µatm pCO_2) on the relaxation time of the Q_A (µs). A. 1 h after light. B. 5 h after light. For each light level, white bars represent 150 µatm CO_2 and grey bars represent 900 µatm CO_2. Dotted bars represent values measured during ambient illumination at the growth conditions and checkered bars represent values measured after acclimation to dark. Errors are ±1 standard deviation (n=3). Significances between groups were determined by One-Way ANOVA ($p<0.05$) followed by a Scheffe Post Hoc test. Different letters represent significant differences between groups.

Fig. 9: The influence of different light (50 and 200 µmol photons m^{-2} s^{-1}) and CO_2 levels (150 and 900 µatm pCO_2) on: A. The fraction of open photosystem II (PSII) Reaction centers. B. PSII electron transfer rate (ETR, electrons $cell^{-1}$ s^{-1}). White bars represent 150 µatm CO_2 and grey bars represent 900 µatm CO_2. Errors are ±1 standard deviation (n=6). Significances between groups were determined by One-Way ANOVA (Sig<0.05) followed by a Scheffe Post Hoc test. Different letters represent significant differences between groups, asterisk represent value that is significantly different from the low light values according to T-test ($p<0.01$).

Fig. 10: A schematic comparison of the changes taking place in *Trichodesmium* IMS101 when acclimated to 150 µatm / 50 µmol photons m^{-2} s^{-1} and 900 µatm / 200 µmol photons m^{-2} s^{-1}. A) Fluxes, protein pools and σ_{PSII} under low CO_2 and low light (150 µatm / 50 µmol photons m^{-2} s^{-1}). B) Fluxes, protein pools and σ_{PSII} under high CO_2 and high light (150 µatm / 50 µmol photons m^{-2} s^{-1}). Amount of protein complexes are taken as the average values from table 3.,PSI:PSII ratios are the values corresponding to Fig. 5B (77K measurements). Fluxes of Carbon fixation, CO_2 uptake, N_2 fixation and O_2 evolution, as well as growth rates are from Kranz et al., (this volume). The difference between protein pool sizes and fluxes are represented proportionally by changes in the subunit/flux arrow area, with panel A as the base line amounts and changes in panel B are relative to panel A. N_2 fixation and CO_2 uptake rates (marked with asterisks) are not presented in proportion the changes were too big to plot. Protein subunits colored grey, represent proteins that we suggest to be post-translationally regulated by pCO_2 and light. Dotted lines and shapes represent fluxes that were not measured.

Figures

Figure 1:

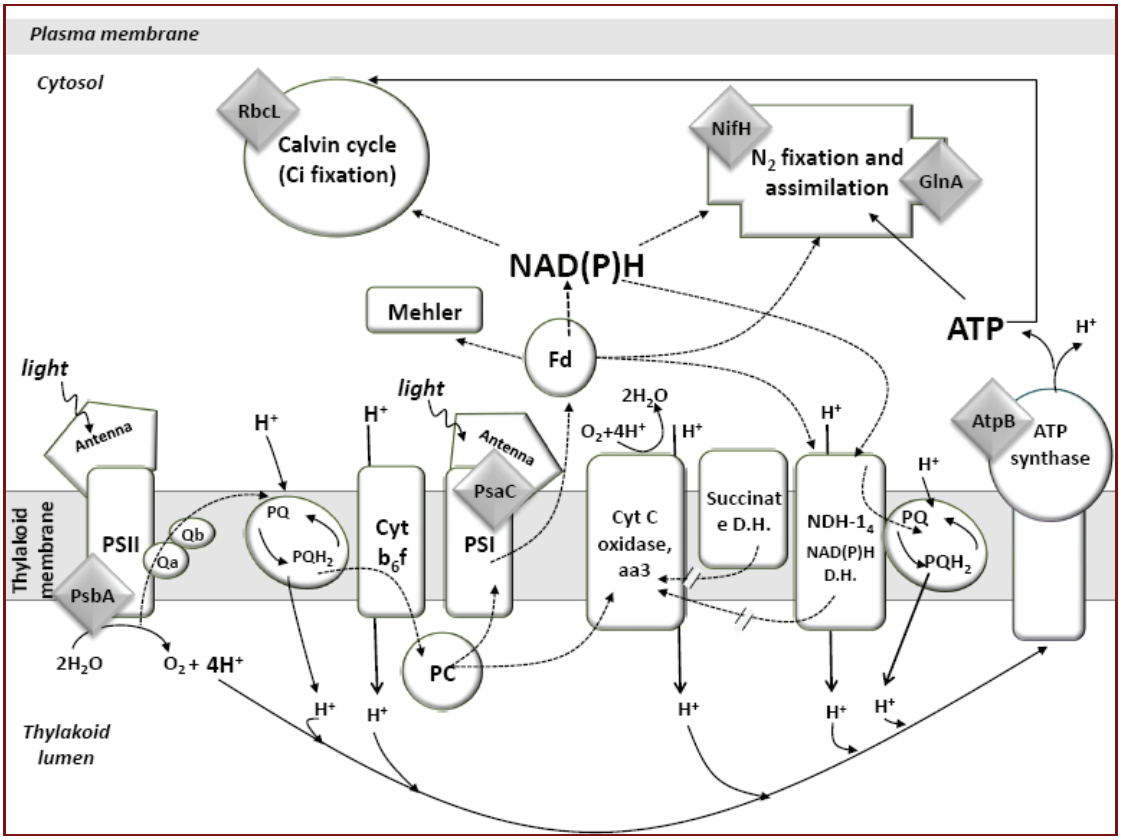

Figure 2:

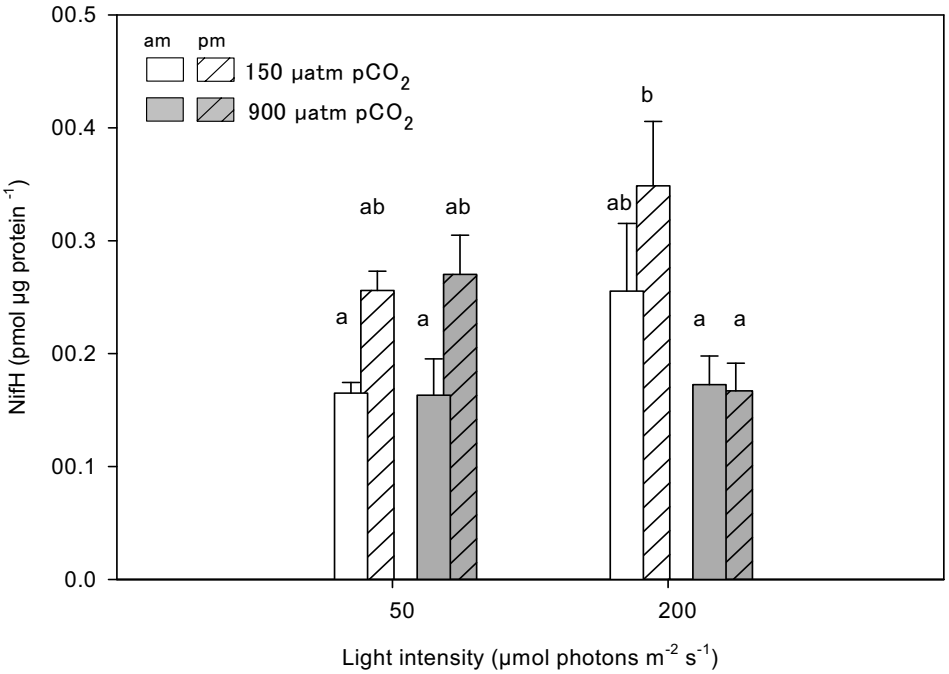
00.5
00.4
00.3
00.2
00.1
0.0
NifH (pmol µg protein -1)
am
pm
150 µatm pCO2
900 µatm pCO2
a
ab
a
ab
ab
b
a
a
50
200
Light intensity (µmol photons m-2 s-1)

Figure 3:

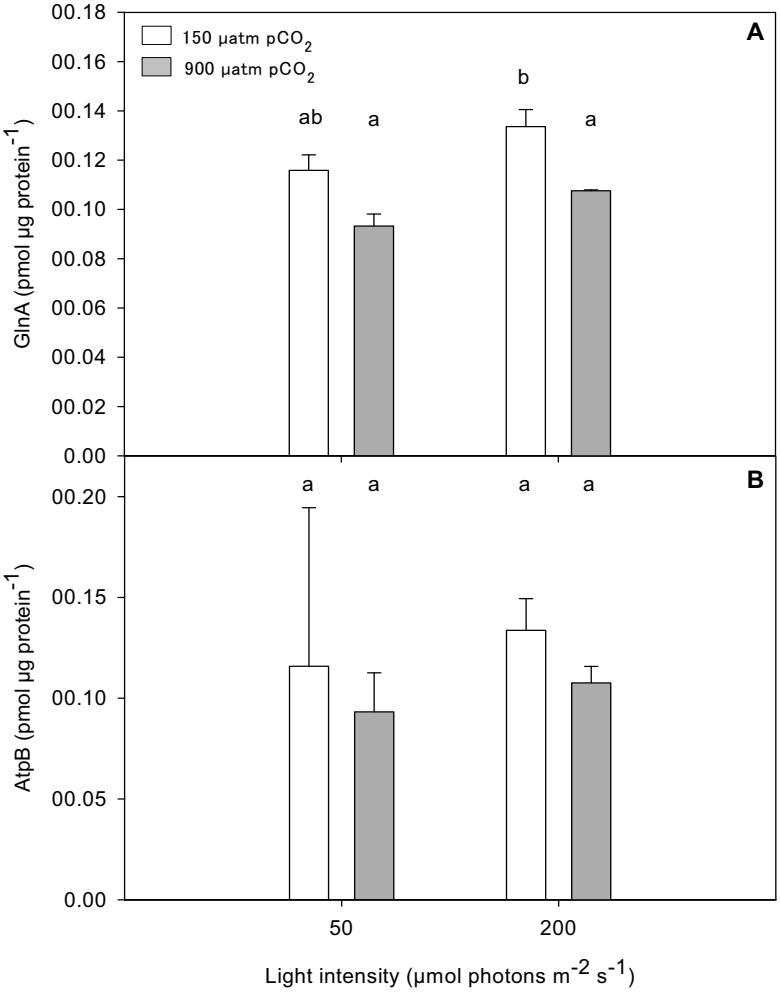
150 µatm pCO2
900 µatm pCO2
A
B
GlnA (pmol µg protein-1)
AtpB (pmol µg protein-1)
00.18
00.16
00.14
00.12
00.10
00.08
00.06
00.04
00.02
0.00
00.20
00.15
00.10
00.05
0.00
ab
a
b
a
a
a
a
a
50
200
Light intensity (µmol photons m-2 s-1)

Figure 4:

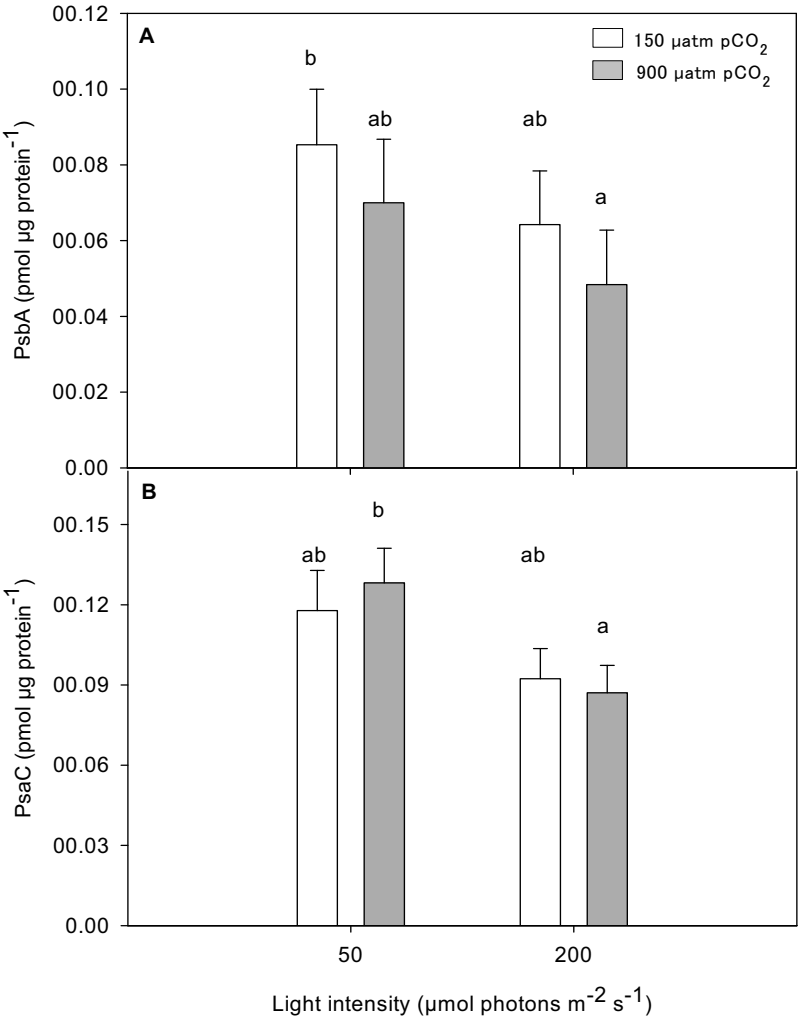
A
B
150 µatm pCO2
900 µatm pCO2
PsbA (pmol µg protein-1)
PsaC (pmol µg protein-1)
00.12
00.10
00.08
00.06
00.04
00.02
00.00
00.15
00.12
00.09
00.06
00.03
00.00
b
ab
ab
a
b
ab
ab
a
50
200
Light intensity (µmol photons m-2 s-1)

Figure 5:

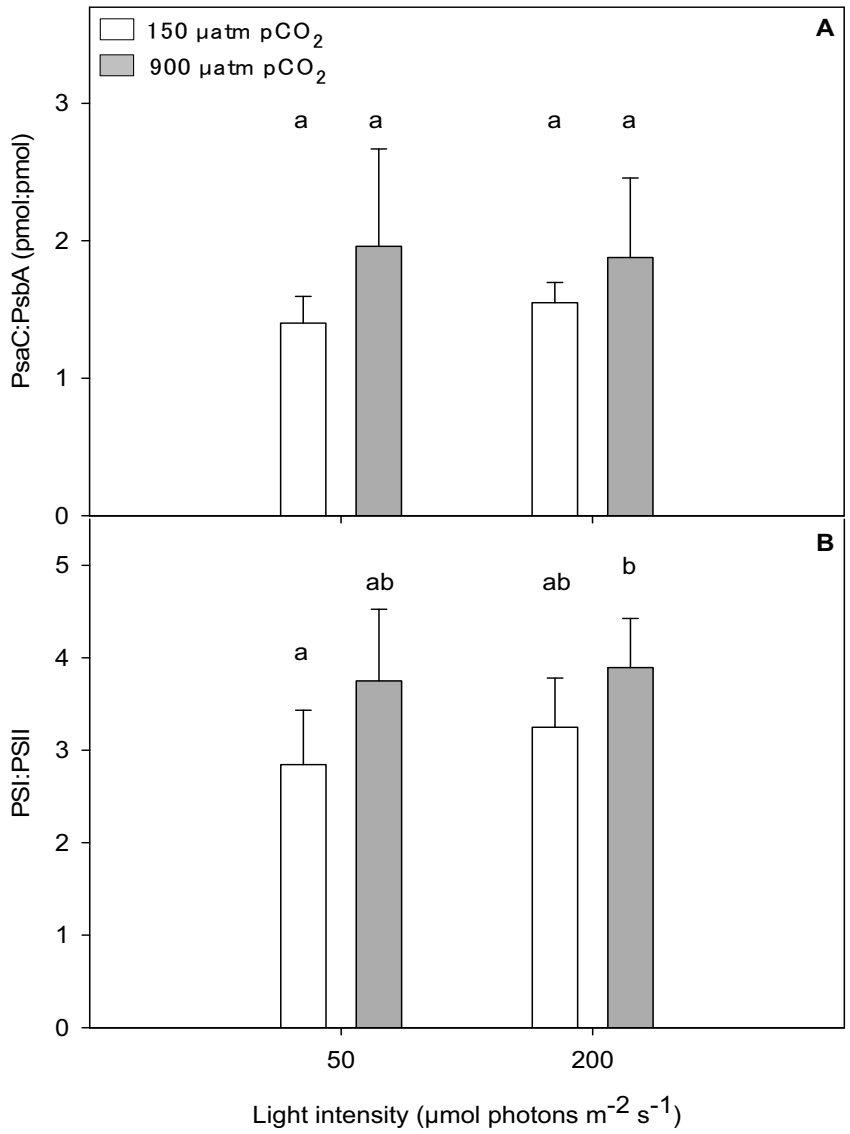
150 µatm pCO2
900 µatm pCO2
A
B
PsaC:PsbA (pmol:pmol)
PSI:PSII
a
a
a
a
a
ab
ab
b
0
1
2
3
4
5
50
200
Light intensity (µmol photons m-2 s-1)

Figure 6:

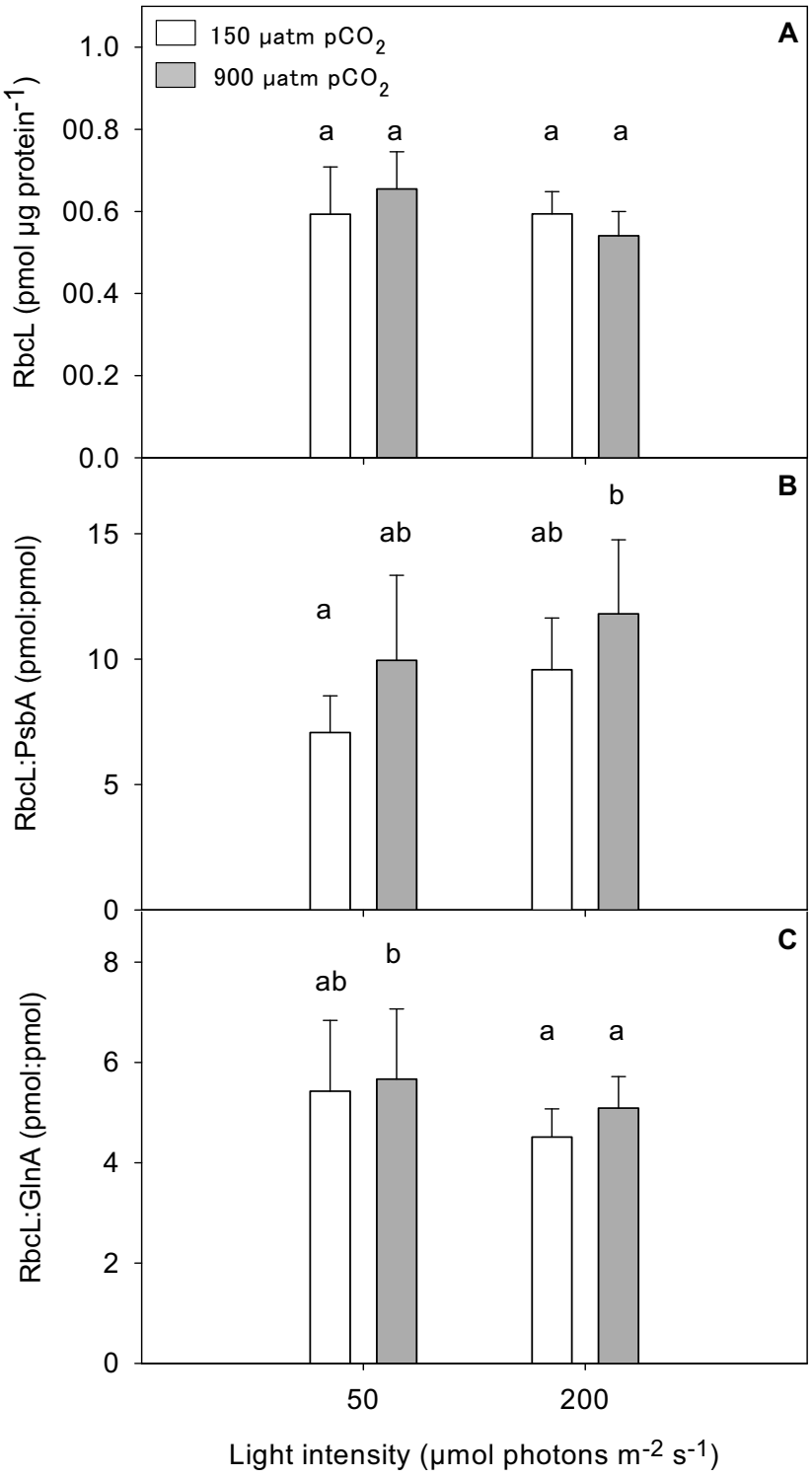
150 µatm pCO2
900 µatm pCO2
A
B
C
RbcL (pmol µg protein-1)
RbcL:PsbA (pmol:pmol)
RbcL:GlnA (pmol:pmol)
1.0
00.8
00.6
00.4
00.2
0.0
15
10
5
0
8
6
4
2
0
a a a a
a ab ab b
ab b a a
50
200
Light intensity (µmol photons m-2 s-1)

Figure 7:

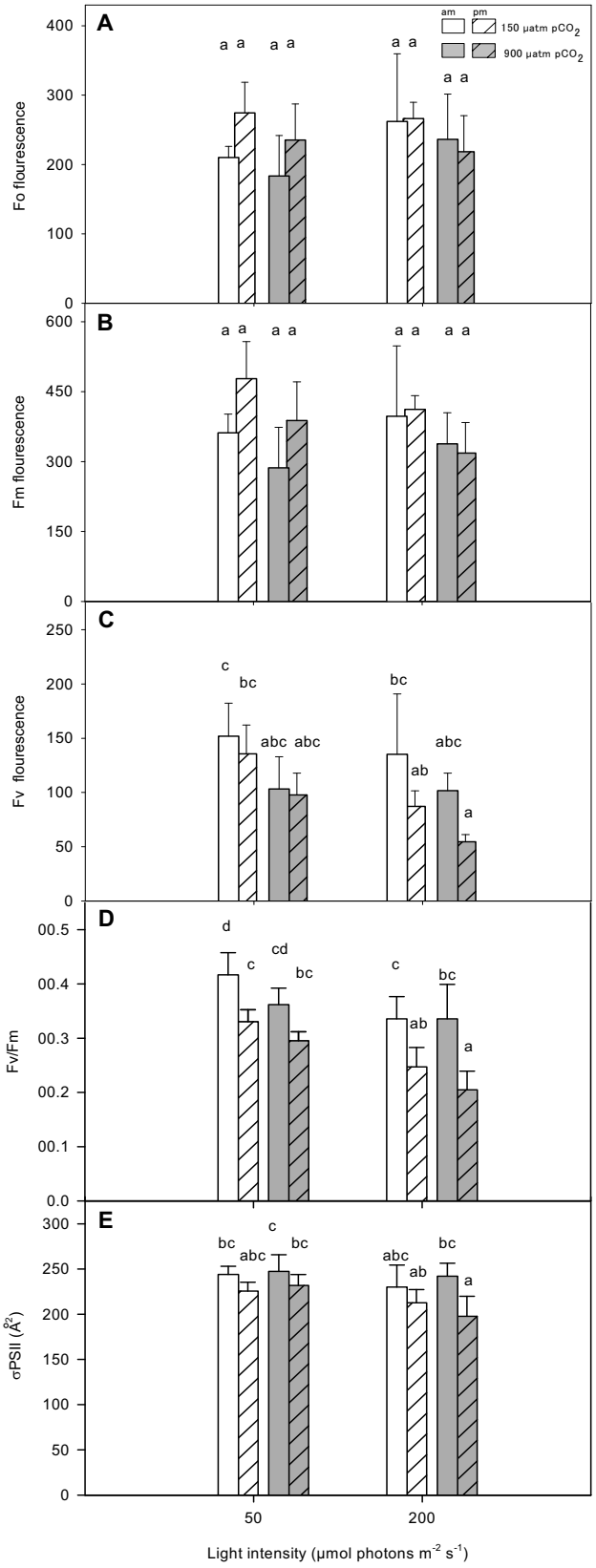
A
B
C
D
E
am
pm
150 µatm pCO2
900 µatm pCO2
Fo flourescence
Fm flourescence
Fv flourescence
Fv/Fm
σPSII (Å2)
Light intensity (µmol photons m-2 s-1)
50
200

Figure 8:

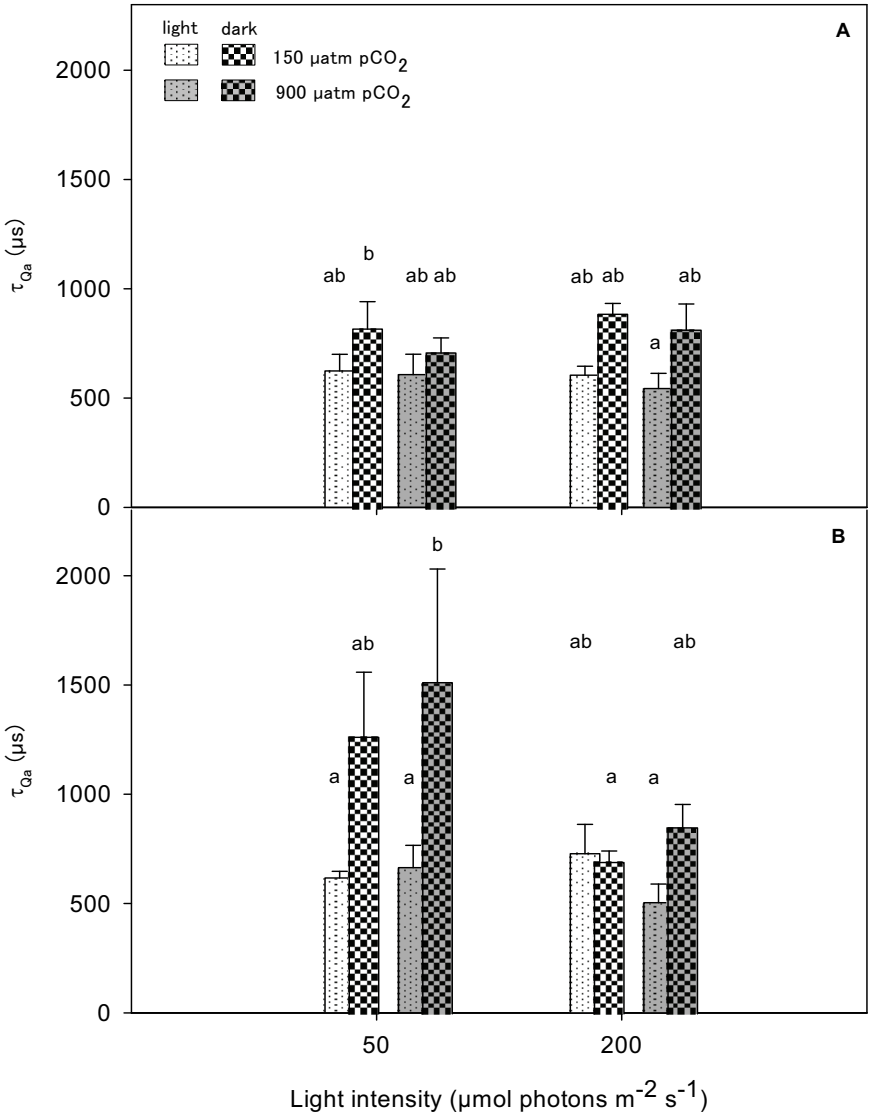
light
dark
150 µatm pCO2
900 µatm pCO2
A
B
τQa (µs)
2000
1500
1000
500
0
ab
b
ab ab
ab ab
ab
a
a
ab
b
ab
ab
a
a
a
50
200
Light intensity (µmol photons m-2 s-1)

Figure 9:

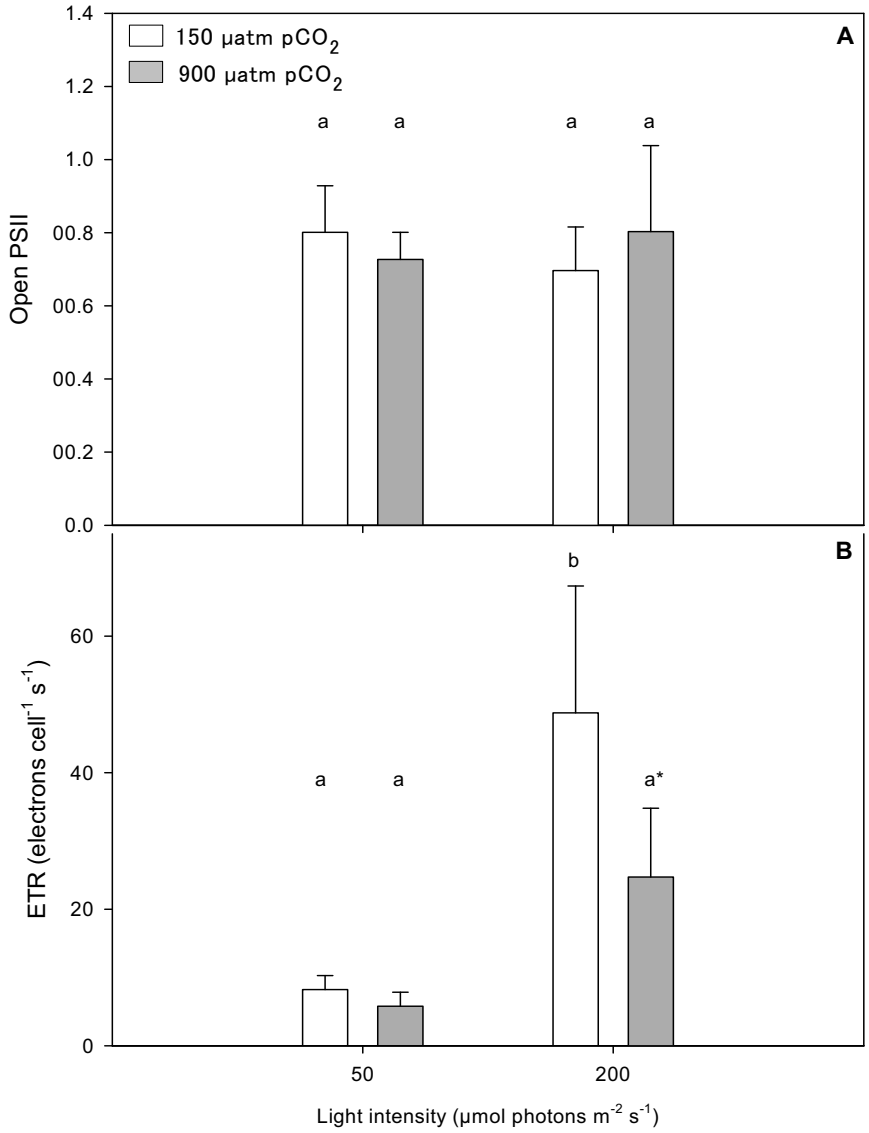
150 µatm pCO2
900 µatm pCO2
A
B
Open PSII
ETR (electrons cell-1 s-1)
Light intensity (µmol photons m-2 s-1)
a
a
a
a
b
a
a
a*
50
200

Figure 10:

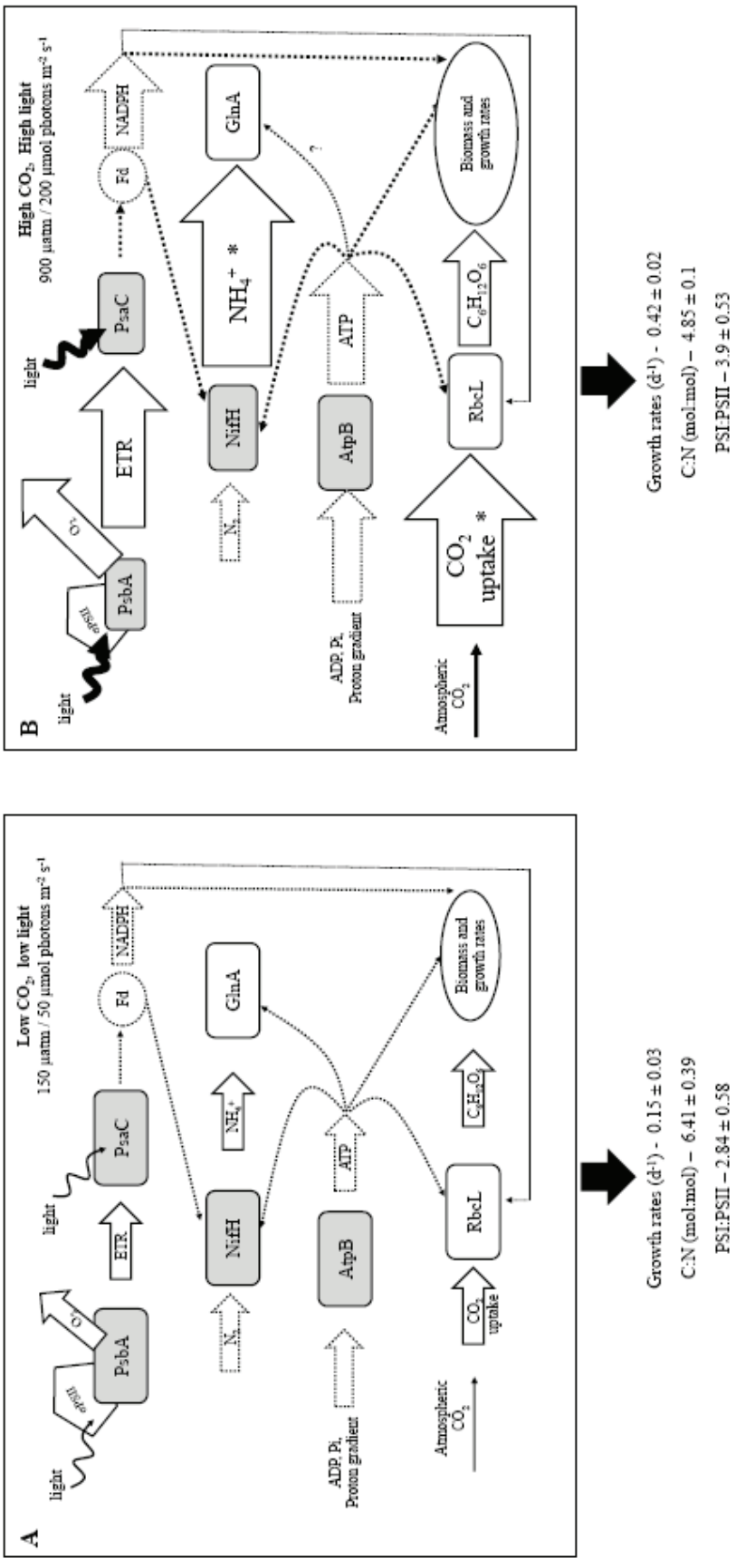
A
Low CO_2, low light
150 µatm / 50 µmol photons m^{-2} s^{-1}
light
PsbA
O_2
H2O
ETR
light
PsaC
Fd
NADPH
N_2
NifH
NH_4^+
GlnA
ADP, Pi,
Proton gradient
AtpB
ATP
Atmospheric
CO_2
CO_2
uptake
RbcL
$C_6H_{12}O_6$
Biomass and
growth rates
Growth rates (d^{-1}) - 0.15 ± 0.03
C:N (mol:mol) – 6.41 ± 0.39
PSI:PSII – 2.84 ± 0.58
B
High CO_2, High light
900 µatm / 200 µmol photons m^{-2} s^{-1}
light
PsbA
O_2
H2O
ETR
light
PsaC
Fd
NADPH
N_2
NifH
NH_4^+ *
GlnA
ADP, Pi,
Proton gradient
AtpB
ATP
Atmospheric
CO_2
CO_2
uptake *
RbcL
$C_6H_{12}O_6$
Biomass and
growth rates
Growth rates (d^{-1}) - 0.42 ± 0.02
C:N (mol:mol) – 4.85 ± 0.1
PSI:PSII – 3.9 ± 0.53

Appendix II

Chapter 12

Fluorescence as a tool to understand changes in photosynthetic electron flow regulation

Peter J Ralph[1], Christian Wilhelm[2], Johann Lavaud[3] Torsten Jakob[2] Katherina Petrou[1] and Sven A. Kranz[4]

[1] University of Technology, Sydney, Plant Function Biology & Climate Change Cluster,PO Box 123 Broadway, Sydney NSW Australia
[2] University of Leipzig, Department of Plant Physiology D-04103 Leipzig, Johannisallee 23 Germany
[3] CNRS UMR6250 'LIENSs', Institute of Coastal and Environmental Research (ILE), University of La Rochelle, France
[4] Alfred Wegener Institute for Polar and Marine Research, Am Handelshafen 12, 27570 Bremerhaven

Abbreviations
ADP: adenine diphosphate
ADRY: accelerators of deactivation reactions of the water-splitting system Y
ATP: adenine triphosphate
AX: antheraxanthin
Ci: inorganic carbon
DBMIB: 2,5-dibromo-3-methyl-6-isopropyl-p-benzoquinone
DCMU: 3'-(3,4-dichlorophenyl)-1',1'-dimethylurea
DD: diadinoxanthin
DT: diatoxanthin
E_k: minimum saturating irradiance
FCCP: carbonyl cyanide 4-trifluoromethyloxyphenylhydazone
FL: fluctuating light
Fm: maximum fluorescence
Fo: minimum fluorescence
FQR: ferredoxin-plastoquinone reductase
FTIR: Fourier transformed infra-red
GA: glycolaldehyde
LHC: light-harvesting antenna
MV: Methyl viologen (N,N'-Dimethyl-4,4'-bipyridinium dichloride; MV^{2+}
NDH: NADH-dehydrogenase complex
NPQ: non-photochemcial quenching
PAM: pulse amplitude modeluated
PGal: Propyl-gallate
PMS: Phenazine methosulfate
PQ: plastiquinone
PQH_2: reduced plastiquinone
PSI: Photosystem I
PSII: Photosystem II
PTOX: plastoquinol terminal oxidase
Q_A: primary electron acceptor
Q_B: secondary electron acceptor
qE: energy-dependent quenching
qI : photoinhibition quenching
qP: photochemical quenching
qT: state-transition quenching
SL: sine light
XC: xanthophyll cycle
ZX: zeaxanthin

I. Introduction

The physiological state of a chloroplast is strongly influenced by both biotic and abiotic conditions. Unfavourable growth conditions lead to photosynthetic stress. Chlorophyll *a* fluorescence is a widely used probe of photosynthetic activity (specifically PSII), and therefore stress which specifically targets the electron transport pathway and associated alternative electron cycling pathways. By manipulating the processes that control photosynthesis, affecting the chlorophyll *a* fluorescence which yields detailed insight into the biochemical pathways. Light that is captured by a chlorophyll molecule can be utilised in

three competing processes; electron transport, energy dissipation (via heat) and chlorophyll *a* fluorescence emission. Electrons produced by water-splitting are not always used in carbon fixation; if the incident irradiance generates more electrons than the dark reactions can use in carbon fixation, otherwise damage will occur to the photosynthetic apparatus. If carbon fixation is inhibited by temperature or reduced inorganic carbon (Ci), ATP or NADPH availability, then the photosystem dynamically adjusts and uses alternate sinks for electrons, such as molecular oxygen (water-water cycle or Mehler ascorbate peroxidase reaction). The process of stress acclimation leads to a number of photoprotective pathways and we describe how inhibitors can be used to identify these particular processes. In this chapter, we describe the processes controlling electron transport as influenced by light-induced stress.

Electron usage in photosynthesis

Photosynthesis drives the light reactions which ultimately lead to carbon fixation; however predicting photosynthetic rates from fluorescence is a complex issue. As outlined in other chapters of this book (Laney & Oxenborough, 2008; Suggett et al., 2008) different fluorescence tools are available to measure the electron flow through Photosystem II (PSII). The quantum yield of PSII can be multiplied by the amount of absorbed quanta which can be obtained from the incident light and either the PSII absorption cross section or the spectral overlap between the light spectrum and the *in-situ* absorption spectra. From these data, the electron transport rate per chlorophyll molecule over time can be assessed for an entire day to determine the daily primary production (Wagner et al., 2005). However, growth and photosynthesis are rarely equivalent. Electrons transported by PSII can follow several competing pathways: the majority of the electrons are normally used to reduce CO_2 to carbohydrates, allowing the synthesis of other cellular macromolecules like proteins, lipids or nucleotides, but some of them might be lost by alternate cellular processes (see alternate electron cycling) or dissipated (non-photochemical quenching). Therefore, the ratio of electron per carbon incorporated into the biomass may vary tremendously, either by losses or by the synthesis of highly reduced biomolecules like proteins or lipids.

Alternative electron cycling (AEC)

In principle, PSII electron transport rates should match the gross rates of oxygen evolution. Studies have tried to verify this assumption with divergent results (Falkowski et al., 1986; Kolber et al., 1998; Suggett et al., 2001; Jakob et al., 2005). It was shown that linearity between PSII electron transport and oxygen evolution can be found, but non-linear behaviour was also observed, especially under conditions when photosynthesis was over-saturated (excess irradiance). These experiments indicated that PSII electron transport might over-estimate the primary production under some conditions, because oxygen evolution rates were found to be lower than PSII electron flow (Gilbert et al., 2000). Several explanations for this disparity have been suggested:

a. cyclic electron flow around PSII (Prasil et al., 1996; Lavaud et al., 2002),
b. water-water cycle (Asada, 1999) where oxygen uptake on the acceptor side of PSI leads to superoxide which is then dismutated to H_2O_2 and then detoxified to water and,
c. cyclic electron flow around PSI (Bendall & Manesse, 1996).

These processes can be summarised as alternative electron cycling (AEC) which are not energetic losses (such as non-photochemical quenching: NPQ), because at least the water-water cycle and the cyclic flow around PSI generate a proton gradient which can be used for additional ATP synthesis. Therefore, it is suggested that alternative electron cycling is a normal stress response and might be of less importance under balanced growth conditions. Recently, Wagner et al. (2005) described an experimental setup to estimate the alternative

electron cycling activity by comparing the electron flow through PSII with oxygen evolution relative to the amount of absorbed quanta. The result is shown in Figure 1.

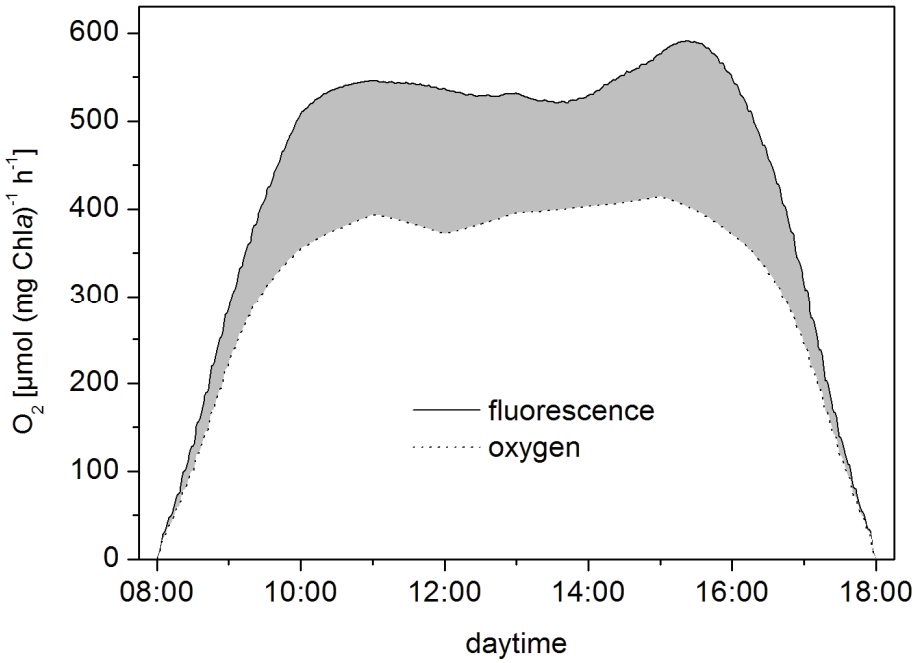

Figure 1: Modelling of fluorescence and oxygen-based photosynthesis rates in *Phaeodactylum tricornutum* grown in a turbidostat under sine light conditions (10 h light period). Photosynthesis-irradiance curves were measured hourly and fitted using the dynamic model of Eilers & Peters (1988). With the derived fitting parameters, oxygen and fluorescence-based electron transport rates can be calculated for any given light intensity during the daily course of the light climate. The difference between fluorescence-based electron transport rates and oxygen-based photosynthesis rates (grey area between the curves) is linked to the proportion of alternative electron cycling.

Obviously, at low light intensities in the morning and in the late afternoon, the fluorescence-based electron transport rates closely match the oxygen evolution rates as measured by a Clark-type electrode, whereas at high light intensities the "alternative electron cycling" can account for up to 40% of the fluorescence-based electron transport. This mismatch is not due to inappropriate measuring techniques, but to the physiological variability between linear and alternative electron pathways across the photosynthetic membrane. Interestingly, the ratio of linear to alternative electron cycling is not only light-dependent, but can be linked to species-specific physiological regulation, as shown in Figure 2.

When light pulse frequency is manipulated, the relationship between electron transport and oxygen evolution is further altered. In the sine light (SL) climate which simulates a sunny day, the ratio PAM/oxygen is always higher than in the exponentially fluctuating light (FL) climate (Fig. 2), when the light intensity oscillates with a frequency of half an hour between the maximum value and zero. The green alga *Chlorella vulgaris* performs much more alternative electron transport than the diatom *Phaeodactylum tricornutum* under both light conditions (FL and SL). In the sine light where the cells are exposed to a photon flux which exceeds the capacity of the Calvin cycle, the alternative electron cycling is highest indicating, that it can act as a photoprotective mechanism which compliments other photoprotective processes. Given that alternative electron cycling in the green alga was higher than in the diatom, this corresponds with the observation that in diatoms the energy dissipation capacity of the diadinoxanthin/diatoxanthin xanthophyll cycle is more active than in green algae or higher plants (Ruban et al., 2004; Goss et al., 2006) and will be discussed later in this chapter.

It should be noted that green algae and higher plants have a different suite of xanthophyll pigments to diatoms and dinoflagellates.

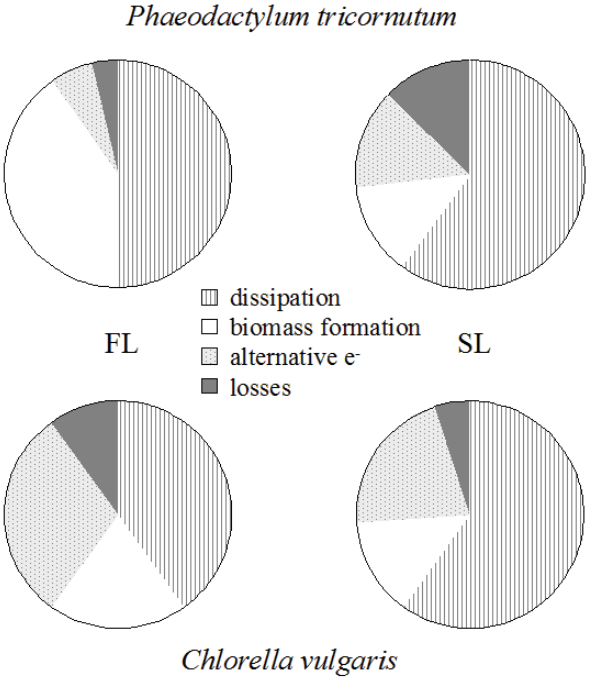

Figure 2: The fate of absorbed photons in the comparison of *Phaeodactylum tricornutum* and *Chlorella vulgaris* grown in a turbidostat under dynamic light conditions (fluctuating light, FL; sine light, SL). Data are given as percentage of absorbed quanta (Q_{phar}). Energy losses by dissipation include the conversion of absorbed light into heat and fluorescence and were derived from $[(1\text{-}q_P)^{x} Q_{phar}]$, where q_P is the photosynthetic quantum efficiency at Photosystem II measured by PAM fluorescence. The amount of quanta lost by alternative electron sinks was calculated from the difference of fluorescence and oxygen-based photosynthesis rates and the assumption of a quantum efficiency of 0.125 [mol O_2 (mol quanta)$^{-1}$]. The amount of quanta used for biomass formation was derived from Φ_μ according to Jakob et al. (2007). Energy losses which are not directly quantifiable as absorbed quanta, like mitochondrial respiration, have been depicted as 'losses'.

Electron usage to produce new biomass

Under continuous light, the oxygen production or the uptake of inorganic carbon shows a clear linear relationship with biomass production (Toepel et al., 2004) indicating that 55-60 µmol oxygen released is equivalent to 1 mg dry weight. However, the ratio of oxygen released to carbon incorporated is highly variable, for several reasons. Firstly, the reduction in biomass strongly depends on the species and the environmental conditions (Kroon & Thoms, 2006). For example, under N or P limitation, the relative proportion of carbon incorporated into carbohydrates is strongly increased and therefore the reduction in biomass is relatively low. The energetic cost of converting the products of the Calvin cycle into lipid or proteins are incorporated by higher rates of mitochondrial respiration. Therefore, it can not be expected that the ratio of oxygen production in the light, per oxygen molecule consumed in the dark to be constant. This ratio is modulated, not only by the availability of nutrients and the reduction in biomass, but also by the turn-over rates of proteins and lipids. It is well documented that cells growing under high-light have significantly higher mitochondrial respiration rates, as well as under nutrient replete conditions and optimal temperature (Wilhelm & Wild, 1984). Table 1 shows that the ratio photosynthesis/respiration varies not only in response to the light climate (sine versus fluctuating light) but also with the C/N ratio. Therefore, the ratio of photosynthetic electrons to carbon incorporated into the newly formed cells has to be variable. However, such parameters have not been measured under an adequate range of conditions or with sufficient species to make broad speculation.

The conversion of electron transport rates into actual new biomass requires accurate estimates for the ratio of electrons per carbon in the macromolecules of the new biomass. In future, the FTIR spectroscopy (Stehfest et al., 2005) might become a tool to measure this parameter, and is also possible with single cells. This opens the perspective to improve the robustness of estimates for primary production measure by using advanced fluorescence techniques.

Table 1: Comparison of *Phaeodactylum tricornutum* and *Chlorella vulgaris* with respect to the activity of alternative electron transport (expressed as the ratio of fluorescence-based to oxygen-based photosynthesis rates; P_F/P_O), to C/N ratios (given as mol mol^{-1}), and the activity of mitochondrial respiration (expressed as the ratio of respiration rate to net photosynthesis rate; R/Pnet). Algal cultures were grown in a turbidostat under dynamic light conditions (10h and 12h light periods) which have been applied either as a non-fluctuating sine light climate or as oscillating light (osc. Light). In addition, *P. tricornutum* was exposed to nitrate-limited conditions (N-limited). Data are adapted from Wagner et al. (2006) and Jakob et al. (2007).

Species	Growth condition	P_F/P_O	C/N	R/Pnet
P.tricornutum.	Replete – sine light (10 h)	1.4	7.7	0.8
P.tricornutum.	Replete – osc. light (10 h)	1.3	7.9	1.0
P.tricornutum	Replete – sine light (12 h)	1.6	6.6	0.4
P.tricornutum	Replete – osc. light (12 h)	1.1	6.7	1.4
P.tricornutum	N-limited – sine light (10 h)	1.6	14.5	0.7
P.tricornutum	N-limited – osc. light (10 h)	1.2	10.8	1.5
C.vulgaris.	Replete – sine light (12 h)	2.1	6.8	0.4
C.vulgaris	Replete – osc. light (12 h)	2.0	6.8	0.9

II. Effect of light stress on fluorescence signatures and their interpretation

When captured light energy cannot be completely utilized for metabolic processes, the excess energy accumulates within the photosynthetic apparatus (Nixon and Mullineaux, 2001). This typically occurs when the light intensity is too high (over minimum saturating irradiance: E_k). However, this also occurs when the cells are suddenly switched from a dark/low light environment or to a higher irradiance (not necessarily over E_k) depending on the physiological state of the cells and their response to other environmental cues. Accumulation of excess energy within the photosynthetic apparatus can be harmful for photosynthesis, and especially for the activity of PSII, because the over-reduction of the primary electron acceptor (Q_A) generates free radicals which leads to oxidative stress (Ledford and Niyogi, 2005); stress which will ultimately cause a decrease in the photosynthetic rate (i.e. photoinhibition). Photosynthetic organisms have developed a number of fast photoprotective (or photoacclimative) processes to minimize the level of oxidative stress, especially linked to the dissipation of the excess absorbed energy (Niyogi, 2000). Non-photochemical quenching (NPQ) is believed to be one of the most important of these mechanisms for the fast regulation of photosynthesis in higher plants as well as in algae (Szabo et al., 2005; Demmig-Adams and Adams, 2006; Lavaud, 2007). It should be noted that NPQ is not a form of AEC, but rather it is especially efficient for organisms growing in a fluctuating light environment where it helps to balance the absorption of light energy with its use, and ultimately plays a role in the maintenance of their fitness (Külheim et al., 2002; Demmig-Adams and Adams, 2006; Lavaud, 2007).

Non-photochemical quenching (NPQ) originates in the light-harvesting antenna (LHC) of PSII. When the available excitation energy exceeds the photochemical capacity, it can then be dissipated as heat (or reallocated) before it reaches the PSII reaction center. This process arise from reactions not directly related to photochemistry, which have been defined as 'non-photochemical quenching' to be distinguished from the processes dealing with the 'photochemical quenching' (qP) which is directly related to photochemistry and the linear transport of electrons (Fig. 3a) (Maxwell and Johnson, 2000; Baker, 2008). In that framework,

the redox state of quinones (Q_A and Q_B) and plastoquinones can strongly influence the emission of fluorescence in parallel to NPQ under high light conditions (Perkins et al., 2006). NPQ reduces the lifetime of excited chlorophylls (^{1}Chl*) and thereby the quantum yield of Chl *a* fluorescence, which is seen by a decrease of F_m to F_m' level (see Fig. 3a). For that reason, it is calculated as $(F_m-F_m')/F_m'$ (or F_o-F_o'/F_o'; Lavaud et al., 2002). In higher plants, green algae and dinoflagellates, where the NPQ mechanism has been investigated, it consists of three components (Fig. 3a) (Stroch et al., 2004; Szabo et al., 2005): the energy-dependent quenching (qE) which is regulated by the built-up of a trans-thylakoid proton gradient (ΔpH) and the operation of the xanthophyll cycle (XC); state-transition quenching (qT); which relies on the redistribution of excitation energy between photosystems by physical modulation of the cross-section of light-harvesting antennas (Ruban and Johnson, 2009) and the sustained quenching which is heterogeneous (Demmig-Adams and Adams, 2006) which partially depends on xanthophylls (Garcia-Mendoza and Colombo-Pallotta, 2007) as well as on photoinactivation/photoinhibition (qI) of PSII (Stroch et al., 2004). Quantification of these three components is either based on their relaxation kinetics in the dark (Müller et al., 2001) or requires photosynthetic inhibitors (Horton & Hague, 1988). The characteristics of their relaxation kinetics can vary according to environmental stresses and between groups of organisms. Such that, qE relaxes very rapidly (within tens of seconds after the offset of light), qT takes several minutes (shorter for cyanobacteria and rhodophytes), while qI is sustained and can last for hours even days under certain extreme environmental conditions (Demmig-Adams and Adams, 2006; Garcia-Mendoza and Colombo-Pallotta, 2007). Furthermore, in diatoms qE usually relaxes very slowly in comparison to higher plants (compare the two organisms in Fig. 3b) so that it could be confounded with qI due to overlaps with time. In general, with non-stressed leaves, qE is the major component under moderate to saturating irradiance. qI can become prominent under over-saturating irradiances and possibly in combination with other stresses (nutrient/water deficiency, temperature and salinity) (Demmig-Adams and Adams, 2006). In this context, qT is not as relevant since it generally only makes a small contribution to overall relaxation of fluorescence (see Fig. 3a) (Nixon and Mullineaux, 2001). qT is usually significant only under low light levels (Mullineaux and Emlyn-Jones, 2005) while some dinoflagellates increase qT under thermal and light stress (Hill et al., 2005). The amplitude and kinetics of the whole NPQ process and the importance of each component (Fig. 3b) can be extremely divergent between taxa, especially among microalgal groups (Casper-Lindley and Bjorkman, 1998; Juneau and Harrison, 2005), and even between species within a taxonomic group (Lavaud et al., 2004; Lavaud et al., 2007). For example, qE shows high amplitude and fast onset in diatoms and brown macroalgae, while being of minor importance in most of the green microalgae (Finazzi et al., 2006) and cyanobacteria (Kirilovsky, 2007). Nevertheless, within the diatoms (see the Chapter 7) as well as higher plants (Johnson et al., 1993) there are clear differences in qE amplitude that have been highlighted. Whereas, qT is currently unknown in diatoms (Owens, 1986) and brown macroalgae (Fork et al., 1991), and of only moderate importance in higher plants and dinoflagellates (Hill et al., 2005), yet highly developed in some green microalgae and cyanobacteria (Finazzi, 2005; Mullineaux and Emlyn-Jones, 2005).

Amongst the three components of NPQ, qE is a major influence on the Chl *a* fluorescence signal under normal growth conditions (Logan et al., 2007); see also the Chapter 7). The interpretation of qE is possibly the most complex of the NPQ components, as it is linked to faster regulation of photosynthesis than qT and qI with most organisms, especially under naturally fluctuating environment (Lavaud, 2007). (Frenkel et al., 2007) demonstrated that qE is critical for maintaining the fitness of plants under natural temperate-light conditions, rather than qT. Also, in cyanobacteria and green microalgae, qT has no significant physiological importance in photoprotection towards high-light stress, yet is more relevant in low light

conditions (Mullineaux and Emlyn-Jones, 2005) and for acclimation to different light quality (Pfannschmidt, 2005). The qT mechanism has been documented, as well as its impact on the fluorescence signal, especially in cyanobacteria and green microalgae (see (Campbell et al., 1998; Nixon and Mullineaux, 2001; Finazzi, 2005; Mullineaux and Emlyn-Jones, 2005). Even though qI has been well documented in some species of higher plants growing in extreme environments (Demmig-Adams and Adams, 2006), its occurrence and control mechanism remains unknown in some of the algal groups. Also, the part of qI which depends on xanthophylls is also linked to the qE process (Demmig-Adams and Adams, 2006), although clear mechanistic differences have only been recently demonstrated (Dall'Osto et al., 2005).

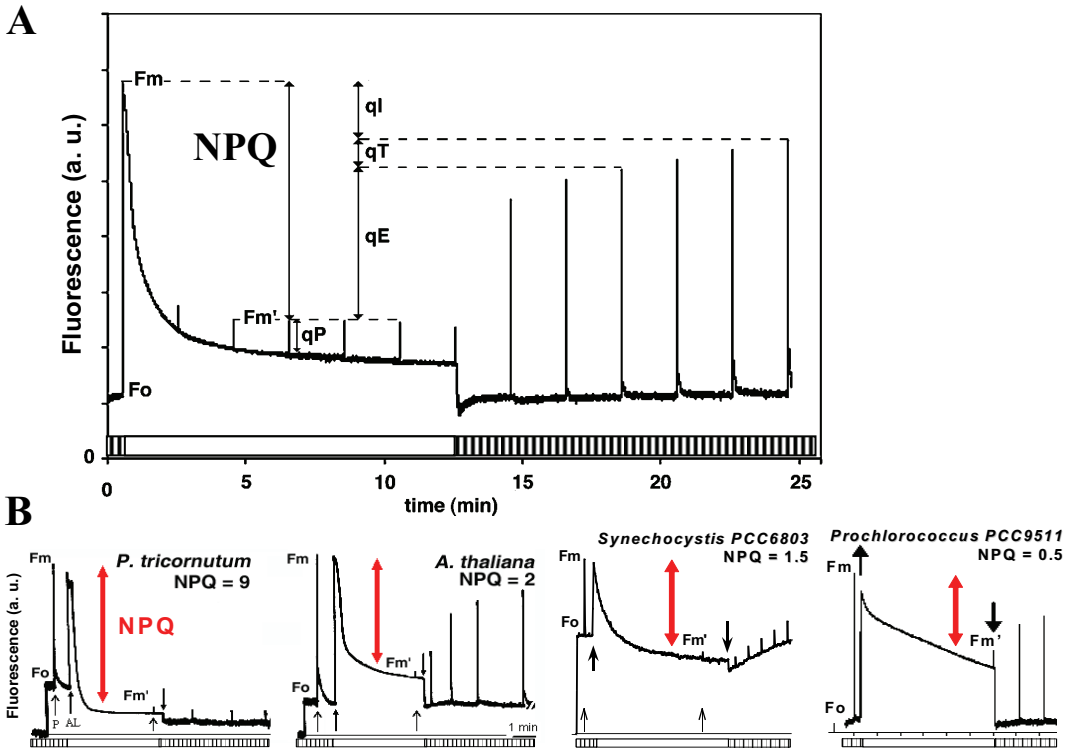

Figure 3. (A) Chlorophyll *a* (Chl *a*) fluorescence signal as measured with a PAM fluorometer on an *Arabidopsis thalania* leaf. After dark-adaptation, in the presence of the detector beam (dashed bottom bar), the minimal fluorescence level (F_o) is measured. When a saturating light pulse (P) is given, the photosynthetic light reactions become saturated and fluorescence reaches a maximum level (F_m). Upon continuous actinic light (AL On, white bottom bar) with moderately excess light (750 µmol photons m^{-2} s^{-1}; growth light was 130 µmol photons m^{-2} s^{-1}), a combination of qP and NPQ lowers the fluorescence yield. NPQ (qE + qT + qI) is the difference between F_m and the measured maximal fluorescence after a saturating light pulse during illumination (F_m'): NPQ = (F_m-F_m')/F_m'. After switching off the actinic light (AL Off), the quenching on the F_o level can be observed (F_o'). Also, the recovery of F_m' within a few minutes reflects relaxation of the qE component of NPQ. qT takes a longer time to relax while qI is a sustained quenching. Adapted from Müller et al. (2001). **(B)** Characteristic Chl *a* fluorescence signals as measured with a PAM fluorometer in cells of the diatom *Phaeodactylum tricornutum*, leaf of the higher plant *Arabidopsis thalania*, cells of the cyanobacterium *Synechocystis* PCC6803, and cells of the Prochlorophyte *Prochlorococcus* PCC9511, illumination was: 5 min-2000 µmol photons m^{-2} s^{-1}. The time scale is given on the *A. thaliana* trace. Adapted from Ruban et al. (2004), Cadoret et al. (2004), Bailey et al. (2005). For (A) and (B): F_o, minimum fluorescence level in the dark; F_o', minimum fluorescence level after light exposure (detector beam only for both); F_m, maximum fluorescence level in the dark; F_m', maximum fluorescence level at light; AL, actinic continuous light (bold arrow up/down: AL on/off); P, over-saturating pulses (600-800 ms duration, thin arrows: pulse fire). Bars: dashed, detector beam only; white; detector beam+AL on.

The qE mechanism has been described in a molecular context for higher plants and green microalgae (Standfuss et al., 2005; Cogdell, 2006; Ruban et al., 2007). The machinery triggering and controlling qE amplitude and kinetics is now quite well known for groups of algae like the diatoms and brown macroalgae (Goss et al., 2006; Lavaud, 2007), as well as in the cyanobacteria and prochlorophytes (Bailey et al., 2005; Kirilovsky, 2007). The NPQ process is based on a feed-back reaction from the linear electron transport through the build-up of a trans-thylakoid ΔpH and subsequent acidification of the thylakoid lumen (see (Nixon and Mullineaux, 2001). Consequently, the activity of the ATP synthase (Dal Bosso et al.,

2004) the cytochrome b_6f (Munekage et al., 2001), or the cyclic electron flow around PSI (Miyake et al., 2005) can indirectly influence qE. Hence, in a simple direct relationship, the higher the irradiance, the higher the electron transport rate, the higher the accumulation of protons in the lumen, the higher qE. In some organisms such as diatoms, it appears there is a relative independence of the PSII redox-state from the proton-motive electron transfer and subsequent NPQ (Ruban et al., 2004; Lavaud et al., 2007). To summarize NPQ responses, the lumen acidification triggers two events (Fig. 4): 1) the protonation of specific sites of the LHC antenna, and 2) the activation of an enzyme, a de-epoxidase, which drives the conversion of epoxized xanthophyll to a de-epoxidized form. This conversion is reversible as the backward reaction is driven by an epoxidase which also depends on the trans-thylakoid ΔpH. The accumulation of de-epoxidized xanthophylls thus depends on the balance between the activity of both enzymes within the xanthophyll cycle (XC) (see (Lavaud, 2007) for a detailed description). In higher plants, green microalgae and brown macroalgae, the XC involves the conversion of violaxanthin to zeaxanthin (ZX) via antheraxanthin (AX) (Fig. 4) while the diatoms and dinoflagellates use diadinoxanthin (DD) which is converted to diatoxanthin (DT) under elevated light (see Chapter 7). Both protonated LHC protein(s) and the presence of DT or ZX/AX in the LHC antenna of PSII are thought to act together as the trigger of the qE. The whole LHC antenna switches into a dissipative mode when excess excitation energy should be converted into heat while Chl *a* fluorescence is quenched (Fig. 4) (Stroch et al., 2004; Szabo et al., 2005). More precisely, protonation would promote and transduce conformational changes ('aggregations') which bring pigments closer together and especially chlorophyll/xanthophyll molecules. In higher plants the 'special' polypeptide which undergoes protonation is PsbS (Niyogi et al., 2005). The function of PsbS is essentially to sense the lumen pH, ths is linked to several H^+-binding amino acids residues present on the luminal loops of this protein (Dominici et al., 2002; Li et al., 2002). In green microalgae (Graham & Niyogi, pers. com.) and diatoms (Zhu and Green, 2008), the Li-818 proteins which are up-regulated under high light, could play a similar role as PsbS in qE. Simultaneously, with PsbS protonation, de-epoxidized xanthophylls would also act as 'allosteric regulators' by amplifying the conformational changes within the whole LHC antenna. The physical process by which excitation energy is effectively converted into heat has only recently been understood (Holt et al., 2005; Pascal et al., 2005; Ruban et al., 2007). The qE mechanism is rather similar in other organisms like the diatoms and the brown macroalgae given some peculiarities (see Chapter 7). In other groups like the red algae, cyanobacteria and prochlorophytes, the process is quite different even though it involves xanthophylls and special proteins of the antenna system (Lavaud, 2007). Therefore, qE in these taxa is not as controlled as in higher plants or diatoms since these organisms do not display a finely regulated xanthophyll cycle, also cyanobacteria and prochlorophytes show no involvement of a trans-thylakoid ΔpH (Kirilovsky, 2007).

Quenching based in the PSII reaction center (as opposed to LHC antenna) has also been observed in higher plants (Bukhov et al., 2001; Stroch et al., 2004) and green microalgae (Finazzi et al., 2004), and possibly in diatoms (Eisenstadt et al.). Appearance of reaction centre quenching depends on the balance between light and carbon fixation fluxes (Finazzi et al., 2004) along with a clear temperature influence (Kornyeyev et al., 2004). This quenching appears to drive both qE and qI components of NPQ with both fast and slow relaxation kinetics, respectively. In contrast to the antenna-based quenching, it cannot cause changes in the F_o level (Maxwell and Johnson, 2000). Nevertheless, as well as the antenna-based quenching it requires thylakoid acidification, but it does not require de-epoxidized xanthophylls (Bukhov et al., 2001; Finazzi et al., 2004). The qI part of this reaction center based quenching is associated with a reversible inactivation of a sub-population of the PS II (Finazzi et al., 2004) as well as with PSII photodamage (Kornyeyev et al., 2004).

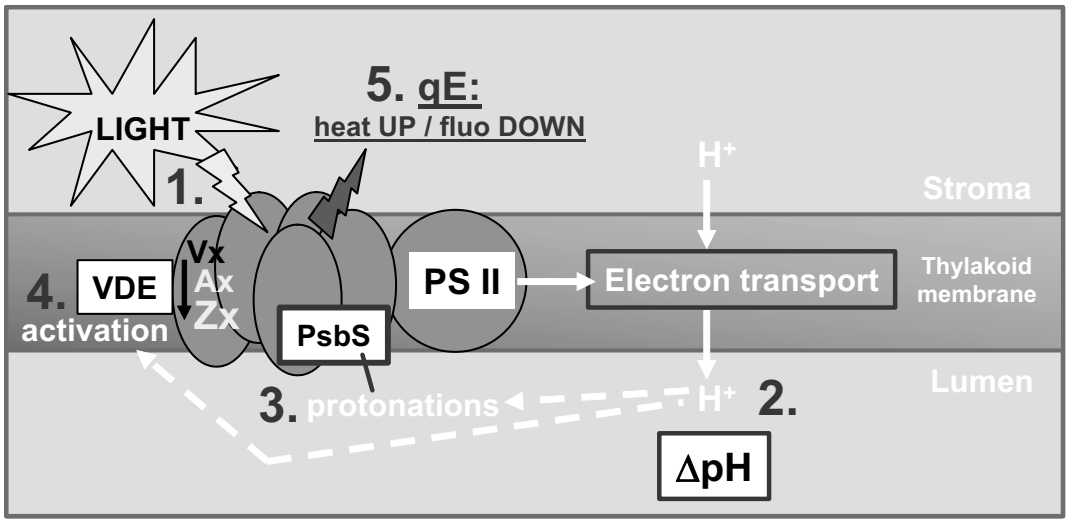

Figure 4. Simplified model of the qE mechanism in higher plants (see the text for a full description). The numbering refers to the sequence of the qE process steps. AX, antheraxanthin; H^+, protons; PS II, photosystem II; VDE, violaxanthin de-epoxidase; VX, violaxanthin; ZX, zeaxanthin; ΔpH, transthylakoid proton gradient. Adapted from Lavaud (2007).

III. Use of chemicals for the differentiation of photosynthetic processes

Photosynthesis is a complex interaction of complementary processes such as alternate electron cycling (AEC) and non-photochemical quenching (NPQ). A common method of isolating specific processes is using biochemical inhibitors such as herbicides. Electron transport inhibitors, uncouplers, artificial electron acceptors and donors have all proved to be essential tools in elucidating the function of various components of the photosynthetic electron transport chain, metabolic pathways and photosynthetic regulatory processes. Using herbicides to understand the regulation of photosynthesis and related biochemical pathways requires the basic understanding of how these herbicides interact with the photosynthetic apparatus.

Determining the appropriate concentration of herbicide is very important and often problematic, because depending on the organism, cells can have different cell wall composition, membrane transporters and a variation in the number of reaction centres per cell, thus requiring different concentrations of herbicide (Durnford et al., 1998). Therefore, any concentrations specified herein are only an indication of what has been used based the range of concentrations found in the literature. The most effective and correct way to determine the concentration at which a cellular response occurs is by titration of the herbicide against a known cell density or chlorophyll *a* concentration while measuring the physiological impact (oxygen evolution or chl *a* fluorescence).

Inhibitors of linear electron transport

DCMU (3'-(3,4-dichlorophenyl)-1',1'-dimethylurea), also known as Diuron, is the most extensively used inhibitor of photosynthetic electron transport. DCMU inhibits electron transport between PSII and PSI, impacting on the acceptor side of PSII by supplanting a bound plastoquinone from the Q_B^- binding site of PSII (Fig 5). Binding of this herbicide to the Q_B^- site of PSII, results in the effective blocking of electron flow and leads to the subsequent inhibition of photosynthesis. Blocking of electron flow is a consequence of the herbicide being incapable of receiving electrons, and therefore electrons remain trapped in Q_A, the first quinone acceptor (Kleczkowski, 1994). This trapping of electrons prevents the reduction of plastoquinone, by holding the electrons in the D1 dimer, thus affecting the redox state of the PQ pool, which becomes completely oxidised (Durnford et al., 1998).

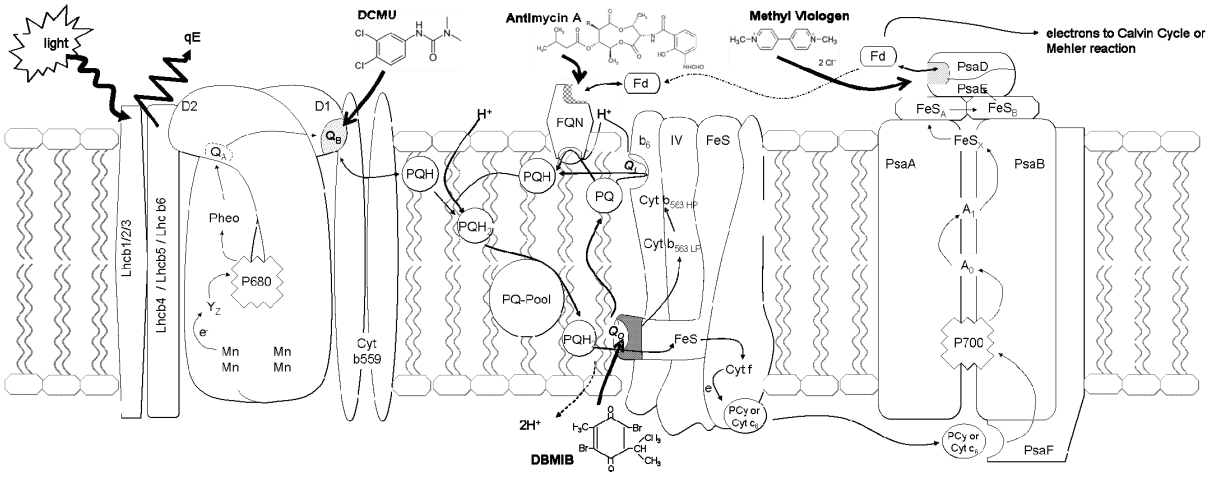

Figure 5. Electron transport flow through PSII, cytochrome *b6f* complex and PSI. The D1, D2 and Cyt b559 proteins are shown. The thin arrows indicate the electron flow pathway through PSII, while the thick arrow indicates the site of inhibition by DCMU. The figure shows the DCMU molecule binding to the Q_B site of PSII, thereby effectively blocking the continuation of electron flow from PSII to the plastoquinone, cytochrome *b6f* complex and onto PSI. After Q_B the thin arrows indicate electron flow pathways and proton (H^+) pathways. The thick arrow in the lower middle of the diagram indicates the site of impact by the inhibitors DBMIB and antimycin A. One DBMIB molecule competes with the PQH_2 resulting in the blocking of the release of electrons from the plastoquinone to PSI at the Fe-S complex. Antimycin A (upper middle) inhibits the reduction of ferrodoxin in PSI, intercepting electron transport at the ferrodoxin-plastoquinone reductase, resulting in the blocking of cyclic electron transport. Electrons move through PSI indicated by thin arrows, while the thick arrow (RHS) indicates the impact site of methyl viologen. Methyl viologen interacts at the binding site of ferredoxin, accepting the terminal electron, thus preventing the reduction of ferredoxin and the continued pathway of the electron to carbon fixation or cyclic electron transport.

DCMU causes a rapid increase to maximum fluorescence (F_m), where all PSII reaction centres are closed and the plastoquinone pool fully oxidised (Trebst, 2007). DCMU has no impact on the membrane potential of the thylakoid in darkness, yet completely inhibits light-induced membrane pH gradient. The amount of DCMU required for the inhibition of 50% of PSII reaction centres will vary depending on cell concentration and species. Published concentrations range from 1-20 μM (Falkowski & Raven, 2007). However, incremental increases in the amount of DCMU added to cells will result in changes in variable fluorescence and the rate of Q_A re-oxidation (Durnford et al., 1998), which will invariably allow for the determination of the appropriate concentration of DCMU needed to elicit the desired effect. In addition, the light acclimation state of the cells needs to taken into account, as cells grown at low PFD will have a plastiquinone (PQ) pool that is predominantly oxidized and therefore the addition of DCMU will have very little effect on the redox state of the PQ pool (Durnford et al., 1998) similarly, chlororespiration can alter the PQ redox state, allowing fluorescence yield to occur with saturating DCMU concentrations (Wilhelm & Duval, 1990). In the presence of saturating DCMU concentrations, fluorescence yield becomes maximum ($Fo \Rightarrow F_m$ so $F_v/F_m \Rightarrow 0$), as Q_A can no longer pass electrons to PQ, so electron transport stops and the maximum amount of captured energy is dissipated as fluorescence.

Like DCMU, DBMIB (2,5-dibromo-3-methyl-6-isopropyl-p-benzoquinone) is also an inhibitor of electron transport, however it blocks further along the electron transport chain near the Cytochrome b_6f complex (Trebst, 2007). DBMIB is thought to interfere at the Reiske iron-sulfur centre (Trebst, 2007), thus blocking photosynthetic electron flow through the Cytochrome b_6f complex. DBMIB binds close to the Qo pocket (Cramer et al., 2006), the plastoquinol binding site of the Cytochrome b_6f complex (Fig. 5), inhibiting the reoxidation of PQH_2 thus keeping the PQ pool completely reduced (Trebst, 1980).

Some precaution should be taken when using DBMIB, because site of action is concentration dependent, as well as redox sensitive, where DBMIB becomes reduced under light and oxidised in the dark (Bukhov et al., 2003). At low concentrations, DBMIB inhibits electron transport on the reducing side of the PQ, but at higher concentrations excess DBMIB will inhibit the Q_B site of PSII, located on the oxidising side of the PQ (Moreland, 1980; Rich

et al., 1991). To prevent fluorescence quenching from oxidised DBMIB, it can be used in conjunction with an excess of sodium ascorbate (Kufryk & Vermaas, 2006). For every Cytochrome b_6f complex, one molecule of $DBMIB_{red}$ is needed for complete inhibition of electron transfer through the Cytochrome b_6f complex (Rich et al., 1991). DBMIB can also inhibit mitochondrial electron transport (Durnford et al., 1998). This is a good example of co-inhibition, where some inhibitors have more than one impact site, and therefore interpretation of results must carefully consider the possibility of an alternate component of the cell machinery being affected by the inhibitor. DBMIB reduces minimum fluorescence (F_o) as well as the rise of variable fluorescence (F_v). While $DBMIB_{red}$ quenches chlorophyll *a* fluorescence, it does so less efficiently than the oxidised form ($DBMIB_{ox}$) and both forms alter NPQ estimates (Tyystjarvi et al., 1999).

Inhibitors of cyclic electron transport

The antibiotic, antimycin A, is an effective inhibitor of one of the alternate electron cycles (AEC), cyclic electron transport around PSI (Tagawa et al., 1963). It has been proposed that inhibition of photosynthetic electron transport by antimycin A is associated with the ferredoxin-plastoquinone reductase (FQR) activity in cyclic electron transport (Simonis & Urbach, 1973; Moss & Bendall, 1984; Cleland & Bendall, 1992). In addition to inhibiting cyclic electron transport, antimycin A is also known to inhibit excess light energy dissipation measured through NPQ (Oxborough & Horton, 1987). The decline in q_E (energy-dependent quenching) formation in the presence of this antibiotic is due to a change in the redox state of the electron transport chain. However, since antimycin A has no direct impact on linear electron transport rate, the redox change is most likely the result of a change in the redox state of a component located in the cytochrome complex (Oxborough & Horton, 1987). Before inhibiting cyclic electron transport, it is important to understand that there are two potential transport pathways that cycle around PSI (Joët et al., 2001; Munekage et al., 2004). The first, cycles electrons from ferrodoxin to the PQ pool and is sensitive to antimycin A, while the second, involves the NDH complex which is insensitive to the antibiotic (Joët et al., 2001). In the case of the NDH cycle, it is not yet fully understood and no known inhibitor has been identified. Published concentrations of antimycin A range from 0.1-50 μM (Falkowski & Raven, 2007).

Inhibitors of alternative electron cycling (AEC)

Distinguishing between different electron pathways is important to describe the discrepancies often seen between oxygen evolution and chlorophyll *a* fluorescence under stressful conditions. Molecular oxygen can be reduced downstream of PSII at various sites, using different forms of AEC. In the case of the Mehler reaction, oxygen is reduced at the acceptor side of PSI (Mehler, 1951) where it competes for electrons with both linear and cyclic electron transport pathways (Heber, 2002). The Mehler reaction itself can not be inhibited; however, the addition of potassium cyanide (KCN) can be used to inhibit the formation of H_2O and monodehydroascorbate (MDA) during the ascorbate peroxidase reaction, which is part of the Mehler cycle (Neubauer & Yamamoto 1992). The inhibition of H_2O formation as a result of altered peroxide turnover, impacts on the zeaxanthin-dependent light energy dissipation, by suppressing zeaxanthing formation and consequently NPQ (Neubauer and Yamamoto 1992). In fluorescence, the addition of KCN results in a decline in NPQ as well as a decrease in linear electron flow, shown as a suppression of q_P (Neubauer and Yamamoto 1992). Published KCN concentrations vary from 0.1mM to 3mM (Neubauer and Yamamota 1992, Hormann et al 1994, Singh et al 1996).

Another more recently discovered pseudo-cyclic electron transport pathway which cycles around PSII via the plastoquinol terminal oxidase (PTOX), reduces molecular oxygen by

utilising electrons from the PQ pool to generate H_2O (Cournac et al., 2000; Peltier & Cournac, 2002; Josse et al., 2003). This alternative electron flow around PSII (upstream of PSI & Cytochrome b_6f) is believed to be advantageous in both a high-light environment and under iron limitation (Bailey et al., 2008), as it alleviates PSII excitation pressure by transporting electrons directly to oxygen while simultaneously ensuring that the electrons bypass the iron-demanding cytochrome b_6f and PSI complexes (Mackey et al., 2008). Propyl-gallate (PGal) is an oxidase inhibitor specific to PTOX (Cournac et al., 2000; Bailey et al., 2008). PGal helps determine the role PTOX plays in alternative electron flow, and establish whether or not electrons are being used to reduce oxygen through PTOX activity (Mackey et al., 2008). The addition of 1 mM PGal results in a decrease in electron flow through PSII (Bailey et al., 2008; Mackey et al., 2008), highlighting the role the oxidase plays in keeping the PSII reaction centres oxidised in cells where Cytochrome b_6f and PSI activity are limiting. As in the case of DBMIB, PGal has more than one impact site in eukaryotes, as it can also lead to the inhibition of mitochondrial electron transport (Bailey et al., 2008).

Inhibitors of CO_2 fixation

Iodoacetamide has been used as an inhibitor of carbon fixation (Miller et al., 1988; Miller & Canvin, 1989), however when added during steady state photosynthesis, it inhibits CO_2 very slowly and may induce O_2 uptake in the light (Miller & Canvin, 1989). An alternative inhibitor of CO_2 fixation is D, L-glyceraldehyde (Stokes & Walker 1972), which at very high concentrations (>25 mM) completely inhibits CO_2 fixation (Shelp & Canvin, 1989) and blocks the conversion of triose-P to ribulose-1,5-bisphosphate (Stokes & Walker, 1972). However, more recently, glycolaldehyde (GA) has become the preferred inhibitor of CO_2 fixation, as it uses concentrations an order of magnitude lower than those of D, L-glyceraldehyde, while rapidly and effectively inhibiting CO_2 fixation (Sicher, 1984) without inhibiting CO_2 or HCO_3^- transport (Miller & Canvin, 1989; Rotatore et al., 1992). The addition of GA to cells eliminates the chlorophyll *a* fluorescence quenching that is seen with the addition of inorganic carbon; however, oxygen evolution is greatly impacted by the presence of GA (Miller & Canvin, 1989).

Electron transport uncouplers

Uncouplers function by dissociating electron transport from ATP synthesis during photosynthetic phosphorylation (Moreland, 1980; McCauley et al., 1987). This is accomplished by dissipating the energised state (H^+) of the membrane (ΔpH) before the energy can be utilised in ADP phosphorylation (Moreland, 1980) and thus prevent the formation of the trans-thylakoid ΔpH gradient. In addition to this major effect on the energy budget of the cell, the electron flow continues but the collapsed proton gradient no longer regulates electron transport rate. This type of inhibitor can be useful when examining processes triggered by ΔpH, such as NPQ and in particular qE. Common uncouplers of photophosphorylation include ammonia chloride (HN_4Cl), carbonyl cyanide 4-trifluoromethyloxyphenylhydazone (FCCP) and nigericin.

Ammonium chloride (NH_4Cl) is a potent uncoupler of electron transport. As described above, it works in the classical way by relaxing the pH gradient across the thylakoid membrane, inhibiting ATP synthesis. The addition of NH_4Cl before the application of saturating light will prevent all quenching of F_m'. In contrast, if the uncoupler is added after fluorescence quenching has already formed (following a series of saturating pulses), it will result in a complete reversal of all F_m' quenching (Delphin et al., 1998).

Carbonyl cyanide p-trifluoromethoxy phenylhydrazone (FCCP) is a powerful uncoupler of photophosphorylation. It acts as an ionophore completely dissipating the pH gradient, while leaving the electron transport system uninhibited (Canaani & Havaux, 1990). FCCP prevents

the long-term fluorescence induction, meaning that the inhibition of the induction is likely the result of an increase in the dark decay processes (Canaani & Havaux, 1990). Typical concentrations of FCCP are 1-10 μM (Shyam et al., 1993; Sigalat et al., 1993; Singh et al., 1996). At low concentrations FCCP quenches PSII fluorescence, indicative of the reoxidation of Q_A^- (McCauley et al., 1987), while it requires much higher concentrations to perform in its function as an uncoupler of oxidative phosphorylation (Canaani & Havaux, 1990). When incubated with cells under photoinhibitory light, FCCP accelerates photoinhibition and rapidly quenches fluorescence yield (McCauley et al., 1987; Shyam et al., 1993; Singh et al., 1996).

Another type of uncoupler is the protonophore, such as nigericin which dissipates the proton gradient across the thylakoid membrane. Nigericin relaxes the ΔpH gradient by antiporting H^+ at the expense of K^+ across membranes, resulting in the collapse q_E (Pressman et al., 1967). As a result of a breakdown in the pH gradient, the addition of nigericin to illuminated samples, results in an increase in F_m' and strong inhibition of NPQ with a concomitant large increase in steady state fluorescence F_t. The typical concentration range for nigericin is 1-5 mM (Falkowski & Raven, 2007).

Electron acceptors

Electron acceptors are compounds with very strong reducing capacity, such as methyl viologen (N,N'-Dimethyl-4,4'-bipyridinium dichloride; MV^{2+}) also known as Paraquat. Methyl viologen is an artificial electron acceptor, intercepting electron flow between PSI and the Calvin cycle by competing with ferrodoxin for the binding site at PSI (Fig. 5) (Dan Hess, 2000). MV^{2+} is an extremely powerful electron acceptor, due to the nature of the bipyridinium salts, which temporarily become a stable radical with the addition of an electron, neutralising the positive charge of the cation (Moreland, 1980; Peon et al., 2001). MV^{2+} oxidizes the primary acceptor (ferrodoxin) of linear electron transport, allowing a ΔpH to become established. However, this temporary neutral radical rapidly reverts back to its ion form, a process that results in the production of superoxide radicals (Hormann et al., 1993; Dan Hess, 2000). MV^{2+} can be used to demonstrate damage to the electron transport chain beyond PSI (typically Calvin cycle), where incubation with MV^{2+} will oxidise the electron transport chain and increase Φ_{PSII} by supplementing the slow carbon fixation rate. In the presence of MV^{2+}, non-photochemical quenching (NPQ) is reduced, because the excess electrons that are usually held up by the Calvin cycle, are being accepted by the MV^{2+} allowing for continual rapid electron transport and a reduced need for excess light energy dissipation in the form of NPQ. Published concentrations of MV^{2+} range from 0.05 to 1 mM (Falkowski & Raven, 2007).

In conclusion, we have illustrated how photosynthetic electron transport is strongly influenced by a range of internal feedback processes (AEC and NPQ) to ensure maximum efficiency, whilst preventing potential damage from excess excitation energy. Light stimulated processes such as non-photochemical quenching are closely linked with pigments, however the control mechanisms are species-specific and show wide variability. Chemical inhibitors can be used to isolate specific components of the electron transport chain allowing a mechanistic understanding of the control of these photosynthetic pathways.

References

Asada K (1999) The water-water cycle in chloroplasts: Scavenging of Active Oxygens and Dissipation of Excess Photons. Annu Rev Plant Physio Plant Mol Biol 50: 601-639.

Babin et al 2008 THIS BOOK

Baena-Gonzalez E, Allahverdiyeva Y, Svab Z et al. (2003) Deletion of the tobacco plastid psbA gene triggers an upregulation of the thylakoid-associated NAD(P)H dehydrogenase complex and the plastid terminal oxidase (PTOX) Plant Journal 35(6): 704-716.

Baker NR (2008) Chlorophyll fluorescence: A probe of photosynthesis *in vivo*. Annu Rev Plant Biol 59: 89-113.

Bailey S, Mann NH, Robinson C, Scanlan P (2005) The occurrence of rapidly reversible non-photochemical quenching of chlorophyll a fluorescence in cyanobacteria. FEBS Lett 579: 275-280.

Bailey S, Melis A, Mackey KRM, Cardol P, van Dijken FGG, Berg G, Arrigo KR, Shrager J, Grossman A (2008) Alternative photosynthetic electron flow to oxygen in marine *Synechococcus*. Biochimica et Biophysica Acta (BBA) 1777: 269-276.

Bukhov NG, Heber U, Wiese C, Shuvalov VA (2001) Energy dissipation in photosyntesis: Does the quenching of chlorophyll fluorescence originate from antenna complexes of photosystem II or from the reaction center? Planta 212: 749-758.

Bukhov NG, Sridharan G, Egorova EA, Carpentier R (2003) Interaction of exogenous quinones with membranes of higher plant chloroplasts: modulation of quinone capacities as photochemical and non-photochemical quenchers of energy in Photosystem II during light-dark transitions. Biochimica et Biophysica Acta (BBA) - Bioenergetics, 1604: 115-123.

Campbell D, Hurry V, Clarke AK, Gustafsson P, Oquist G (1998) Chlorophyll fluorescence analysis of cyanobacterial photosynthesis and acclimation. Microbiol Mol Biol Rev 62: 667-683.

Canaani O, Havaux M (1990) Evidence for a Biological Role in Photosynthesis for Cytochrome b-559-A Component of Photosystem II Reaction Center. PNAS, 87: 9295-9299.

Casper-Lindley C, Bjorkman O (1998) Fluorescence quenching in four unicellular algae with different light-harvesting and xanthophyll-cycle pigments. Photosynth Res 56: 277-289.

Cleland RE, Bendall DS (1992) Photosystem I cyclic electron transport: Measurement of ferredoxin-plastoquinone reductase activity. Photosynth. Res. 34: 409-418.

Cogdell RJ (2006) The structural basis of non-photochemical quenching revealed? TRENDS Plant Sci 11: 59-60.

Cournac L, Redding K, Ravenel J, Rumeau D, Josse EM, Kuntz M, Peltier G (2000) Electron flow between photosystem II and oxygen in chloroplasts of photosystem I-deficient algae is mediated by a quinol oxidase involved in chlororespiration. J Biol Chem 275:17256–17262.

Cramer WA, Zhang H, Yan J, Kurisu G, Smith JL (2006) Transmembrane Traffic in the Cytochrome b 6 f Complex. Annual Review of Biochemistry, 75: 769-790.

Dal Bosso C, Lezhneva L, Biehl A, Leister D, Strotmann H, Wanner G, Meurer J (2004) Inactivation of the chloroplast ATP synthase g subunit results in high non-photochemical fluorescence quenching and altered nuclear gene expression in Arabidopsis thaliana. J Biol Chem 279: 1060-1069.

Dall'Osto L, Caffarri S, Bassi R (2005) A mechanism of non-photochemical energy dissipation, independent from PsbS, revealed by a conformational change in the antenna protein CP26. Plant Cell 17: 1217-1232.

Dan Hess F (2000) Review: light-dependent herbicides: an overview. Weed Science 48:160-170.

Delphin E, Duval JC, Etienne AL, et al. (1998) Delta pH-dependent photosystem II fluorescence quenching induced by saturating, multiturnover pulses in red algae. Plant Physiology 118(1): 103-113.

Demmig-Adams B, Adams WWIII (2006) Photoprotection in an ecological context: the remarkable complexity of thermal energy dissipation. New Phytol 172: 11-21.

Dominici P, Caffarri S, Armenante F, Ceoldo S, Crimi M, Bassi R (2002) Biochemical properties of the PsbS subunit of photosystem II either purified from chloroplast or recombinant. J Biol Chem 25: 22750-22758.

Durnford DG, Prasil O, Escoubas JM, Falkowski P (1998) Assessing the potential for chloroplast redox regulation of nuclear gene expression. Methods in Enzymology, 297: 220-234.

Eisenstadt D, Ohad I, Keren N, Kaplan A (2008) Changes in the photosynthetic reaction centre II

in the diatom *Phaeodactylum tricornutum* result in non-photochemical fluorescence quenching. Environ Microbiol *In press*

Falkowski PG, Raven JA (2007) Aquatic Photosynthesis 2nd edition. Princeton University Press pp. 484.

Falkowski PG, Wyman K, Ley AC, Mauzerall DC (1986) Relationship of steady-state photosynthesis to fluorescence in eukaryotic algae. Biochim Biophys Acta 849: 183-192.

Finazzi G (2005) The central role of the green alga *Chlamydomonas reinhardtii* in revealing the mechanism of state transitions. J Exp Bot 56: 383-388.

Finazzi G, Johnson GN, Dallosto L, Joliot P, Wollman F-A, Bassi R (2004) A zeaxanthin-independent nonphotochemical quenching mechanism localized in the photosystem II core complex. Proc Natl Acad Sci USA 101: 12375-12380.

Finazzi G, Johnson GN, Dall'Osto L, Zito F, Bonente G, Bassi R, Wollman F-A (2006) Non-photochemical quenching of chlorophyll fluorescence in *Chlamydomonas reinhardtii*. Biochemistry 45: 1490-1498.

Fork DC, Herbert SK, Malkin S (1991) Light energy distribution in the brown alga *Macrocystis pyrifera* (giant kelp). Plant Physiol 95: 731-739.

Frenkel M, Bellafiore S, Rochaix J-D, Jansson S (2007) Hierarchy amongst photosynthetic acclimation responses for plant fitness. Physiol Plant 129: 455-459.

Garcia-Mendoza E, Colombo-Pallotta MF (2007) The giant kelp *Macrocystis pyrifera* presents a different non-photochemical quenching control than in higher plants. New Phytol 173: 526-536

Gilbert M, Richter M, Wilhelm C (2000) Bio-optical modelling of oxygen evolution using *in-vivo* fluorescence: comparison of measured and calculated P-I curves in four representative phytoplankton species. J. Plant Physiol. 157: 307-314.

Goss R, Ann Pinto E, Wilhelm C, Richter M (2006) The importance of a highly active and delta-pH-regulated diatoxanthin epoxidase for the regulation of the PS II antenna function in diadinoxanthin cycle containing algae. J Plant Physiol 163: 1008-1021.

Heber U (2002) Irrungen, Wirrungen? The Mehler reaction in relation to cyclic electron transport in C3 plants. Photosynthesis Research 73: 223-231.

Hill R, Frankart C, Ralph PJ (2005) Impact of bleaching conditions on the components of non-photochemical quenching in the zooxanthellae of a coral. Journal of Experimental Marine Biology and Ecology 322: 83-92.

Holt NE, Zigmantas D, Valkunas L, Li XP, Niyogi KK, Fleming GR (2005) Carotenoid cation formation and the regulation of photosynthetic light harvesting. Science 307: 433-436.

Hormann H, Neubauer C, Asada K, Schreiber U (1993) Intact chloroplasts display pH 5 optimum of O2-reduction in the absence of methyl viologen: Indirect evidence for a regulatory role of superoxide protonation. Photosynthesis Research, 37: 69-80.

Horton P, Hague A (1988) Studies on the induction of chlorophyll fluorescence in isolated barley protoplasts. IV. Resolution of non-photochemical quenching. Biochim Biophys Acta 932: 107–115.

Jakob T, Schreiber U, Kirchesch V, Langner U, Wilhelm C (2005) Estimation of chlorophyll content and daily primary production of the major algal groups by means of multiwavelength-excitation PAM chlorophyll fluorometry: performance and methodological limits. Photosynth. Res. 83:343-361.

Jakob T, Wagner H, Stehfest K, Wilhelm C (2007) Uncoupling of growth rates and biomass production under nitrate limitation in combination with dynamic light conditions in the diatom *Phaeodactylum tricornutum*. J. Exp Bot. 58: 2101-2113.

Joët T, Cournac L, Horváth EM, Medgyesy P, Peltier G (2001) Increased sensitivity of photosynthesis to antimycin A induced by inactivation of the chloroplast *ndhB* gene. Evidence for a participation of the NADH-dehydrogenase complex to cyclic electron flow around photosystem I. Plant Physiol. 125, pp. 1919–1929.

Johnson GN, Young AJ, Scholes JD, Horton P (1993) The dissipation of excess excitation energy in British plant species. Plant Cell Envir 16: 673-679.

Juneau P, Harrison PJ (2005) Comparison by PAM fluorometry of photosynthetic activity of nine marine phytoplankton grown under identical conditions. Photochem Photobiol 81: 649-653.

Kirilovsky D (2007) Photoprotection in cyanobacteria: the orange carotenoid protein (OCP)-related non-photochemical quenching mechanism. Photosynth Res 93: 7-16.

Kleczkowski LA (1994) Glucose activation and metabolism through UDP-glucose pyrophosphorylase in plants. Phytochemistry 37, pp. 1507–1515.

Kolber ZS, Prasil O, Falkowski PG (1998) Measurements of variable chlorophyll fluorescence using fast repetition rate techniques: defining methodology and experimental protocols. Biochim Biophys Acta 1367: 88-106.

Kornyeyev D, Holaday AS, Logan BA (2004) Minimization of the photon energy absorbed by 'closed' reaction centers of photosystem 2 as a photoprotective strategy in higher plants. Photosynthetica 42: 377-386.

Kroon BM, Thoms S (2006) From electron to biomass: a mechanistic model to describe phytoplankton photosynthesis and steady state growth rates. J. Phycol. 42: 593-609.

Kufryk GI, Vermaas WFJ (2006) Sll1717 Affects the Redox State of the Plastoquinone Pool by Modulating Quinol Oxidase Activity in Thylakoids. Journal of Bacteriology, 188(4) 1286-1294.

Külheim C, Agren J, Jansson S (2002) Rapid regulation of light harvesting and plant fitness in the field. Science 297: 91-93.

Laney and Oxborough, 2008 THIS BOOK

Lavaud J (2007) Fast regulation of photosynthesis in diatoms: Mechanisms, evolution and ecophysiology. Funct Plant Sci Biotech 1: 267-287.

Lavaud J, Strzepek RF, Kroth PG (2007) Photoprotection capacity differs among diatoms: Possible consequences on the spatial distribution of diatoms related to fluctuations in the underwater light climate. Limnol Oceanogr 52: 1188-1194.

Lavaud J, Rousseau B, Etienne A-L (2004) General features of photoprotection by energy dissipation in planktonic diatoms (Bacillariophyceae). J Phycol 40: 130-137.

Lavaud J, Rousseau B, van Gorkom HJ, Etienne A-L (2002) Influence of the diadinoxanthin pool size on photoprotection in a marine planktonic diatom *Phaeodactylum tricornutum*. Plant Physiol. 129: 1398-1406.

Ledford HK, Niyogi KK (2005) Singlet oxygen and photo-oxidative stress management in plants and algae. Plant Cell Envir 28: 1037-1045.

Li X-P, Phippard A, Pasari J, Niyogi KK (2002) Structure-function analysis of photosystem II subunit S (PsbS) *in vivo*. Funct Plant Biol 29: 1131-1139.

Logan BA, Adams WWIII, Demmig-Adams (2007) Avoiding common pitfalls of chlorophyll fluorescence analysis under field conditions. Funct Plant Biol 34: 853-859.

Mackey K, Paytan A, Grossman A Bailey S (2008) A photosynthetic strategy for coping in a high-light, low nutrient environment. Limnology and Oceanography, 53: 900-913.

Maxwell K, Johnson GN (2000) Chlorophyll fluorescence-a practical guide. J Exp Bot 51: 659-668.

McCauley S, Melis A, Tang G, Arnon D (1987) Protonophores Induce Plastoquinol Oxidation and Quench Chloroplast Fluorescence: Evidence for a Cyclic, Proton-Conducting Pathway in Oxygenic Photosynthesis. Proceedings of the National Academy of Sciences of the United States of America 84(23): 8424-8428.

Mehler AH (1951) Studies on reactions of illuminated chloroplasts I. Mechanism of the reduction of oxygen and other Hill reagents. Arch. Biochem. Biophys. 33: 65-77.

Miller AG, Canvin DT (1989) Glycoaldehyde inhibits CO_2 fixation in the cyanobacterium *Synechococcus* UTEX 625 without inhibiting the accumulation of inorganic carbon or the associated quenching of chlorophyll *a* fluorescence. Plant Physiol. 91: 1044–1049.

Miller AG, Espie GS, Canvin DT (1988) Active transport of CO_2 by the cyanobacterium *Synechococcus* UTEX 625. Plant Physiol. 86: 677–683.

Miyake C, Horiguchi S, Makino A, Shinzaki Y, Yamamoto H, Tomizawa K-I (2005) Effects of light intensity on cyclic electron flow around PSI and its relationship to non-photochemical quenching of Chl fluorescence in tobacco leaves. Plant Cell Physiol 46: 1819-1830.

Moreland DE (1980) Mechanisms of Action of Herbicides. Annual Review of Plant Physiology 31: 597-638.

Moss DA, Bendall DS (1984) Cyclic electron transport in chloroplasts. The Q-cycle and the site of action of antimycin. Biochim. Biophys. Acta 767: 389–395.

Müller P, Li X-P, Niyogi KK (2001) Non-photochemical quenching. A response to excess light energy. Plant Physiol 125: 1558-1566.

Mullineaux CW, Emlyn-Jones D (2005) State-transitions: and example of acclimation to low-light stress. J Exp Bot 56: 389-393.

Munekage Y, Takeda S, Endo T, Jahns P, Hashimoto T, Shikanai T (2001) Cytochrome *b6f* mutation specifically affects thermal dissipation of absorbed light energy in *Arabidopsis*. Plant J 28: 351-359.

Munekage Y, Hashimoto M, Miyake C, Tomizawa K, Endo T, Tasaka M, Shikanai T (2004) Cyclic

electron flow around photosystem I is essential for photosynthesis. Nature 429: 579–582.

Neubauer C, Yamamoto HY (1992) Mehler-peroxidase reaction mediates zeaxanthin formation and zeaxanthin-related fluorescence quenching in intact chloroplasts. Plant Physiology 99(4): 1354-1361.

Nixon PJ, Mullineaux CW (2001) Regulation of photosynthetic electron transport. In Aro E-M, Andersson B [ed.] Regulation of Photosynthesis. Kluwer Academic Publishers, Dordrecht, The Netherlands, pp. 533-555.

Niyogi KK (2000) Safety valves for photosynthesis. Curr Opin Plant Biol 3: 455-460.

Niyogi KK, Li XP, Rosenberg V, Jung H-S (2005) Is PsbS the site of non-photochemical quenching in photosynthesis? J Exp Bot 56: 375-382.

Owens TG (1986) Light-harvesting function in the diatom *Phaeodactylum tricornutum* II. Distribution of excitation energy between the photosystems. Plant Physiol 80: 739-746.

Oxborough K, Horton P (1987) Characterization of the effects of antimycin A upon high energy state quenching of chlorophyll fluorescence (qE) in spinach and pea chloroplasts. Photosynth. Res. 12: 119-128.

Pascal AA, Zhenfeng L, Broess K, van Oort B, van Amerongen H, Wang C, Horton P, Robert B, Chang W, Ruban A (2005) Molecular basis of photoprotection and control of photosynthetic light-harvesting. Nature 436: 134-137.

Peltier G, Cournac L (2002) Chlororespiration. Annu Rev Plant Physiol Plant Mol Biol 53: 523-550.

Peon J, Tan X, Hoerner D, Xia C, Luk YF, Kohler B (2001) Excited State Dynamics of Methyl Viologen. Ultrafast Photoreduction in Methanol and Fluorescence in Acetonitrile. J. Phys. Chem, 105: 5768-5777.

Perkins R, Mouget J-L, Lefebvre S, Lavaud, J (2006) Light response curve methodology and possible implications in the application of chlorophyll fluorescence to benthic diatoms. Mar Biol 149: 703-712.

Pfannschmidt T (2005) Acclimation to varying light qualities: toward the functional relationship of state transitions and adjustment of photosystem stochiometry. J Phycol 41: 723-725.

Prasil O, Kolber Z, Berry JA, Falkowski PG (1996) Cyclic electron flow around PSII in vivo. Photosynth. Res. 48: 395-410.

Pressman BC, Harris EJ, Jagger WC, Johnson JH (1967) Antibiotic-mediated transport of alkali ions across lipid bilayers. Proceedings of the National Academy of Sciences of the U.S.A. 58**:** 1949–1956.

Ralph PJ, Polk S, Moore KA, Orth RJ, Smith WA (2002) Operation of the xanthophyll cycle in the seagrass *Zostera marina* in response to variable light. Journal of Experimental Marine Biology and Ecology, 271: 189-207.

Rich P, Madgwick S, Moss D (1991) The interaction of duroquinol, DBMIB and NQNO with the chloroplast cytochrome *bf* complex. Biochimica et Biophysica Acta (BBA), 1058: 312-328.

Rotatore C, Lew RR, Colman B (1992) Active uptake of CO_2 during photosynthesis in the green alga *Eremosphaera viridis* is mediated by a CO_2-ATPase. Planta 188: 539–545.

Ruban AV, Johnson MP (2009) Dynamics of higher plant photosystem cross-section associated with state-transitions. Photosynth Res 99: 173-183.

Ruban AV, Berera R, Ilioaia C, van Stokkum IHM, Kennis JTM, Pascal AA, van Amerongen H, Robert B, Horton P, van Grondelle R (2007) Identification of a mechanism of photoprotective energy dissipation in higher plants. Nature 450: 575-579.

Ruban VA, Lavaud J, Rousseau B, Guglielmi G, Horton P, Etienne A-L (2004) The super-excess energy dissipation in diatom algae: comparative analysis with higher plants. Photosynth Res 82: 165-175.

Serra T, Borrego C, Quintana X, Calderer R, Lopez R, Colomer J (2009) Quantification of the effect of nonphotochemical quenching on the determination of *in vivo* chl a from phytoplankton along the water column of a freshwater reservoir. Photochem Photobiol 85: 321-331.

Shelp BJ, Canvin DT (1984) Evidence for bicarbonate accumulation by *Anacystis nidulans*. Can J Bot 62: 1398-1403.

Shyam R, Raghavendra AS, Sane PV (1993) Role of dark respiration in photoinhibition of photosynthesis and its reactivation in the cyanobacterium *Anacystis nidulans.* Physiol Plant 88: 446-452.

Sicher RC (1984) Glycolaldehyde inhibition of photosynthetic carbon assimilation by isolated chloroplasts and protoplasts. In C Sybesma, ed, Advances in Photosynthetic Research, Vol III. Martinus Nijhoff/Dr W Junk, The Hague, pp 413-416.

Sigalat C, Haraux F, de Kouchkovsky Y (1993) Force-flow relationship in lettuce thylakoids. 1. Strict control of election flow by internal pH. Biochemistry 32: 10201-10208.

Simonis, W. and Urbach, W. 1973: Photophosphorylation in Vivo. Annual Review of Plant Physiology, 24: 89-114.

Singh K, Shyam R, Sane PV (1996) Reactivation of photosynthesis in the photoinhibited green alga *Chlamydomonas reinhardtii:* Role of dark respiration and of light. Photosynthesis Research, 49: 11-20.

Standfuss J, van Scheltinga ACT, Lamborghini M, Kühlbrandt W (2005) Mechanisms of photoprotection and non-photochemical quenching in pea light-harvesting complex at 2.5 Å resolution. EMBO J 24: 919-928.

Stehfest K, Toepel J, Wilhelm C (2005) The application of micro-FTIR spectroscopy to analyze nutrient stress-related changes in biomass composition of phytoplankton algae. Plant Physiology and Biochemistry, 43: 717-726.

Stokes DM, Walker DA (1972) Photosynthesis by isolated chloroplasts. Inhibition by DL-glyceraldehyde of carbon dioxide fixation. Biochem. J. 128: 1147-1157.

Stroch M, Spunda V, Kurasova I (2004) Non-radiative dissipation of absorbed excitation energy within photosynthetic apparatus of higher plants. Photosynthetica 42: 323-337.

Suggett D, Kraay G, Holligan P, Davey M, Aiken J, Geider R (2001) Assessment of photosynthesis in a spring cyanobacterial bloom by use of a fast repetition rate fluorometer. Limnol. Oceanogra 46: 802-810.

Suggett et al 2008 THIS BOOK

Szabo I, Bergantino E, Giacometti GM (2005) Light and oxygenic photosynthesis: energy dissipation as a protection mechanism against photo-oxidation. EMBO Rep 6: 629-634.

Tagawa K, Tsujimoto HY, Arnon DI (1963) Role of chloroplast ferredoxin in the energy conversion process of photosynthesis. Proc. Natl. Acad. Sci. USA 49: 567-572

Toepel J, Domin A, Gilbert M, Wilhelm C (2004) Quantitative Estimates to convert photosynthetic electron transport rates into biomass. Archiv für Hydrobiologie 160: 515-526.

Trebst A (1980) Inhibitors in electron flow: Tools for the functional and structural localization of carriers and energy conservation sites. Methods in Enzymology, 69: 675–715.

Trebst A (2007) Inhibitors in the functional dissection of the photosynthetic electron transport system. Photosynthesis Research, 92: 217-224.

Tyystjarvi E, Koski A, Keranen M, Nevalainen O (1999) The Krautsky curve is a built-in barcode. Biophysical J. 77:1159-1167.

Velthuys B (1981) Electron-dependent competition between plastoquinone and inhibitors for binding to photosystem 11. FEBS Lett. 126: 277-281.

Wagner H, Jakob T, Wilhelm C (2005) Balancing the energy flow from captured light to biomass under fluctuating light conditions. New Phytol. 169: 95-108.

Wagner H, Gilbert M, Goss R, Wilhelm C (2006) Light emission originating from photosystem II radical pair recombination is sensitive to zeaxanthin related non-photochemical quenching (NPQ) J. Photochem. Photobiol. 83: 172-179.

Wilhelm C, Duval JC (1990) Fluorescence induction kinetics as a tool to detect chlororespiratorian activity in the prasinophycean alga *Mantoniella squamata.* Biochim. Biophys. Acta. 1016: 197-202.

Wilhelm C, Wild A (1984) The variability of the photosynthetic unit in *Chlorella* II. The effect of light intensity and cell development on photosynthesis, P-700 and cytochrome f in homocontinuous and synchronous cultures of *Chlorella.* J. Plant Physiol. 115: 124-135, 1984.

Zhu S-H, Green BR (2008) Light-harvesting and photoprotection in diatoms: Identification and expression of L818-like proteins. *In* Photosynthesis. Energy from the Sun: 14th International Congress on Photosynthesis, Allen J-F, Gantt, E, Golbeck JH, Osmond B (*Eds*), Springer, The Netherlands, pp 261-264.

Acknowledgements:
PR thanks the Australian Research Council for financial support. CW and TJ thank the deutsche Forschungsgemeinschaft for financial support Wi 764/12. JL thanks the Centre National de la Recherche Scientifique (CNRS), the Agence Nationale de la Recherche (ANR program VasiRéMi) and the deutsche Forschungsgemeinschaft (DFG, grant LA2368/2-1) for their financial support. Ross Hill is thanked for editorial comments.

Sven A. Kranz
Blessmannstrasse 1
27570 Bremerhaven
Sven.Kranz@awi.de

Bremerhaven, den 05.03.2010

Erklärung gemäß §6 (5) PromO (vom 14. März 2007):

Hiermit erkläre ich, dass ich die vorliegende Doktorarbeit mit dem Titel:

"Carbon and nitrogen acquisition of the diazotroph *Trichodesmium* in a high CO_2 world"

1. ohne unerlaubte fremde Hilfe angefertigt habe,
2. keine anderen als die von mir angegebenen Quellen und Hilfsmittel benutzt habe
3. die den benutzen Werken wörtlich oder inhaltlich entnommenen Stellen als solche kenntlich gemacht habe.

Ebenfalls erkläre ich hiermit eidesstattlich, dass es sich bei den von mir abgegebenen Arbeiten um 3 identische Exemplare handelt.

…….
Sven Kranz